Structural Investigation of Marine Biomolecules by Tandem Mass Spectrometry

by

©Trevena Nabil Youssef

A dissertation submitted to the School of Graduate Studies

in partial fulfillment of the requirements for the degree of

Doctor of Philosophy

in

Department of Biochemistry

Memorial University

St. John's, Newfoundland, Canada

May 2025

Abstract

A wealth of undiscovered scientific information is held within our oceans. Elucidation of this scientific information will play a leading role in understanding the aqueous environment.

This thesis focuses on two main research goals. The first one involves the qualitative and quantitative investigations of the protein composition of Atlantic cod (*Gadus morhua*) otoliths. Cod otoliths have been sampled for decades; however, a wealth of information remains to be uncovered. With advancements in novel scientific technologies, we are beginning to probe the physiological and biochemical blueprints of their proteins and biomarker components. This research will help clarify how the aqueous environment influences the full life history of fish.

Most importantly, it will contribute to efforts aimed at preserving fish populations for future generations. The detailed study of otolith protein composition is an emerging scientific field that seeks to explain the diverse roles of otolith proteins and their relationships with physiological and biochemical growth functions.

The second goal of this thesis involves the structural elucidation of lipopolysaccharide (LPS) components from marine Gram-negative bacteria that impact aquaculture ventures. The LPS of bacterial cell walls contains lipid A, which is essential for fish vaccine development and is used as a vaccine adjuvant. Therefore, we will explore the molecular structure of two lipid A molecules, isolated from different Gram-negative marine bacteria belonging to the *Vibrionaceae and Aeromonadaceae* families.

Acknowledgments

From the bottom of my heart, I extend my deepest thanks to my Lord, God, and Savior, Jesus Christ. His love and grace have been my unwavering companions throughout my journey.

I extend my sincere thanks to Dr. Joseph H. Banoub, Adjunct Professor of Biochemistry at Memorial University of Newfoundland and Head of Special Projects, Science Branch, Department of Fisheries and Oceans, Canada. His exemplary guidance, persistent help, and constant encouragement have been crucial to the success of my Ph.D. studies.

I am also profoundly grateful to my supervisory committee members, Dr. Travis Fridgen and Dr. Mark Berry, whose expertise, insightful criticism, and invaluable advice have shaped my research work.

I am also profoundly grateful to Professor Sherri L. Christian for her invaluable guidance and support throughout my work on protein analysis. Her expertise was crucial in achieving the final version of this study, and I could not have reached this point without her assistance and guidance.

I would like to extend my heartfelt gratitude to Professor David R. Goodlett and Dr. Abanoub Micheal for their help in MS AND MS/MS analysis and guidance throughout my research on bacterial lipid A.

My heartfelt thanks are extended to the Biochemistry Department at the Memorial University of Newfoundland and the Department of Fisheries and Oceans (DFO) at St.

John's. The resources and support provided by these esteemed institutions have been essential in facilitating my research endeavours.

I would like to extend my sincere appreciation to the School of Graduate Studies (SGS) at the Memorial University of Newfoundland. Their financial support throughout my degree program has been invaluable in my academic journey.

Finally, I would like to express my profound gratitude to my family for their immeasurable love, unwavering support, and constant encouragement. Your guidance and care have been invaluable to me. To my lovely mother, Trevosa Sorial, my father, Nabil Youssef, my brother, Kerolos, and all my friends, I owe my deepest appreciation. I also extend my heartfelt thanks to Father Faltaaos and my dear friend, Martyr Filomena, for their steadfast support and prayers, which have been the cornerstone of my personal and academic journey.

Table of Contents

List of Figures

List of Tables

List of Schemes

List of Abbreviations and Symbols

Full Name	Abbreviation
A	
2-Amino-2-deoxy-D-galactose	GalN
2-Amino-2-deoxy-D-glucopyranose	GlcpN
4-Amino-4-deoxy-L-arabinose phosphate	Ara4N-p
AP-3 complex subunit mu-2	PA3
Alternating current	AC
ATP-binding cassette sub-family B	MDR/TAP
Acyl carrier protein	ACP
Aeromonas hydrophila	*A. hydrophila*
Alpha and acetyl-CoA acetyltransferase 1	ACAT1
Ammonium bicarbonate	NH_4HCO_3
Arrestin-domain containing protein 1	Arrdc1
Auto gain control	AGC
C	
95% Confidence intervals	CIs
Calcium carbonate	$CaCO_3$
Calmodulin	CaM
Calmodulin 2a phosphorylase kinase	CaMKII
Carbonic anhydrase	CA

Cation calcium	Ca^{2+}
Cation exchange chromatography	SCX
Cell division control protein 42 homolog	CDC42
Chemical Ionization	CI
Chondroadherin-like b	CHADL
Coelomic fluid	CF
Collision-induced dissociation	CID
Compensation voltage	CV
Core oligosaccharide	OS
Cys-Cys-Gly amino acid motif	CCG motif

D

2,3-Diamino-2,3-dideoxy-D-glucosamine	GlcN3N
3-Deoxy-D-manno-oct-2-ulosonic acid	Kdo
D-2-Amino-2-deoxyglucitol	GlcNol
Di-phosphorylated Lipid A	DPLA
Direct current	DC
Dithiothreitol	DTT

E

Electron Ionization	EI
Electrospray Ionization	ESI
Ethanolamine di-phosphate	EtNPP
Eukaryotic translation elongation factor 2	EEF2

Extracellular matrix	ECM
F	
FK-506 binding protein	FKBP
Fast Fourier transforms	FFT
Field Asymmetric Waveform Ion Mobility Spectrometry	FAIMS
Flavin adenine dinucleotide	FAD
Fourier transform ion cyclotron resonance	FTICR
Frequency	ω
G	
G-protein-coupled-Receptors	GPCRs
Galactose	Gal
Galacturonic Acid	GalA
Gas chromatography	GC
Gene ontology	GO
Glucosamine residues	GlcN
Glucose	Glc
H	
3-Hydroxy-myristic	C14:0(3-OH)
Heat shock proteins	HSPs
Heparan sulfate proteoglycans	HSPG
High mobility group	HMG
High-performance liquid chromatography	HPLC

High-performance liquid chromatography, electrospray ionization, and tandem mass spectrometry	HPLC-ESI- MS/MS
Higher-energy Collisional Dissociation	HCD
Hydrophilic Interaction Liquid Chromatography	HILIC
I	
Inner membrane	IM
Intermediate filament protein ON3-like	IFs
Iodoacetamide	$IAcNH_2$
Ion Mobility Spectrometry	
Isoelectric point	pI
K	
Kendrick mass defect	KMD
L	
L-glycero-D-manno-heptose	Hep
Lauric acid/ Lauroyl group	C12:0
Linear ion traps	LIT
Lipopolysaccharides	LPS
Liquid chromatography	LC
M	
Malate dehydrogenase	MDH
Mass spectrometry	MS
Mass-to-charge ratio	*m/z*

Matrix-Assisted Laser Desorption/Ionization	MALDI
Membrane-derived oligosaccharides	MDO
Mono- phosphorylated Lipid A	MPLA
Motile Aeromonas septicemia	MAS
Multi-reflecting TOF	MR-TOF
Myelin basic protein	MBP
Myristic acid/myristoyl group	C14:0
Myristyl-oxy-lauric acid	C14:0(3-O-12:0)

N

Nucleobindin 1	NUCB1

O

One-dimensional gel electrophoresis	1-DGE
One-dimensional sodium dodecyl sulfate polyacrylamide gel electrophoresis	1D-SDS-PAGE
Otoconin-90	OC90
Otolith matrix protein-1	OMP-1
Outer membrane	OM
Outer mitochondrial membrane	OMM
Ovarian fluid	OF

P

Palmitic acid/ palmitate	C16:0
Pathogen-associated molecular pattern	PAMP

Peroxiredoxin-1	PRX1
Phospho-ethanolamine	PEtN
Plasma membrane calcium ATPase isomer 2	PMCA2
Polycyclic aromatic hydrocarbons	PAHs
Protein–protein interaction	PPI
Purine-rich element binding protein Ab	PURA

Q

Quadrupole	Q
Quadrupole Mass Analyzer	QMA

R

RAN binding protein 2	RANBP2
Radio frequency	RF
Ribonucleoprotein	RNP

S

Second heptose	HepII
Small cellular or pericellular matrix proteoglycan	SLRP
Small leucine-rich proteins	SLRPS
Sodium dodecyl sulphate-polyacrylamide gel electrophoresis	SDS-PAGE
Sodium/potassium-transporting ATPase subunit beta	NKA
Spring viremia of carp virus	SVCV

T

Tandem mass spectrometry	MS^2, MS/MS
Time-of-flight	TOF
Total potential	Φo
Trans-Golgi network	TGN
Transketolase b	TKT
Trichloroacetic acid	TCA
Triethyl ammonium acetate buffer	TEAA
Trifluoroacetic acid	TFA
Triple-quadrupole	QqQ
Tubulin alpha-1A chain	TUBA 1A
Two-dimensional gel electrophoresis	2-DGE

U

UDP-2,3-di-acylglucosamine	UDP-2,3-di-acyl-GlcN
UDP-3-acyl-glucosamine	UDP-3-O-acyl-GlcN
Uridine di-phosphate-N-acetylglucosamine	UDP-GlcNAc
Uridine monophosphate	UMP

V

Variance stabilization normalization	VSN
Vibrio anguillarum	*V. anguillarum*
Voltage-dependent anion-selective channel 2	VDAC2
Vitellogenin	VTG

Co-authorship statement

The research presented in this thesis has been conducted by the principal author, Trevena Youssef, for the Doctor of Philosophy degree under the supervision of Prof. Joseph Banoub.

Trevena Youssef planned and designed the study, conducted most of the experiments, interpreted the data, and prepared the manuscript. Collaborators provided important support, including help with data analysis, manuscript revisions, and contributions from other authors.

1. **J. Banoub, T. Youssef, and A. Mikhael, "Proteomic technology applications for fisheries research,"** ***Tech. Report. Fish. Aquat. Sci.,*** **vol. 3465, pp. xi-668, May, 2022.** Trevena Youssef performed the manuscript preparation. This work was used as part of the application of proteomic technology in Chapter 1 of this thesis. The manuscript was edited by Dr. Mikhael and Dr. Banoub.
2. **R. M. Rideout, T. N. Youssef, A. T. Adamack, R. John, A. M. Cohen, T. D. Fridgen, and J. H. Banoub, "Qualitative Shotgun proteomics strategy for protein expression profiling of fish otoliths,"** ***BioChem*****., vol. 3, no. 3, pp. 102-117, Jul, 2023.** DOI: https://doi.org/10.3390/biochem3030008. This work is included in Chapter 2. Trevena Youssef performed all data interpretation and manuscript preparation. The manuscript was edited by Dr. Rideout, Dr. Adamack, Dr. John, Dr. Cohen, Dr. Fridgen, and Dr. Banoub.

3. **T. N. Youssef, S. L. Christian, R. Rideout, A. Adamack, P. Thibault, E. Bonneil, T. D. Fridgen, and J. Banoub, "Proteomic blueprint of Atlantic Cod (Gadus morhua) otoliths revealing environmental stress insights through label-free quantitative shotgun proteomics," *Biochem.*, vol. 4, no. 2, pp. 144-165, Jun, 2024.** DOI: https://doi.org/10.3390/biochem4020008. This work is included in Chapter 3. Trevena Youssef performed all data interpretation and manuscript preparation. The manuscript was edited by Dr. Christian, Dr. Rideout, Dr. Adamack, Dr. Thibault, Dr. Bonneil, Dr. Fridgen, and Dr. Banoub.
4. **T. N. Youssef, A. Mikhael, D. R. Goodlett, T. D. Fridgen, and J. Banoub, "Benefits of field asymmetric ion mobility spectrometry (FAIMS) and Kendrick mass defect plots in lipid A analysis, ".** This work is currently submitted for publication in the journal the journal J. Am. Soc. Mass Spectrom. and included in Chapter 4. Trevena Youssef performed all data interpretation and manuscript preparation. The manuscript was edited by Dr. Mikhael, Dr. Goodlett, Dr. Fridgen, and Dr. Banoub.
5. **T. N. Youssef, A. Mikhael, D. R. Goodlett, T. D. Fridgen, and J. Banoub, "Structural elucidation of a novel unique mixture of lipid A obtained from the phenol-phase soluble lipopolysaccharide of Vibrio anguillarum serovar SJ-41,"** This work is currently submitted for publication in the journal Rapid Commun. Mass Spectrom. and included in Chapter 5. Trevena Youssef performed all data interpretation and manuscript preparation. The manuscript was edited by Dr. Mikhael, Dr. Goodlett, Dr. Fridgen, and Dr. Banoub.

Chapter 1 Introduction:

In this introduction, I will provide the literature background for this work, offering the fundamental information necessary to understand the two research studies presented. We will discuss the advantages of structurally investigating Atlantic cod otolith proteins, the structural elucidation of lipid A biomolecules from marine Gram-negative bacteria, and the principles of mass spectrometry along with its applications in these studies.

1.1. Atlantic cod (*Gadus Morhua*)

Atlantic cod (*Gadus morhua*) is a species of great ecological and economic importance, known for its role in the North Atlantic ecosystem and its value in commercial fisheries [1-3]. These fish inhabit all waters overlying the continental shelves of the Northwest and the Northeast Atlantic Ocean [4]. However, their population is impacted by both overfishing and climate change [5, 6].

In Canada, Atlantic cod are found continuously along the east coast from Georges Bank and the Bay of Fundy in the south, moving northward along the Scotian Shelf, throughout the Gulf of St. Lawrence, around the island of Newfoundland, and extending along the eastern shores of Labrador and Baffin Island, Nunavut. There are also three landlocked populations of Atlantic cod on Baffin Island [4]. They are known for their remarkable adaptability to different environments, including variations in temperature and salinity. This adaptability is evident in the Baltic Sea, where cod populations are managed

as distinct western and eastern stocks, each exhibiting unique physiological and life-history traits [1].

1.1.1. Atlantic Cod's Otolith

Fish otoliths are biominerals found in the inner ear commonly used for tracking fish bio-chronologies and as a model system for biomineralization [7]. The inner ear of the Atlantic cod, like other teleost bony fishes (**Figure 1-1**), includes three semicircular canals (anterior, posterior, and horizontal), three otolithic end organs: the saccule, utricle, and lagena, each housing a specific otolith: the sagitta, lapillus, and asteriscus, respectively [8-10]. These otoliths are encased within fluid-filled sacs known as the end organs of the inner ear. The fluid, known as endolymph, is rich in both inorganic materials and proteins, which play a crucial role in the growth and maintenance of otoliths [11]. Each otolith organ contains a macula, a specialized sensory region covered with hair cells. The movement of these otoliths causes the hair cells in the macula to bend, converting mechanical stimuli into electrical signals that are then recognized by the nervous system (**Figure 1-1 A**) [12, 13].

The sagitta, being the largest, is most commonly studied due to its detailed growth rings, which provide valuable insights into the fish's age and growth patterns [14, 15]. Otoliths are dense structures composed primarily of calcium carbonate ($CaCO_3$) embedded in an organic matrix, and they grow incrementally through daily deposition of concentric layers [16-21].

A)

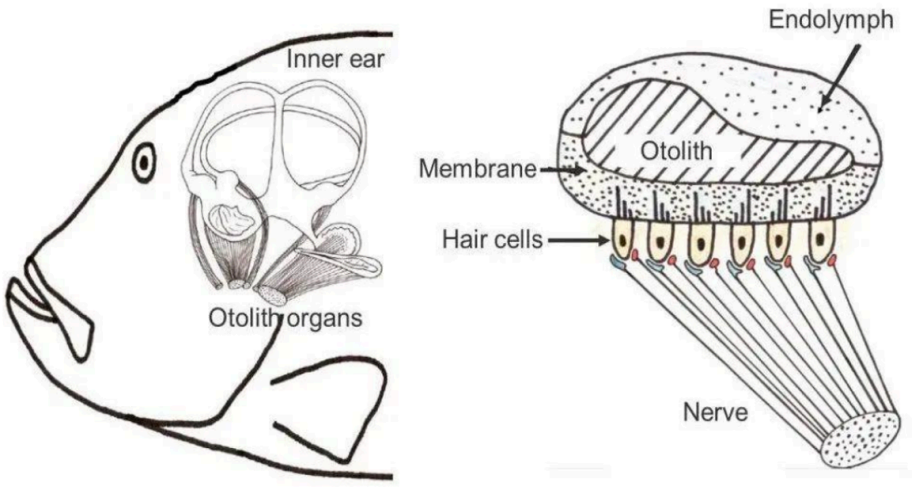
Inner ear
Otolith organs
Endolymph
Otolith
Membrane
Hair cells
Nerve

B)

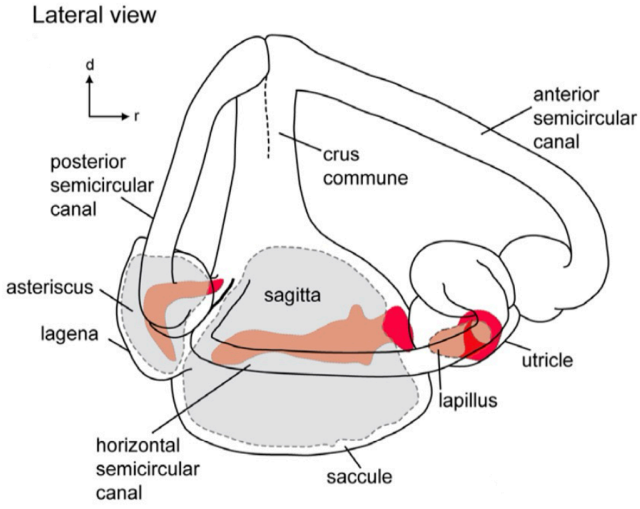
Lateral view
d
r
anterior
semicircular
canal
crus
commune
posterior
semicircular
canal
asteriscus
sagitta
lagena
utricle
lapillus
horizontal
semicircular
canal
saccule

C)

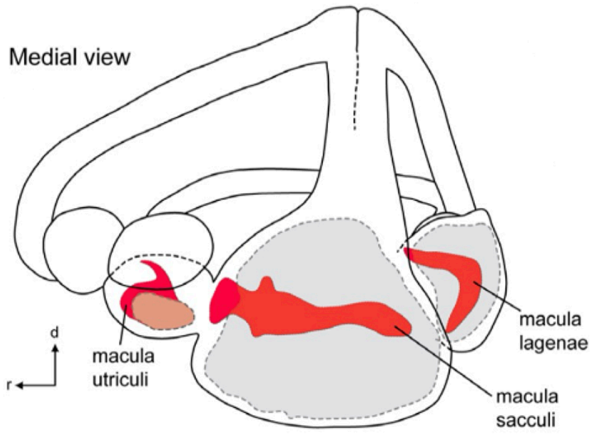

Figure 1-1. Inner ears of teleost fish. A) Otolith structure of a fish. B-C) Right labyrinth with semicircular canals and end organs with otoliths shown in shaded gray and maculae shown in red in lateral view (B) and medial view (C). This figure is reprinted from Open Access sources [13, 22].

The role of otoliths extends beyond their structural composition; they are integral to the fish's sensory systems, particularly in hearing and balance. Otoliths detect sound and motion, transmitting vibrations to the sensory hair cells in the inner ear, which then relay this information to the brain [23, 24]. Unlike other calcified tissues, otoliths are metabolically inert [25], meaning that the materials deposited throughout the fish's life remain unchanged. This makes them valuable for studying environmental influences on fish physiology, as the composition of the otoliths can reflect changes in water chemistry and temperature over time [16, 21, 25, 26]. Moreover, the continuous growth of otoliths serves as a biological record, providing critical data for fisheries research, including insights into the fish's life history, migration patterns, and environmental interactions [5, 27].

The detailed analysis of otolith structure and composition has enabled researchers to better understand the impacts of various environmental factors, such as temperature fluctuations and habitat changes, on Atlantic cod populations [5, 27]. For instance, studies have shown that the shape and size of otoliths can vary depending on the cod's growth conditions, which can be influenced by factors such as food availability, water temperature, and salinity. This makes otoliths an essential tool not only for age determination but also for assessing the overall health and viability of cod stocks in different regions [5, 27].

1.1.2. Identified Otolith Proteins

Proteins, constituting only 2-3% of the otolith's composition, play a critical role in the biomineralization process that shapes and maintains these structures [28, 29]. The protein matrix within the otolith provides a substrate for $CaCO_3$ deposition and influences the polymorphism of the deposited $CaCO_3$, determining whether it forms as aragonite or calcite [28-30]. These proteins are crucial in the biomineralization process that shapes and maintains these structures [14, 31].

One of the primary proteins involved in this process is otolin-1, a glycoprotein that forms a scaffold for calcium carbonate deposition, which is crucial for the biomineralization of otoliths. It contains a C1q-like structural domain forming a stable trimer in the presence of calcium ions and is responsible for protein trimerization and Ca^{2+} binding, which are essential for the biomineralization of otoliths [30]. Otolin-1 has also been identified as a component of the otolithic membrane, which binds the otolith to the sensory macula [8, 23, 32]. In zebrafish, the knockdown of otolin-1 results in reduced

otolith growth rates, larger and malformed otoliths, and even the fusion of sagitta with lapilli within 72 hours post-fertilization [23, 32]. Otolith matrix protein-1 (OMP-1) is directly involved in otolith growth through coordinating hydrogen carbonate deposition and is essential for the proper placement of otolin-1 on the growing discontinuous zone of otolith [23, 32]. The importance of OMP-1 is highlighted by studies in zebrafish, where its knockdown leads to smaller, misshapen otoliths, emphasizing its essential role in otolith formation and growth [32].

Otoconin-90 (OC90) is crucial in nucleating $CaCO_3$ crystals within the otolith. This highly acidic protein can bind to calcium ions and is required to recruit other proteins into the otolith organic matrix [30, 33]. Cochlin, another matrix protein, also plays a role in maintaining the structural integrity of the otolith [34]. Proteins like starmaker and its homolog, starmaker-like protein, are key regulators of crystal polymorph selection and serve as a template for $CaCO_3$ crystal nucleation [23, 35, 36].

Osteopontin plays an important role in otolith mineralization, inhibiting excessive mineral deposition and thereby contributing to the precise formation of otolith layers [14, 37]. Other proteins, like the precerebellin-like protein, are believed to interact with otolin-1 during matrix assembly [23, 38].

Beyond structural proteins, the otolith contains anchoring proteins such as otoglin, otoglin-like, and α-tectorin [14, 30, 32, 39]. Otogelin and otogelin-like specifically anchor the otolith to the macula, which is essential for accurate sensory perception [23, 40]. α-Tectorin is thought to be essential for cell adhesion [23, 40]. However, the complete protein composition within otoliths has yet to be fully studied [30].

Then, I will describe the background of the second part of this work, which deals with the molecular structure elucidation of bacterial lipid A.

1.2. Marine Gram-Negative Bacteria

Marine Gram-negative bacteria are a diverse and ecologically critical group of microorganisms inhabiting the world's oceans. Their unique cell wall structure, particularly the presence of lipopolysaccharides (LPS), is essential for their survival and interactions within the marine environment [41, 42]. LPS plays a key role in protecting these bacteria from harsh conditions and mediating interactions with host organisms, making it a focal point in understanding their pathogenic potential and ecological significance [41].

These bacteria are essential for maintaining the health of marine ecosystems and serve as a rich source of novel bioactive compounds with promising applications in biotechnology and medicine. The pharmaceutical industry is increasingly exploring these microorganisms for new compounds, particularly those that can combat antibiotic-resistant pathogens [41, 43, 44].

Usually, conventional Gram stain tests will distinguish the group of bacteria by colour. The Gram-positive bacteria show a blue or purple colour after staining and possess a thick cell wall. Gram-negative bacteria display a pink or red colour and show a thin wall, reflecting differences in the cell envelope architecture [45, 46]. Gram-positive and -negative bacteria possess a cytoplasmic membrane composed of a phospholipid bilayer bordering the cytosol and provides a semipermeable barrier that regulates the movement

of molecules in and out of the cell [45]. However, Gram-positive bacteria have a thick peptidoglycan layer and lack an outer phospholipid bilayer or lipopolysaccharides (LPS), which are characteristic of Gram-negative bacteria (**Figure 1-2)** [45, 47].

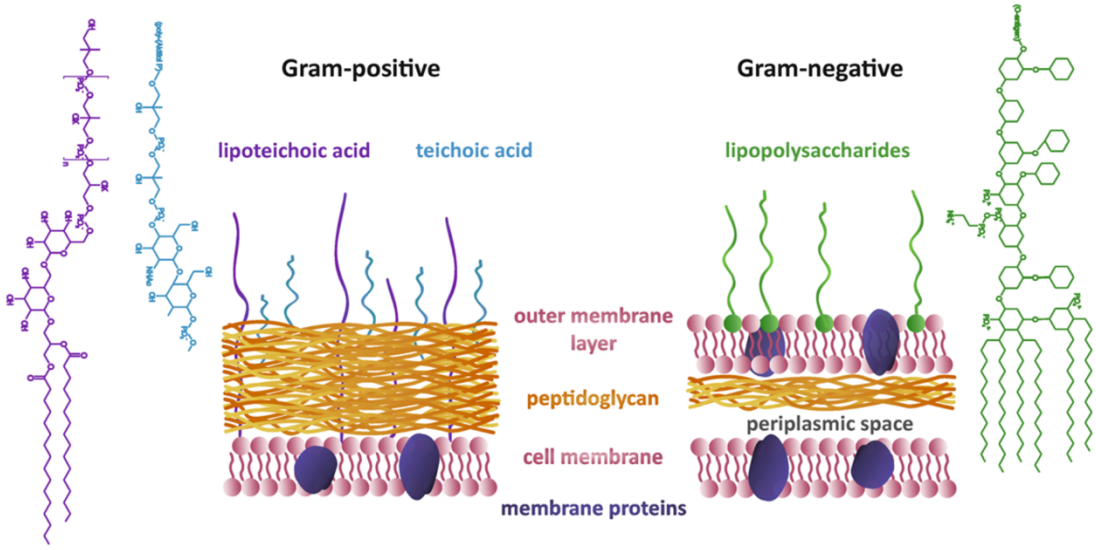

Figure 1-2. Differences between Gram-positive and Gram-negative bacterial cell walls. This figure is reprinted from an Open Access source [47].

The structural diversity of LPS among different marine Gram-negative bacteria is especially significant, as certain pathogenic strains can cause substantial damage to marine life, leading to economic losses in aquaculture and fisheries [41, 48]. Understanding these structural features is crucial for developing effective therapeutic strategies and mitigating the impact of these bacteria on marine industries [41, 48].

1.2.1. The Cell Envelope of Gram-Negative Bacteria

There are three principal layers in the envelope: the outer membrane (OM), the thin peptidoglycan cell wall, and the cytoplasmic or inner membrane (IM), as shown in **Figure 1-3** [46, 49].

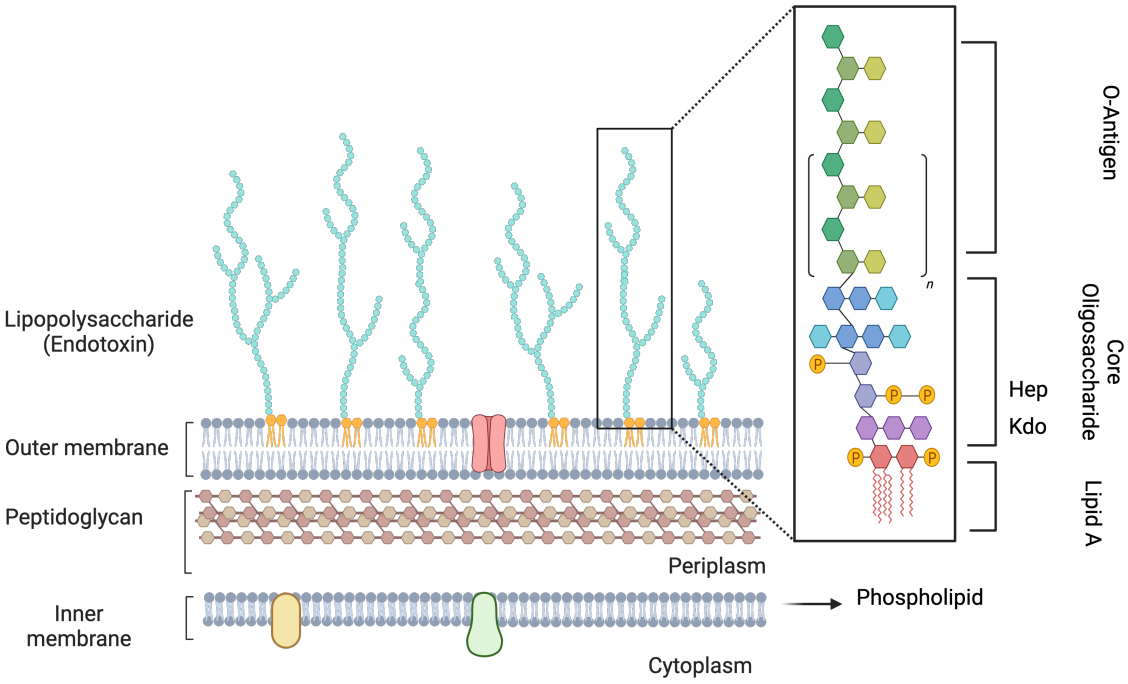

Figure 1-3. Schematic of the Gram-negative cell envelope. The outer membrane is an asymmetric bilayer with the inner leaflet. The inner leaflet is composed of phospholipids and proteins. The outer leaflet contains lipopolysaccharides, proteins, and phospholipids. Kdo, 3-deoxy-D-manno-octulosonic acid and Hep, L-glycero-D-manno-heptose. This figure was created by BioRender.

The OM is a unique asymmetric phospholipid bilayer in which the inner leaflet is composed of glycerophospholipids; however, the external leaflet is rich in LPS, which covers up to the majority of the cell surface [50, 51]. Rooted in the OM are integral membrane proteins like porins, which serve as channels for the passage of small hydrophilic molecules, as well as lipoproteins [50, 51].

The cell wall peptidoglycan (also called murein) is a rigid layer that confers shape and osmotic strength to the bacterial cell and encloses the cytoplasmic membrane. The polymeric network of the peptidoglycan is formed by carbohydrate backbone chains of N-acetyl-D-glucosamine and N-acetylmuramic acid that are cross-linked by penta-peptide chains [45, 46].

1.2.1.1. LPS Structure

LPSs, also known as endotoxins, are the primary component of the outer leaflet of the OM of Gram-negative bacteria and are critical for their viability [49]. In most bacteria, LPS displays a common structural architecture that includes three domains: a lipophilic moiety known as lipid A, a hydrophilic polymeric molecule called the *O*-specific polysaccharide, and a relatively shorter oligosaccharide known as the core oligosaccharide (OS) (**Figure 1-4**). The core OS can be further divided into two regions: the inner core OS, which is proximal and attached to lipid A, and the outer core OS, which is distal and adjacent to the O-antigen [45, 50, 52]. The complete LPS comprising all three regions is termed “smooth” (S) LPS, while LPS lacking the O-chain and/or portions of core OS the LPS is called “rough” [53].

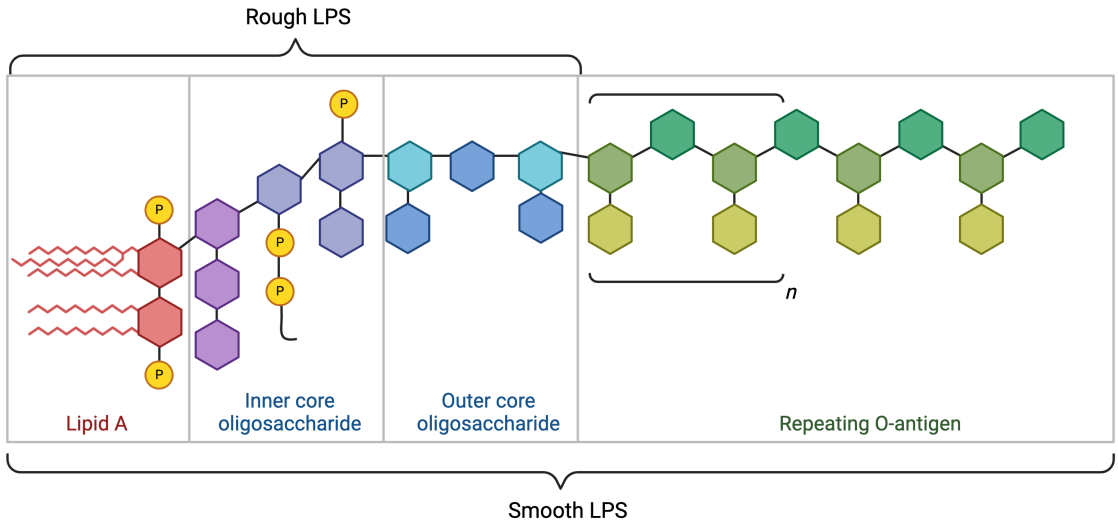

Figure 1-4. The general structure of LPS from Gram-negative bacteria: All known forms of LPS consist of a lipid A domain and a covalently linked saccharide moiety composed of the core region (oligosaccharide) (Rough LPS), plus a polysaccharide portion, the O-antigen (Smooth LPS). This figure was created by BioRender.

LPSs are an effective permeability barrier, protecting bacteria against external stress factors [54]. It plays an essential structural role in the assembly and stability of the OM, which is vital for bacterial survival [45, 51]. LPS is a heat-stable, amphiphilic complex of macromolecules that provides a permeability barrier to various organic molecules, biomolecules, and metals [45, 51]. On the bacterial surface, LPSs act as a pathogen-associated molecular pattern (PAMP) that is recognized by the host immune system, typically leading to pathogen elimination [55, 56].

Gram-negative bacteria can modify the LPS structures to evade the immune system detection and resist defense factors such as complement and antibiotics. These modifications often involve changes in the lipid A region of LPS or alterations to the O-antigen, making it harder for immune cells to detect and attack the bacteria. This highlights the high variability of LPS in the cell wall [57-61].

Extensive research has been conducted to uncover the structure and biosynthesis of various components of LPS molecules [45, 62-66], as well as the mechanisms of LPS-induced immune activation [45, 67, 68].

1.2.1.1.1. LPS *O*-Specific Antigens

The O-specific chain, also called the *O*-antigen, is a repetitive polysaccharide polymer composed of up to 50 repeating oligosaccharide units, with each unit consisting of 2 to 8 monosaccharide residues [53, 58, 69]. The structure and composition of the O-antigen vary across different bacterial genera and serotypes due to differences in sugar units, glycosidic linkages, and non-carbohydrate components [53, 69]. This diversity results from genetic variability and leads to unique O-chain structures, which can be linear or branched [53, 70-81].

The presence or absence of the *O*-antigen determines whether the bacterial LPS is classified as smooth or rough. A full-length *O*-antigen renders the LPS smooth, while the absence of *O*-antigen chains results in a rough LPS. Additionally, semi-rough LPS structures contain a single *O*-chain unit attached to the core-lipid A oligosaccharide (**Figure 1-4**) [53, 82, 83].

1.2.1.1.2. LPS Core Oligosaccharide

The core oligosaccharide is situated between the *O*-antigen region of the LPS and the lipid A region. Compared to the *O*-antigen, the core oligosaccharide is more conserved in both structure and composition and can be divided into inner and outer subdomains [53].

The inner core typically contains unique residues, such as 3-deoxy-D-manno-oct-2-ulosonic acid (Kdo) and L-glycero-D-manno-heptose (Hep), which are hallmarks of the LPS [53, 69, 84]. The presence of the Kdo residue at the reducing end of the core oligosaccharide is crucial for the biological activity of the LPS [53, 61]. KdoI is linked to lipid A through a glycosidic bond at the O-6' position of lipid A [45, 53].

The outer core in LPSs generally consists of an oligosaccharide chain of up to six sugar units linked to the second heptose (HepII) in the inner core. It is often branched with glucose (Glc), galactose (Gal), or their derivatives [53].

1.2.1.1.3. LPS Lipid A

Lipid A is the portion of the LPS that anchors it to the bacterial cell membrane [53]. In most Gram-negative bacteria, lipid A is the most conserved LPS region. However, structural variations exist across bacterial species [45, 85]. Typically, the disaccharide backbone of lipid A is composed of 2-amino-2-deoxy-D-glucopyranose (Glc*p*N). In some species, 2,3-diamino-2,3-dideoxy-D-glucosamine (GlcN3N) is present, or a mixture of both may occur [85]. The 1- and 4'-positions are typically substituted with phosphate (P) or phosphate esters but can also be substituted with hydrogen or galacturonic acid. The degree of acylation varies from 4 to 8 acyl groups depending on the species [85].

In most Gram-negative bacteria, lipid A consists of a disaccharide structure, β-D-Gl*cp*N-(1→6)-α-D-Gl*cp*N. Phosphorylation typically occurs at the 1-position D- Gl*cp*N I residue (reducing end) and at 4'- position the β-D- Gl*cp*N II residue (non-reducing).

Acylation occurs at the C-2, C-2', C-3, and C-3' positions of both D-Gl*cp*N residues via amide and ester linkages [45].

The first structurally elucidated lipid A was from *E. coli,* consisting of β-D-Gl*cp*N-(1→6)-α-D-Gl*cp*N. It is N-acylated at positions 2 and 2' and O-acylated at positions 3 and 3' of both Gl*cp*N residues, with (R)-3-hydroxy-myristoyl groups (C14:0(3-OH)) as primary fatty acids. Both primary acyl groups attached to Gl*cp*N II are esterified at their 3-hydroxy group with two secondary fatty acids: the amide-linked fatty acid bears a lauroyl group (C12:0), and the ester-linked fatty acid carries a myristoyl group (C14:0) (**Figure 1-5**) [45].

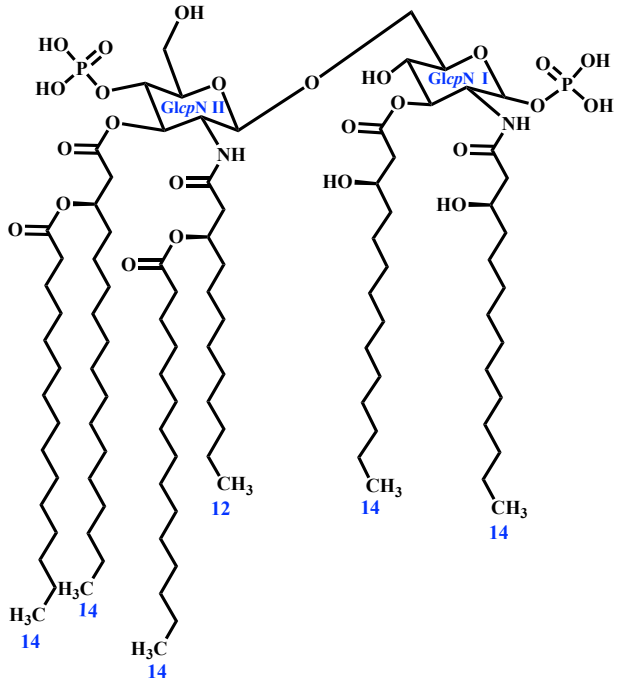

Figure 1-5. Structure of lipid A of *E*. Coli. This figure was generated using ChemDraw Prime.

Lipid A structures with GlcN3N disaccharide backbone have been identified in various bacterial species, such as *Aquifex pyrophilus [86]*, *Brucella abortus* [87],

Bacteriovorax stolpii [88], *Caulobacter crescentus [89], Mesorhizobium huakuii [90]*, *Bradyrhizobium elkanii [91]*, *Bartonella henselae [92]*, *Legionella pneumophila* [93]. The major lipid A structural variant of *Campylobacter jejuni*, a bacterium responsible for gastrointestinal diseases, contains a hybrid backbone of a GlcN3N-(1→6)-Gl*cp*N disaccharide (**Figure 1-6**) [94].

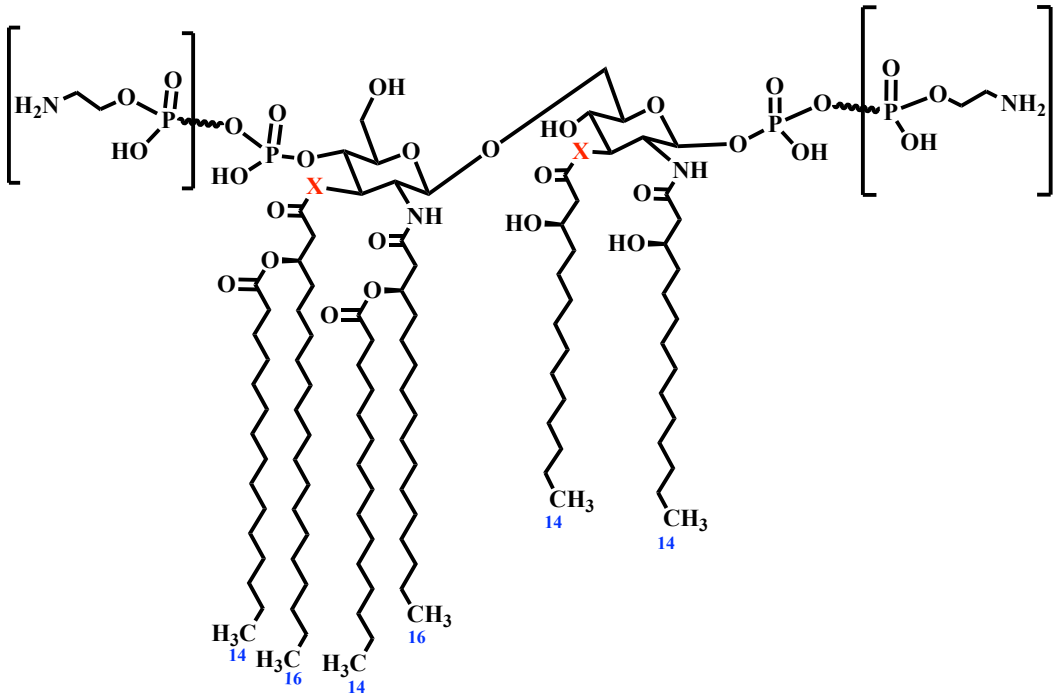

Figure 1-6. Schematic structure of lipid A from *C. jejuni* wild-type 11168. Variable acyl linkages are indicated in red (X), representing either oxygen (O) or nitrogen (NH), depending on whether GlcpN or GlcN3N is present. Variable phosphoethanolamine group(s) are shown in brackets. This figure was generated using ChemDraw Prime.

Variations in lipid A across bacterial species involve differences in the sugar backbone, phosphate modifications, and the number, type, and distribution of fatty acids [45]. These structural differences may occur between genera or even within species of the same genus. (**Table 1-1)** [45].

Table 1-1. Substitution patterns of the lipid A disaccharide backbone in various studied bacteria [45].

Bacteria	Glc*p*N[a] II or (GlcN3N[b] II)			Glc*p*N[a] I or (GlcN3N[b] I)		
	O-4'	**O-3'**	**N-2'**	**O-3**	**N-2**	**O-1**
Acinetobacter radioresistens[c] **[95]**	P[e]	C12:0 [3-O (C12:0)]	C12:0 [3-O (C12:0)]	C12:0 (3-OH)	C12:0/C14 :0 [3-O (C12:0)]	P[e]
Acinetobacter baumannii[c] **[96]**	P[e]	C12:0 [3-O(C12:0)]	C14:0 [3-O (C12:0(2-OH)]	C12:0 (3-OH)	C14:0 [3-O (C12:0)]	P[e]
Aeromonas salmonicida[c] ***[97]***	P[e]	C14:0 [3-O (C16:1)]	C14:0 [3-O (C12:0)]	C14:0 (3-OH)	C14:0 (3-OH)	–
Agrobacterium tumefaciens[c] **[98]**	P[e]	C14:0 (3-OH)	C16:0 [3-O (28:0(27-O (C4:0 (3-OH)]	C14:0 (3-OH)	C16:0 (3-OH)	P[e]
Alteromonas macleodii[c] ***[99]***	P[e]	C12:0 (3-OH)	C12:0 [3-O (12:0)]	C12:0 (3-OH)	C12:0 (3-OH)	P[e]
A. pyrophilus[d] **[86]**	GalA[f]	C14:0 [3-O (C18:0)]	C16:0 (3-OH)	C14:0 (3-OH)	C14:0 (3-OH)	GalA[f]
A. lipoferrum[c] **[100]**	–	C14:0 (3-OH)	C16:0 [3-O (C18:1/C18: 0)]	C14:0 (3-OH)	C16:0 (3-OH)	GalA[f]
B. stolpii[c] **[88]**	EtNPP[g]	C14:0 [3-O (iso-C13:0)]	C14:0 [3-O (iso-C13:0)]	C14:0/iso-C15:0 (3-OH)	C14:0/iso-C15:0 (3-OH)	P[e]
Bartonella henselae[d] **[92]**	P[e]	C12:0 (3-OH)	C16:0 (3-O (C28:0(27-OH)	C12:0 (3-OH)	C16:0 (3-OH)	P[e]
Bordetella parapertussis[c] **[101]**	P[e]	C10:0 (3-OH)	C14:0 [3-O (C14:0)]	C16:0	C14:0 (3-O H)	P[e]
B. pertussis[c] ***[101]***	GalN-P	C14:0 (3-OH]	C14:0 [3-O (C14:0)]	C10:0 (3-OH)	C14:0 (3-OH)	P-GalN[h]
B. cepacia complex[c] ***[102]***	Ara4N-P	C14:0 [3-O (14:0)]	C16:0 [3-O (C14:0)]	C14:0 (3-OH)	C16:0 (3-OH)	P-Ara4N[i]
B. abortus[d] **[87]**	P[e]	C16:0 [3-O (C28:0 (27-OH)]	C14:0 (3-OH)	C14:0 (3-O (C18:0)]	C12:0 (3-OH)	P[e]
Chlamydia trachomatis[c] **[103]**	P[e]	C14:0/C 16:0	C20:0 [3-O (18:0-21:0)]	C14:0/C15:0	C20:0 (3-OH)	P[e]

Coxiella burnetii [c] ***[104]***	P[e]	C16:0/C 15:0	C16:0 (3-OH)	C16:0	C16:0 (3-OH)	P[e]
Francisella victoria [c] **[105]**	Man[j]-P	–	C18:0 (3-O (C16:0))	C18:0 (3-OH)	C18:0 (3-OH)	P-GalN
Fusobacterium nucleatum [c] **[106]**	P[e]	C14:0/C 16:0 [3-O (C14:0)]	C16:0 (3-O (C14:0))	C14:0 (3-OH)	C14:0/C16 :0 (3-OH)	P[e]
H. alvei [c] **[107]**	P[e]	C14:0 [3-O(C14:0)]	C12:0 [3-O (C12:0)]	C14:0 (3-OH)	C14:0 [3-O(C16:0)]	P[e]
H. magadiensis [c] **[108]**	P[e]	C12:0 [3-O (C18:1/C 16:0)]	C12:0 [3-O (C14:0)]	C12:0 (3-OH)	C12:0 [3-O (C10:0)]	P[e]
L. interrogans [d] **[109]**	–	C12:0 [3-O (C12:1/C 14:1)]	C16:0 [3-O (C12:1/C14: 1)]	C12:0 (3-OH)	C16:0 (3-OH)	P-Me[k]
M. vaga [c] ***[110]***	–	–	C12:0 [3-O (C12:0(3-OH)]	C12:0 (3-OH)	C12:0 [3-O (C10:0/C1 2:0)]	P[e]
Porphyromonas gingivalis [c] ***[111]***	P[e]	iso-C15:0 [3- OH)]	iso-C17:0 [3-O (C16:0)]	16:0 (3-OH)	iso -17:0 (3-OH)	P/PEtN[l]
Pseudolateromonas nigrificans [c] ***[112]***	P[e]	C10:0 (3-O H)	C12:0 (3-OH)	C10:0 (3-OH)	C12:0 [3-O (12:0)]	P[e]
Rhodospirillum fulvu [c] **[113]**	Heptose	C14:0 [3-O (C12:0)]	C14:0 [3-O (C16:0)]	C14:0 (3-OH]	C14:0 (3-OH)	GalA[f]
Shewanella pacific [c] **[114]**	P[e]	C13:0 [3-O (C13:0)]	C12:0 [3-O (13:0)]	C13:0 (3-OH)	C13:0 (3-OH)	P[e]
Xanthomonas campestris[c] **[67]**	EtNPP[g]	C10:0/13 :0 [3-O (C10:0/C 11:0)]	C12:0 (3-OH)	C10-13:0 [3-O (10:0/11:0)]	C12:0 [3-OH)	PPEtN[g]

[a] 2-amino-2-deoxy-D-glucopyranose (Gl*cp*N)
[b] 3-amino-3-deoxy-D-glucosamine (GlcN3N)
[c] Lipid A that has a di-Gl*cp*N backbone.
[d] Lipid A that has a di-GlcN3N backbone.
[e] Phosphate (p)
[f] Galacturonic Acid (GalA)
[g] Ethanolamine di-phosphate (EtNPP)
[h] 2-amino-2-deoxy-D-galactose (GalN)
[i] 4-Amino-4-deoxy-L-arabinose phosphate (Ara4N-p)
[j] Mannose (Man)
[k] Methyl group (Me)
[l] Phospho-ethanolamine (PEtN).

The phosphate groups on the glucosamine backbone can be substituted by polar groups, such as ethanolamine (EtN), phospho-ethanolamine (PEtN), and 4-amino-4-deoxy-L-arabinose (Ara4N), which are often present in non-stoichiometric quantities. Other charged and non-charged substituents are listed in **Table 1-1** [45]**.** It can also be replaced with another acid, or one of the phosphate groups may be absent. Kdo I residues of the inner core are typically linked at the 6' position of GlcpN II [45].

Lipid A structures in some bacteria, such as *Bordetella* and *Mesorhizobium huakuii*, include differences in acyl chain lengths and types. For example, *Bordetella* has the same amide-linked, two (C14:0(3-OH)) fatty acids, while the ester-linked C10:0 (3-OH) and C14:0(3-OH) fatty acids differ (**Figure 1-7 A**) [101]. *M. huakuii* contains a mixture of shorter and longer chains, including iso-C12:0(3-OH), C14:0(3-OH), and C20:0(3-OH) (**Figure 1-7 B**) [90].

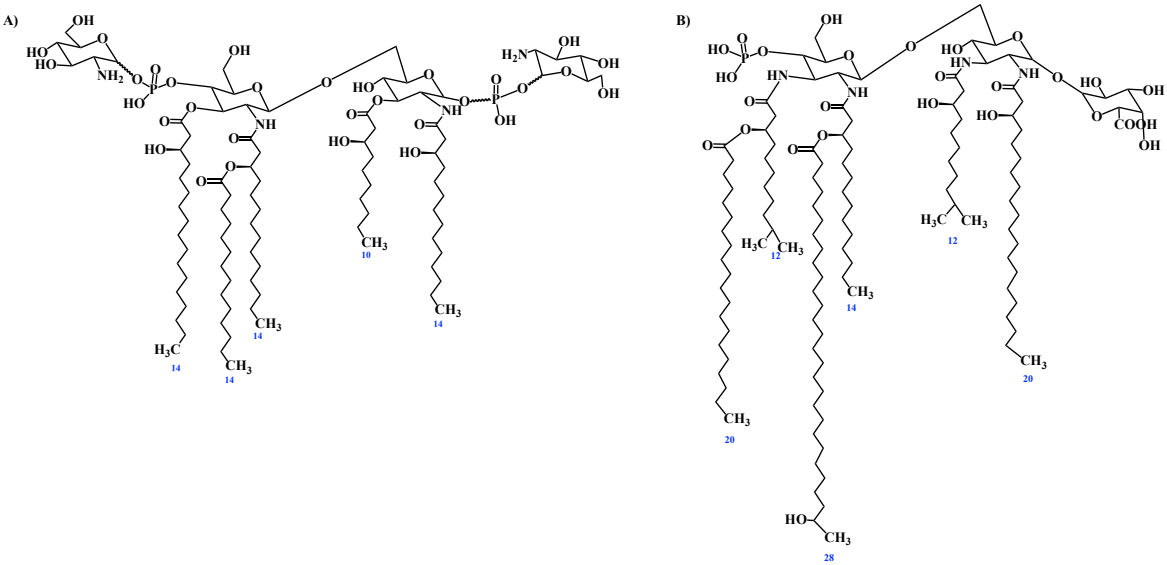

Figure 1-7. Structures of lipid A of (A) *Bordetella bronchiseptica* 4650 and (B) *M. huakuii IF*O 15243. This figure was generated using ChemDraw Prime.

In some cases, lipid A is chemically modified, as seen in *Rhizobiaceae* (**Figure 1-8 A and A'**) and *Agrobacterium elkanii* (**Figure 1-8 B**), where the secondary C28:0 (27-OH) fatty acid is partially O-acylated with 3-hydroxy-butanoic acid [90, 91, 98, 115, 116].

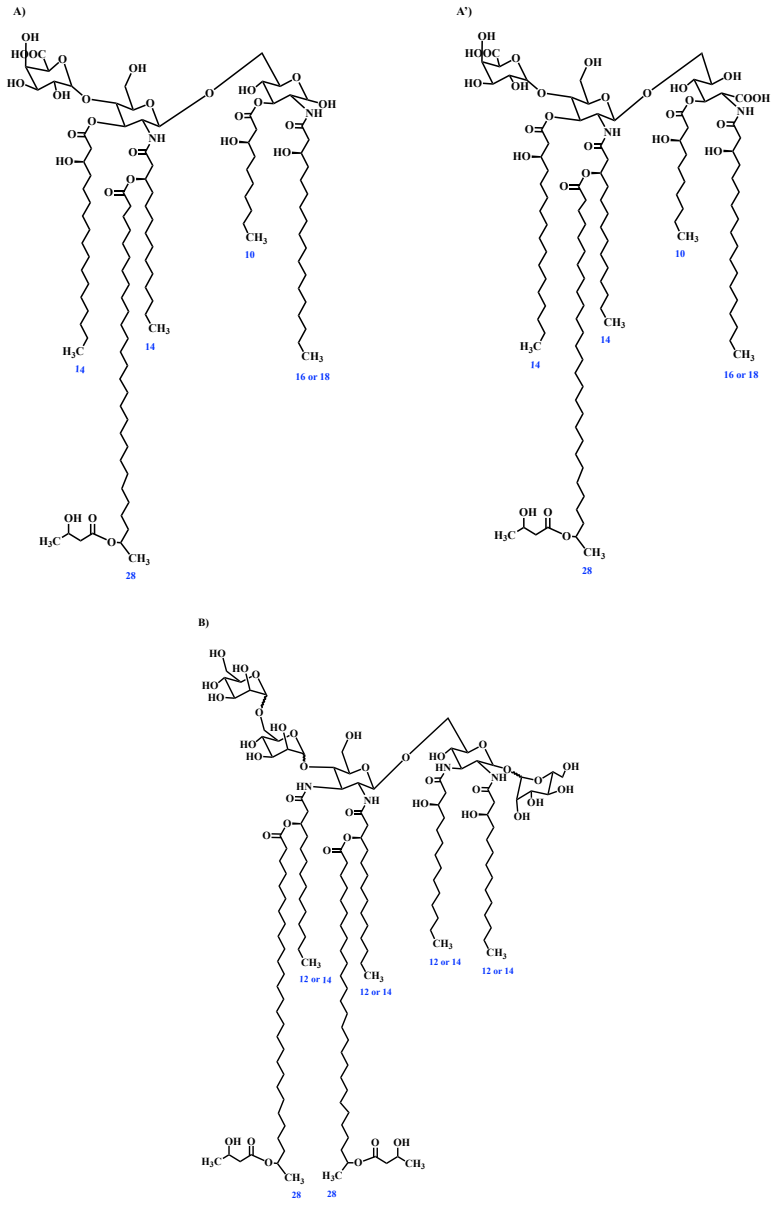

Figure 1-8. Structures of lipid A of (A, A') *Rhizobium etli* CE3 and (B) *B. elkanii*. This figure was generated using ChemDraw Prime.

Regarding biological activity, bis-phosphorylated, hexa-acylated lipid A with an asymmetric acyl group distribution (4 + 2) is the most potent activator for LPS-responsive human cells [45, 50, 51, 117]. Hexa-acylated, mono-phosphorylated lipid A from *Salmonella* shows moderate activity and acts as an adjuvant [118-120]. In contrast, the tetra-acyl precursor lipid IVA from *E. coli* is a classical antagonist of the human immune system [45]. The presence of Ara4N shields the negative charges of lipid A, providing resistance to antimicrobial peptides [45, 121]. Additionally, the length of the fatty acid chains influences lipid A's biological activity, with extended chain lengths being associated with lower endotoxic activity [45, 93].

1.2.1.1.3.1. Biosynthesis of Lipid A

The biosynthesis of lipid A has been extensively studied using *Escherichia coli* and *Salmonella typhimurium* as model organisms [45, 122]. As defined by Raetz and Whitfield [50], this pathway consists of nine constitutive enzymatic steps that occur in multiple cellular regions (**Figure 1-9**) [123-125].

The initial stages of lipid A biosynthesis take place in the cytoplasm. The first enzyme in this pathway is LpxA, a cytoplasmic acyltransferase that selectively transfers β-(C14:0(3-OH)) from acyl carrier protein (ACP) to the 3-OH position of the precursor molecule uridine di-phosphate-N-acetyl-glucosamine (UDP-GlcNAc), forming an ester linkage. LpxA is described as having a "hydrocarbon ruler," enabling the selection of long or short β-hydroxy-acyl chains across various bacterial species [45, 50, 84, 122, 124-127]. This selective mechanism is essential for maintaining the proper structure and function of

lipid A, and it explains variations in lipid A acylation observed across different organisms [45, 124, 126]. For example, the active site of *E. coli* LpxA shows a preference for β-(C14:0(3-OH))-ACP, while the *Pseudomonas aeruginosa* LpxA prefers β-(C10:0(3-OH))-ACP [45, 124, 126, 128].

Following LpxA-mediated acylation, the Zn^{2+}-dependent deacetylase LpxC produces UDP-3-acyl-glucosamine (UDP-3-O-acyl-GlcN) by deacetylating UDP-3-O-acyl-GlcNAc at the N-2 position. Then, the acyltransferase LpxD transfers a second acyl chain to form UDP-2,3-di-acylglucosamine (UDP-2,3-di-acyl-GlcN) [45, 126, 128, 129].

The subsequent steps in lipid A synthesis take place on the cytoplasmic face of the IM, where the lipid A backbone is assembled and modified. The pyrophosphate hydrolase LpxH cleaves UDP-2,3-di-acyl-GlcN to form uridine monophosphate (UMP), and a key intermediate, 2,3-di-acyl-GlcN-1-phosphate, which is known as lipid X. Then, LpxB condenses lipid X with another molecule of UDP-2,3-di-acyl-GlcN, forming the β-1,6 linkage characteristic of lipid A. The membrane-bound 4' kinase LpxK then phosphorylates the disaccharide 1-phosphate, producing lipid IV_A, which also functions as pharmacological endotoxin antagonists in human cells [45, 126, 129].

Next, two Kdo sugars are incorporated at the O-6 position of the lipid IV_A by a Kdo transferase kdtA to produce Kdo_2-lipid IV_A [130, 131]. The final hexa-acylated lipid A species is produced by the sequential of two acyltransferases, LpxL and LpxM, which catalyze the addition of secondary acyl chains to the distal GlcN in a specific order due to strict substrate preference [45, 132, 133]. LpxL first transfers a (C12:0) group to the 2'-

position of Kdo_2-lipid IV_A, followed by the addition of a (C14:0) group by LpxM at the 3'-position, forming Kdo_2-lipid A [45, 132, 133].

After synthesis, Kdo_2-lipid A is conjugated to the core OS. Subsequently, MsbA, an ATP-binding cassette transporter, flips Kdo_2-lipid A from the cytoplasmic leaflet to the periplasmic (outer) leaflet of the IM, where the *O*-antigen is attached to the core OS linked to lipid A [45, 65, 125, 134]. Finally, The LPS transport system transfers LPS from the IM to the OM in Gram-negative bacteria [45, 123].

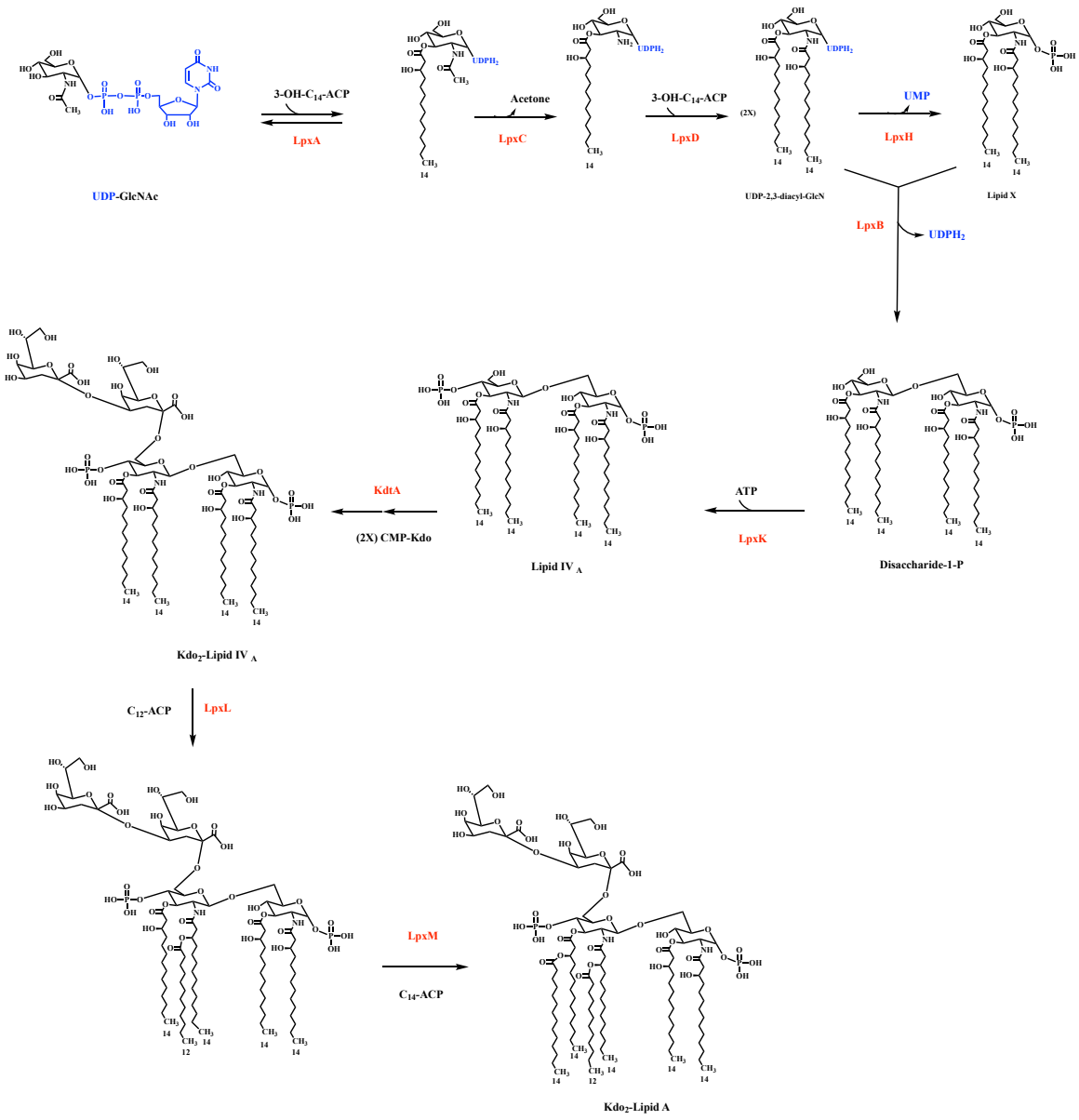

Figure 1-9. The Raetz Pathway for Kdo2-Lipid Biosynthesis in *E. coli* and *Salmonella typhimurium*, Highlighting Enzymes in red and Reactions Involved. UDP (shown in blue) is a key component in lipid A biosynthesis. This figure was generated using ChemDraw Prime.

Diverse modifications of the lipid A moiety may occur during its synthesis or transit from the IM to the OM. These modifications may be regulated by environmental factors such as temperature, enzyme activity, genetic regulation, mutations in the synthetic

enzymes, and bacterial stress responses, which significantly impact bacterial virulence [45, 123, 128, 135, 136]. The diversity of lipid A structures in Gram-negative bacteria is vast, with modifications and variations continuing to be discovered [137]. These modifications are not only crucial for bacterial survival and virulence but also offer new avenues for therapeutic applications, particularly in vaccine development as vaccine adjuvants [137]. Novel lipid A structures will undoubtedly be identified and reported in the future, offering valuable models for structural variation and modification [137].

1.2.1.1.3.2. The Vital Role of LPS and Lipid A in Bacterial Research

The study of LPS, particularly their lipid A component, is vital because it is essential due to their roles in bacterial pathogenicity and immune system interaction, which have significant implications for vaccine development and therapeutic strategies [120, 137, 138]. Lipid A is essential for bacterial viability and is responsible for the endotoxic properties of the LPS [45, 50, 117, 139, 140]. It is the primary agent responsible for the toxic effects observed in conditions like Toxic Shock Syndrome and sepsis [45, 85, 119].

Lipid A also acts as a potent stimulator of the innate immune system via recognition by the toll-like receptor TLR4 [45, 85, 119]. Some studies focused on modifying the structure of lipid A in various Gram-negative bacteria species, such as *E. coli* and *Salmonella*, to reduce its toxicity while maintaining its immunostimulatory properties by altering acylation patterns and creating synthetic analogs [141, 142]. As a result, lipid A has become a key target for developing synthetic analogs such as mono-

phosphoryl lipid A (MPLA), which retains immune-stimulating properties with reduced toxicity and are widely used as adjuvants in vaccines [142].

By understanding the structural diversity of lipid A across different bacterial species, researchers can better counteract bacterial immune evasion and develop tailored vaccines and therapies that enhance immune recognition without triggering harmful inflammation [143, 144].

The development of vaccines faces significant challenges due to various factors, such as strain variability within species, which complicates the targeting of specific bacterial strains. This is further complicated by structural variability within lipid A, as these molecules differ significantly across bacterial species and even within strains [58, 145, 146]. Therefore, discovering new lipid A structures is critical for advancing strategies to combat bacterial infections, particularly those caused by Gram-negative pathogens. Understanding these variations will help design more effective vaccines targeting a broader range of bacterial strains while overcoming immune evasion mechanisms [58, 145, 146].

1.2.2. Gram-Negative Bacteria: *Aeromonadaceae* and *Vibrionaceae* Family

The *Aeromonadaceae* family comprises Gram-negative bacteria predominantly found in aquatic environments, including freshwater and marine ecosystems, as well as soil. The genus *Aeromonas* within this family is significant due to its pathogenic species that affect both humans and animals [147-150]. These bacteria exhibit remarkable versatility, thriving under various conditions, including extreme salinity, low temperatures, and even the presence of disinfectants. As facultative anaerobes, they can survive in both

oxygen-rich and oxygen-poor environments, contributing to their broad distribution [151, 152]. Pathogenic *Aeromonas* species are linked to diseases in fish, amphibians, reptiles, and humans, utilizing toxins, hemolysins, and enzymes to invade host tissues [149].

One notable species, *Aeromonas hydrophila*, is a pathogen recognized for causing hemorrhagic septicemia in fish, which results in high mortality rates and significant economic losses in aquaculture [153-155]. Its virulence stems from various factors, including enterotoxins, cytotoxins, and tissue-invasive enzymes such as proteases and lipases. *A. hydrophila* is adept at forming biofilms and protective layers, enhancing its resistance to environmental stressors, including disinfectants, making it a persistent threat in aquatic environments [156, 157]. However, the lipid A structure of *Aeromonas hydrophila* has not been extensively studied, leaving gaps in understanding its specific role in virulence and immune evasion.

Similarly, the *Vibrionaceae* family encompasses Gram-negative bacteria that thrive in diverse marine habitats, ranging from coastal to deep-sea environments [158].

Members of this family play essential roles in nutrient cycling by contributing to the decomposition of organic matter and nutrient recycling within marine ecosystems [158-160]. These bacteria can exist as free-swimming plankton or form symbiotic or pathogenic relationships with marine organisms [160]. One key pathogen from this family is *Vibrio anguillarum,* known for causing vibriosis in fish, which has severe economic impacts on aquaculture [161, 162]. Despite its clinical importance, the lipid A structure of *Vibrio anguillarum* has not been fully explored, presenting an opportunity for future research to elucidate its role in pathogenesis and immune interactions.

Then, I will describe the background and advantages of the tandem mass spectrometry used in this work.

1.3. Mass spectrometry

Mass spectrometry (MS) is a powerful analytical technique used to identify and quantify molecules based on their mass-to-charge ratio (*m/z)*. It plays a crucial role in structural and biochemical research, providing detailed insights into the composition and function of biological molecules [163]. It plays an essential role in analytical chemistry due to its sensitivity, selectivity, structural information, low sample consumption, and relatively fast analysis [164-168].

The technique determines the masses of molecules by placing an electrical charge on the molecule, resulting in separated ions based on their *m/z.* This technique can be used for the qualitative structural determination of analytes and their quantitation [169]. There are numerous types of MSs, varying by the types of ionization source and the mass analyzer configuration [170-173]. The MS is typically composed of three main components: an ionization source, a mass analyzer, and a detector (**Figure 1-10**).

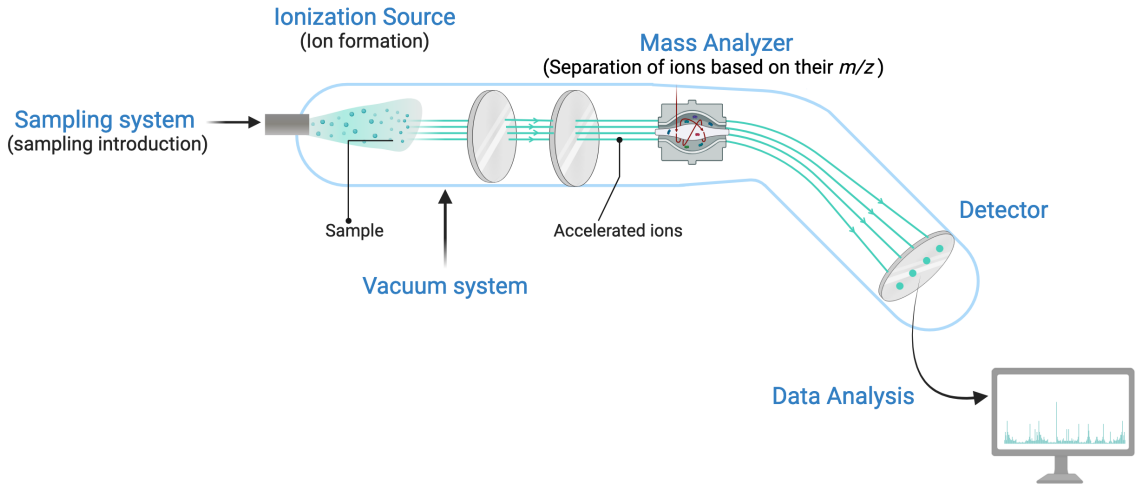

Figure 1-10. Diagrammatic overview of a mass spectrometer. The MS typically consists of an ionization source, an analyzer such as an Orbitrap, and a detector. This figure was created by BioRender.

Liquid chromatography (LC), gas chromatography (GC), and high-performance liquid chromatography (HPLC) are essential techniques in analytical chemistry, often coupled with MS for the detailed analysis of complex mixtures [174]. These techniques allow for the separation of complex mixtures into their individual components, enabling the identification and quantification of each component in a single analytical run [174]. Field asymmetric ion mobility spectrometry (FAIMS), another valuable technique, separates gas-phase ions based on their mobility in alternating strong and weak electric fields. FAIMS is especially useful in MS for the analysis of complex samples, such as lipopolysaccharides (LPS) [175].

1.3.1. Ionization sources

Ionization sources in mass spectrometry are crucial for generating charged particles from analytes, enabling their detection and analysis [176-178]. Ionization sources are classified as hard and soft ionization sources based on the quantity of internal energy transferred to the molecule during the ionization process [179]. Hard ionization methods typically impart high energy, leading to extensive fragmentation, while soft ionization methods transfer less energy, preserving the molecular structure and resulting in minimal fragmentation [179].

Soft ionization methods are the most widely used, especially for the analysis of biomolecules, as they allow for the analysis of a wide range of molecules, from small metabolites to large biomolecules like proteins and nucleic acids [180-183].

The following sections provide an overview of the distinctive features of two common soft ionization sources: Electrospray Ionization (ESI) and Matrix-Assisted Laser Desorption Ionization (MALDI).

1.3.1.1. Electrospray Ionization (ESI)

ESI is widely used for its ability to ionize large biomolecules, making it ideal for proteomics and other biological studies [184]. ESI operates by introducing a dilute solution containing the analyte of interest, dissolved in a suitable polar solvent, through a capillary tube at a slow flow rate (0.1-10 μL/min) [180]. A high voltage (2–5 kV) is applied to the capillary, with the polarity (positive or negative) based on the type of analyte, which in turn controls whether cations or anions accumulate at the emitter tip, thus producing

protonated ($[M + H]^+$) or deprotonated ($[M - H]^-$) ions, depending on the analyte's structure [185, 186].

This applied voltage creates a strong electric field gradient, causing charge separation at the surface of the liquid [180, 187]. Consequently, the liquid extends outward from the capillary tip, forming a cone shape known as the Taylor cone. This cone results from the balance between Coulombic repulsion forces among the surface charges and the surface tension of the liquid **(Figure 1-11)** [180, 187].

The resulting droplets undergo rapid solvent evaporation, shrinking in size and increasing charge density [186]. When these charged droplets reach the Rayleigh limit, Coulombic repulsion forces exceed surface tension. A Coulomb explosion then breaks each droplet into multiple smaller, highly charged droplets. This process continues, producing tiny droplets with high charge density [185, 188, 189]. A stream of hot nitrogen gas aids in evaporating the solvent and accelerates droplet drying and desolvation. This process leaves behind dry, charged ions, which are directed into the mass analyzer for detection [163]. The key advantage of ESI is its compatibility with HPLC and other LC systems, enhancing its application for complex sample analysis [190-192].

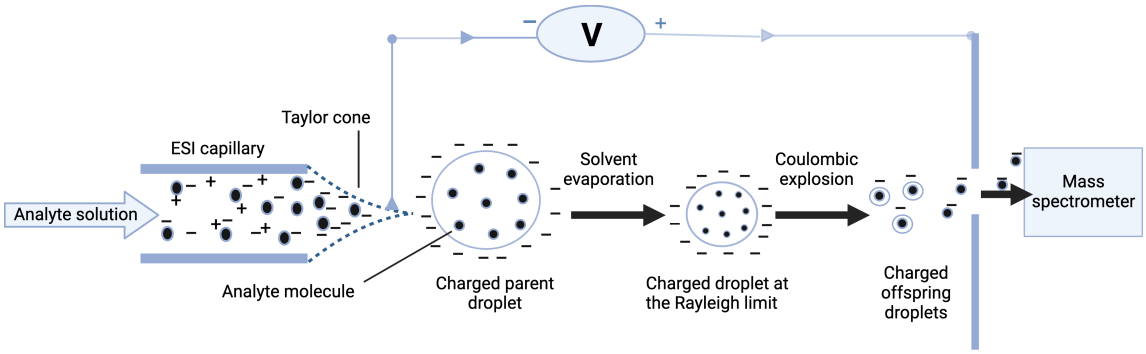

Figure 1-11. Schematic representation of charged droplet production during the ES (Negative ion mode) ionization. This figure was created by BioRender.

1.3.1.2. Matrix-Assisted Laser Desorption Ionization (MALDI)

MALDI is a soft ionization technique widely used in mass spectrometry to analyze large biomolecules like proteins, peptides, and polymers, which are otherwise difficult to ionize [174].

In MALDI, the sample is mixed with a matrix, a small organic molecule that absorbs laser light. Various types of matrices are used depending on the specific class of biomolecules being analyzed, ensuring optimal ionization efficiency [193-196]. The process begins by mixing the matrix solution with the analyte and then spotting this mixture onto a MALDI plate. The dried droplet method is the most common technique, leaving the mixture spot in the room, which evaporates the solvent and enables the analyte to co-crystallize with the matrix [193].

When a laser pulse strikes the dried spot on the MALDI plate, the matrix absorbs the laser energy (hv), causing its molecules to enter an excited state. These excited matrix molecules then transfer part of their energy to the analyte [188]. This interaction leads to the desorption and ionization of both matrix and analyte. The ionization of analytes occurs

through a proton transfer reaction triggered by the collision between matrix and analyte molecules in gas-phase clusters. This method generates intact, gas-phase ions of large, non-volatile, and thermally sensitive compounds, making MALDI essential in fields like proteomics, genomics, and polymer science **(Figure 1-12)** [123, 174, 188].

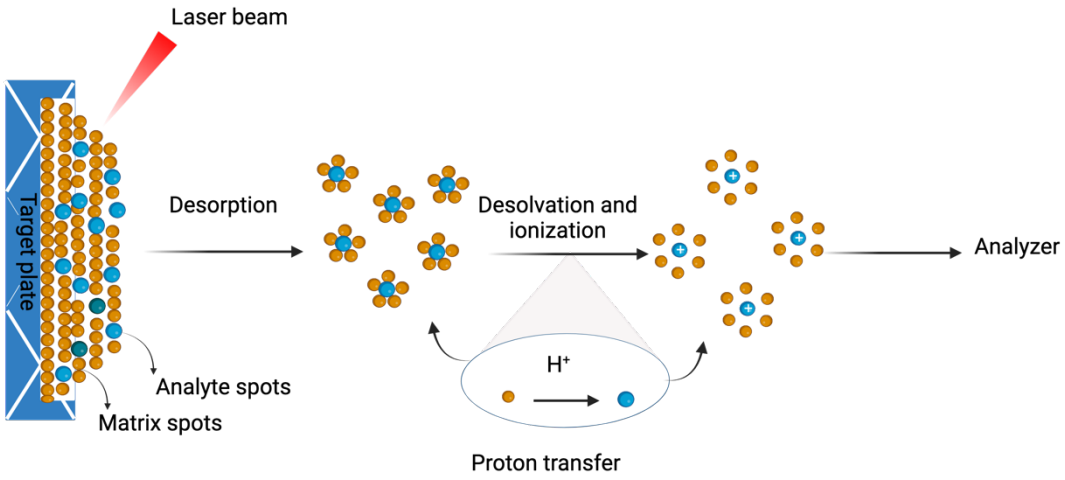

Figure 1-12. Schematic representation of the principle of MALDI. This figure was created by BioRender.

1.3.2. Mass Analyzers

Once gas-phase ions are produced, they must be separated according to their *m/z* to determine their masses accurately. Unlike measuring mass alone, the mass analyzer measures the *m/z* ratio, which is particularly important for multiplying charged ions, as their apparent *m/z* values are fractional parts of their actual masses [174].

Several types of mass analyzers have been developed to separate ions based on their *m/z* ratio through various methods [174]. The upcoming section covers the common types of mass analyzers specifically used for biomolecule analysis presented in this PhD thesis research work [174].

1.3.2.1. Time-of-Flight (TOF)

The TOF mass analyzer is a high-speed, versatile tool applied across various scientific disciplines, including proteomics, genomics, and materials science, due to its capability to analyze a broad range of ion masses without relying on magnetic fields [197-199].

In the TOF analyzer, ions are generated from an ion source and introduced into the TOF analyzer as short packets. These ions are then accelerated in an acceleration region by an electric field, imparting them with uniform kinetic energy, which is crucial for accurate time-of-flight measurements [186]. After acceleration, the ions enter a field-free drift space where they can travel unimpeded. In this region, ions begin to separate based on their *m/z* ratios. The lighter ions travel faster and reach the detector sooner, while the heavier ions take longer ((**Figure 1-13**) [186].

Another advanced configuration of the TOF analyzer contains a reflectron-TOF addition. This includes a reflection, which is a series of electrodes that creates a retarding electric field, reversing the direction of ions toward the detector [197]. This adjustment extends the ions' flight path and corrects for slight kinetic energy differences among ions of the same *m/z* ratio, resulting in significantly improved resolution without requiring a larger instrument. This feature makes reflectron-TOF particularly valuable for high-precision applications, enhancing the mass accuracy and resolution of the data collected. Once the ions reach the detector, their arrival times are recorded and processed into a detailed mass spectrum, providing insightful details into the sample's composition.

However, TOF analyzers can encounter limitations in the ultra-high mass range, where resolution and mass accuracy may decrease [200, 201].

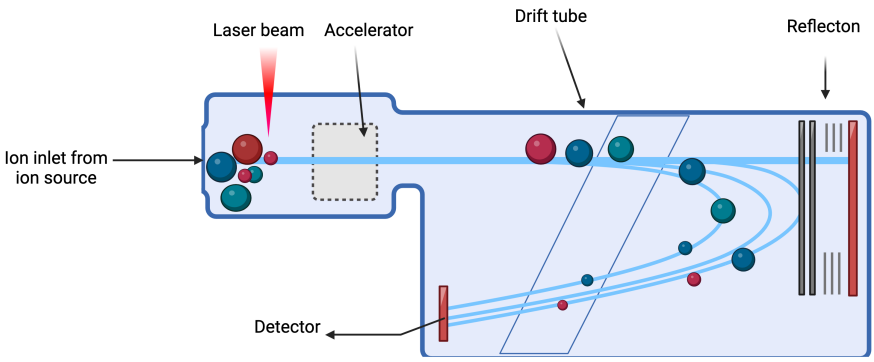

Figure 1-13. Schematic representation of the reflectron-TOF showing the fight of ions to reach the detector. This figure was created by BioRender.

1.3.2.2. Orbitrap Mass Analyzer

The Orbitrap is a highly advanced instrument developed to meet the demands of analyzing complex mixtures in mass spectrometry, offering high resolving power and mass accuracy capabilities [202, 203]. The Orbitrap consists of a spindle-like central electrode, and the outer electrode has the shape of cups facing each other with a hair-thin dielectric gap in between (**Figure 1-14**) [202]. When voltage is applied between the outer and central electrodes, the resulting electric field is strictly linear along the axis, enabling purely harmonic oscillations. Simultaneously, the radial electric field confines ions in stable, nearly circular trajectories around the central electrode by balancing their tangential velocity with an opposing centrifugal force [202]. The axial electric field, shaped by the conical geometry of the electrodes, pushes ions toward the widest part of the trap, initiating harmonic axial oscillations [202].

The outer electrodes have dual roles: they confine ions axially by creating a trapping field and serve as receiver plates for detecting the image current produced by oscillating ions. This image current is converted into a time-domain signal, which is then transformed into the frequency domain using the Fourier transform (FFT) equation and ultimately into a mass spectrum [202-205]. Ion frequencies are measured non-destructively by detecting time-domain image current transients. Each frequency corresponds to a specific *m/z* ratio, as the frequency of ion oscillation is inversely proportional to the square root of its *m/z* value [202, 204].

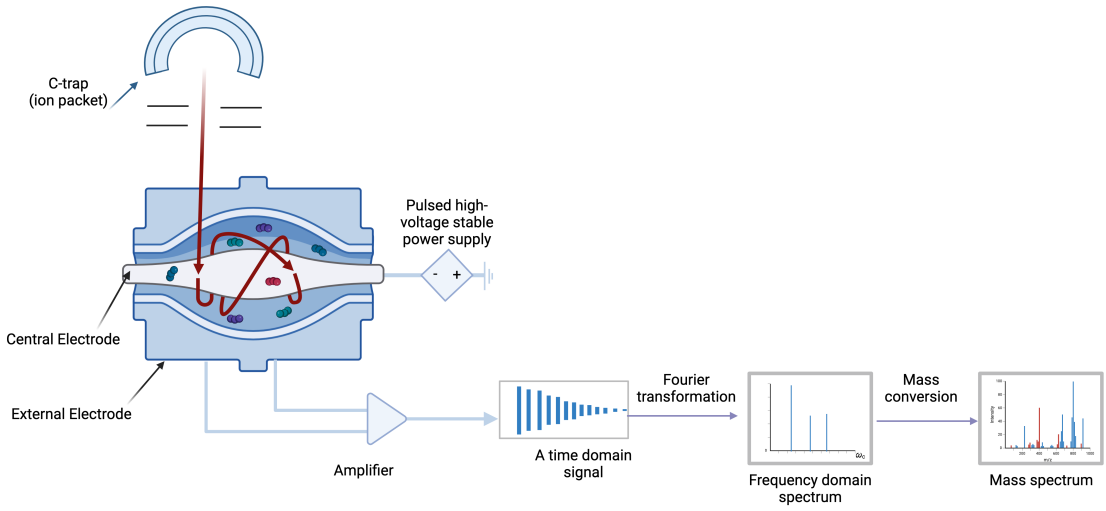

Figure 1-14. Schematic representation of an orbitrap mass analyzer. This figure was created by BioRender.

An additional C-trap is positioned before the Orbitrap to improve ions preparation for the analysis [173]. This trap stores and cools the ions before sending them to the Orbitrap. As a result, the practical *m/z* range of ions that can be injected simultaneously

into the Orbitrap is increased, enhancing performance, resolution, and sensitivity in the mass spectrometric analysis [173].

1.3.2.3. Quadrupole Mass Analyzer (QMA)

QMF has been one of the most commonly used mass analyzers over the past few decades [206, 207]. However, the QMF also has significant limitations that restrict its utility in more demanding analytical applications. Specifically, QMFs typically offer a low resolution, often below 3000 Da, which can hinder their ability to distinguish between closely related *m/z* ratios [208]. QMF is composed of four parallel metal rods **(Figure 1-15 A)**. DC and radiofrequency (RF) potentials are applied to the four rods to create two positively charged rods (on the x-direction) and two negatively charged rods (on the y-direction) **(Figure 1-15 B)** [209, 210].

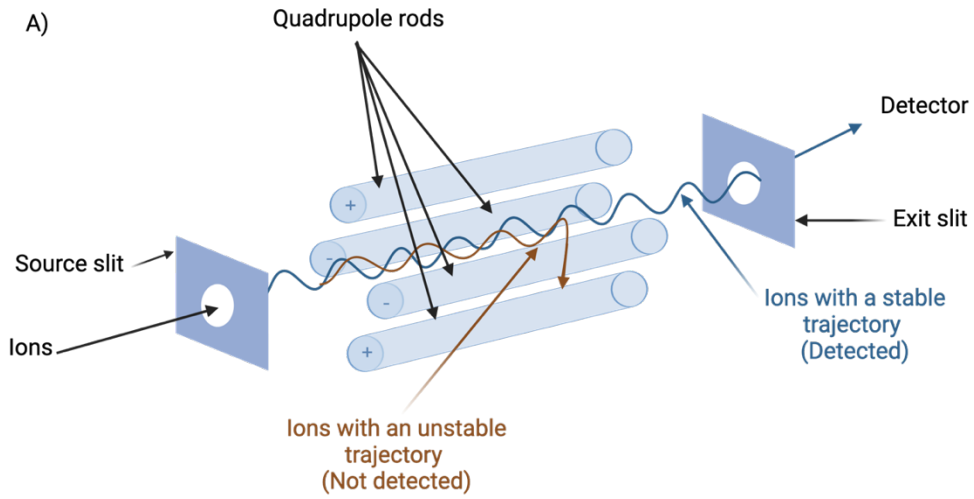

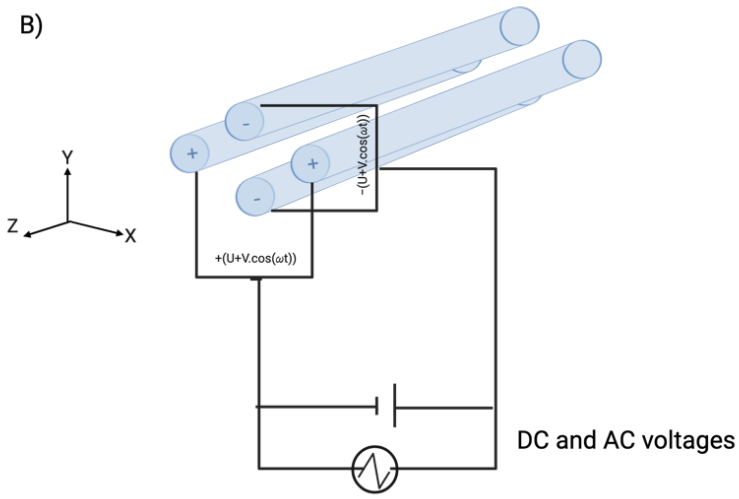

Figure 1-15. A) Schematic representation of a QMA showing the trajectory of ions to reach the detector. B) The x- and y-axes are indicated, with the z-axis being perpendicular to the plane of the paper. One pair of rods has a potential of + (U + Vcosωt) applied to it, and the other pair has – (U + V cos ωt) applied. U is a fixed potential, and Vcosωt represents a radio frequency (RF) field of amplitude (V) and frequency (ω). This figure was created by BioRender.

As an ion enters the quadrupole assembly along the z-axis, it experiences an attractive force from one of the rods, which has a charge opposite to that of the ion. If the voltage applied to the rods is periodic, the forces of attraction and repulsion will alternate in both the x- and y-directions over time since the electric force's polarity changes periodically. The applied voltage is a combination of a DC voltage (U) and an RF voltage (V) with a frequency (ω). The total potential applied to the rods, Φ_o, is expressed as $\Phi_o = \pm(U + V\cos \omega t)$, where Φo represents the voltage applied to the rods, U is the DC voltage, V is the RF voltage amplitude, and ω is the frequency [163].

Only ions with a stable trajectory, which are controlled by the specific combination of DC and RF potentials, will successfully traverse the quadrupole, while others will collide with the rods and be neutralized [210].

1.3.2.4. Linear ion trap (LIT)

A two-dimensional (2D) ion trap, commonly known as a LIT, is a mass analyzer that is increasingly being utilized in various areas of MS due to its superior performance characteristics [211, 212]. LIT is composed of two pairs of hyperbolic rods, each divided into three axial sections. The central section is approximately three times the length of the two end sections, and a small slit is cut along one of the rods in the central section to enable ion ejection for external detection (**Figure 1-16**) [188].

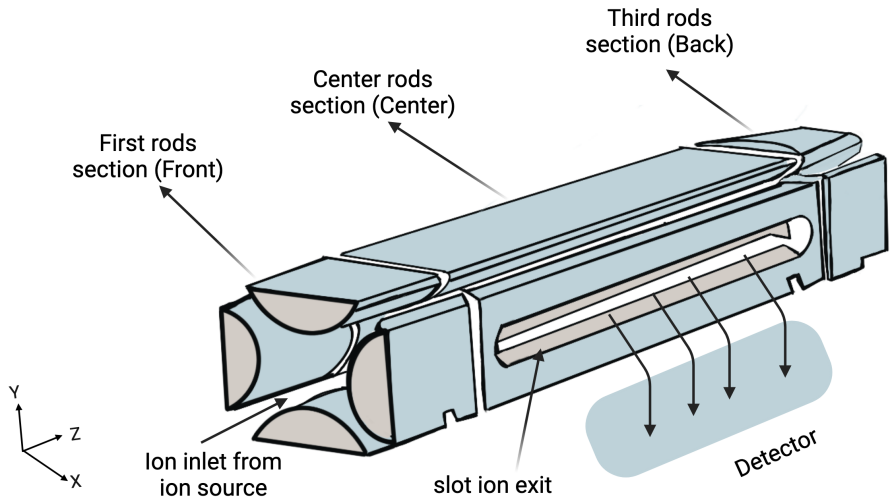

Figure 1-16. Schematic representation of a linear ion trap mass analyzer showing the trajectory of ions to reach the detector. This figure was created by Procreate and BioRender.

In each section, the opposite rods are connected electrically. In the axial direction (YZ-plane), ions are trapped by applying separate DC voltages to each of the three sections of the trap. For radial trapping (in the XY-plane, the main RF voltage is applied between the x- and y-electrode pairs. Additionally, a two-phase supplemental alternating current (AC) voltage is applied to the x-electrodes (exit rods) to facilitate ion activation, isolation,

and controlled ejection, enhancing the functionality and flexibility of the LIT for various mass spectrometry applications [188].

The LIT uses a mass-selective instability mode, where the RF voltage gradually increases. As the voltage rises, ions of specific *m/z* ratios become unstable and are ejected radially through exit slots. Additionally, a supplemental AC voltage can be applied to match the ions' natural oscillation frequency, enhancing their radial movement and enabling selective ejection [188]. One of the main advantages of a linear ion trap (LIT) is its flexibility in operation. The trapping function can be switched on and off, allowing the LIT to act either as a trap for qualitative studies, including MS^n (e.g., MS^3) experiments or as a transmission-only quadrupole. This dual functionality enables the instrument to perform as a QqQ (triple quadrupole) mass spectrometer when needed, thus enhancing both structural elucidation and quantitative performance within a single platform [213].

1.3.3. Tandem Mass Spectrometry

Tandem mass spectrometry (MS^2, or MS/MS) is a powerful technique for obtaining structural information about molecules by using at least two stages of mass analysis (n=2) [185, 214]. The core principle of MS/MS involves isolating a precursor ion in the first mass analyzer, followed by fragmentation through collision with an inert gas. A second mass analyzer then analyzes the resulting product ions (**Figure 1-17)** [185, 214]. Fragmentation may occur naturally or can be induced through activation techniques such as collision-induced dissociation (CID), where ions collide with neutral gas molecules to produce specific product ions and neutral fragments, which are subsequently analyzed [185, 214].

MS/MS can be conceived in two ways: tandem in space or tandem in time [174, 214] **(Figure 1-18)**.

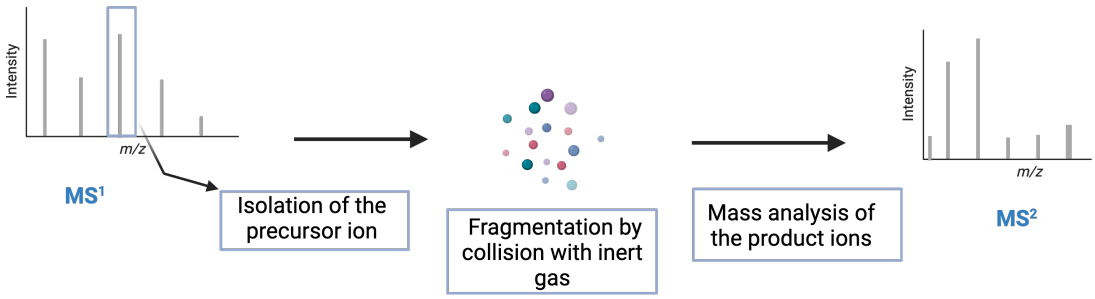

Figure 1-17. Schematic representation of the principle of MS^n. A precursor ion is isolated by the first mass analyzer, fragmented by collision with an inert gas, and the resulting product ions are analyzed by the second mass spectrometer. This figure was created by BioRender.

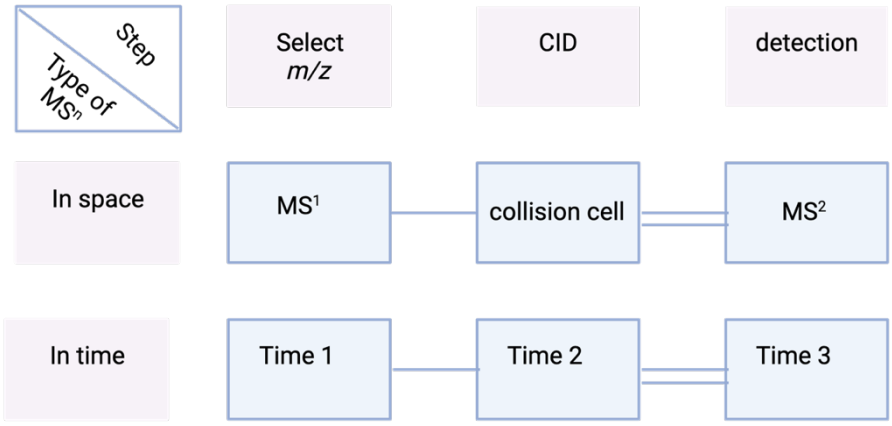

Figure 1-18. Schematic representation of comparing a simple MS^n product ion scan performed by either a space- or a time-based instrument. This figure was created by BioRender.

Common MS/MS in space configurations involves at least two mass analyzers and a collision cell where the selected precursor ion experiences CID, a collision with a neutral gas, which results in the fragmentation of the precursor ion to its characteristic product

ions, for example, combine a TOF with other types of analyzers like quadrupoles, TOF, orbitrap or linear ion traps [174, 215]. An instance of this approach is Orbitrap Fusion™ Lumos™ Tribrid™ Mass Spectrometer (Thermo Scientific, Waltham, MA, USA), which integrates a quadrupole mass filter, a linear ion trap, and an Orbitrap mass analyzer. This instrument was selected for use in our study due to its high sensitivity **(Figure 1-19)** [216].

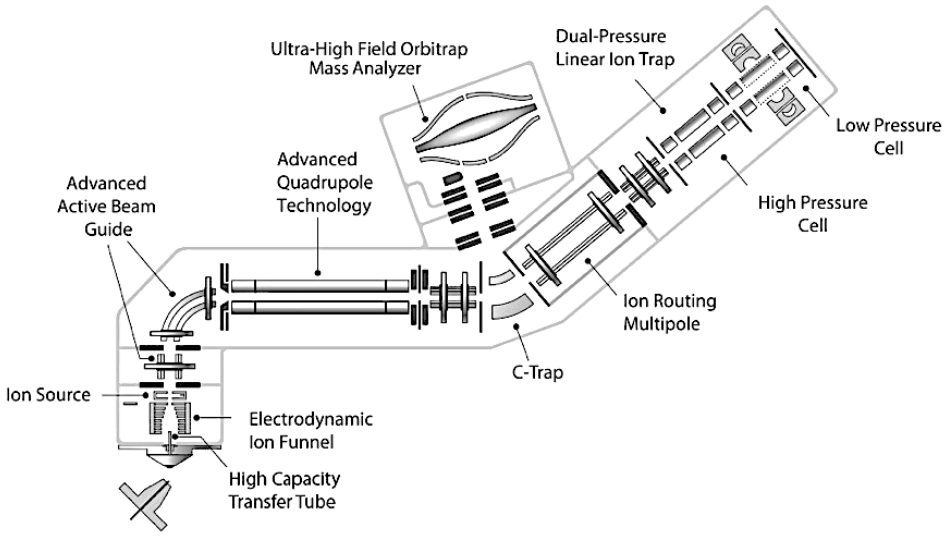

Figure 1-19. Orbitrap Fusion™ Lumos™ Tribrid™ Mass Spectrometer. The tribrid architecture includes a quadrupole mass filter, linear ion trap and an Orbitrap mass analyzer. This Figure was reproduced with permission from Thermo Fisher Scientific [216].

In the case of MS/MS in time, all events that occur in MS/MS in space, such as isolation, fragmentation, and detection, happen in the same place (mass analyzer) but sequentially in time, such as orbitrap [163, 174, 215] **(Figure 1-18)**. Hybrid mass spectrometers use different types of analyzers for the first and second stages of mass analysis in tandem mass spectrometry (MS/MS) experiments. These additional analyzers could consist of TOF, quadrupole, quadrupole ion trap, and linear ion trap [163, 174, 215].

1.3.4. Mass Spectrometry Analysis of Biomolecules

The determination of molecular weight has long been one of the primary measurements used to characterize biopolymers. Until the late 1970s, the only available techniques for obtaining this information were chromatographic or ultracentrifugation methods [174]. However, these methods often produced results with significant variability (10-100% relative error on average) as they were influenced by factors other than molecular weight, such as conformation and hydrophobicity. Consequently, the only reliable way to determine the exact molecular weight of a macromolecule was through calculation based on its chemical structure [174]. At the beginning of the 1990s, two new ionization methods, ESI and MALDI, coupled with TOF analyzers, were developed to avoid such limitations. These advancements catalyzed subsequent developments that have progressively expanded the capabilities and applications of MS in biological research to the present day [174].

Today, MS has become one of the most widely used analytical techniques in the life sciences. It is extensively applied in the analysis of various classes of biomolecules, such as peptides, proteins, nucleic acids, oligosaccharides, and lipids, contributing significantly to various *omics* fields, including proteomics, genomics, metabolomics, and lipidomics [174, 215, 217-220].

1.3.4.1. Mass Spectrometry Analysis of Proteins

1.3.4.1.1. Classical Approach in MS-Based Proteomics

The classical MS-proteomic has been used extensively in fisheries research over the last decades [221, 222]. This approach provides rapid, sensitive, and qualitative or quantitative protein characterization combined with separation techniques such as gel electrophoresis (DGE) and LC [223-225]. The process begins with protein extraction from specific fish tissues, followed by separation using one- or two-dimensional gel electrophoresis (1- or 2-DGE). Proteins of interest are then excised, digested by enzymes like trypsin, and analyzed by MS, creating a peptide mass fingerprint valuable for protein identification [226-228]. Additionally, peptides can undergo MS/MS for further identification and sequencing, enabling assumption-free peptide determination, with peak intensities reflecting relative abundance **(Figure 1-20)** [228, 229].

A widely used 1- or 2-DGE method is sodium dodecyl sulfate-polyacrylamide gel electrophoresis (SDS-PAGE) [223]. In 2-D-SDS-PAGE, proteins are separated horizontally by isoelectric point (pI) and vertically by molecular mass [223]. In contrast, 1-D-SDS-PAGE separates proteins solely by molecular weight [230]. Protein spots are visualized and analyzed using software such as Progenesis SameSpots or PDQuest, allowing for comparative analysis across samples to identify protein upregulation or downregulation [223]. However, this approach can be time-consuming and challenging, particularly for complex samples [231].

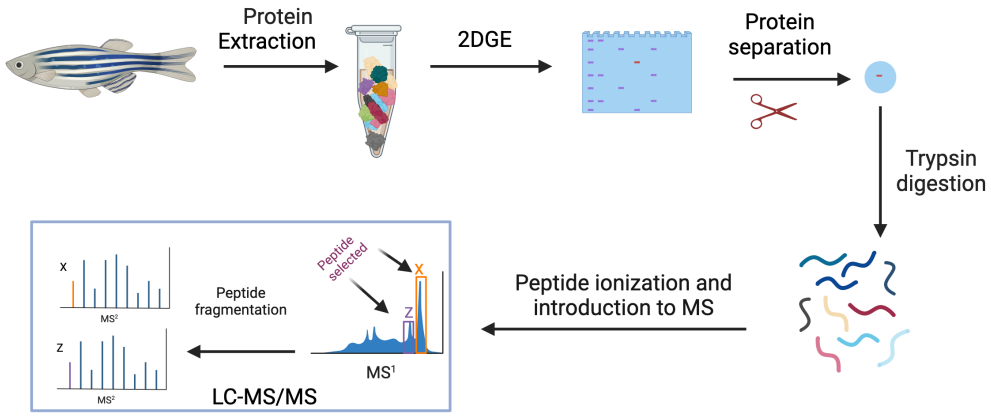

Figure 1-20. Schematic representation of the classical MS-proteomic approach. This figure was created by BioRender.

1.3.4.1.2. Recent Advances in MS-Based Proteomic Strategies

Various efficient and effective MS-based proteomics strategies have been developed to address biological and analytical challenges [223, 232-234]. Protein identification via MS is usually performed either through top-down proteomics or by bottom-up proteomics, as shown in **(Figure 1-21)** [223, 232-234].

In top-down proteomics, proteins are analyzed directly without enzymatic digestion. Proteins are typically separated by LC, followed by identification (amino acid sequencing) through fragmentation in an MS/MS experiment **(Figure 1-21)** [232, 235, 236].

Bottom-up proteomics employs either gel-based or gel-free strategies [237]. The gel-based approach is similar to the classical method [237]. This technique is particularly suitable for species with unknown protein sequences and is effective in identifying biological markers within proteomes [237, 238]. The resulting peptides can then be

identified using LC-MS/MS and MALDI-TOF-MS/MS techniques **(Figure 1-21)** [234-236].

Alternatively, the gel-free approach, known as shotgun proteomics or multi-dimensional protein identification, is a highly sensitive bottom-up method for analyzing complex protein mixtures [239]. In this approach, extracted proteins are digested directly without a separation step, and peptides are separated by LC-MS. Peptide mixtures are separated by charge via strong cation exchange chromatography (SCX) and/or by hydrophobicity via reverse-phase chromatography before MS analysis, followed by MS/MS for further identification [234, 235, 240-242].

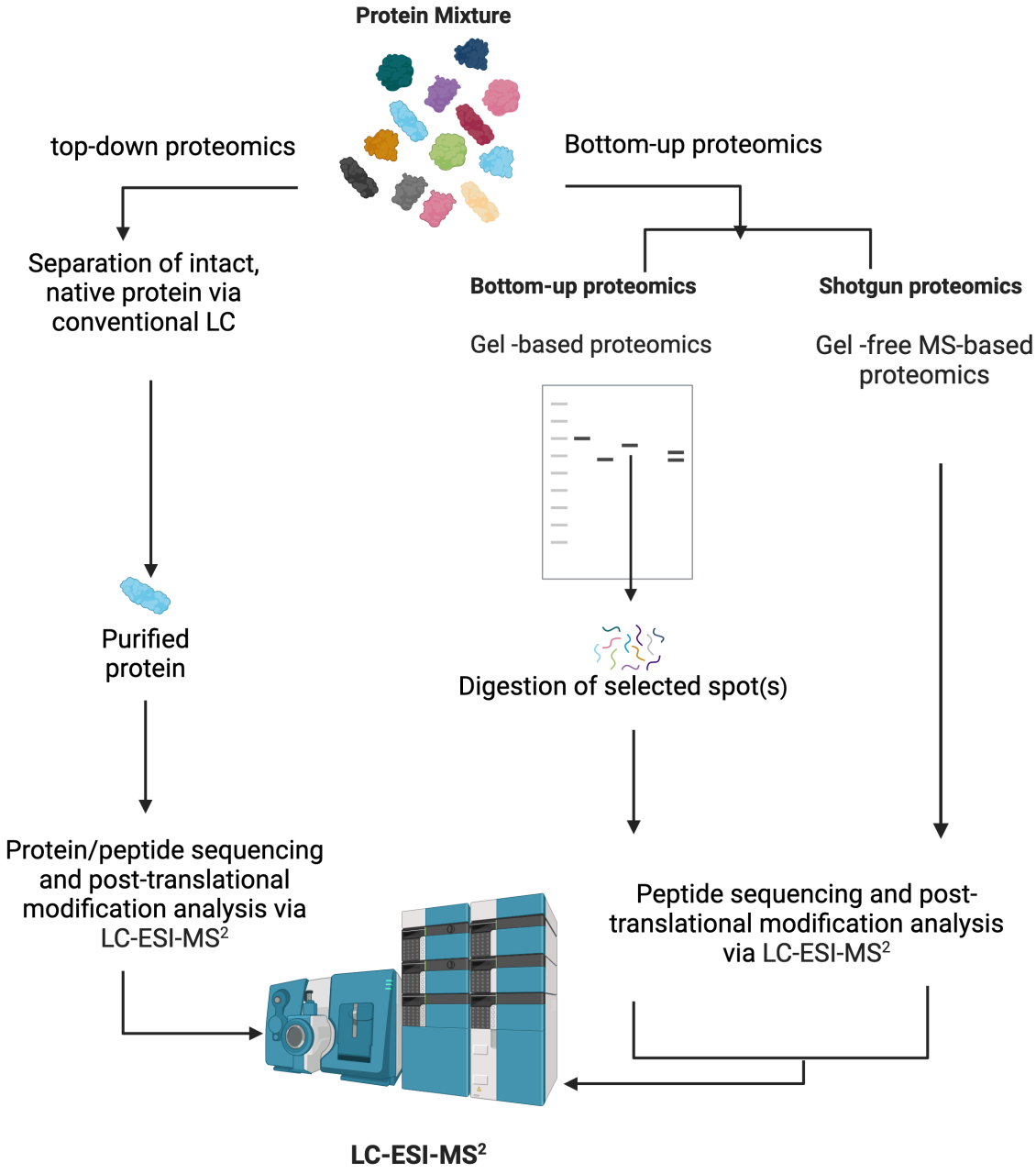

Figure 1-21. A schematic representation of comparing the top-down and bottom-up approaches used in proteomic studies. This figure was created by BioRender.

Following MS-proteomics experiments, peptide sequence identification is achieved by comparing experimentally obtained MS/MS spectra with available database

fragmentation spectra **(Figure 1-22)**. The fragmentation spectra for each specific peptide sequence are unique and distinguish between isomass peptides with a different amino acid sequence. Peptide mass fingerprinting is thus advantageous for accurately identifying unknown protein sequences [231, 232, 243, 244].

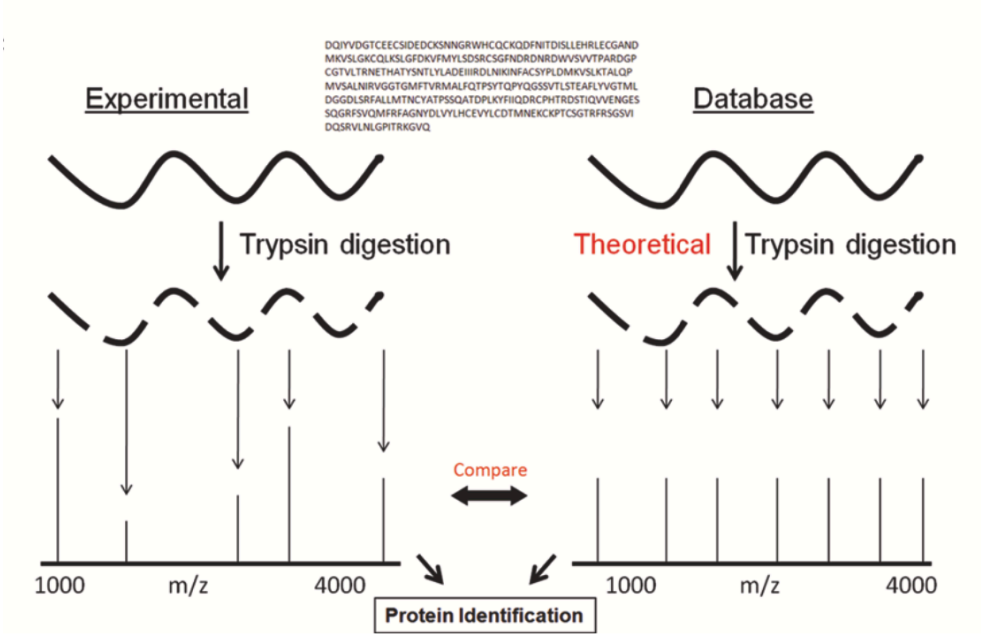

Figure 1-22. A peptide mass fingerprinting: In the MALDI-TOF-MS, one peak corresponds to one peptide, and many peaks correspond to many peptides, either from one protein or more proteins. Database searches of the MALDI-MS spectra usually identify that single protein or those proteins through a process named peptide mass fingerprinting. This figure was reproduced with permission from [231].

Beyond qualitative analysis, MS-based proteomics also enables protein quantification. Changes in specific protein quantity and/or MS-peak intensity under certain conditions can aid in biomarker identification [231, 232, 243, 244]. A widely used quantification technique is the label-free quantitation method, which is fast, cost-effective, and implemented through spectral counting. In spectral counting, proteins are quantified

based on the total number of MS/MS spectra that link peptides to a specific protein, with abundance directly proportional to the matched peptides [231, 245, 246].

If the protein is not available in the database, *de novo* sequencing of peptides is required [247], which can be done with software like PEAKS and DeNovoX [248]. This approach has proven successful in de novo sequencing of fish allergens such as parvalbumins and shrimp arginine kinases [249, 250].

1.3.4.1.3. Applications of Proteomics in Fish Research

Fish seminal plasma provides an optimal environment for spermatozoa storage before spawning, with proteins playing a crucial role in sperm protection and functionality [223, 251-254]. Comprehensive proteomic analysis of seminal plasma proteins in species like carp (*Cyprinus carpio*) and rainbow trout has been instrumental in understanding the complexity of fish seminal proteins [255]. Advanced shotgun proteomics using 1D-SDS-PAGE and HPLC-ESI-MS/MS has significantly propelled this field, enabling the identification of a diverse array of seminal plasma proteins in rainbow trout and carp [256, 257]. This approach has cataloged 206 proteins in rainbow trout sperm and 348 in carp sperm, shedding light on species-specific differences and the potential role of these proteins in reproductive success [251, 258, 259].

Ovarian fluid (OF), the biological fluid surrounding eggs within the ovary of female fish, plays a vital role in maintaining oocyte health and readiness for fertilization [260]. Proteomic analysis of OF in rainbow trout produced the first comprehensive identification of 54 proteins, many of which were previously unreported, through 1-D-SDS-PAGE and

HPLC-ESI-MS/MS[261]. These protein identifications may facilitate biomarker discovery for assessing oocyte quality, potentially impacting fish breeding and conservation strategies [261].

Proteomics has also enhanced our understanding of disease processes in fish. For instance, in a study on adult zebrafish infected with spring viremia of carp virus (SVCV), LC-MS/MS analysis identified novel biomarkers and provided a detailed plasma protein profile in infected fish [262]. In total, 3062 proteins were identified in control fish, with 137, 63, and 31 proteins significantly abundant at 1, 2, and 5 days post-infection, respectively, highlighting immune response over time after infection [262].

Additionally, proteomics has proven to be a robust tool for environmental monitoring, offering insights into the effects of contaminants on marine life through the identification of critical protein biomarkers [263]. For example, in Atlantic cod, LC-MS/MS proteomics was employed to investigate the impact of polycyclic aromatic hydrocarbons (PAHs) on the plasma proteome [264]. PAHs are toxic, hydrophobic compounds associated with carcinogenic and immunotoxic effects in aquatic organisms [265]. This study identified 369 proteins, with 12 showing significant changes, such as upregulated immunoglobulin components and downregulated antifreeze proteins, suggesting an immune response to PAH exposure. Apolipoproteins were notably prominent among identified proteins, indicating their role as potential biomarkers for PAH exposure [264].

Finally, proteomic responses to environmental temperature changes have also been studied [266]. A label-free quantitative LC-MS/MS analysis using the UniProt Atlantic

salmon (*Salmo salar*) database identified and quantified cardiac proteins in salmon exposed to water temperatures 4 °C warmer than usual [266]. The analysis revealed differential abundance in 79 proteins between control (0 °C) and elevated (+4 °C) temperature treatments, showing increased levels of proteins involved in oxidative metabolism and a corresponding expansion of compact myocardium. These findings underscore the potential for proteomics to reveal adaptive responses to climate change in aquatic species [266].

1.3.4.2. Mass Spectrometry Applications in Lipid A Analysis

MS-structural studies of lipid A are critical for understanding its biological function, particularly its role in immunological responses [267-270]. Due to lipid A's pro-inflammatory properties [137], structural analysis aids in developing synthetic analogs, some of which serve as antagonists to *E. coli* lipid A [271, 272]. These structural insights lay the groundwork for designing lipid A analogs to either mimic or inhibit its effects [271, 272].

1.3.4.2.1. Analysis of Lipid A Structures from *Aeromonas liquefaciens* SJ-19a

The Gram-negative bacterium *Aeromonas liquefaciens* SJ-19a is associated with hemorrhagic septicemia in cultured fish. Its complex lipid A structures, especially when exposed to phages, reveal significant structural insights [270]. Lipid A molecules were isolated via the aqueous phenol method, purified by chromatography, and analyzed using ESI-MS. A triple-quadrupole (QqQ) analyzer confirmed asymmetric fatty acid attachment to the lipid A disaccharide backbone **(Figure 1-23 and Table 1-2)** [270].

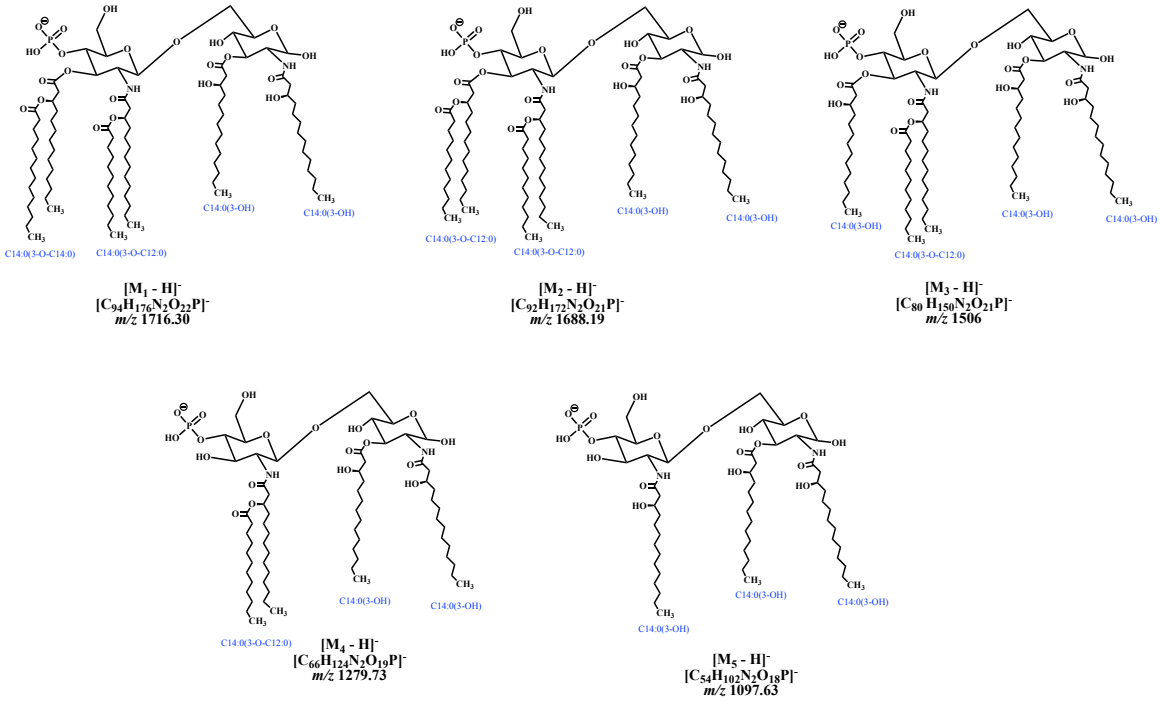

Figure 1-23. Schematic representation of lipid A Structures Extracted from *A. liquefaciens SJ-19a*. This figure was generated using ChemDraw Prime.

Table 1-2. Assignments of the deprotonated mono-phosphorylated molecules observed in negative mode ESI-QqQ-MS of the native mixture of lipid A_{1-5} extracted from the LPS of *Aeromonas liquefaciens* SJ-19a.

Deprotonated molecules	Empirical formula	*m/z* Observed; Calculated	δ ppm
[M$_1$ - H]$^-$	$C_{94}H_{176}N_2O_{22}P$	1716.30; 1716.24	-10
[M$_2$ - H]$^-$	$C_{92}H_{172}N_2O_{21}P$	1688.19; 1688.21	- 11.8
[M$_3$ - H]$^-$	$C_{80}H_{150}N_2O_{21}P$	1506.10; 1506.05	33.1
[M$_4$ - H]$^-$	$C_{66}H_{124}N_2O_{19}P$	1279.83; 1279.85	- 15.6
[M$_5$ - H]$^-$	$C_{54}H_{102}N_2O_{18}P$	1097.63; 1097.68	- 45.5

The identified lipid A variants, labelled lipid A_1 to A_5, along with their product anions, were identified through ESI-CID-MS/MS analysis **(Figure 1-19)** [270]. The CID-MS/MS spectrum of Lipid A_1 $[M-H]^-$ anion at *m/z* 1716.30 produced several productions, including *m/z* 1516.02, 1488.08, 1226.92, 1053.82, 1017.12, and 692.39, as illustrated in

(**Scheme 1-1).** The most abundant anion, *m/z* 1516.02, represented the loss of (C12:0) acid, indicating its attachment at the N-2′ position. Likewise, the anion at *m/z* 1488.08 corresponds to the removal of (C14:0) acid from O-3′. The anion at *m/z* 1226.92 suggests consecutive losses of the branched (C14:0(3-O-C14:0)) fatty acid and two water molecules. The anion at *m/z* 1053.62 resulted from the loss of (C14:0(3-O-C14:0)) ketene and (C14:0(3-OH)) ketene from the O-3′ and O-3 positions, respectively. The ion at *m/z* 1017.12 was a secondary ion formed by eliminating two water molecules from the *m/z* 1053.62 ion. The *m/z* 692.39 anion, formed by glycosidic cleavage of the β-D-Gl*cp*N-(1→6)-α-D-Gl*cp*N disaccharide backbone following the loss of (C14:0) and (C12:0) acids from the O-3 and N-2 positions (**Scheme 1-1)** [270].

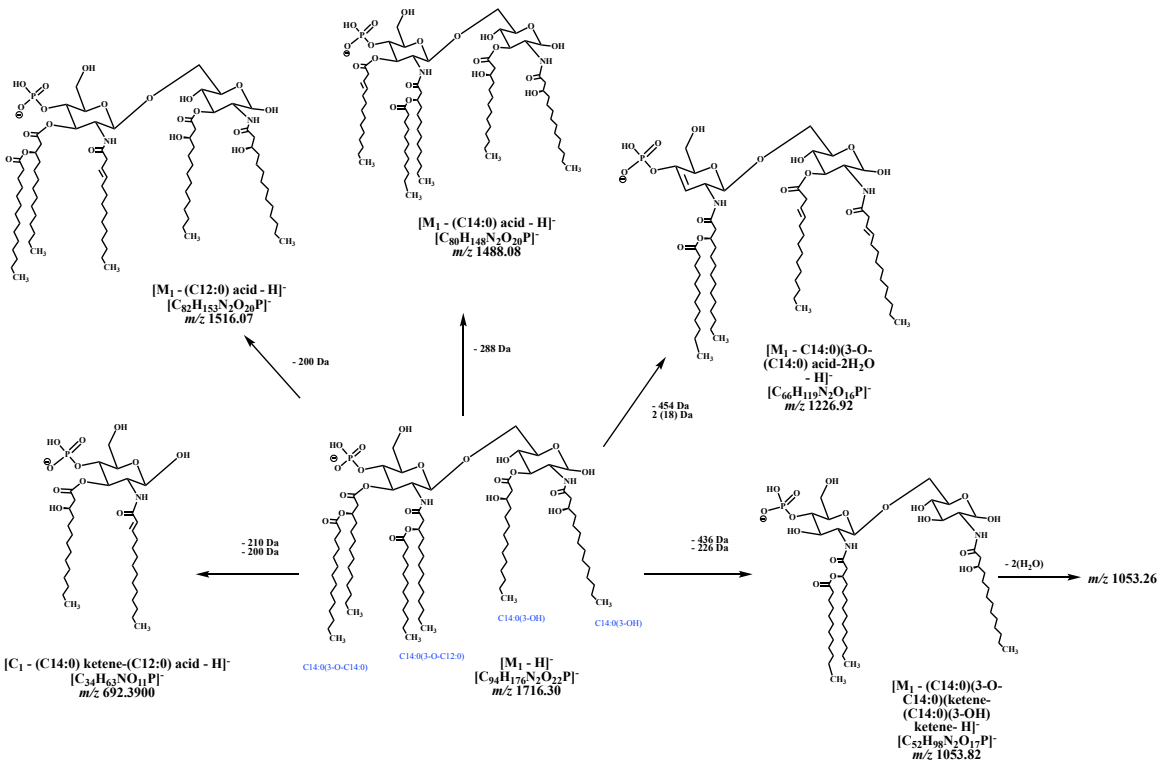

Scheme 1-1. Proposed fragmentation pathways obtained by CID-QqQ-MS/MS of the deprotonated Lipad A_1 molecules at *m/z* 1716.30. This figure was generated using ChemDraw Prime.

1.3.4.2.2. Analysis of Lipid A Structures from *Aeromonas salmonicida*

Aeromonas salmonicida, which is one of the most important primary pathogens in salmonids, is responsible for significant economic losses [273]. Using ESI-QqToF-MS/MS, the lipid A structure of *Aeromonas salmonicida* using ESI-QqToF-MS/MS unveiled a degree of microheterogeneity, presenting structural complexity with different phosphorylation states and fatty acid variations [269]. The lipid A molecules analyzed contained both mono- and bi-phosphorylated forms, evident by unique *m/z* ratios. Bi-phosphorylated lipid A (M_B) exhibited anions at *m/z* 883.5826 and 1768.1972, representing doubly and singly charged states, respectively. The mono-phosphorylated lipid A (M_M) is characterized by an ion at *m/z* 1688.2144 [269]. Further MS/MS studies confirmed their structures in **Figure 1-24 and Table 1-3**.

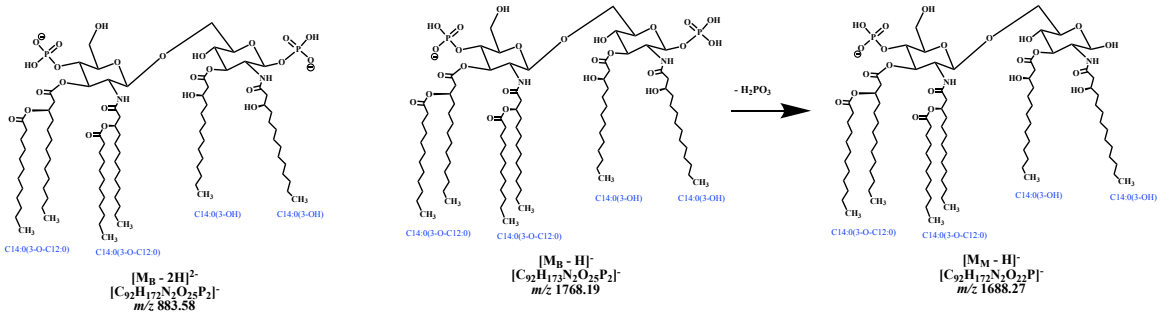

Figure 1-24. Schematic representation of lipid A Structures Extracted from *Aeromonas salmonicida*. This figure was generated using ChemDraw Prime.

Table 1-3. Assignments of the diagnostic ions observed in the QqToF mass spectrum of native lipid A extract acquired at DP = - 60 [269].

Diagnostic ion	Empirical formula	*m/z* Calculated; Observed	**δ ppm**
$[M_B - H]^{-}$ [a]	$C_{92}H_{173}N_2O_{25}P_2$	1768.1802; 1768.1972	9.6
$[M_B - 2H]^{2-}$	$C_{92}H_{172}N_2O_{25}P_2$	883.5862; 883.5826	4.0
$[M_M - H]^{-}$ [b]	$C_{92}H_{172}N_2O_{22}P$	1688.2139; 1688.2144	0.3

[a] M_B: Bi-phosphorylated lipid A.
[b] M_M: Mono-phosphorylated lipid A.

MS/MS fragmentation of the singly charged monophosphorylated lipid A $[M_M - H]^{-}$ species at *m/z* 1688.2139 fragmentation pathway presented in **Schemes 1- 2**. The product anion at *m/z* 1444.07 confirmed the loss of (C14:0(3-OH)) from the O-2 position. This fragmentation pathway further led to the formation of anions at *m/z* 1261.85, 1243.87, and 1035.67, indicating consecutive losses of fatty acid residues and water molecules [269]. The detection of anions at *m/z* 1261.85 and 1279.86 confirmed that the (C14:0(3-O-12:0)) acid residues were linked at both the N-2′ and O-3′ positions. Similarly, ions at *m/z* 1444.07 and 1017.67 provided evidence for the presence of (C14:0(3-OH)) acid residues at the reducing end [269].

The product anion at *m/z* 1488.08 confirms the loss of (C12:0) acid from the non-reducing end. This ion was a crucial diagnostic marker for the presence of (C14:0(3-O-12:0)) acid at the N-2' or O-3' positions. The ion at *m/z* 1279.86 was formed by the loss of both (C12:0) ketene and (C14:0) acid ketene. These eliminations confirmed the presence of (C14:0(3-O-12:0)) acyl chains at the non-reducing end (**Scheme 1-2)**.

These analyses highlight the structural diversity in lipid A from *Aeromonas* species, providing key insights into bacterial immune evasion and guiding potential vaccine targets to counteract these pathogens' virulence mechanisms [269].

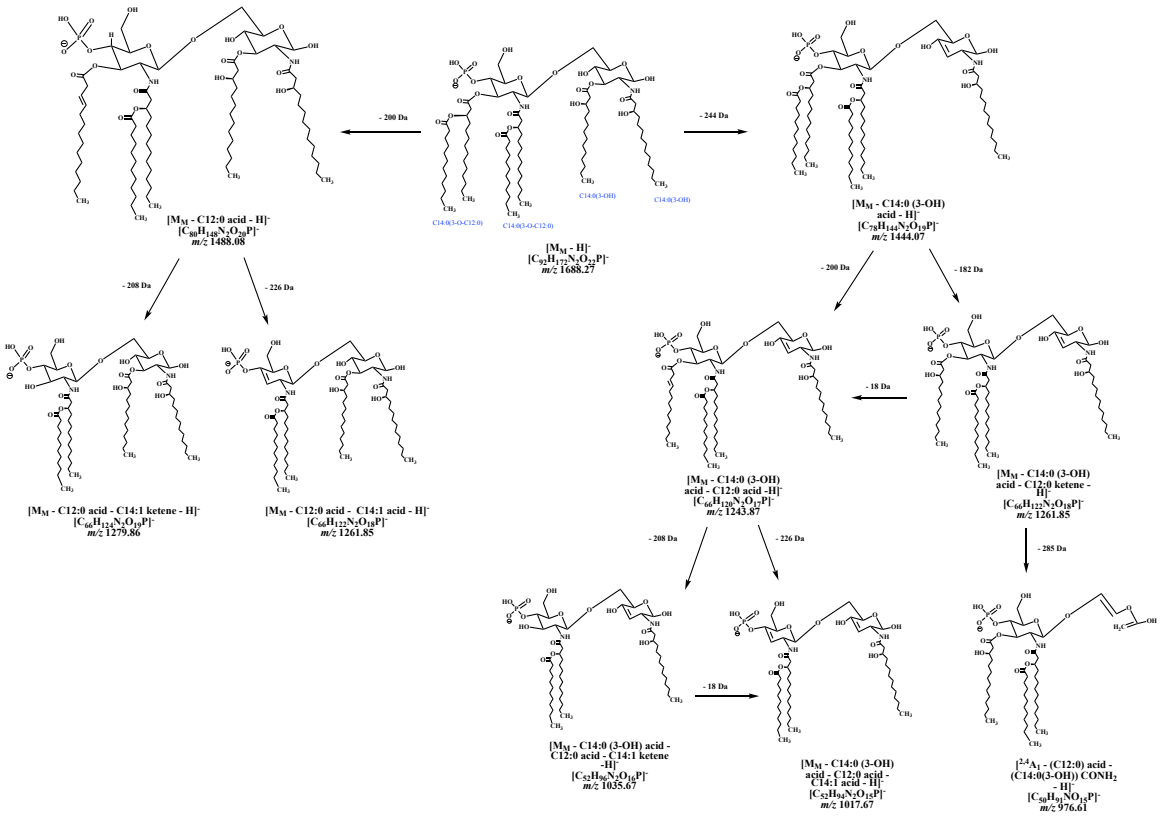

Scheme 1-2. Proposed fragmentation pathways of the selected precursor mono-phosphorylated lipid A $[M_M - H]^-$ ion at *m/z* 1688.2. This figure was generated using ChemDraw Prime.

The following section will introduce the separation techniques employed in this study to improve MS characterization.

1.3.5. Ion Mobility Spectrometry (IMS)

An IMS is an analytical technique that separates ionized molecules in the gas phase based on their mobility through a buffer gas under the influence of an electric field [274]. This separation is influenced by the ion's size, shape, and charge, allowing IMS to distinguish between isomers and conformers that might be indistinguishable by MS alone

[275]. Consequently, IMS is frequently coupled with MS (IMS-MS) to enhance analytical specificity and provide structural information about analytes [276, 277].

A notable advancement in this field is Field Asymmetric Waveform Ion Mobility Spectrometry (FAIMS). FAIMS enhances the traditional IMS concept by applying an asymmetric high-voltage waveform between two electrodes, separating ions based on differences in their mobility under high and low electric fields. This orthogonal and highly selective separation enhances specificity prior to MS analysis [277, 278].

1.3.5.1. Principle of FAIMS:

In FAIMS, ions are introduced between two electrodes in a flowing carrier gas and subjected to an asymmetric waveform that alternates between high and low electric field intensities [279]. The field strength causes ions to experience non-linear mobility behaviour due to energetic collisions with the gas molecules. The ion's velocity (cm/s) relative to the applied field (V/cm) is described by its mobility (K, $cm^2/V \cdot s$) [280]. While K is typically constant at low field strengths, at higher electric fields, ion mobility becomes field-dependent. Three general types of ion behaviour have been described. Type A ions show an increase in ion mobility with increasing field strength. Type B ions display an initial rise in ion mobility with increasing fields, followed by decreasing mobility as the field strength rises further. Type C ions show a decrease in ion mobility with increasing field strength. More recent experimental and theoretical studies have shown that these differences in ion behaviour depend on multiple parameters, including ion structure, collision cross-section, and instrumental settings [279].

Compensation voltage (CV) is a critical parameter in FAIMS operations [279]. CV is applied to counteract the net ion displacement caused by the asymmetric waveform, allowing only ions with specific differential mobility (ΔK) to traverse the FAIMS cell and reach the mass spectrometer. Unlike drift tube IMS, which samples ion packets in discrete time intervals, FAIMS acts as a continuous filtration system, selectively transmitting ions in real time based on the applied CV [280].

1.3.5.2. Applications of FAIMS:

FAIMS has found diverse applications across multiple branches of analytical science, notably enhancing the performance of MS. In proteomics, FAIMS is particularly beneficial for reducing chemical noise, thereby improving the detection of low-abundance peptides. It achieves this by filtering out interfering ions and selectively transmitting ions based on their differential mobility, enhancing both the dynamic range and detection sensitivity in MS-based workflows. For example, LC-FAIMS-MS has demonstrated significant improvements in the detection and quantification of peptides in complex biological samples [280]. Furthermore, when combined FAIMS with parallel reaction monitoring, FAIMS has been shown to increase the sensitivity of targeted proteomic assays in formalin-fixed, paraffin-embedded tissue analyses, improving the signal-to-noise ratio for targeted proteins [281].

In lipidomics, the structural diversity and isomeric complexity of lipids present unique analytical challenges. FAIMS has been effectively employed to improve the separation of lipid classes and isomeric species, enabling more comprehensive lipidomic

analyses. For instance, the use of Hydrophilic Interaction Liquid Chromatography (HILIC) combined with FAIMS-MS allows for the separation of lipids based on headgroup polarity and fatty acyl chain composition, facilitating detailed lipid profiling in biological samples [282]. Additionally, FAIMS has advanced shotgun lipidomics techniques by enhancing the detection and characterization of gangliosides, a complex class of glycosphingolipids. By improving the separation of isomeric species, FAIMS supports more detailed analyses of lipid compositions in biological systems [283].

FAIMS also addresses a major analytical challenge in carbohydrate analysis: distinguishing isomeric forms such as anomers, linkage isomers, and positional isomers, which often share identical masses. Traditional mass spectrometry alone struggles to resolve these isomers effectively. However, FAIMS enables rapid and sensitive separation of disaccharide isomers without the need for prior purification or chromatographic fractionation [284].

The following section will introduce the techniques employed in this study to enhance the characterization of bacterial lipid A.

1.3.6. Kendrick mass defect plots (KMD)

Mass spectra are often highly complex, making data interpretation challenging. Among the various data mining tools available, KMD analysis has become a powerful visualization and data processing tool for the mass spectra of different mixtures such as oils and LPSs [175, 285, 286]. KMD plots are particularly valuable for classifying and sorting structurally related ions in complex mixtures [175, 287-291]. This method

transforms *m/z* values from the mass spectrum into Kendrick Mass (KM) values by multiplying the given *m/z* value by the ratio of the nominal mass of a repeating unit to its IUPAC exact mass [288]. Historically, KMD analysis involved a change of basis from the IUPAC mass scale to a KM scale, where the nominal mass of the methylene group base unit (CH_2) is set at 14 a.u. [175] .

The KM is calculated as follows [286]:

$$\text{KM} = \text{experimental } m/z \times \frac{14.00000}{14.01565} \qquad \text{Eq.1}$$

The KMD is then determined as [286]:

$$\text{KMD} = \text{nominal KM} - \text{exact KM} \qquad \text{Eq.2}$$

In a KMD plot, the relationship between the KMD and the nominal KM is visually represented. Using CH_2 as the base unit, ions differing only by the number of CH_2 units align horizontally, as they share the same KMD value **(Figure 1-25)**. Ions whose elemental composition differs by several CH_2 units also share the same KMD and line up horizontally in the plot [175]. Conversely, ions with different KMD values align vertically, with differences reflecting variations in double bond equivalents (DBE) or heteroatom counts; higher DBE or heteroatom numbers result in higher mass defects [175].

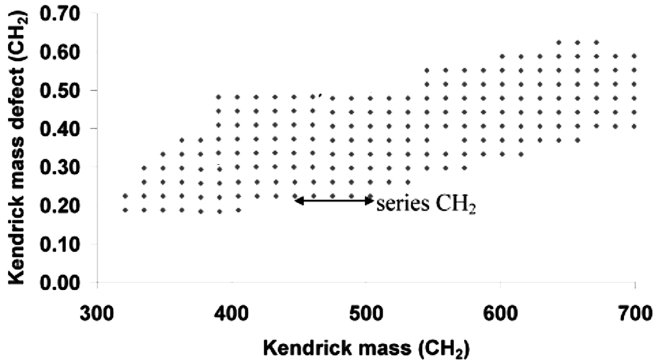

Figure 1-25. KMD plot of an organic compounds sample using CH_2 as a base unit. This figure was reprinted with permission from [292].

When the repeat unit of a homopolymer does not match the base unit used for the KMD calculation, points deviate from horizontal alignment and instead align diagonally in the KMD plot [285, 293, 294]. Modifications of KMD analysis introduced alternative base units tailored to the polymer type [285, 286]. Furthermore, a fractional base unit (i.e., repeat unit/X) can significantly expand the KMD dimension, amplifying KMD variations across peaks, which enhances the plot's resolution **(Figure 1-26)** [285]. Fractional base units have demonstrated the ability to discriminate isotopes (e.g., ^{12}C and ^{13}C) and resolve components in polymeric blends and copolymers into distinct clusters [285].

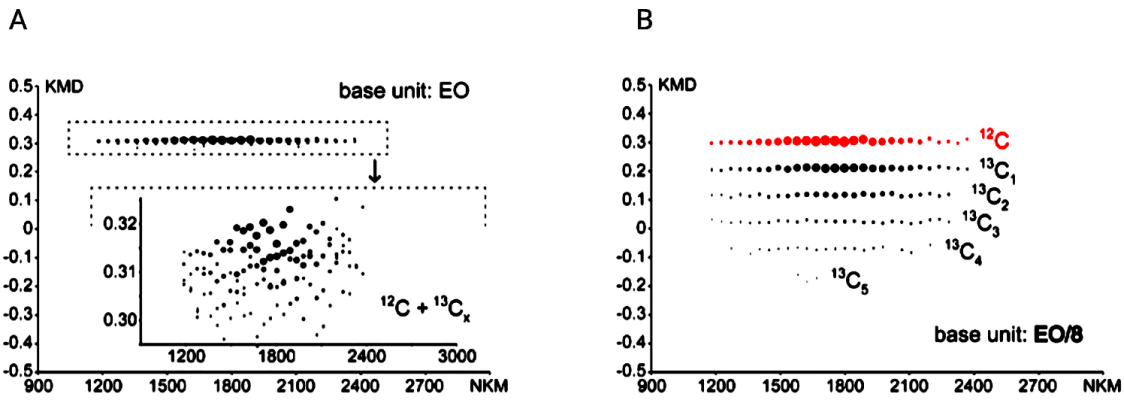

Figure 1-26. Comparison between KMD plots of poly (ethylene oxide) (PEO) with integer and fractional (EO/8) units as the base. (A) Full-scale EO-based KMD plot and its magnification in inset. (B) Full-scale KMD plot using a fractional EO/8 as the base unit. This figure was reprinted with permission from [285].

1.4. Hypotheses and Research Goals

The main work described in this introduction establishes the context of my PhD, outlining the motivation and significance of this research. It provides the necessary background on two key research areas: the structural investigation of Atlantic cod otolith proteins and the structural elucidation of bacterial lipid A from marine Gram-negative bacteria.

For the study on Atlantic cod otolith proteins, we hypothesize that cod otolith proteins can represent the protein profile of fish from embryo to death. The aims of this research are to characterize and quantify the protein composition of cod otoliths using the shotgun proteomic technique. This work sheds light on the physiological and biochemical roles these proteins play in fish growth and life history, which are essential for sustainable fisheries management.

Additionally, the analysis of lipid A from marine Gram-negative bacteria of the *Vibrionaceae* and *Aeromonadaceae* families aims to provide critical insights into the impact of bacterial endotoxins on fish health. By employing FAMIS-ESI-MS and MS/MS techniques, along with Kendrick mass defect analysis, we seek to reveal the molecular structures of lipid A and offer novel insights into its biological function.

Together, these studies pave the way for a deeper understanding of the biochemical complexity of marine environments and set the foundation for future advancements in marine ecosystem management and conservation.

1.5. References

[1] P. Weist, F. M. Schade, M. Damerau, J. M. I. Barth, J. Dierking, C. André, C. Petereit, T. Reusch, S. Jentoft, R. Hanel, and U. Krumme, "Assessing SNP-markers to study population mixing and ecological adaptation in Baltic cod," *PLOS One,* vol. 14, no. 6, pp. e0218127, Jun, 2019. DOI: https://doi.org/10.1371/journal.pone.0218127.

[2] T. Fischer, *The effects of climate induced temperature changes on cod (Gadus morhua L.): linking ecological and physiological investigations*, Bremerhaven, Bremen:Alfred-Wegener-Institut für Polar- und Meeresforschung; Vertrieb durch K. Kamloth, 2003.

[3] J. Hemmer-Hansen, E. E. Nielsen, N. O. Therkildsen, M. I. Taylor, R. Ogden, A. J. Geffen, D. Bekkevold, S. Helyar, C. Pampoulie, T. Johansen, and G. R. Carvalho, "A genomic island linked to ecotype divergence in Atlantic cod," *Mol. Ecol.,* vol. 22, no. 10, pp. 2653-2667, May, 2013. DOI: https://doi.org/10.1111/mec.12284.

[4] COSEWIC, *COSEWIC assessment and status report on the Atlantic cod Gadus morhua in Canada,* ISBN 978-1-100-15988-1, Committee on the Status of Endangered Wildlife in Canada, 2010.

[5] T. Norin, P. Canada, J. A. Bailey, and A. K. Gamperl, “Thermal biology and swimming performance of Atlantic cod (*Gadus morhua*) *and haddock* (*Melanogrammus aeglefinus*),” *PeerJ.,* vol. 7, pp. e7784, Oct, 2019. DOI: https://doi.org/10.7717/peerj.7784.

[6] R. J. Lilley, and R. K. F. Unsworth, “Atlantic Cod (*Gadus morhua*) benefits from the availability of seagrass (*Zostera marina*) nursery habitat,” *Global. Ecol. Conserv.,* vol. 2, pp. 367-377, Dec, 2014. DOI: https://doi.org/10.1016/j.gecco.2014.10.002.

[7] M. Kalka, K. Bielak, M. Ptak, J. Stolarski, P. Dobryszycki, and M. Wojtas, “Calcium carbonate polymorph selection in fish otoliths: A key role of phosphorylation of Starmaker-like protein,” *Acta Biomater,* vol. 174, pp. 437-446, Jan, 2024. DOI: https://doi.org/10.1016/j.actbio.2023.11.039.

[8] E. Murayama, Y. Takagi, T. Ohira, J. G. Davis, M. I. Greene, and H. Nagasawa, “Fish otolith contains a unique structural protein, otolin-1,” *Eur. J. Biochem.,* vol. 269, no. 2, pp. 688-696, Jan, 2002. DOI: https://doi.org/10.1046/j.0014-2956.2001.02701.x.

[9] O. Lowenstein, "7 The labyrinth," *Sensory systems and electric organs*, Fish Physiology W. S. Hoar and D. J. Randall, eds.Cambridge, MA, USA: Academic Press, 1971. pp. 207-240.

[10] A. N. Popper, J. Ramcharitar, and S. E. Campana, “Why otoliths? Insights from inner ear physiology and fisheries biology,” *Mar. Freshw. Res.,* vol. 56, no. 5, pp. 497-504, May, 2005. DOI: https://doi.org/10.1071/mf04267.

[11] O. R. B. Thomas, S. E. Swearer, E. A. Kapp, P. Peng, G. Q. Tonkin-Hill, A. Papenfuss, A. Roberts, P. Bernard, and B. R. Roberts, "The inner ear proteome of fish," *FEBS J.,* vol. 286, no. 1, pp. 66-81, Jan, 2019. DOI: https://doi.org/10.1111/febs.14715.

[12] M. Tanimoto, Y. Ota, M. Inoue, and Y. Oda, "Origin of inner ear hair cells: morphological and functional differentiation from ciliary cells into hair cells in zebrafish inner ear," *J. Neurosci.,* vol. 31, no. 10, pp. 3784-3794, Mar, 2011. DOI: https://doi.org/10.1523/JNEUROSCI.5554-10.2011.

[13] H. Yuan, Y. Zhou, and P. Chen, "Research on the Acoustic conditioning taming on fish and application in marine ranching," *Water,* vol. 15, no. 1, Dec, 2022. DOI: https://doi.org/10.3390/w15010071.

[14] Y. W. Lundberg, Y. Xu, K. D. Thiessen, and K. L. Kramer, "Mechanisms of otoconia and otolith development," *Dev. Dyn.,* vol. 244, no. 3, pp. 239-253, Sep, 2015. DOI: https://doi.org/10.1002/dvdy.24195.

[15] A. N. Popper, and A. D. Hawkins, "An overview of fish bioacoustics and the impacts of anthropogenic sounds on fishes," *J. Fish Biol.,* vol. 94, no. 5, pp. 692-713, May, 2019. DOI: https://doi.org/10.1111/jfb.13948.

[16] P. Payan, H. De Pontual, G. Bœuf, and N. Mayer-Gostan, "Endolymph chemistry and otolith growth in fish," *Comptes. Rendus. Palevol.,* vol. 3, no. 6-7, pp. 535-547, Oct, 2004. DOI: https://doi.org/10.1016/j.crpv.2004.07.013.

[17] Y. Takagi, "Otolith formation and endolymph chemistry: A strong correlation between the aragonite saturation state and pH in the endolymph of the trout otolith

organ," *Mar. Ecol. Prog. Ser.,* vol. 231, pp. 237-245, Apr, 2002. DOI: https://doi.org/10.3354/meps231237.

[18] R. R. Fay, "The goldfish ear codes the axis of acoustic particle motion in three dimensions," *Science,* vol. 225, no. 4665, pp. 951-954, Aug, 1984. DOI: https://doi.org/10.1126/science.6474161.

[19] L. Schnetz, C. Pfaff, E. Libowitzky, Z. Johanson, R. Stepanek, and J. Kriwet, "Morphology and evolutionary significance of phosphatic otoliths within the inner ears of cartilaginous fishes (Chondrichthyes)," *BMC Evol. Biol.,* vol. 19, no. 1, pp. 238, Dec, 2019. DOI: https://doi.org/10.1186/s12862-019-1568-z.

[20] G. Panella, "Fish otoliths: Daily growth layers and periodical patterns," *Science,* vol. 173, no. 4002, pp. 1124-1127, Sep, 1971. DOI: https://doi.org/10.1126/science.173.4002.1124.

[21] C. S. Romanek, and R. W. Gauldie, "A predictive model of otolith growth in fish based on the chemistry of the endolymph," *Comp. Biochem. Physiol. Part A Physiol.,* vol. 114, no. 1, pp. 71-79, May, 1996. DOI: https://doi.org/10.1016/0300-9629(95)02094-2.

[22] T. Schulz-Mirbach, M. Hess, and M. Plath, "Inner ear morphology in the Atlantic molly *Poecilia mexicana*-first detailed microanatomical study of the inner ear of a *cyprinodontiform* species," *PLOS One,* vol. 6, no. 11, pp. e27734, Nov, 2011. DOI: https://doi.org/10.1371/journal.pone.0027734.

[23] O. R. B. Thomas, and S. E. Swearer, "Otolith biochemistry—A Review," *Rev. Fish. Sci. Aquac.,* vol. 27, no. 4, pp. 458-489, Jul, 2019. DOI: https://doi.org/10.1080/23308249.2019.1627285.

[24] M. Yasuo, "Diurnal rhythm in otolith formation in the rainbow trout, Salmo gairdneri: Seasonal reversal of the rhythm in relation to plasma calcium concentrations," *Comp. Biochem. Physiol. Part A Physiol.,* vol. 78, no. 2, pp. 289-293, Jan, 1984. DOI: https://doi.org/10.1016/0300-9629(84)90149-x.

[25] M. C. F. Disspain, S. Ulm, and B. M. Gillanders, "Otoliths in archaeology: Methods, applications and future prospects," *J. Archaeol. Sci. Rep.,* vol. 6, pp. 623-632, May, 2016. DOI: https://doi.org/10.1016/j.jasrep.2015.05.012.

[26] C. Koppl, V. Wilms, I. J. Russell, and H. G. Nothwang, "Evolution of endolymph secretion and endolymphatic potential generation in the vertebrate inner ear," *Brain Behav. Evol.,* vol. 92, no. 1-2, pp. 1-31, Nov, 2018. DOI: https://doi.org/10.1159/000494050.

[27] A. T. Pinhorn, "Fishery and biology of Atlantic cod (*Gadus morhua*) off the Southwest Coast of Newfoundland," *J. Fish. Res. Board. Can.,* vol. 26, no. 12, pp. 3133-3164, 1969. DOI: https://doi.org/10.1139/f69-298.

[28] S. E. Campana, "Chemistry and composition of fish otoliths:pathways, mechanisms and applications," *Mar. Ecol. Prog. Ser.,* vol. 188, pp. 263-297, 1999. DOI: https://doi.org/10.3354/meps188263.

[29] G. Falini, S. Albeck, S. Weiner, and L. Addadi, “Control of aragonite or calcite polymorphism by Mollusk shell macromolecules,” *Science,* vol. 271, no. 5245, pp. 67-69, Oct, 1996. DOI: https://doi.org/10.1126/science.271.5245.67.

[30] S. Huang, and S. Qian, “Advances in otolith-related protein research,” *Front. Neurosci.,* vol. 16, no. 7, pp. 956200, Jul, 2022. DOI: https://doi.org/10.3389/fnins.2022.956200.

[31] K. Bielak, D. Benkowska-Biernacka, M. Ptak, J. Stolarski, M. Kalka, A. Ozyhar, and P. Dobryszycki, “Otolin-1, an otolith- and otoconia-related protein, controls calcium carbonate bioinspired mineralization,” *Biochim. Biophys Acta. Gen. Subj.,* vol. 1867, no. 5, pp. 130327, May, 2023. DOI: https://doi.org/10.1016/j.bbagen.2023.130327.

[32] E. Murayama, P. Herbomel, A. Kawakami, H. Takeda, and H. Nagasawa, “Otolith matrix proteins OMP-1 and Otolin-1 are necessary for normal otolith growth and their correct anchoring onto the sensory maculae,” *Mech. Dev.,* vol. 122, no. 6, pp. 791-803, Jun, 2005. DOI: https://doi.org/10.1016/j.mod.2005.03.002.

[33] J. A. Petko, B. B. Millimaki, V. A. Canfield, B. B. Riley, and R. Levenson, “Otoc1: a novel otoconin-90 ortholog required for otolith mineralization in zebrafish,” *Dev. Neurobiol.,* vol. 68, no. 2, pp. 209-222, Feb, 2008. DOI: https://doi.org/10.1002/dneu.20587.

[34] K. N. Robillard, E. de Vrieze, E. van Wijk, and J. J. Lentz, “Altering gene expression using antisense oligonucleotide therapy for hearing loss,” *Hear. Res.,*

vol. 426, pp. 108523, Dec, 2022. DOI: https://doi.org/10.1016/j.heares.2022.108523.

[35] C. Sollner, M. Burghammer, E. Busch-Nentwich, J. Berger, H. Schwarz, C. Riekel, and T. Nicolson, "Control of crystal size and lattice formation by starmaker in otolith biomineralization," *Science,* vol. 302, no. 5643, pp. 282-286, Oct, 2003. DOI: https://doi.org/10.1126/science.1088443.

[36] B. Bajoghli, M. Ramialison, N. Aghaallaei, T. Czerny, and J. Wittbrodt, "Identification of starmaker-like in medaka as a putative target gene of Pax2 in the otic vesicle," *Dev. Dyn.,* vol. 238, no. 11, pp. 2860-2866, Nov, 2009. DOI: https://doi.org/10.1002/dvdy.22093.

[37] V. G. Fonseca, V. Laize, M. S. Valente, and M. L. Cancela, "Identification of an osteopontin-like protein in fish associated with mineral formation," *FEBS J.,* vol. 274, no. 17, pp. 4428-4439, Sep, 2007. DOI: https://doi.org/10.1111/j.1742-4658.2007.05972.x.

[38] Y. J. Kang, A. K. Stevenson, P. M. Yau, and R. Kollmar, "Sparc protein is required for normal growth of zebrafish otoliths," *J. Assoc. Res. Otolaryngol.,* vol. 9, no. 4, pp. 436-451, Dec, 2008. DOI: https://doi.org/10.1007/s10162-008-0137-8.

[39] E. Mulry, and K. Parham, "Inner ear proteins as potential biomarkers," *Otol. Neurotol.,* vol. 41, no. 2, pp. 145-152, Feb, 2020. DOI: https://doi.org/10.1097/MAO.0000000000002466.

[40] G. A. Stooke-Vaughan, N. D. Obholzer, S. Baxendale, S. G. Megason, and T. T. Whitfield, "Otolith tethering in the zebrafish otic vesicle requires Otogelin and

alpha-Tectorin," *Development,* vol. 142, no. 6, pp. 1137-1145, Mar, 2015. DOI: https://doi.org/10.1242/dev.116632.

[41] M. A. Anwar, and S. Choi, "Gram-negative marine bacteria: structural features of lipopolysaccharides and their relevance for economically important diseases," *Mar. Drugs,* vol. 12, no. 5, pp. 2485-2514, Apr, 2014. DOI: https://doi.org/10.3390/md12052485.

[42] C. C. de Carvalho, and P. Fernandes, "Production of metabolites as bacterial responses to the marine environment," *Mar. Drugs,* vol. 8, no. 3, pp. 705-727, Mar, 2010. DOI: https://doi.org/10.3390/md8030705.

[43] H. Machado, E. C. Sonnenschein, J. Melchiorsen, and L. Gram, "Genome mining reveals unlocked bioactive potential of marine Gram-negative bacteria," *BMC Genomics,* vol. 16, no. 1, pp. 158, Mar, 2015. DOI: https://doi.org/10.1186/s12864-015-1365-z.

[44] A. Undabarrena, F. Beltrametti, F. P. Claverias, M. Gonzalez, E. R. Moore, M. Seeger, and B. Camara, "Exploring the diversity and antimicrobial potential of marine *Actinobacteria* from the Comau Fjord in Northern Patagonia, Chile," *Front. Microbiol.,* vol. 7, pp. 1135, Jul, 2016. DOI: https://doi.org/10.3389/fmicb.2016.01135.

[45] Y. A. Knirel, and M. A. Valvano, *Bacterial lipopolysaccharides*, 1 ed., Springer Vienna, 2011.

[46] T. J. Silhavy, D. Kahne, and S. Walker, “The bacterial cell envelope,” *Cold Spring Harb. Perspect. Biol.,* vol. 2, no. 5, pp. a000414, May, 2010. DOI: https://doi.org/10.1101/cshperspect.a000414.

[47] W. Pajerski, D. Ochonska, M. Brzychczy-Wloch, P. Indyka, M. Jarosz, M. Golda-Cepa, Z. Sojka, and A. Kotarba, “Attachment efficiency of gold nanoparticles by gram-positive and Gram-negative bacterial strains governed by surface charges,” *J. Nanopart. Res.,* vol. 21, no. 8, Jul, 2019. DOI: https://doi.org/10.1007/s11051-019-4617-z.

[48] T. R. L. Senadheera, A. Hossain, and F. Shahidi, “Marine bioactives and their application in the food industry: A review,” *Appl. Sci.,* vol. 13, no. 21, pp. 12088, Nov, 2023. DOI: https://doi.org/10.3390/app132112088.

[49] J. Zhou, Y. Cai, Y. Liu, H. An, K. Deng, M. A. Ashraf, L. Zou, and J. Wang, “Breaking down the cell wall: Still an attractive antibacterial strategy,” *Front. Microbiol.,* vol. 13, pp. 952633, Sep, 2022. DOI: https://doi.org/10.3389/fmicb.2022.952633.

[50] C. R. Raetz, and C. Whitfield, “Lipopolysaccharide endotoxins,” *Annu. Rev. Biochem.,* vol. 71, pp. 635-700, Nov, 2002. DOI: https://doi.org/10.1146/annurev.biochem.71.110601.135414.

[51] A. Silipo, C. De Castro, R. Lanzetta, M. Parrilli, and A. Molinaro, "Lipopolysaccharides," *Prokaryotic cell wall compounds*, H. König, H. Claus and A. Varma, eds. Springer Berlin Heidelberg, 2010. pp. 133-153.

[52] O. Holst, and A. Molinaro, "Core region and lipid A components of lipopolysaccharides," *Microbial Glycobiology*, A. P. Moran, O. Holst, P. Brennan and M. von Itzstein, eds., 2010. pp. 29-55.

[53] J. H. Banoub, A. E. Aneed, A. M. Cohen, and N. Joly, "Structural investigation of bacterial lipopolysaccharides by mass spectrometry and tandem mass spectrometry," *Mass Spectrom. Rev.,* vol. 29, no. 4, pp. 606-650, Apr, 2010. DOI: https://doi.org/10.1002/mas.20258.

[54] H. Nikaido, "Molecular basis of bacterial outer membrane permeability revisited," *Microbiol. Mol. Biol. Rev.,* vol. 67, no. 4, pp. 593-656, Dec, 2003. DOI: https://doi.org/10.1128/MMBR.67.4.593-656.2003.

[55] N. Chaudhuri, and I. Sabroe, "Basic science of the innate immune system and the lung," *Paediatr. Respir. Rev.,* vol. 9, no. 4, pp. 236-242, Dec, 2008. DOI: https://doi.org/10.1016/j.prrv.2008.03.002.

[56] S. Ranf, "Immune sensing of lipopolysaccharide in plants and animals: Same but different," *PLoS Pathog.,* vol. 12, no. 6, pp. e1005596, Jun, 2016. DOI: https://doi.org/10.1371/journal.ppat.1005596.

[57] R. F. Maldonado, I. Sa-Correia, and M. A. Valvano, "Lipopolysaccharide modification in Gram-negative bacteria during chronic infection," *FEMS Microbiol. Rev.,* vol. 40, no. 4, pp. 480-493, Jul, 2016. DOI: https://doi.org/10.1093/femsre/fuw007.

[58] M. Matsuura, "Structural modifications of bacterial lipopolysaccharide that facilitate Gram-negative bacteria evasion of host innate immunity," *Front.*

Immunol., vol. 4, pp. 109, May, 2013. DOI: https://doi.org/10.3389/fimmu.2013.00109.

[59] B. W. Simpson, and M. S. Trent, "Pushing the envelope: LPS modifications and their consequences," *Nat. Rev. Microbiol.,* vol. 17, no. 7, pp. 403-416, Jul, 2019. DOI: https://doi.org/10.1038/s41579-019-0201-x.

[60] V. I. Band, and D. S. Weiss, "Mechanisms of antimicrobial peptide resistance in Gram-negative bacteria," *Antibiotics (Basel),* vol. 4, no. 1, pp. 18-41, Mar, 2015. DOI: https://doi.org/10.3390/antibiotics4010018.

[61] M. Caroff, and A. Novikov, "LPS Structure, function, and heterogeneity," *Endotoxin detection and control in pharma, limulus, and mammalian systems*, Springer International Publishing, 2019. pp. 53-93.

[62] J. Banoub, A. El Aneed, A. Cohen, and P. Martin, "Characterization of the O-4 phosphorylated and O-5 substituted Kdo reducing end group and sequencing of the core oligosaccharide of Aeromonas salmonicida ssp salmonicida lipopolysaccharide using tandem mass spectrometry," *Eur. J. Mass Spectrom.,* vol. 10, no. 5, pp. 715-730, May, 2004. DOI: https://doi.org/10.1255/ejms.673.

[63] J. H. Banoub, and D. H. Shaw, "Structural investigations on the core oligosaccharide of *Aeromonas hydrophila* (chemotype III) lipopolysaccharide," *Carbohydr. Res.,* vol. 98, no. 1, pp. 93-103, Dec, 1981. DOI: https://doi.org/10.1016/s0008-6215(00)87145-1.

[64] J. H. Banoub, Y. M. Choy, F. Michon, and D. H. Shaw, "Structural investigations on the core oligosaccharide of *Aeromonas hydrophila* (Chemotype II)

lipopolysaccharide," *Carbohydr. Res.,* vol. 114, no. 2, pp. 267-276, Apr, 1983. DOI: https://doi.org/10.1016/0008-6215(83)88193-2.

[65] M. S. Trent, "Biosynthesis and membrane assembly of lipid A," *Microb. Glycobiol.*, 2010. pp. 305-318.

[66] X. Xiao, K. Sankaranarayanan, and C. Khosla, "Biosynthesis and structure–activity relationships of the lipid a family of glycolipids," *Curr. Opin. Chem. Biol.,* vol. 40, pp. 127-137, Oct, 2017. DOI: https://doi.org/10.1016/j.cbpa.2017.07.008.

[67] A. Silipo, A. Molinaro, L. Sturiale, J. M. Dow, G. Erbs, R. Lanzetta, M. A. Newman, and M. Parrilli, "The elicitation of plant innate immunity by lipooligosaccharide of *Xanthomonas campestris*," *J Biol Chem,* vol. 280, no. 39, pp. 33660-33668, Sep, 2005. DOI: https://doi.org/10.1074/jbc.M506254200.

[68] J. N. Rapicavoli, B. Blanco-Ulate, A. Muszynski, R. Figueroa-Balderas, A. Morales-Cruz, P. Azadi, J. M. Dobruchowska, C. Castro, D. Cantu, and M. C. Roper, "Lipopolysaccharide O-antigen delays plant innate immune recognition of Xylella fastidiosa," *Nat. Commun.,* vol. 9, no. 1, pp. 390, Jan, 2018. DOI:10.1038/s41467-018-02861-5.

[69] M. Caroff, and D. Karibian, "Structure of bacterial lipopolysaccharides," *Carbohydr. Res.,* vol. 338, no. 23, pp. 2431-2447, Nov, 2003. DOI: https://doi.org/10.1016/j.carres.2003.07.010.

[70] K. A. Mattos, A. R. Todeschini, N. Heise, C. Jones, J. O. Previato, and L. Mendonca-Previato, "Nitrogen-fixing bacterium Burkholderia brasiliensis

produces a novel yersiniose A-containing O-polysaccharide," *Glycobiology,* vol. 15, no. 3, pp. 313-321, Mar, 2005. DOI: https://doi.org/10.1093/glycob/cwi009.

[71] L. L. MacLean, M. B. Perry, and E. Vinogradov, "Characterization of the antigenic lipopolysaccharide O chain and the capsular polysaccharide produced by *Actinobacillus pleuropneumoniae* serotype 13," *Infect. Immun.,* vol. 72, no. 10, pp. 5925-5930, Oct, 2004. DOI: https://doi.org/10.1128/IAI.72.10.5925-5930.2004.

[72] E. Vinogradov, L. Nossova, M. B. Perry, and W. W. Kay, "Structural characterization of the O-polysaccharide antigen of *Edwardsiella tarda MT 108*," *Carbohydr. Res.,* vol. 340, no. 1, pp. 85-90, Jan, 2005. DOI: https://doi.org/10.1016/j.carres.2004.10.015.

[73] L. S. Forsberg, and R. W. Carlson, "The structures of the lipopolysaccharides from *Rhizobium etli* strains CE358 and CE359. The complete structure of the core region of R. etli lipopolysaccharides," *J. Biol. Chem.,* vol. 273, no. 5, pp. 2747-2757, Jan, 1998. DOI: https://doi.org/10.1074/jbc.273.5.2747.

[74] L. L. MacLean, A. C. Webb, and M. B. Perry, "Structural elucidation of the O-antigenic polysaccharide from enterohemorrhagic (EHEC) *Escherichia coli* O48:H21," *Carbohydr. Res.,* vol. 341, no. 15, pp. 2543-2549, Nov, 2006. DOI: https://doi.org/10.1016/j.carres.2006.08.008.

[75] E. Vinogradov, and M. Caroff, "Structure of the Bordetella trematum LPS O-chain subunit," *FEBS Lett.,* vol. 579, no. 1, pp. 18-24, Jan, 2005. DOI: https://doi.org/10.1016/j.febslet.2004.11.040.

[76] E. Vinogradov, "Structure of the O-specific polysaccharide chain of the lipopolysaccharide of *Bordetella hinzii*," *Carbohydr. Res.,* vol. 337, no. 10, pp. 961-963, May, 2002. DOI: https://doi.org/10.1016/s0008-6215(02)00071-x.

[77] J. Kumirska, J. Szafranek, M. Czerwicka, M. Paszkiewicz, H. Dziadziuszko, D. Kunikowska, and P. Stepnowski, "The structure of the O-polysaccharide isolated from the lipopolysaccharide of Salmonella Dakar (serogroup O:28)," *Carbohydr. Res.,* vol. 342, no. 14, pp. 2138-2143, Oct, 2007. DOI: https://doi.org/10.1016/j.carres.2007.05.035.

[78] S. Larocque, J. R. Brisson, H. Therisod, M. B. Perry, and M. Caroff, "Structural characterization of the O-chain polysaccharide isolated from Bordetella avium ATCC 5086: variation on a theme(1)," *FEBS Lett.,* vol. 535, no. 1-3, pp. 11-16, Jan, 2003. DOI: https://doi.org/10.1016/s0014-5793(02)03843-7.

[79] R. Eserstam, T. P. Rajaguru, P. E. Jansson, A. Weintraub, and M. J. Albert, "The structure of the O-chain of the lipopolysaccharide of a prototypal diarrheagenic strain of *Hafnia alvei* that has characteristics of a new species under the genus *Escherichia*," *Eur. J. Biochem.,* vol. 269, no. 13, pp. 3289-3295, Jul, 2002. DOI: https://doi.org/10.1046/j.1432-1033.2002.03009.x.

[80] O. Kooistra, E. Luneberg, Y. A. Knirel, M. Frosch, and U. Zahringer, "N-Methylation in polylegionaminic acid is associated with the phase-variable epitope of *Legionella pneumophila serogroup 1* lipopolysaccharide. Identification of 5-(N,N-dimethylacetimidoyl)amino and 5-acetimidoyl(N-methyl)amino-7-acetamido-3,5,7,9-tetradeoxynon-2-ulosonic acid in the O-chain polysaccharide,"

Eur. J. Biochem., vol. 269, no. 2, pp. 560-572, Jan, 2002. DOI: https://doi.org/10.1046/j.0014-2956.2001.02683.x.

[81] E. Vinogradov, A. Korenevsky, and T. J. Beveridge, "The structure of the O-specific polysaccharide chain of the *Shewanella algae BrY* lipopolysaccharide," *Carbohydr. Res.,* vol. 338, no. 4, pp. 385-388, Feb, 2003. DOI: https://doi.org/10.1016/s0008-6215(02)00469-x.

[82] S. E. Paradis, D. Dubreuil, S. Rioux, M. Gottschalk, and M. Jacques, "High-molecular-mass lipopolysaccharides are involved in Actinobacillus pleuropneumoniae adherence to porcine respiratory tract cells," *Infect. Immun.,* vol. 62, no. 8, pp. 3311-3319, Aug, 1994. DOI: https://doi.org/10.1128/iai.62.8.3311-3319.1994.

[83] A. Banemann, H. Deppisch, and R. Gross, "The lipopolysaccharide of Bordetella bronchiseptica acts as a protective shield against antimicrobial peptides," *Infect. Immun.,* vol. 66, no. 12, pp. 5607-5612, Dec, 1998. DOI: https://doi.org/10.1128/IAI.66.12.5607-5612.1998.

[84] B. Bertani, and N. Ruiz, "Function and biogenesis of lipopolysaccharides," *EcoSal. Plus.,* vol. 8, no. 1, Aug, 2018. DOI: https://doi.org/10.1128/ecosalplus.ESP-0001-2018.

[85] S. Kim, Dhilon S. Patel, S. Park, J. Slusky, Jeffery B. Klauda, G. Widmalm, and W. Im, "Bilayer properties of lipid a from various Gram-negative bacteria," *Biophys. J.,* vol. 111, no. 8, pp. 1750-1760, Jun, 2016. DOI: https://doi.org/10.1016/j.bpj.2016.09.001.

[86] B. M. Plotz, B. Lindner, K. O. Stetter, and O. Holst, "Characterization of a novel lipid A containing D-galacturonic acid that replaces phosphate residues. The structure of the lipid a of the lipopolysaccharide from the hyperthermophilic bacterium *Aquifex pyrophilus*," *J. Biol. Chem.,* vol. 275, no. 15, pp. 11222-11228, Apr, 2000. DOI: https://doi.org/10.1074/jbc.275.15.11222.

[87] N. Qureshi, K. Takayama, U. Seydel, R. Wang, R. J. Cotter, P. K. Agrawal, C. A. Bush, R. Kurtz, and D. T. Berman, "Structural analysis of the lipid A derived from the lipopolysaccharide of *Brucella abortus*," *J. Endotoxin Res.,* vol. 1, no. 3, pp. 137-148, 1994. DOI: https://doi.org/10.1177/096805199400100303.

[88] S. Beck, F. D. Muller, E. Strauch, L. Brecker, and M. W. Linscheid, "Chemical structure of *Bacteriovorax stolpii* lipid A," *Lipids,* vol. 45, no. 2, pp. 189-198, Feb, 2010. DOI: https://doi.org/10.1007/s11745-010-3383-6.

[89] J. Smit, I. A. Kaltashov, R. J. Cotter, E. Vinogradov, M. B. Perry, H. Haider, and N. Qureshi, "Structure of a novel lipid A obtained from the lipopolysaccharide of *Caulobacter crescentus*," *Innate Immun.,* vol. 14, no. 1, pp. 25-37, Feb, 2008. DOI: https://doi.org/10.1177/1753425907087588.

[90] A. Choma, and P. Sowinski, "Characterization of *Mesorhizobium huakuii* lipid A containing both D-galacturonic acid and phosphate residues," *Eur. J. Biochem.,* vol. 271, no. 7, pp. 1310-1322, Apr, 2004. DOI: https://doi.org/10.1111/j.1432-1033.2004.04038.x.

[91] I. Komaniecka, A. Choma, B. Lindner, and O. Holst, "The structure of a novel neutral lipid A from the lipopolysaccharide of *Bradyrhizobium elkanii* containing

three mannose units in the backbone," *Chemistry,* vol. 16, no. 9, pp. 2922-2929, Mar, 2010. DOI: https://doi.org/10.1002/chem.200902390.

[92] U. Zähringer, B. Lindner, Y. A. Knirel, W. M. R. Van Den Akker, R. Hiestand, H. Heine, and C. Dehio, "Structure and biological activity of the short-chain lipopolysaccharide from *Bartonella henselae* ATCC 49882T," *J. Biol. Chem.,* vol. 279, no. 20, pp. 21046-21054, Feb, 2004. DOI: https://doi.org/10.1074/jbc.m313370200.

[93] U. Zahringer, Y. A. Knirel, B. Lindner, J. H. Helbig, A. Sonesson, R. Marre, and E. T. Rietschel, "The lipopolysaccharide of *Legionella pneumophila* serogroup 1 (strain Philadelphia 1): chemical structure and biological significance," *Prog. Clin. Biol. Res.,* vol. 392, no. 1, pp. 113-139, 1995.

[94] A. van Mourik, L. Steeghs, J. van Laar, H. D. Meiring, H. J. Hamstra, J. P. van Putten, and M. M. Wosten, "Altered linkage of hydroxyacyl chains in lipid A of *Campylobacter jejuni* reduces TLR4 activation and antimicrobial resistance," *J. Biol. Chem.,* vol. 285, no. 21, pp. 15828-15836, May, 2010. DOI: https://doi.org/10.1074/jbc.M110.102061.

[95] S. Leone, A. Molinaro, E. Pessione, R. Mazzoli, C. Giunta, L. Sturiale, D. Garozzo, R. Lanzetta, and M. Parrilli, "Structural elucidation of the core-lipid A backbone from the lipopolysaccharide of *Acinetobacter* radioresistens S13, an organic solvent tolerant Gram-negative bacterium," *Carbohydr. Res.,* vol. 341, no. 5, pp. 582-590, Apr, 2006. DOI: https://doi.org/10.1016/j.carres.2006.01.016.

[96] E. Fregolino, G. Fugazza, E. Galano, V. Gargiulo, P. Landini, R. Lanzetta, B. Lindner, L. Pagani, M. Parrilli, O. Holst, and C. De Castro, "Complete lipooligosaccharide structure of the clinical isolate *Acinetobacter baumannii*, Strain SMAL," *Eur. J. Org. Chem.,* vol. 2010, no. 7, pp. 1345-1352, 2010. DOI: https://doi.org/10.1002/ejoc.200901396.

[97] Z. Wang, J. Li, and E. Altman, "Structural characterization of the lipid A region of *Aeromonas salmonicida* subsp. salmonicida lipopolysaccharide," *Carbohydr. Res.,* vol. 341, no. 17, pp. 2816-2825, Dec, 2006. DOI: https://doi.org/10.1016/j.carres.2006.09.020.

[98] A. Silipo, C. De Castro, R. Lanzetta, A. Molinaro, and M. Parrilli, "Full structural characterization of the lipid A components from the *Agrobacterium tumefaciens* strain C58 lipopolysaccharide fraction," *Glycobiology,* vol. 14, no. 9, pp. 805-815, Sep, 2004. DOI: https://doi.org/10.1093/glycob/cwh096.

[99] V. Liparoti, A. Molinaro, L. Sturiale, D. Garozzo, E. L. Nazarenko, R. P. Gorshkova, E. P. Ivanova, L. S. Shevcenko, R. Lanzetta, and M. Parrilli, "Structural analysis of the deep rough lipopolysaccharide from Gram-negative bacterium *Alteromonas macleodii* ATCC 27126T: the first finding of β-Kdo in the inner core of lipopolysaccharides," *Eur. J. Org. Chem.,* vol. 2006, no. 20, pp. 4710-4716, 2006. DOI: https://doi.org/10.1002/ejoc.200600489.

[100] A. Choma, and I. Komaniecka, "Characterization of a novel lipid A structure isolated from *Azospirillum lipoferum* lipopolysaccharide," *Carbohydr. Res.,* vol.

343, no. 4, pp. 799-804, Mar, 2008. DOI: https://doi.org/10.1016/j.carres.2008.01.006.

[101] N. Marr, A. Tirsoaga, D. Blanot, R. Fernandez, and M. Caroff, "Glucosamine found as a substituent of both phosphate groups in *Bordetella* lipid A backbones: role of a BvgAS-activated ArnT ortholog," *J. Bacteriol.,* vol. 190, no. 12, pp. 4281-4290, Jun, 2008. DOI: https://doi.org/10.1128/jb.01875-07.

[102] A. De Soyza, A. Silipo, R. Lanzetta, J. R. Govan, and A. Molinaro, "Chemical and biological features of *Burkholderia cepacia* complex lipopolysaccharides," *Innate Immun.,* vol. 14, no. 3, pp. 127-144, Jun, 2008. DOI: https://doi.org/10.1177/1753425908093984.

[103] S. Rund, B. Lindner, H. Brade, and O. Holst, "Structural analysis of the lipopolysaccharide from *Chlamydia trachomatis* serotype L2," *J. Biol. Chem.,* vol. 274, no. 24, pp. 16819-16824, Jun, 1999. DOI: https://doi.org/10.1074/jbc.274.24.16819.

[104] R. Toman, P. Garidel, J. Andra, K. Slaba, A. Hussein, M. H. Koch, and K. Brandenburg, "Physicochemical characterization of the endotoxins from *Coxiella burnetii* strain Priscilla in relation to their bioactivities," *BMC Biochem.,* vol. 5, no. 1, pp. 1, Jan, 2004. DOI: https://doi.org/10.1186/1471-2091-5-1.

[105] W. Kay, B. O. Petersen, J. O. Duus, M. B. Perry, and E. Vinogradov, "Characterization of the lipopolysaccharide and beta-glucan of the fish pathogen *Francisella victoria*," *FEBS J.,* vol. 273, no. 13, pp. 3002-3013, Jul, 2006. DOI: https://doi.org/10.1111/j.1742-4658.2006.05311.x.

[106] Y. Asai, Y. Makimura, A. Kawabata, and T. Ogawa, “Soluble CD14 discriminates slight structural differences between lipid as that lead to distinct host cell activation,” *J. Immunol.,* vol. 179, no. 11, pp. 7674-7683, Dec, 2007. DOI: https://doi.org/10.4049/jimmunol.179.11.7674.

[107] J. Lukasiewicz, W. Jachymek, T. Niedziela, L. Kenne, and C. Lugowski, “Structural analysis of the lipid A isolated from *Hafnia alvei* 32 and PCM 1192 lipopolysaccharides,” *J. Lipid Res.,* vol. 51, no. 3, pp. 564-574, Mar, 2010. DOI: https://doi.org/10.1194/jlr.M001362.

[108] A. Silipo, L. Sturiale, D. Garozzo, Cristina d. Castro, R. Lanzetta, M. Parrilli, William D. Grant, and A. Molinaro, “Structure elucidation of the highly heterogeneous lipid a from the lipopolysaccharide of the gram-negative extremophile bacterium *Halomonas Magadiensis* Strain 21 M1,” *Eur. J. Org. Chem.,* vol. 2004, no. 10, pp. 2263-2271, 2004. DOI: https://doi.org/10.1002/ejoc.200400048.

[109] N. L. Que-Gewirth, A. A. Ribeiro, S. R. Kalb, R. J. Cotter, D. M. Bulach, B. Adler, I. S. Girons, C. Werts, and C. R. Raetz, “A methylated phosphate group and four amide-linked acyl chains in *leptospira interrogans* lipid A. The membrane anchor of an unusual lipopolysaccharide that activates TLR2,” *J. Biol. Chem.,* vol. 279, no. 24, pp. 25420-25429, Jun, 2004. DOI: https://doi.org/10.1074/jbc.M400598200.

[110] I. N. Krasikova, N. V. Kapustina, V. V. Isakov, A. S. Dmitrenok, P. S. Dmitrenok, N. M. Gorshkova, and T. F. Solov'eva, “Detailed structure of lipid A isolated from lipopolysaccharide from the marine *proteobacterium Marinomonas vaga* ATCC

27119," *Eur. J. Biochem.,* vol. 271, no. 14, pp. 2895-2904, Jul, 2004. DOI: https://doi.org/10.1111/j.1432-1033.2004.04212.x.

[111] H. Kumada, Y. Haishima, T. Umemoto, and K. Tanamoto, "Structural study on the free lipid A isolated from lipopolysaccharide of *Porphyromonas gingivalis*," *J. Bacteriol.,* vol. 177, no. 8, pp. 2098-2106, Apr, 1995. DOI: https://doi.org/10.1128/jb.177.8.2098-2106.1995.

[112] I. N. Krasikova, N. V. Kapustina, V. I. Svetashev, R. P. Gorshkova, S. V. Tomshich, E. L. Nazarenko, N. A. Komandrova, E. P. Ivanova, N. M. Gorshkova, L. A. Romanenko, V. V. Mikhailov, and T. F. Solov'eva, "Chemical characterization of lipid A from some marine proteobacteria," *Biochemistry (Mosc),* vol. 66, no. 9, pp. 1047-1054, Sep, 2001. DOI: https://doi.org/10.1023/a:1012338113514.

[113] A. B. Schromm, K. Brandenburg, H. Loppnow, A. P. Moran, M. H. Koch, E. T. Rietschel, and U. Seydel, "Biological activities of lipopolysaccharides are determined by the shape of their lipid A portion," *Eur. J. Biochem.,* vol. 267, no. 7, pp. 2008-2013, Apr, 2000. DOI: https://doi.org/10.1046/j.1432-1327.2000.01204.x.

[114] S. Leone, A. Molinaro, C. De Castro, A. Baier, E. L. Nazarenko, R. Lanzetta, and M. Parrilli, "Absolute configuration of 8-Amino-3,8-dideoxyoct-2-ulosonic acid, the chemical hallmark of lipopolysaccharides of the genus Shewanella," *J. Nat. Prod.,* vol. 70, no. 10, pp. 1624-1627, Oct, 2007. DOI: https://doi.org/10.1021/np0702988.

[115] C. De Castro, A. Molinaro, R. Lanzetta, A. Silipo, and M. Parrilli, "Lipopolysaccharide structures from *Agrobacterium* and *Rhizobiaceae* species," *Carbohydr. Res.,* vol. 343, no. 12, pp. 1924-1933, Aug, 2008. DOI: https://doi.org/10.1016/j.carres.2008.01.036.

[116] N. L. Que, S. Lin, R. J. Cotter, and C. R. Raetz, "Purification and mass spectrometry of six lipid A species from the bacterial endosymbiont *Rhizobium etli.* Demonstration of a conserved distal unit and a variable proximal portion," *J. Biol. Chem.,* vol. 275, no. 36, pp. 28006-28016, Sep, 2000. DOI: https://doi.org/10.1074/jbc.M004008200.

[117] O. Takeuchi, and S. Akira, "Pattern recognition receptors and inflammation," *Cell,* vol. 140, no. 6, pp. 805-820, Mar, 2010. DOI:10.1016/j.cell.2010.01.022.

[118] L. Vernacchio, H. Bernstein, S. Pelton, C. Allen, K. MacDonald, J. Dunn, D. D. Duncan, G. Tsao, V. LaPosta, J. Eldridge, S. Laussucq, D. M. Ambrosino, and D. C. Molrine, "Effect of monophosphoryl lipid A (MPL) on T-helper cells when administered as an adjuvant with *pneumococcoccal*-CRM197 conjugate vaccine in healthy toddlers," *Vaccine,* vol. 20, no. 31-32, pp. 3658-3667, Nov, 2002. DOI: https://doi.org/10.1016/s0264-410x(02)00413-9.

[119] C. W. Cluff, "Monophosphoryl lipid A (MPL) as an adjuvant for anti-cancer vaccines: clinical results," Springer New York, 2009. pp. 111-123.

[120] V. Mata-Haro, C. Cekic, M. Martin, P. M. Chilton, C. R. Casella, and T. C. Mitchell, "The vaccine adjuvant monophosphoryl lipid A as a TRIF-biased agonist of TLR4,"

Science, vol. 316, no. 5831, pp. 1628-1632, Jun, 2007. DOI: https://doi.org/10.1126/science.1138963.

[121] J. J. Zik, S. H. Yoon, Z. Guan, G. Stankeviciute Skidmore, R. R. Gudoor, K. M. Davies, A. M. Deutschbauer, D. R. Goodlett, E. A. Klein, and K. R. Ryan, "Caulobacter lipid A is conditionally dispensable in the absence of fur and in the presence of anionic sphingolipids," *Cell. Rep.,* vol. 39, no. 9, pp. 110888, May, 2022. DOI: https://doi.org/10.1016/j.celrep.2022.110888.

[122] M. S. Trent, "Biosynthesis, transport, and modification of lipid A," *Biochem. Cell Biol.,* vol. 82, no. 1, pp. 71-86, Feb, 2004. DOI: https://doi.org/10.1139/o03-070.

[123] C. R. Raetz, C. M. Reynolds, M. S. Trent, and R. E. Bishop, "Lipid A modification systems in Gram-negative bacteria," *Annu. Rev. Biochem.,* vol. 76, pp. 295-329, Feb, 2007. DOI: https://doi.org/10.1515/cclm-2019-0868.

[124] C. R. Raetz, Z. Guan, B. O. Ingram, D. A. Six, F. Song, X. Wang, and J. Zhao, "Discovery of new biosynthetic pathways: the lipid A story," *J. Lipid Res.,* vol. 50 Suppl, no. Suppl, pp. S103-108, Apr, 2009. DOI: https://doi.org/10.1194/jlr.R800060-JLR200.

[125] A. Emiola, J. George, and S. S. Andrews, "A complete pathway model for lipid a biosynthesis in *Escherichia coli*," *PLOS One,* vol. 10, no. 4, pp. e0121216, Apr, 2014. DOI: https://doi.org/10.1371/journal.pone.0121216.

[126] R. E. Bishop, "Lipid A," *Handbook of hydrocarbon and lipid microbiology*, Springer Berlin Heidelberg, 2010. pp. 409-416.

[127] S. O. Opiyo, R. L. Pardy, H. Moriyama, and E. N. Moriyama, “Evolution of the Kdo2-lipid A biosynthesis in bacteria,” *BMC Evol. Biol.,* vol. 10, no. 1, pp. 362, Nov, 2010. DOI: https://doi.org/10.1186/1471-2148-10-362.

[128] R. E. Bishop, "Lipid A," Springer International Publishing, 2016. pp. 1-12.

[129] B. L. Ray, G. Painter, and C. R. Raetz, “The biosynthesis of Gram-negative endotoxin. Formation of lipid A disaccharides from monosaccharide precursors in extracts of *Escherichia coli*,” *J. Biol. Chem.,* vol. 259, no. 8, pp. 4852-4859, Apr, 1984. DOI:https://doi.org/10.1016/S0021-9258(17)42924-3.

[130] K. A. Brozek, K. Hosaka, A. D. Robertson, and C. R. Raetz, “Biosynthesis of lipopolysaccharide in *Escherichia coli*. Cytoplasmic enzymes that attach 3-deoxy-D-manno-octulosonic acid to lipid A,” *J. Biol. Chem.,* vol. 264, no. 12, pp. 6956-6966, Apr, 1989. DOI: https://doi.org/10.1016/s0021-9258(18)83524-4.

[131] C. J. Belunis, and C. R. Raetz, “Biosynthesis of endotoxins. Purification and catalytic properties of 3-deoxy-D-manno-octulosonic acid transferase from *Escherichia coli*,” *J. Biol. Chem.,* vol. 267, no. 14, pp. 9988-9997, May, 1992.

[132] T. Clementz, J. J. Bednarski, and C. R. Raetz, “Function of the htrB high temperature requirement gene of *Escherichia co*li in the acylation of lipid A: HtrB catalyzed incorporation of laurate,” *J. Biol. Chem.,* vol. 271, no. 20, pp. 12095-12102, May, 1996. DOI: https://doi.org/10.1074/jbc.271.20.12095.

[133] T. Clementz, Z. Zhou, and C. R. Raetz, “Function of the *Escherichia coli* msbB gene, a multicopy suppressor of htrB knockouts, in the acylation of lipid A. Acylation by MsbB follows laurate incorporation by HtrB,” *J. Biol. Chem.,* vol.

272, no. 16, pp. 10353-10360, Apr, 1997. DOI: https://doi.org/10.1074/jbc.272.16.10353.

[134] P. S. Padayatti, S. C. Lee, R. L. Stanfield, P. C. Wen, E. Tajkhorshid, I. A. Wilson, and Q. Zhang, "Structural insights into the lipid A transport pathway in MsbA," *Structure,* vol. 27, no. 7, pp. 1114-1123 e1113, Jul, 2019. DOI: https://doi.org/10.1016/j.str.2019.04.007.

[135] Z. Zhou, S. Lin, R. J. Cotter, and C. R. Raetz, "Lipid A modifications characteristic of Salmonella typhimurium are induced by NH4VO3 in Escherichia coli K12. Detection of 4-amino-4-deoxy-L-arabinose, phosphoethanolamine and palmitate," *J. Biol. Chem.,* vol. 274, no. 26, pp. 18503-18514, Jun, 1999. DOI: https://doi.org/10.1074/jbc.274.26.18503.

[136] B. D. Needham, and M. S. Trent, "Fortifying the barrier: the impact of lipid A remodelling on bacterial pathogenesis," *Nat. Rev. Microbiol.,* vol. 11, no. 7, pp. 467-481, Jul, 2013. DOI:10.1038/nrmicro3047.

[137] K. Kawahara, "Variation, modification and engineering of lipid A in endotoxin of Gram-negative bacteria," *Int. J. Mol. Sci.,* vol. 22, no. 5, pp. 1-15, Feb, 2021. DOI: https://doi.org/10.3390/ijms22052281.

[138] D. H. Persing, R. N. Coler, M. J. Lacy, D. A. Johnson, J. R. Baldridge, R. M. Hershberg, and S. G. Reed, "Taking toll: lipid A mimetics as adjuvants and immunomodulators," *Trends Microbiol.,* vol. 10, no. 10 Suppl, pp. S32-37, Oct, 2002. DOI: https://doi.org/10.1016/s0966-842x(02)02426-5.

[139] E. F. Eckel, and B. N. Ametaj, “Bacterial endotoxins and their role in periparturient diseases of dairy cows: mucosal vaccine perspectives,” *Dairy,* vol. 1, no. 1, pp. 61-90, May, 2020. DOI: https://doi.org/10.3390/dairy1010006.

[140] M. S. Trent, C. M. Stead, A. X. Tran, and J. V. Hankins, “Diversity of endotoxin and its impact on pathogenesis,” *J. Endotoxin Res.,* vol. 12, no. 4, pp. 205-223, 2006. DOI: https://doi.org/10.1179/096805106X118825.

[141] A. Shimoyama, and K. Fukase, “Lipid A-mediated bacterial-host chemical ecology: Synthetic research of bacterial lipid As and their development as adjuvants,” *Molecules,* vol. 26, no. 20, pp. 6294-6294, Oct, 2021. DOI: https://doi.org/10.3390/molecules26206294.

[142] A. Zamyatina, and S. Strobl, "Synthesis of bioactive lipid A and analogs," *Recent trends in carbohydrate chemistry*, Elsevier Inc., 2020. pp. 51-102.

[143] H. Heine, and A. Zamyatina, “Therapeutic targeting of TLR4 for inflammation, infection, and cancer: A perspective for disaccharide lipid A mimetics,” *Pharmaceuticals (Basel),* vol. 16, no. 1, pp. 23, Dec, 2022. DOI: https://doi.org/10.3390/ph16010023.

[144] C. R. Alving, “Lipopolysaccharide, lipid A, and liposomes containing lipid A as immunologic adjuvants,” *Immunobiology,* vol. 187, no. 3-5, pp. 430-446, 1993. DOI: https://doi.org/10.1016/s0171-2985(11)80355-4.

[145] Y. Torres-Corral, A. Girons, O. Gonzalez-Barreiro, R. Seoane, A. Riaza, and Y. Santos, “Effect of bivalent Vaccines against *Vibrio anguillarum* and *Aeromonas salmonicida* Subspecie achromogenes on health and survival of Turbot,” *Vaccines*

(Basel), vol. 9, no. 8, pp. 906, Aug, 2021. DOI: https://doi.org/10.3390/vaccines9080906.

[146] J. A. Hammerl, J. M. Ritchie, F. Leoni, S. Banerjee, and E. Strauch, “Editorial: Molecular adaptations of vibrionaceae to changing environments, volume ii,” *Front. Microbiol.,* vol. 13, pp. 863038, Mar, 2022. DOI: https://doi.org/10.3389/fmicb.2022.863038.

[147] M. E. Martino, L. Fasolato, and B. Cardazzo, "*Aeromonas*," *Encyclopedia of food and health*, 2016. pp. 61-67.

[148] M. D’Agostino, and N. Cook, "Foodborne pathogens," *Encyclopedia of food and health*, 2016. pp. 83-86.

[149] A. N. Schuetz, “Emerging agents of gastroenteritis: *Aeromonas, Plesiomonas, and the diarrheagenic* pathotypes of Escherichia coli,” *Semin Diagn. Pathol.,* vol. 36, no. 3, pp. 187-192, May, 2019. DOI: https://doi.org/10.1053/j.semdp.2019.04.012.

[150] G. Huys, "The family *Aeromonadaceae*," *The prokaryotes*, Springer Berlin Heidelberg, 2014. pp. 27-57.

[151] J. M. Tomas, “The main Aeromonas pathogenic factors,” *ISRN Microbiol,* vol. 2012, pp. 256261, Sep, 2012. DOI: https://doi.org/10.5402/2012/256261.

[152] A. Sadique, S. B. Neogi, T. Bashar, M. Sultana, F. T. Johura, S. Islam, N. A. Hasan, A. Huq, R. R. Colwell, and M. Alam, “Dynamics, diversity, and virulence of *Aeromonas* spp. in homestead pond water in coastal bangladesh,” *Front. Public Health,* vol. 9, pp. 692166, Jul, 2021. DOI: https://doi.org/10.3389/fpubh.2021.692166.

[153] D. Stratev, and O. A. Odeyemi, “Antimicrobial resistance of *Aeromonas hydrophila* isolated from different food sources: A mini-review,” *J. Infect. Public Health,* vol. 9, no. 5, pp. 535-544, Sep-Oct, 2016. DOI: https://doi.org/10.1016/j.jiph.2015.10.006.

[154] A. Semwal, A. Kumar, and N. Kumar, “A review on pathogenicity of *Aeromonas hydrophila* and their mitigation through medicinal herbs in aquaculture,” *Heliyon,* vol. 9, no. 3, pp. e14088, Mar, 2023. DOI: https://doi.org/10.1016/j.heliyon.2023.e14088.

[155] M. Pang, J. Jiang, X. Xie, Y. Wu, Y. Dong, A. H. Kwok, W. Zhang, H. Yao, C. Lu, F. C. Leung, and Y. Liu, “Novel insights into the pathogenicity of epidemic *Aeromonas hydrophila* ST251 clones from comparative genomics,” *Sci. Rep.,* vol. 5, no. 1, pp. 9833, May, 2015. DOI: https://doi.org/10.1038/srep09833.

[156] A. K. Bhunia, "Opportunistic and emerging foodborne pathogens: *Aeromonas hydrophila*, *Plesiomonas shigelloides, Cronobacter sakazakii, and Brucella abortus*," *Foodborne microbial pathogens*, Food Science Text Series Springer New York, 2018. pp. 343-350.

[157] C. R. Rasmussen-Ivey, M. J. Figueras, D. McGarey, and M. R. Liles, “Virulence factors of *Aeromonas hydrophila*: In the wake of reclassification,” *Front. Microbiol.,* vol. 7, pp. 1337, Aug, 2016. DOI: https://doi.org/10.3389/fmicb.2016.01337.

[158] A. F. Takemura, D. M. Chien, and M. F. Polz, “Associations and dynamics of Vibrionaceae in the environment, from the genus to the population level,” *Front*

Microbiol, vol. 5, no. FEB, pp. 38, Feb, 2014. DOI: https://doi.org/10.3389/fmicb.2014.00038.

[159] A. Palit, and G. B. Nair, "Bacteria: Other vibrios," *Encyclopedia of food safety*, 2014. pp. 570-573.

[160] R. Dryselius, K. Kurokawa, and T. Iida, "Vibrionaceae, a versatile bacterial family with evolutionarily conserved variability," *Res. Microbiol.,* vol. 158, no. 6, pp. 479-486, Jul-Aug, 2007. DOI: https://doi.org/10.1016/j.resmic.2007.04.007.

[161] B. Rajan, J. Lokesh, V. Kiron, and M. F. Brinchmann, "Differentially expressed proteins in the skin mucus of Atlantic cod (*Gadus morhua*) upon natural infection with Vibrio anguillarum," *BMC Vet. Res.,* vol. 9, no. 1, pp. 103, May, 2013. DOI: https://doi.org/10.1186/1746-6148-9-103.

[162] M. Bekaert, N. Goffin, S. McMillan, and A. P. Desbois, "Essential Genes of *Vibrio anguillarum* and Other Vibrio spp. Guide the Development of New Drugs and Vaccines," *Front. Microbiol.,* vol. 12, pp. 755801, Oct, 2021. DOI: https://doi.org/10.3389/fmicb.2021.755801.

[163] J. H. Gross, *Mass spectrometry: A textbook*, 3 ed., Cham, Switzerland:Springer International Publishing, 2017.

[164] A. El-Aneed, A. Cohen, and J. Banoub, "Mass spectrometry, review of the basics: electrospray, maldi, and commonly used mass analyzers," *Appl. Spectrosc. Rev.,* vol. 44, no. 3, pp. 210-230, May, 2009. DOI: https://doi.org/10.1080/05704920902717872.

[165] M. Ibáñez, J. V. Sancho, L. Bijlsma, A. L. N. van Nuijs, A. Covaci, and F. Hernández, "Comprehensive analytical strategies based on high-resolution time-of-flight mass spectrometry to identify new psychoactive substances," *TrAC, Trends Anal. Chem.,* vol. 57, pp. 107-117, May, 2014. DOI: https://doi.org/10.1016/j.trac.2014.02.009.

[166] A. K. Meher, and Y. C. Chen, "Analysis of volatile compounds by open-air ionization mass spectrometry," *Anal. Chim. Acta.,* vol. 966, pp. 41-46, May, 2017. DOI: https://doi.org/10.1016/j.aca.2017.03.005.

[167] D. R. Letourneau, and D. A. Volmer, "Mass spectrometry-based methods for the advanced characterization and structural analysis of lignin: A review," *Mass Spectrom. Rev.*, pp. mas.21716-mas.21716, Jun, 2021. DOI: https://doi.org/10.1002/mas.21716.

[168] A. Mikhael, "Mass spectrometric structural elucidation of Sporopollenin and Lignin," Chemistry department, Memorial university, Canada, 2021.

[169] I. K. Perera, J. Perkins, and S. Kantartzoglou, "Spin-coated samples for high resolution matrix-assisted laser desorption/ionization time-of-flight mass spectrometry of large proteins," *Rapid Commun. Mass Spectrom.,* vol. 9, no. 2, pp. 180-187, Dec, 2005. DOI: https://doi.org/10.1002/rcm.1290090215.

[170] I. Ojanpera, M. Kolmonen, and A. Pelander, "Current use of high-resolution mass spectrometry in drug screening relevant to clinical and forensic toxicology and doping control," *Anal. Bioanal. Chem.,* vol. 403, no. 5, pp. 1203-1220, May, 2012. DOI: https://doi.org/10.1007/s00216-012-5726-z.

[171] R. J. B. Peters, A. A. M. Stolker, J. G. J. Mol, A. Lommen, E. Lyris, Y. Angelis, A. Vonaparti, M. Stamou, C. Georgakopoulos, and M. W. F. Nielen, "Screening in veterinary drug analysis and sports doping control based on full-scan, accurate-mass spectrometry," *TrAC, Trends Anal. Chem.,* vol. 29, no. 11, pp. 1250-1268, Dec, 2010. DOI: https://doi.org/10.1016/j.trac.2010.07.012.

[172] G. Hopfgartner, D. Tonoli, and E. Varesio, "High-resolution mass spectrometry for integrated qualitative and quantitative analysis of pharmaceuticals in biological matrices," *Anal. Bioanal. Chem.,* vol. 402, no. 8, pp. 2587-2596, Mar, 2012. DOI: https://doi.org/10.1007/s00216-011-5641-8.

[173] Agnieszka Kraj, D. M. Desiderio, and N. M. Nibbering, *Mass spectrometry: instrumentation, interpretation, and applications*, John Wiley & Sons, 2008.

[174] E. Hoffmann, and V. Stroobant, *Mass spectrometry principles and applications*, 3 ed., 2016.

[175] A. Mikhael, D. Hardie, D. Smith, H. Petrosova, R. K. Ernst, and D. R. Goodlett, "Structural elucidation of intact rough-type lipopolysaccharides using field asymmetric ion mobility spectrometry and Kendrick mass defect plots," *Analy. Chem.,* vol. 95, no. 46, pp. 16796–16800, Jul, 2023. DOI: https://doi.org/10.1021/acs.analchem.3c02947.

[176] G. J. Van Berkel, "An overview of some recent developments in ionization methods for mass spectrometry," *Eur. J. Mass Spectrom.,* vol. 9, no. 6, pp. 539-562, Feb, 2003. DOI: https://doi.org/10.1255/ejms.586.

[177] T. Portoles, E. Pitarch, F. J. Lopez, F. Hernandez, and W. M. Niessen, “Use of soft and hard ionization techniques for elucidation of unknown compounds by gas chromatography/time-of-flight mass spectrometry,” *Rapid Commun. Mass Spectrom.,* vol. 25, no. 11, pp. 1589-1599, Jun, 2011. DOI: https://doi.org/10.1002/rcm.5028.

[178] Y. Wang, J. Sun, J. Qiao, J. Ouyang, and N. Na, “A "Soft" and "Hard" ionization method for comprehensive studies of molecules,” *Anal. Chem.,* vol. 90, no. 24, pp. 14095-14099, Dec, 2018. DOI: https://doi.org/10.1021/acs.analchem.8b04437.

[179] V. Gabelica, and E. De Pauw, “Internal energy and fragmentation of ions produced in electrospray sources,” *Mass Spectrom. Rev.,* vol. 24, no. 4, pp. 566-587, Jul-Aug, 2005. DOI: https://doi.org/10.1002/mas.20027.

[180] N. B. Cech, and C. G. Enke, “Practical implications of some recent studies in electrospray ionization fundamentals,” *Mass Spectrom. Rev.,* vol. 20, no. 6, pp. 362-387, Nov, 2001. DOI: https://doi.org/10.1002/mas.10008.

[181] D. B. Robb, T. R. Covey, and A. P. Bruins, “Atmospheric pressure photoionization: an ionization method for liquid chromatography-mass spectrometry,” *Anal. Chem.,* vol. 72, no. 15, pp. 3653-3659, Aug, 2000. DOI: https://doi.org/10.1021/ac0001636.

[182] L. H. Cohen, and A. I. Gusev, “Small molecule analysis by MALDI mass spectrometry,” *Anal. Bioanal. Chem.,* vol. 373, no. 7, pp. 571-586, Aug, 2002. DOI: https://doi.org/10.1007/s00216-002-1321-z.

[183] J. Banoub, J. Miller-Banoub, F. Jahouh, N. Joly, and P. Martin, "Overview of recent developments in the mass spectrometry of nucleic acid and constituents," J. H. Banoub and P. A. Limbach, eds. CRC Press, 2009. pp. 1-90.

[184] S. Banerjee, and S. Mazumdar, "Electrospray ionization mass spectrometry: A technique to access the information beyond the molecular weight of the analyte," *Int. J. Anal. Chem.,* vol. 2012, pp. 1-40, Nov, 2012. DOI: https://doi.org/10.1155/2012/282574.

[185] J. K. Prasain, *Tandem mass spectrometry - applications and principles*, Croatia:InTech, 2012.

[186] J. B. Lambert, S. Gronert, H. F. Shurvell, and D. R. G. Lightner, *Organic structural spectroscopy*, 2 ed., the United States of America:Pearson Education, Inc., 2013.

[187] C. S. Ho, C. W. Lam, M. H. Chan, R. C. Cheung, L. K. Law, L. C. Lit, K. F. Ng, M. W. Suen, and H. L. Tai, "Electrospray ionisation mass spectrometry: principles and clinical applications," *Clin. Biochem. Rev.,* vol. 24, no. 1, pp. 3-12, Feb, 2003.

[188] C. Dass, *Fundamentals of contemporary mass spectrometry*, Hoboken, NJ, USA:John Wiley & Sons, Inc., 2007.

[189] M. Mann, and J. B. Fenn, "Electrospray mass spectrometry," *Mass Spectrom.*, Springer US, 1992. pp. 1-35.

[190] A. Kruve, K. Herodes, and I. Leito, "Electrospray ionization matrix effect as an uncertainty source in HPLC/ESI-MS pesticide residue analysis," *J. AOAC Int.,* vol. 93, no. 1, pp. 306-314, Jan-Feb, 2010. DOI: https://doi.org/10.1002/0471140864.10.1093/jaoac/93.1.306.

[191] S. H. Hansen, and L. Reubsaet, "High-performance liquid chromatography (HPLC) and high-performance liquid chromatography-mass spectrometry (LC-MS)," *Bioanalysis of pharmaceuticals*, 2015. pp. 123-172.

[192] S. Schmid, M. C. Jecklin, and R. Zenobi, "Electrosonic spray ionization-an ideal interface for high-flow liquid chromatography applications," *J. Chromatogr A,* vol. 1218, no. 23, pp. 3704-3710, Jun, 2011. DOI: https://doi.org/10.1002/0471140864.10.1016/j.chroma.2011.04.030.

[193] M. A. Meier, and U. S. Schubert, "Evaluation of a new multiple-layer spotting technique for matrix-assisted laser desorption/ionization time-of-flight mass spectrometry of synthetic polymers," *Rapid Commun. Mass Spectrom.,* vol. 17, no. 7, pp. 713-716, Jan, 2003. DOI: https://doi.org/10.1002/rcm.961.

[194] N. C. Wamer, C. N. Morse, J. N. Gadient, T. A. Dodson, E. A. Carlson, and E. G. Prestwich, "Comparison of small biomolecule ionization and fragmentation in *Pseudomonas aeruginosa* using common MALDI matrices," *J. Am. Soc. Mass Spectrom.,* vol. 34, no. 3, pp. 355-365, Mar, 2023. DOI: https://doi.org/10.1021/jasms.2c00157.

[195] M. L. Williams, A. A. Olomukoro, R. V. Emmons, N. H. Godage, and E. Gionfriddo, "Matrix effects demystified: Strategies for resolving challenges in analytical separations of complex samples," *J. Sep. Sci.,* vol. 46, no. 23, pp. e2300571, Dec, 2023. DOI: https://doi.org/10.1002/jssc.202300571.

[196] J. Leopold, Y. Popkova, K. M. Engel, and J. Schiller, “Recent developments of useful MALDI matrices for the mass spectrometric characterization of lipids,” *Biomolecules,* vol. 8, no. 4, Dec, 2018. DOI: https://doi.org/10.3390/biom8040173.

[197] B. A. Mamyrin, “Time-of-flight mass spectrometry (concepts, achievements, and prospects),” *Int. J. Mass Spectrom.,* vol. 206, no. 3, pp. 251-266, Mar, 2001. DOI: https://doi.org/10.1016/s1387-3806(00)00392-4.

[198] D. Suckau, A. Resemann, M. Schuerenberg, P. Hufnagel, J. Franzen, and A. Holle, “A novel MALDI LIFT-TOF/TOF mass spectrometer for proteomics,” *Anal. Bioanal. Chem.,* vol. 376, no. 7, pp. 952-965, Aug, 2003. DOI: https://doi.org/10.1007/s00216-003-2057-0.

[199] T. Bonk, and A. Humeny, “MALDI-TOF-MS analysis of protein and DNA,” *Neuroscientist,* vol. 7, no. 1, pp. 6-12, Feb, 2001. DOI: https://doi.org/10.1177/107385840100700104.

[200] A. N. Verenchikov, M. I. Yavor, and T. V. Pomozov, “Control of time front tilts in planar multi-reflection time-of-flight mass analyzers by local wedge fields,” *Int. J. Mass Spectrom.,* vol. 469, Aug, 2021. DOI: https://doi.org/10.1016/j.ijms.2021.116680.

[201] J. Lee, and P. T. Reilly, “Limitation of time-of-flight resolution in the ultra high mass range,” *Anal. Chem.,* vol. 83, no. 15, pp. 5831-5833, Aug, 2011. DOI: https://doi.org/10.1021/ac201537b.

[202] R. A. Zubarev, and A. Makarov, “Orbitrap mass spectrometry,” *Anal. Chem.,* vol. 85, no. 11, pp. 5288-5296, Apr, 2013. DOI: https://doi.org/10.1021/ac4001223.

[203] R. H. Perry, R. G. Cooks, and R. J. Noll, “Orbitrap mass spectrometry: Instrumentation, ion motion and applications,” *Mass Spectrom. Rev.,* vol. 27, no. 6, pp. 661-699, May, 2008. DOI: https://doi.org/10.1002/MAS.20186.

[204] P. J. Amorim Madeira, P. A, and C. M, "High Resolution Mass Spectrometry Using FTICR and Orbitrap Instruments," *Fourier transform - materials analysis*, 2012.

[205] S. Eliuk, and A. Makarov, “Evolution of orbitrap mass spectrometry instrumentation,” *Annu. Rev. Anal. Chem.,* vol. 8, pp. 61-80, Jul, 2015. DOI: https://doi.org/10.1146/annurev-anchem-071114-040325.

[206] R. E. March, and J. F. J. Todd, "The development of the quadrupole mass filter and quadrupole ion trap," *The encyclopedia of mass spectrometry*, M. L. Gross and R. M. Caprioli, eds.Boston: Elsevier, 2016. pp. 43-60.

[207] D. L. Shinholt, S. N. Anthony, A. W. Alexander, B. E. Draper, and M. F. Jarrold, “A frequency and amplitude scanned quadrupole mass filter for the analysis of high *m/z* ions,” *Rev. Sci. Instrum.,* vol. 85, no. 11, pp. 113109, Nov, 2014. DOI: https://doi.org/10.1063/1.4900627.

[208] G. Kaklamanos, E. Aprea, and G. Theodoridis, "Mass spectrometry: Principles and instrumentation," *Encyclopedia of food and health*, 2016. pp. 661-668.

[209] S. U. Syed, T. J. Hogan, M. J. Antony Joseph, S. Maher, and S. Taylor, “Quadrupole mass filter: design and performance for operation in stability zone 3,” *J. Am. Soc. Mass Spectrom.,* vol. 24, no. 10, pp. 1493-1500, Oct, 2013. DOI: https://doi.org/10.1007/s13361-013-0704-z.

[210] C. G. Herbert, and R. A. Johnstone, *Mass spectrometry basics*, 1 ed., London New York Washington, D.C.:CRC press, 2002.

[211] D. J. Douglas, A. J. Frank, and D. Mao, “Linear ion traps in mass spectrometry,” *Mass Spectrom. Rev.,* vol. 24, no. 1, pp. 1-29, Jan-Feb, 2005. DOI:10.1002/mas.20004.

[212] Á. Somogyi, "Mass spectrometry instrumentation and techniques," *Medical applications of mass spectrometry*, 2008. pp. 93-140.

[213] G. Hopfgartner, E. Varesio, V. Tschappat, C. Grivet, E. Bourgogne, and L. A. Leuthold, “Triple quadrupole linear ion trap mass spectrometer for the analysis of small molecules and macromolecules,” *J. Mass Spectrom.,* vol. 39, no. 8, pp. 845-855, Aug, 2004. DOI: https://doi.org/10.1002/jms.659.

[214] P. Suder, "Tandem mass spectrometry," *Mass Spectrom.*, 2019. pp. 231-259.

[215] J. Prasain, *Tandem mass spectrometry: applications and principles*, 1 ed., InTech, 2012.

[216] "Orbitrap Tribrid Mass Spectrometer," https://www.thermofisher.com/ca/en/home/industrial/mass-spectrometry/liquid-chromatography-mass-spectrometry-lc-ms/lc-ms-systems/orbitrap-lc-ms/orbitrap-tribrid-mass-spectrometers.html.

[217] A. Silipo, C. De Castro, R. Lanzetta, A. Molinaro, M. Parrilli, G. Vago, L. Sturiale, A. Messina, and D. Garozzo, “Structural characterizations of lipids A by MS/MS of doubly charged ions on a hybrid linear ion trap/orbitrap mass spectrometer,” *J.*

Mass Spectrom., vol. 43, no. 4, pp. 478-484, Apr, 2008. DOI: https://doi.org/10.1002/jms.1333.

[218] J. Banoub, E. Gentip, and D. H. Shaw, "Analysis of the core oligosaccharide of *Aeromonas hydrophila* (Chemotype III) lipopolysaccharide using fast atom bombardment, electrospray and low energy tandem mass spectrometry," *Spectroscopy,* vol. 12, no. 2, pp. 55-68, 1994. DOI: https://doi.org/10.1155/1994/786105.

[219] E. R. Williams, K. D. Henry, F. W. McLafferty, J. Shabanowitz, and D. F. Hunt, "Surface-induced dissociation of peptide ions in Fourier-transform mass spectrometry," *J. Am. Soc. Mass Spectrom.,* vol. 1, no. 5, pp. 413-416, May, 1990. DOI: https://doi.org/10.1016/1044-0305(90)85022-E.

[220] J. Zaia, "Mass spectrometry of oligosaccharides," *Mass Spectrom. Rev.,* vol. 23, no. 3, pp. 161-227, Aug, 2004. DOI: https://doi.org/10.1002/mas.10073.

[221] A. K. Anguraj Vadivel, "Gel-based proteomics in plants: time to move on from the tradition," *Front Plant Sci.,* vol. 6, pp. 369, May, 2015. DOI: https://doi.org/10.3389/fpls.2015.00369.

[222] M. U. Nissa, N. Pinto, H. Parkar, M. Goswami, and S. Srivastava, "Proteomics in fisheries and aquaculture: An approach for food security," *Food Control,* vol. 127, no. November 2020, pp. 108125-108125, Nov, 2021. DOI: https://doi.org/10.1016/j.foodcont.2021.108125.

[223] J. Banoub, T. Youssef, and A. Mikhael, “Proteomic technology applications for fisheries research,” *Tech. Report. Fish. Aquat. Sci.,* vol. 3465, pp. xi- 668, May, 2022.

[224] M. Dzieciatkowska, R. Hill, and K. C. Hansen, “GeLC-MS/MS analysis of complex protein mixtures,” *Methods Mol. Biol.*, pp. 53-66, 2014. DOI: https://doi.org/10.1007/978-1-4939-0685-7_4.

[225] P. Bults, B. Spanov, O. Olaleye, N. C. van de Merbel, and R. Bischoff, “Intact protein bioanalysis by liquid chromatography-high-resolution mass spectrometry,” *J. Chromatogr B Analyt Technol. Biomed. Life Sci.,* vol. 1110-1111, pp. 155-167, Mar, 2019. DOI: https://doi.org/10.1016/j.jchromb.2019.01.032.

[226] A. G. Woods, I. Sokolowska, A. G. Ngounou Wetie, D. Channaveerappa, E. J. Dupree, M. Jayathirtha, R. Aslebagh, K. L. Wormwood, and C. C. Darie, "Mass spectrometry for proteomics-based investigation," *Advancements of mass spectrometry in biomedical research*, A. G. Woods and C. C. Darie, eds.Cham: Springer International Publishing, 2019. pp. 1-26.

[227] H. Sveinsdóttir, S. A. M. Martin, and O. T. Vilhelmsson, "Application of proteomics to fish processing and quality," *Food biochemistry and food processing*, Oxford, UK: Wiley-Blackwell, 2012. pp. 406-424.

[228] M. Carrera, B. Cañas, and J. M. Gallardo, “Proteomics for the assessment of quality and safety of fishery products,” *Food Research International,* vol. 54, no. 1, pp. 972-979, Nov, 2013. DOI: https://doi.org/10.1016/j.foodres.2012.10.027.

[229] M. F. Mazzeo, and R. A. Siciliano, "Proteomics for the authentication of fish species," *J. Proteomics.,* vol. 147, pp. 119-124, Mar, 2016. DOI: https://doi.org/10.1016/j.jprot.2016.03.007.

[230] S. R. Gallagher, "One-dimensional SDS gel electrophoresis of proteins," *Curr. Protoc. Protein Sci.,* vol. 10, pp. 10 11 11-10 11 44, Apr, 2012. DOI: https://doi.org/10.1002/0471140864.

[231] C.-f. Xu, Y. Wang, P. Bryngelson, Z. Sosic, D. Dalton, and D. T. T. Dithiothreitol, *Advancements of mass spectrometry in biomedical research*, Springer, Cham, 2019.

[232] C. Chen, J. Hou, J. J. Tanner, and J. Cheng, "Bioinformatics methods for mass spectrometry-based proteomics data analysis," *Int. J. Mol. Sci.,* vol. 21, no. 8, Apr, 2020. DOI: https://doi.org/10.3390/ijms21082873.

[233] M. Ghahremani, K. A. Stigter, and W. Plaxton, "Extraction and characterization of extracellular proteins and their post-translational modifications from *Arabidopsis thaliana* suspension cell cultures and seedlings: A critical review," *Proteomes,* vol. 4, no. 3, pp. 14-20, Sep, 2016. DOI: https://doi.org/10.3390/proteomes4030025.

[234] X. Han, A. Aslanian, and J. R. Yates, 3rd, "Mass spectrometry for proteomics," *Curr. Opin Chem. Biol.,* vol. 12, no. 5, pp. 483-490, Oct, 2008. DOI: https://doi.org/10.1016/j.cbpa.2008.07.024.

[235] C. Piñeiro, B. Cañas, and M. Carrera, "The role of proteomics in the study of the influence of climate change on seafood products," *Food Res. Int.,* vol. 43, no. 7, pp. 1791-1802, Nov, 2010. DOI: https://doi.org/10.1016/j.foodres.2009.11.012.

[236] V. S. Priyadharshini, and L. M. Teran, "Role of respiratory proteomics in precision medicine," Elsevier, 2020. pp. 255-261.

[237] M. Carrera, C. Pineiro, and I. Martinez, “Proteomic strategies to evaluate the impact of farming conditions on food quality and safety in Aquaculture products,” *Foods,* vol. 9, no. 8, Aug, 2020. DOI: https://doi.org/10.3390/foods9081050.

[238] T. Rabilloud, and C. Lelong, “Two-dimensional gel electrophoresis in proteomics: A tutorial,” *J. Proteomics.,* vol. 74, no. 10, pp. 1829-1841, Feb, 2011. DOI: https://doi.org/10.1016/j.jprot.2011.05.040.

[239] F. R. Dani, and G. Pieraccini, “Proteomics of arthropod soluble olfactory proteins,” *Methods Enzymol.,* vol. 642, pp. 81-102, 2020. DOI: https://doi.org/10.1016/bs.mie.2020.04.069.

[240] E. van Vliet, *Omics and related recent technologies*, 3 ed., Elsevier, 2014.

[241] L.-R. Yu, N. A. Stewart, and T. D. Veenstra, "Proteomics," *Essentials of genomic and personalized medicine*, 2010. pp. 89-96.

[242] Y. Gao, and J. R. Yates, “Protein analysis by shotgun proteomics,” *Mass Spectrom. Chem. Proteomics*, pp. 1-38, Aug, 2019. DOI: https://doi.org/10.1002/9781118970195.ch1.

[243] J. Giacometti, A. B. Tomljanović, and D. Josić, “Application of proteomics and metabolomics for investigation of food toxins,” *Food Res. Int.,* vol. 54, no. 1, pp. 1042-1051, Nov, 2013. DOI: https://doi.org/10.1016/j.foodres.2012.10.019.

[244] M. A. Nessen, D. J. Van Der Zwaan, S. Grevers, H. Dalebout, M. Staats, E. Kok, and M. Palmblad, “Authentication of closely related fish and derived fish products

using tandem mass spectrometry and spectral library matching," *J. Agric. Food Chem.,* vol. 64, no. 18, pp. 3669-3677, Apr, 2016. DOI: https://doi.org/10.1021/acs.jafc.5b05322.

[245] M. P. Y. Lam, E. Lau, D. C. M. Ng, D. Wang, and P. Ping, "Cardiovascular proteomics in the era of big data: Experimental and computational advances," *Clin. Proteomics,* vol. 13, no. 1, pp. 1-14, Dec, 2016. DOI: https://doi.org/10.1186/s12014-016-9124-y.

[246] I. Sokolowska, A. G. N. Wetie, A. G. Woods, and C. C. Darie, "Applications of mass spectrometry in proteomics," *Aust. J. Chem.,* vol. 66, no. 7, pp. 721-721, Jun, 2013. DOI: https://doi.org/10.1071/CH13137.

[247] A. Shevchenko, M. Wilm, and M. Mann, "Peptide sequencing by mass spectrometry for homology searches and cloning of genes," *J. Protein Chem.,* vol. 16, no. 5, pp. 481-490, Sep, 1997. DOI: https://doi.org/10.1023/A:1026361427575.

[248] B. Ma, K. Zhang, C. Hendrie, C. Liang, M. Li, A. Doherty-Kirby, and G. Lajoie, "PEAKS: Powerful software for peptide de novo sequencing by tandem mass spectrometry," *Rapid Commun. Mass Spectrom.,* vol. 17, no. 20, pp. 2337-2342, Aug, 2003. DOI: https://doi.org/10.1002/rcm.1196.

[249] I. Ortea, B. Cañas, and J. M. Gallardo, "Mass spectrometry characterization of species-specific peptides from arginine kinase for the identification of commercially relevant shrimp species," *J. Proteome Res.,* vol. 8, no. 11, pp. 5356-5362, May, 2009. DOI: https://doi.org/10.1021/pr900663d.

[250] M. Carrera, B. Cañas, C. Piñeiro, J. Vázquez, and J. M. Gallardo, "De novo mass spectrometry sequencing and characterization of species-specific peptides from nucleoside diphosphate kinase B for the classification of commercial fish species belonging to the family merlucciidae," *J. Proteome Res.,* vol. 6, no. 8, pp. 3070-3080, Oct, 2007. DOI: https://doi.org/10.1021/pr0701963.

[251] M. A. Dietrich, G. J. Arnold, T. Fröhlich, and A. Ciereszko, "In-depth proteomic analysis of carp (*Cyprinus carpio L*) spermatozoa," *Comp. Biochem. Physiol. Part D,* vol. 12, pp. 10-15, Sep, 2014. DOI: https://doi.org/10.1016/j.cbd.2014.09.003.

[252] J. Nynca, M. A. Dietrich, H. Karol, and A. Ciereszko, "Identification of apolipoprotein C-I in rainbow trout seminal plasma," *Reprod. Fertil. Dev.,* vol. 22, no. 8, pp. 1183-1187, Oct, 2010. DOI: https://doi.org/10.1071/RD10066.

[253] M. Wojtczak, G. J. Dietrich, I. Irnazarow, P. Jurecka, M. Słowińska, and A. Ciereszko, "Polymorphism of transferrin of carp seminal plasma: Relationship to blood transferrin and sperm motility characteristics," *Comp. Biochem. Physiol. B.,* vol. 148, no. 4, pp. 426-431, Aug, 2007. DOI: https://doi.org/10.1016/j.cbpb.2007.07.011.

[254] M. Wojtczak, J. Calka, J. Glogowski, and A. Ciereszko, "Isolation and characterization of alpha1-proteinase inhibitor from common carp (*Cyprinus carpio*) seminal plasma," *Comp. Biochem. Physiol B Biochem. Mol. Biol.,* vol. 148, no. 3, pp. 264-276, Nov, 2007. DOI: https://doi.org/10.1016/j.cbpb.2007.06.004.

[255] A. Ciereszko, M. A. A. Dietrich, and J. Nynca, “Fish semen proteomics — New opportunities in fish reproductive research,” *Aquaculture,* vol. 472, pp. 81-92, Mar, 2017. DOI: https://doi.org/10.1016/j.aquaculture.2016.03.005.

[256] J. Nynca, G. J. Arnold, T. Fröhlich, K. Otte, and A. Ciereszko, “Proteomic identification of rainbow trout sperm proteins,” *Proteomics,* vol. 14, no. 12, pp. 1569-1573, Mar, 2014. DOI: https://doi.org/10.1002/pmic.201300521.

[257] M. A. Dietrich, G. J. Arnold, J. Nynca, T. Fröhlich, K. Otte, and A. Ciereszko, “Characterization of carp seminal plasma proteome in relation to blood plasma,” *J. Proteomics.,* vol. 98, pp. 218-232, Jan, 2014. DOI: https://doi.org/10.1016/j.jprot.2014.01.005.

[258] I. Forné, J. Abián, and J. Cerdà, “Fish proteome analysis: Model organisms and non-sequenced species,” *Proteomics,* vol. 10, no. 4, pp. 858-872, Nov, 2010. DOI: https://doi.org/10.1002/pmic.200900609.

[259] J. Nynca, G. Arnold, T. Fröhlich, and A. Ciereszko, “Proteomic identification of rainbow trout blood plasma proteins and their relationship to seminal plasma proteins,” *Proteomics,* vol. 17, no. 11, pp. 1-41, Apr, 2017. DOI: https://doi.org/10.1002/pmic.201600460.

[260] N. Kodzik, A. Ciereszko, B. Szczepkowska, A. Malinowska, and M. A. Dietrich, “Comparative proteomic analysis of the ovarian fluid and eggs of Siberian sturgeon,” *BMC Genom.,* vol. 25, no. 1, pp. 451, May, 2024. DOI: https://doi.org/10.1002/0471140864.10.1186/s12864-024-10309-y.

[261] J. Nynca, G. J. Arnold, T. Fröhlich, and A. Ciereszko, "Shotgun proteomics of rainbow trout ovarian fluid," *Reprod. Fertil. Dev.,* vol. 27, no. 3, pp. 504-512, Jan, 2015. DOI: https://doi.org/10.1071/RD13224.

[262] R. Medina-Gali, M. Belló-Pérez, S. Ciordia, M. C. Mena, J. Coll, B. Novoa, M. d. M. Ortega-Villaizán, and L. Perez, "Plasma proteomic analysis of zebrafish following spring viremia of carp virus infection," *Fish Shellfish Immunol.,* vol. 86, no. October 2018, pp. 892-899, Oct, 2019. DOI: https://doi.org/10.1016/j.fsi.2018.12.035.

[263] M. López-Pedrouso, Z. Varela, D. Franco, J. A. Fernández, and J. R. Aboal, "Can proteomics contribute to biomonitoring of aquatic pollution? A critical review," *Environ. Pollut.,* vol. 267, Aug, 2020. DOI: https://doi.org/10.1016/j.envpol.2020.115473.

[264] K. Skogland Enerstvedt, M. O. Sydnes, and D. M. Pampanin, "Study of the plasma proteome of Atlantic cod (*Gadus morhua*): Effect of exposure to two PAHs and their corresponding diols," *Chemosphere,* vol. 183, pp. 294-304, May, 2017. DOI: https://doi.org/10.1016/j.chemosphere.2017.05.111.

[265] A. B. Patel, S. Shaikh, K. R. Jain, C. Desai, and D. Madamwar, "Polycyclic aromatic hydrocarbons: sources, toxicity, and remediation approaches," *Front. Microbiol.,* vol. 11, pp. 562813, Nov, 2020. DOI: https://doi.org/10.3389/fmicb.2020.562813.

[266] C. A. Muir, B. S. Bork, B. D. Neff, and S. Damjanovski, "Proteomic analysis of temperature-dependent developmental plasticity within the ventricle of juvenile

Atlantic salmon (*Salmo salar*)," *Curr. Res. Physiol.,* vol. 5, pp. 344-354, Jul, 2022. DOI: https://doi.org/10.1016/j.crphys.2022.07.005.

[267] M. Almostafa, T. D. Fridgen, and J. H. Banoub, "Structural investigation by tandem mass spectrometry analysis of a heterogeneous mixture of Lipid A(n) isolated from the lipopolysaccharide of Aeromonas hydrophila SJ-55Ra," *Rapid Commun. Mass Spectrom.,* vol. 32, no. 3, pp. 167-183, Feb, 2018. DOI: https://doi.org/10.1002/rcm.8017.

[268] A. Mikhael, H. Petrosova, D. Smith, R. K. Ernst, and D. R. Goodlett, "Lipid A double bond position determination using ozone and laser-induced dissociation," *Rapid Commun. Mass Spectrom.,* vol. 38, no. 16, pp. e9854, Aug, 2024. DOI: https://doi.org/10.1002/rcm.9854.

[269] A. El-Aneed, and J. Banoub, "Elucidation of the molecular structure of lipid A isolated from both a rough mutant and a wild strain of *Aeromonas salmonicida* lipopolysaccharides using electrospray ionization quadrupole time-of-flight tandem mass spectrometry," *Rapid Commun. Mass Spectrom.,* vol. 19, no. 12, pp. 1683-1695, Apr, 2005. DOI: https://doi.org/10.1002/rcm.1971.

[270] M. Almostafa, B. Allehyane, S. Egli, C. Bottaro, T. D. Fridgen, and J. Banoub, "Tandem mass spectrometry determination of the putative structure of a heterogeneous mixture of Lipid As isolated from the lipopolysaccharide of the Gram-negative bacteria *Aeromonas liquefaciens* SJ-19a," *Rapid Commun. Mass Spectrom.,* vol. 30, no. 8, pp. 1043-1058, Apr, 2016. DOI: https://doi.org/10.1002/rcm.7540.

[271] A. V. Demchenko, M. A. Wolfert, B. Santhanam, J. N. Moore, and G. J. Boons, “Synthesis and biological evaluation of Rhizobium sin-1 lipid A derivatives,” *J. Am. Chem. Soc.,* vol. 125, no. 20, pp. 6103-6112, May, 2003. DOI: https://doi.org/10.1021/ja029316s.

[272] F. Peri, F. Granucci, B. Costa, I. Zanoni, C. Marinzi, and F. Nicotra, “Inhibition of lipid a stimulated activation of human dendritic cells and macrophages by amino and hydroxylamino monosaccharides,” *Angew Chem. Int. Ed. Engl.,* vol. 46, no. 18, pp. 3308-3312, 2007. DOI: https://doi.org/10.1002/anie.200604932.

[273] S. Y. Park, J. E. Han, H. Kwon, S. C. Park, and J. H. Kim, “Recent Insights into Aeromonas salmonicida and Its Bacteriophages in Aquaculture: A Comprehensive Review,” *J. Microbiol. Biotechnol.,* vol. 30, no. 10, pp. 1443-1457, Oct, 2020. DOI: https://doi.org/10.4014/jmb.2005.05040.

[274] V. Gabelica, "CHAPTER 1. Ion mobility–mass spectrometry: An Overview," *Ion Mobility-Mass Spectrometry*, New Developments in Mass Spectrometry, 2021. pp. 1-25.

[275] G. Nagy, “High-resolution ion mobility separations coupled to mass spectrometry: What's next?,” *J. Mass Spectrom.,* vol. 59, no. 5, pp. e5014, May, 2024. DOI: https://doi.org/10.1002/jms.5014.

[276] V. Gabelica, and E. Marklund, “Fundamentals of ion mobility spectrometry,” *Curr. Opin. Chem. Biol.,* vol. 42, pp. 51-59, Feb, 2018. DOI: https://doi.org/10.1016/j.cbpa.2017.10.022.

[277] J. N. Dodds, and E. S. Baker, “Ion mobility spectrometry: Fundamental concepts, instrumentation, applications, and the road ahead,” *J. Am. Soc. Mass Spectrom.,* vol. 30, no. 11, pp. 2185-2195, Nov, 2019. DOI: https://doi.org/10.1007/s13361-019-02288-2.

[278] A. A. Shvartsburg, and R. D. Smith, “Fundamentals of traveling wave ion mobility spectrometry,” *Anal. Chem.,* vol. 80, no. 24, pp. 9689-9699, Dec 15, 2008. DOI: https://doi.org/10.1021/ac8016295.

[279] B. M. Kolakowski, and Z. Mester, “Review of applications of high-field asymmetric waveform ion mobility spectrometry (FAIMS) and differential mobility spectrometry (DMS),” *Analyst,* vol. 132, no. 9, pp. 842-864, Sep, 2007. DOI: https://doi.org/10.1039/b706039d.

[280] K. E. Swearingen, and R. L. Moritz, “High-field asymmetric waveform ion mobility spectrometry for mass spectrometry-based proteomics,” *Expert. Rev. Proteomics,* vol. 9, no. 5, pp. 505-517, Oct, 2012. 10.1586/epr.12.50.

[281] S. Sweet, D. Chain, W. Yu, P. Martin, M. Rebelatto, A. Chambers, F. Cecchi, and Y. J. Kim, “The addition of FAIMS increases targeted proteomics sensitivity from FFPE tumor biopsies,” *Sci. Rep.,* vol. 12, no. 1, pp. 13876, Aug 16, 2022. DOI: https://doi.org/10.1038/s41598-022-16358-1.

[282] J. Li, J. Stupak, A. S. Haqqani, G. Harris, H. Zhou, S. Williamson, R. Chen, H. H. Xu, and W. Chen, “Development of LC-FAIMS-MS and its application to lipidomics study of *Acinetobacter baumannii* infection,” *J. Lipid Res.,* vol. 65, no. 11, pp. 100668, Nov, 2024. DOI: https://doi.org/10.1016/j.jlr.2024.100668.

[283] K. Hohenwallner, L. M. Lamp, L. Peng, M. Nuske, J. Hartler, G. E. Reid, and E. Rampler, “FAIMS Shotgun lipidomics for enhanced HILIC-like separation and automated annotation of gangliosides,” *ChemRxiv*, 2024. 10.26434/chemrxiv-2024-qht6q.

[284] W. Gabryelski, and K. L. Froese, “Rapid and sensitive differentiation of anomers, linkage, and position isomers of disaccharides using High-Field Asymmetric Waveform Ion Mobility Spectrometry (FAIMS),” *J. Am. Soc. Mass Spectrom.,* vol. 14, no. 3, pp. 265-277, Mar, 2003. DOI: https://doi.org/10.1016/S1044-0305(03)00002-3.

[285] T. Fouquet, and H. Sato, “Improving the resolution of Kendrick mass defect analysis for polymer ions with fractional base units,” *Mass Spectrom.,* vol. 6, no. 1, pp. A0055, Feb, 2017. DOI: https://doi.org/10.5702/massspectrometry.A0055.

[286] T. N. J. Fouquet, R. B. Cody, Y. Ozeki, S. Kitagawa, H. Ohtani, and H. Sato, “On the Kendrick Mass Defect Plots of Multiply Charged Polymer Ions: Splits, Misalignments, and How to Correct Them,” *J. Am. Soc. Mass Spectrom.,* vol. 29, no. 8, pp. 1611-1626, Aug, 2018. DOI: https://doi.org/10.1007/s13361-018-1972-4.

[287] C. A. Hughey, C. L. Hendrickson, R. P. Rodgers, A. G. Marshall, and K. Qian, “Kendrick mass defect spectrum: a compact visual analysis for ultrahigh-resolution broadband mass spectra,” *Anal. Chem.,* vol. 73, no. 19, pp. 4676-4681, Oct, 2001. DOI: https://doi.org/10.1021/ac010560w.

[288] G. Gaiffe, R. B. Cole, A. Sonnette, N. Floch, and M. C. Bridoux, “Identification of postblast residues by DART-high resolution mass spectrometry combined with multivariate statistical analysis of the Kendrick mass defect,” *Anal. Chem.,* vol. 91, no. 13, pp. 8093-8100, Jul, 2019. DOI: https://doi.org/10.1021/acs.analchem.9b00137.

[289] X. Ortiz, K. J. Jobst, E. J. Reiner, S. M. Backus, K. M. Peru, D. W. McMartin, G. O'Sullivan, V. Y. Taguchi, and J. V. Headley, “Characterization of naphthenic acids by gas chromatography-Fourier transform ion cyclotron resonance mass spectrometry,” *Anal. Chem.,* vol. 86, no. 15, pp. 7666-7673, Aug, 2014. DOI: https://doi.org/10.1021/ac501549p.

[290] M. W. Alton, H. J. Stark, M. R. Canagaratna, and E. C. Browne, “Generalized Kendrick analysis for improved visualization of atmospheric mass spectral data,” *Atmos. Meas. Tech.,* vol. 16, no. 12, pp. 3273-3282, Dec, 2023. DOI: https://doi.org/10.5194/amt-16-3273-2023.

[291] T. R. Rosa, G. S. Folli, W. L. S. Pacheco, M. P. Castro, W. Romao, and P. R. Filgueiras, “DropMS: Petroleomics data treatment based in a web server for high-resolution mass spectrometry,” *J. Am. Soc. Mass Spectrom.,* vol. 31, no. 7, pp. 1483-1490, Jul, 2020. DOI: https://doi.org/10.1021/jasms.0c00109.

[292] S. Kim, R. W. Kramer, and P. G. Hatcher, “Graphical method for analysis of ultrahigh-resolution broadband mass spectra of natural organic matter, the van Krevelen diagram,” *Anal. Chem.,* vol. 75, no. 20, pp. 5336-5344, Oct, 2003. DOI: https://doi.org/10.1021/ac034415p.

[293] H. Sato, S. Nakamura, K. Teramoto, and T. Sato, “Structural characterization of polymers by MALDI spiral-TOF mass spectrometry combined with Kendrick mass defect analysis,” *J. Am. Soc. Mass Spectrom.,* vol. 25, no. 8, pp. 1346-1355, Aug, 2014. DOI: https://doi.org/10.1007/s13361-014-0915-y.

[294] T. Fouquet, H. Aizawa, and H. Sato, “Taking MALDI SpiralTOF high-resolution mass spectrometry and mass defect analysis to the next level with ethylene vinyl acetate vinyl alcohol terpolymers,” *Rapid Commun. Mass Spectrom.,* vol. 30, no. 15, pp. 1818-1822, Aug, 2016. DOI: https://doi.org/10.1002/rcm.7653.

Chapter 2 Qualitative Shotgun Proteomics Strategy for Protein Expression Profiling of Fish Otoliths

This Chapter is reproduced with permission from Trevena N. Youssef, Rick M. Rideout, Aaron T. Adamack, Rince John, Alejandro M. Cohen, Travis D. Fridgen and Joseph H. Banoub, "Qualitative Shotgun Proteomics Strategy for Protein Expression Profiling of Fish Otoliths," *BioChem,* vol. 3, no. 3, pp. 102-117, 2023; https://doi.org/10.3390/biochem3030008

2.1. Abstract:

Despite decades of research on fish otoliths and their capacity to serve as biochronological recorders, much remains unknown about their protein composition, the mechanisms by which proteins are incorporated into the otolith matrix, or the potential for using otolith proteins to provide insight into aspects of fish life history. We examined the protein composition of Atlantic cod (*Gadus morhua*) otoliths using a state-of-the-art shotgun proteomics approach with liquid chromatography coupled to an electrospray ionization-FAIMS-orbitrap tandem mass spectrometer. In addition to previously known otolith matrix proteins, we discovered over 2000 proteins not previously identified in cod otoliths and more than 1500 proteins not previously identified in any fish otoliths. These included three novel proteins (Somatolactin, F-actin-capping protein subunit beta, Annexin) primarily involved in binding calcium ions and likely mediating crystal nucleation. However, most of the otolith proteins were not necessarily related to otolith

formation but rather to other aspects of fish physiology. For example, we identified sex-related biomarkers for males (SPATA6 protein) and females (Vitellogenin-2-like protein). We highlight some noteworthy classes of proteins having diverse functions; however, the primary goal here is not to discuss each protein separately. The number and diverse roles of the proteins discovered in the otoliths suggest that proteomics could reveal critical life history information from archived otolith collections that could be invaluable for understanding aspects of fish biology and population ecology. This proof-of-concept methodology paper provides a novel methodology whereby otolith proteomics can be further explored.

2.2. Introduction

Otoliths are dense structures made primarily of calcium carbonate, whose movements in response to sound and motion play a critical role in the hearing and equilibrium of fishes [1]. The otoliths sit within endolymph-filled chambers, and their positioning and vibratory movements are picked up by the long ciliary bundles of sensory epithelial cells and relayed to the brain via the auditory nerve [1-6]. Among the three pairs of otoliths found in fishes, the sagitta are the largest and most widely studied and used in fisheries research.

For fisheries biologists, otoliths are regularly used to reveal critical fish life history information. Otoliths accrue daily and annual growth rings [7-9] and have long been considered invaluable in fish age determination. This information is essential for developing age-based population dynamics models used in the management of fisheries

resources. Therefore most, if not all, fisheries research departments put extensive effort and resources into collecting and ageing fish otoliths [10]. For example, Fisheries and Oceans Canada recently completed a partial internal survey of its fish otolith ageing programs and concluded that several hundred thousand otoliths are aged each year across more than 100 species/fish stocks at an aggregate cost of several million dollars [11].

In addition to aging fish, otoliths can be used to back-calculate growth rates based on the width of annual growth rings [12], marking the first use of otoliths as chronological recorders of fish life history information. Otoliths are composed of a crystalline calcium carbonate structure, usually in the form of aragonite, on a protein matrix [13, 14]. Trace elements from a fish's environment are also incorporated into the otolith. Because fish otoliths are metabolically inert, materials accrued to the otolith in the form of new growth rings become permanent features of the otolith [15-18]. Understanding how the trace elements in otoliths correlate with environmental conditions, coupled with the availability of large libraries of stored otoliths, has resulted in an abundance of research using otoliths to reveal fishes' environmental history [14, 19-21]. For example, the concentration of Strontium or Barium in relation to the amount of Calcium in the otoliths can reveal information about the salinity history of individuals, which has proven particularly useful for tracking the life history of diadromous fishes [14]. Many elements also have isotopes that are more or less prevalent under different environmental conditions, and these isotopes are also recorded in the otoliths. For example, the $\delta^{18}O$ content of otoliths is negatively correlated to water temperature, allowing a fish's temperature history to be gauged from its otoliths [14].

In comparison to trace elements, much less is known about the protein composition of fish otoliths. While proteins make up only a small portion (~2–3%) of the otolith, they are thought to play a critical role in otolith formation [14, 22]. Otoliths grow via the daily formation of alternating mineral-rich and protein-rich bands [13, 15, 23]. The protein matrix not only provides a substrate for calcium carbonate deposition but also appears to play an active role in determining the type of calcium carbonate that is incorporated into the otolith [14, 22, 24]. Proteins that appear to play important roles in otolith formation and maintenance include otolith matrix proteins (OC90, Otolin-1, OMP-1, Cochlin, etc.), otolith anchoring proteins (Otolin, Otoglin, Otoglin-like, Otancorin, α-Tectorin, β-Tectorin, KSPG, etc.), and otolith regulatory proteins (Plasma membrane calcium ATPase isomer 2 (PMCA2), Carbonic anhydrase, Otoptin-1, Otoptin-2, etc.) [7, 21, 24-29]. However, it has also been demonstrated that proteins with no functional role in biomineralization may also become trapped in the otoliths during the basic process of increment formation [20]. It has been proposed that these proteins could serve as biomarkers for aspects of development and physiological change and provide the potential to reconstruct the life histories of fishes to an unprecedented level, opening up new and exciting avenues of research in ecology and fisheries science [20].

The emergence of bottom-up shotgun proteomics approaches has greatly enhanced the capacity to identify proteins in complex mixtures [30, 31]. Here, we performed a preliminary test of the use of shotgun proteomics using liquid chromatography-electrospray tandem mass spectrometry (LC-ESI-MS/MS) to identify proteins in cod

otoliths and evaluated whether archived otoliths contain proteins that could potentially be used as biomarkers to reconstruct aspects of fish life history **(Figure 2-1)**.

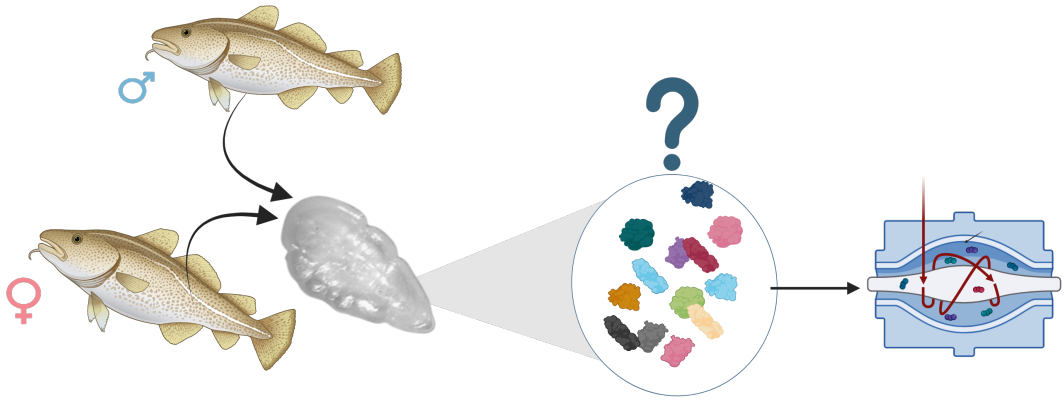

Figure 2-1. The aim of this study is to establish a proof-of-concept for a shotgun proteomics approach to evaluate the proteome of Atlantic cod otoliths. This figure was created by BioRender.

2.3. Materials and Methods

2.3.1. Otoliths

The archived otolith collection at the Northwest Atlantic Fisheries Centre (St. John's, Canada) contains thousands of Atlantic cod otoliths collected over several decades. The methods used to collect otoliths can vary slightly between individual technicians, but in general otoliths were exposed via a dorsal incision in the fish's skull and were removed using forceps. Otoliths were blotted dry with paper towel and stored in small paper envelopes. For this proof-of-concept study, we selected twelve otoliths (6 males, 6 females) collected in 2019 from the northeast coast of Newfoundland, Canada. Otoliths were washed with deionized water prior to protein extraction. Finally, each individual otolith was ground in a mortar using a pestle and then added to a fine powder.Chemicals and Standards

All standards, samples and buffers were prepared using MO; ultra-pure Milli-Q H_2O (18.2 MΩ·cm, Merck Millipore, Darmstadt, Germany). All chemicals were purchased from Sigma Aldrich (Castle Hill, NSW, Australia) and were of the highest available purity. Mass spectrometric grade trypsin was obtained from Promega (Madison, WI, USA). MS-grade solvents for chromatography were obtained from Canadian Life Science.Otolith Protein Extraction

Full powdered otoliths (2 mg) were suspended in 20% w/v trichloroacetic acid (TCA) (10 mL) and incubated overnight at room temperature. Samples were then centrifuged at 10,000× g for 10 min, and the supernatant was discarded. The crystals were washed with 100 µL of ice-cold acetone and recentrifuged. The supernatant and any remaining undissolved otolith were discarded, and the vacuum-dried pellet was processed for in-solution digestion. Briefly, 0.1 mg of the pellet was resuspended in denaturing buffer containing 8 M urea and 0.4 M ammonium bicarbonate (NH_4HCO_3). Then, 10 µL of 0.5 M dithiothreitol (DTT) was added and incubated for 30 min at 60 °C. After cooling for 5 min at room temperature, 20 µL of 0.7 M iodoacetamide ($IAcNH_2$) was added and incubated for 30 min. Next, the sample was diluted with 1.2 mL of H_2O followed by 10 µL of 0.1 M $CaCl_2$. For enzymatic digestion, 100 µL of 0.02 µg/µL trypsin (Promega Trypsin Gold, Mass Spectrometry Grade, Promega) prepared in 50 mM NH_4HCO_3 was added to each sample. The samples were incubated overnight at 37 °C in a shaker. The trypsin activity was inhibited by adding 1 µL of trifluoroacetic acid (TFA), and the samples were acidified to a pH below 3 with formic acid.

The samples were then desalted using Oasis HLB 3cc Extraction Cartridges (Waters Corporation, Milford, MA, USA) connected to a SuperlcoVisiprep DL manifold (Sigma-Aldrich, Darmstadt, Germany). The column was conditioned using 0.5 mL methanol followed by 1 mL of an elution buffer containing 50% ACN and 0.1% TFA and then with 2 mL wash buffer prepared with 0.1% TFA. After loading the sample, the column was washed with 5 mL of wash buffer and eluted twice with 0.5 mL of 50% acetonitrile-0.1% TFA and once with 0.5 mL of 80% ACN-0.1% TFA. The eluant was dried using a vacuum concentrator (SpeedVac Concentrator, Thermo Electron Corp., Gormley, ON, Canada). The dried peptide was reconstituted in 12 µL of resuspension buffer containing 5% acetonitrile and 0.1% formic acid.

2.3.2. Shotgun Proteomics by LC-ESI-MS/MS

The LC separation was carried out using the Ultimate 3000RSLCnano system (Dionex/Thermo Fisher Scientific, San Jose, CA, USA). For analysis, 2 µL (1 mg/mL) of the sample was injected onto an in-house packed capillary column (50 cm × 75 µm, pulled tip, ESI source solutions) packed with Jupiter C18 4 µm chromatographic media (Phenomenex, Torrance, CA, USA) at a flow rate of 300 nL/min. Chromatographic separation was performed with a 120 min method using solvent A (0.1% formic acid in MS-grade water) and solvent B (0.1% formic acid in MS-grade acetonitrile) from 5% to 30% for 90 min, then increasing to 55% for the next 12 min and then to 95% for 8 min before being reduced to 5% B for the remainder of the 120 min run. The column oven temperature was set at 40 °C.

The ESI-MS spectra were obtained using an Orbitrap Fusion Lumos Tribrid Mass Spectrometer (ThermoScientific Waltham, MA, USA) fitted with a Nanospray Flex Ion source and FAIMS Pro sources. The detailed acquisition parameters for mass spectrometry analysis were as follows: for ionization, the spray voltage was 1.8 kV with an ion transfer tube temperature of 300 °C. The data were acquired in data-dependent acquisition mode with a full scan using Orbitrap at a resolution of 120,000 over a mass range of 400–2000 m/z. The FAIMS source was operated at three different compensation voltages (CV = 40, 60 and 80). The auto gain control (AGC) was set in standard mode, and the maximum injection time at auto mode. For each MS/MS, the acquisition of peaks with intensities above 5.0 e^3 was performed using a normalized HCD collision energy of 35%. The cycle time was set at 1 s. The isolation window for MS/MS was set at 1.6 Da. The AGC target was set at standard mode, with the maximum injection time mode as auto. The precursor ions with positive charges 2 to 5 were selected for MS/MS analysis. After every single MS/MS acquisition, the dynamic exclusion time was set at 60 s with a mass tolerance of ±10 ppm.

The MS/MS raw files were acquired using Thermo Scientific Xcalibur 4.5 and Tune 3.5 and searched against the *Gadus morhua* protein database (Taxon ID 8049) downloaded from Uniprot using Proteome Discoverer 2.5 (ThermoFisher, Toronto, ON, Canada). The SequestHT search engine node was used for peptide and protein identification. Two missed cleavages for trypsin digestion were allowed with a 10-ppm precursor mass tolerance and fragment mass tolerance of 0.6 Da. The oxidization of methionine and N-terminal acetylation were set as dynamic modification, and carbamidomethyl cysteine was selected

as a static modification. As a control, we used trypsin-digested bovine serum albumin (BSA) under the same experimental conditions.

2.4. Results and Discussion

The work presented here represents a preliminary experiment and the establishment of a proof-of-concept of a shotgun proteomics approach that could be used to evaluate the proteome of Atlantic Cod otoliths. Although otoliths from only twelve fish (six males, six females) were examined, the sheer number of proteins identified suggest that (1) the proof-of-concept was successful and that this method represents an advancement for further otolith proteomics work, and (2) archived otolith collections intended for ageing purposes are suitable for proteomics work.

A Sequest HT search comparing the MS/MS raw files for the 12 otoliths against the *Gadus morhua* protein database (Taxon ID 8049) downloaded from Uniprot resulted in the identification of well over 2000 otolith proteins **(Tables A1-1 and A1-2, Appendix: Supplementary Materials)**. In addition to previously known otolith matrix proteins, we discovered over 2000 proteins not previously identified in cod otoliths and more than 1500 proteins not previously identified in any fish otoliths.

It is important to state that at this stage our results are only qualitative in nature. The intent is to demonstrate the huge array of proteins identified by the shotgun proteomics approach that had not previously been recorded in cod otoliths. Here, we present detailed lists of proteins for only two representative fish (one male and one female), but note that the total number of otolith proteins identified per individual is variable. The two individuals

highlighted here both contained more than 2000 otolith proteins, even after the exclusion of 27 uncharacterized proteins and 16 potential contaminant proteins (see below). This far exceeds the number of otolith proteins reported elsewhere [26]. The complete list of proteins identified via the shotgun approach is provided in the Appendix: Supplementary Materials **(Tables A1-1 and A1-2)**.

Listing and understanding the role of the thousands of proteins identified in cod otoliths is a daunting task and remains a future challenge. For now, the proteins were filtered according to sequence coverages to identify the most abundant proteins. While the sequence coverage was used as a guideline for protein abundance, we note that these values could also be affected by several factors, including how well a given protein is extracted from the otolith, the effectiveness of it undergoing trypsin digestion, and the readiness of individual peptides dissociate in MS/MS and ionize in the source [31]. Using this approach, we identified 302 proteins that could be considered to be abundant (defined here as having a sequence coverage greater than 20%) in the male otolith and 247 in the female otolith **(Tables A1-3 and A1-4, Appendix: Supplementary Materials).** The number of unique peptides in these proteins ranged from 2 to 107. Nearly half of the abundant proteins were common to both the male and female otoliths, whereas the others were exclusive to one sex or the other **(Figure 2-2, Tables A1-5 - A1-7, Appendix: Supplementary Materials)**.

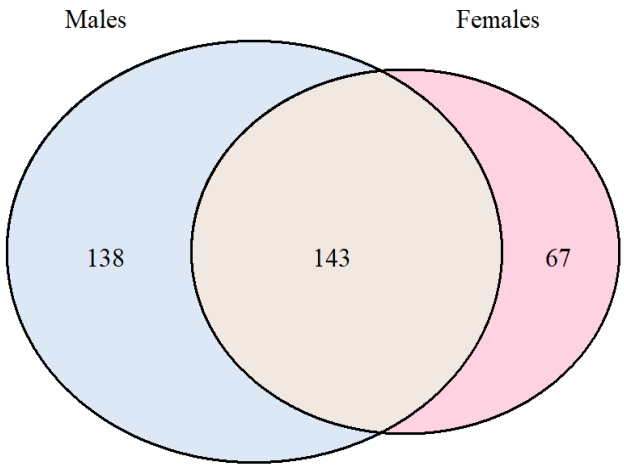

Figure 2-2. Venn diagram of protein expression: male vs. female. The diagram consists of two overlapping circles representing the male and female unique proteomes. The total number of unique proteins in the male sample is 138, while the female sample contains 67 unique proteins. Interestingly, 143 proteins are common to both sexes, indicating shared protein expression. This figure was created in R using the package "VennDiagram"[32].

Previous studies on the otolith proteome have generally focused on identifying proteins important to biomineralization. It has been suggested that otolith biomineralization is produced by three main groups of proteins: (1) otolith matrix proteins, (2) otolith anchoring proteins of the membrane, and (3) otolith regulatory proteins [7, 21, 24-29]. In addition to many of these proteins, we also identified more than 2000 proteins not previously reported in cod otoliths [29, 33] and more than 1500 not previously documented in the otoliths of any fish species [26]. Three of these novel proteins (Somatolactin, F-actin-capping protein subunit beta, Annexin) are primarily involved in binding calcium ions and likely mediating crystal nucleation. However, most of the otolith proteins identified here were not necessarily related to otolith formation, but rather to other aspects of fish physiology, and may have been trapped during otolith formation rather than playing a necessary role in otolith construction.

Here, we noted both similarities and differences **(Tables A1-3 - A1-7, Appendix: Supplementary Materials)** in male and female otolith proteomes, including the presence of sex-related biomarkers for males (SPATA6 protein) and females (Vitellogenin-2-like protein). Similar findings have been reported by Thomas *et al*. [26]. The inner ear of fish, which is enclosed in the braincase and has no direct link to the outside medium or other internal systems such as the circulatory system [2], is generally considered a closed system whereby the organic and inorganic materials necessary for otolith growth are secreted into the endolymph by the surrounding saccular epithelial cells [26]. The observations here and elsewhere [26] of large numbers of proteins in the otolith unrelated to biomineralization suggest that the endolymph and otolith proteomes may also reflect other physiological processes taking place in the fish (growth, maturation, etc.). Clearly, more work is needed to fully understand otolith proteomics in relation to fish physiology, but our results suggest that the presence of these proteins in the otoliths could provide the potential to reconstruct the life histories of fishes to an unprecedented level [26].

The otoliths used in this study were white in colour, with no visible signs of contamination. However, because otoliths were not collected in a sterile environment and were also likely in contact with human hands-on multiple occasions (e.g., as a part of our fish aging program), it was necessary to examine the protein data with respect to the potential for some proteins to be a result of otolith surface contamination. Otoliths were washed with deionized water prior to our analyses, yet we still detected 10 human keratin proteins, suggesting that some surface contamination still existed. We also identified six fish hemoglobin proteins. Although we treated these proteins as likely contaminants on the

otolith surface, we could not definitively determine whether they were surface contaminants or proteins incorporated in the otoliths. Future work using a more thorough surface cleaning should help to answer these questions.

Our results demonstrate that the shotgun approach to proteomics is an effective way to examine the otolith proteome of fishes and is capable of producing much higher resolution results than typically reported. It is not the goal of this proof-of-concept paper to describe all of the observed proteins. However, we take the opportunity below to demonstrate the diverse types of proteins identified in cod otoliths, since these results provide a very different view of otolith proteomics than previous research, which has focused primarily on proteins actively involved in biomineralization. Cod otoliths contained several proteins implicated in protein synthesis.

Here we list **(Table 2-1)** and describe (below) some select noteworthy classes of cod otolith proteins. We chose a subset of proteins with diverse functions and grouped them based on whether their formation was driven by biochemical processes or physiological processes. A complete list of proteins is provided in **Appendix: Supplementary Materials.**

Table 2-1. Proteins were obtained from biochemical and physiological processes involved in the formation of otoliths.

1. Biochemical Processes	
1.1. Protein Synthesis	
A0A8C4ZUE8	40S ribosomal protein S12
A0A8C5BT07	40S ribosomal protein S18
A0A8C5BHD6	40S ribosomal protein S19
A0A8C4ZDL6	40S ribosomal protein S28
A0A8C4YW06	40S ribosomal protein S3a
A0A8C5F524	40S ribosomal protein S9
A0A8C5B226	40S_SA_C domain-containing protein

A0A8C4ZT25	60S acidic ribosomal protein P2
A0A8C4Z3G5	60S ribosomal protein L27
A0A8C5BNH7	60S ribosomal protein L30
A0A8C4Z1D1	60S ribosomal protein L31
A0A8C4ZUJ5	Aminoacyl-tRNA hydrolase
A0A8C4ZR55	Purine-rich element binding protein Ab (PURA)
A0A8C5FJ16	Ribonucloprotein (RNP)
1.2. Biochemical Reaction Processes	
A0A8C5BPU1	Oxoisovalerate dehydrogenase subunit alpha
A0A8C5C4N4	Acetyl-CoA acetyltransferase 1 (ACAT1)
A0A8C5ADH8/ A0A8C5FBY3	Aconitate hydratase
A0A8C4ZEH5	Transketolase b (TKT)
A0A8C4YZP8	Malate dehydrogenase (MDH)
A0A8C4Z702	Peroxiredoxin-1 (PRX1)
P21919	Somatolactin
2. Physiological Processes	
2.1. Brain Function Processes	
A0A8C4ZJE1	14-3-3 protein beta/alpha-1-like protein
A0A8C5A8C5	Alpha-2-HS-glycoprotein-like
A0A8C5BJ01	Aspartate aminotransferase
2.2. Mediated Transport Processes	
A0A8C4Z7S3	AP-3 complex subunit mu-2 (PA3)
A0A8C5F5V1	Adaptor related protein complex 3 subunit sigma 1
2.3. Mitochondrial Processes	
A0A8C4YYC8	ADP/ATP translocase
A0A8C5AUM7	ATP-binding cassette sub-family B (MDR/TAP)
A0A8C4Z154	ATP synthase-coupling factor 6 mitochondria
A0A8C5AGK0/A0A8C4 YZ60	ATP synthase subunit alpha and beta
A0A8C5FKS7	Voltage-Dependent Anion-selective Channel 2 (VDAC2)
2.4. Cytoskeleton and Extracellular Matrixes	
A0A8C5FJI3	Actin, beta protein
A0A8C4ZDZ9	Actin-related protein 2/3 complex subunit 5
A0A8C4ZHY1	Chondroadherin-like b (CHADL)
A0A8C5FEX0	Choclin: extracellular matrix (ECM)
A0A8C4ZF74	Decorin or pericellular matrix proteoglycan (SLRP)
A0A8C5AFR1	the Intermediate filament protein ON3-like (IFs) [47]
A0A8C5C226/A0A8C4 ZFJ9/ A0A8C4YVX1/A0A8C5 B373/ A0A8C4YSX2/A0A8C5 B602/ A0A8C4ZH54	Keratins
A0A8C5FDF8	F-actin-capping protein subunit beta complex
A0A8C5C7G7	Smoothelin a
A0A8C5BEP0	Tubulin alpha-1A chain (TUBA 1A)
2.5. Adhesion and Binding Processes	
A0A8C5BRQ2	Annexin
A0A8C5AI73	Secreted acidic cysteine rich glycoprotein (Sparc)

A0A8C5B6I8	Myelin basic protein (MBP)
2.6. Cellular Signaling Processes	
A0A8C4ZK56	Arrestin-domain containing protein 1 (Arrdc1)
A0A8C5BSR3	Calmodulin 2a phosphorylase kinase (CaMKII)
A0A8C4Z128	Glypicans (Gpi)
A0A8C5BN57/A0A8C4Z2M4	Glycoprotein Tetraspanin
A0A8C4Z782/A0A8C5B4W1	Nucleobindin 1 (NUCB1)
2.7. Cellular Immunological- Processes	
A0A8C5F947	A20/AN1 zinc-finger domain-containing protein
A0A8C5BVB7	Pentraxin
2.8. Nuclear Physiological Processes	
A0A8C5FTZ2/A0A8C4ZQW9/A0A8C4ZTE5	High mobility group (HMG) protein
A0A8C5B042/A0A8C5FQN1/A0A8C5FAA0	Histone protein
2.9. Ions Transport Processes	
A0A8C5AKI2	Sodium/potassium-transporting ATPase subunit beta (NKA)
A0A8C4Z4K1/A0A8C5ASM5	Sodium/potassium-transporting ATPase subunit alpha
2.10. Sexual Differentiation Processes	
A0A8C5A412	SPATA6 protein
A0A8C5CHW7	Vitellogenin-2-like protein
3.Identifiecation of Known Otolith Proteins	
A0A8C4ZKX9	Carbonic anhydrase protein (CA)
A0A8C5CSC6	Cochlin
A0A8C5AZT6	Myosin
A0A8C5F796	Otogelin
A0A8C5CL43	Otolin-1
A0A8C5ASM5/A0A8C5AKI2	Na, K-ATPase proteins
A0A8C5AI73	Secreted acidic cysteine rich glycoprotein (Sparc)
A0A8C5BD06/A0A8C5D2V1/A0A8C5AT89	SERPIN domain-containing protein
A0A8C5AFL5/A0A8C4ZVQ3	α- and β-Tectorins

2.5. Proteins Linked to Biochemical Processes

2.5.1. Protein Synthesis

Cod otoliths contained several proteins implicated in protein synthesis. For example, we identified a series of seven subunit otolith proteins belonging to the regulatory 40S ribosomal proteome known to control an increasing number of essential biochemical

mechanisms of the cellular lifecycle, including DNA synthesis, repair, transcription, translation and cell signal transduction [34]. In addition to the 40S ribosome proteins, we also identified four large 60S subunits [35]. We also identified the presence of aminoacyl-tRNA hydrolase protein, which is responsible for the termination steps of protein biosynthesis [36]. Similarly, we identified the purine-rich element binding protein Ab (PURA), which is a single-stranded DNA-binding protein implicated in the control of DNA replication and transcription [37]. A final example of protein synthesis proteins identified was RNP, which is in charge of cellular processes such as transcription, translation and regulating gene expression and the metabolism of RNA [38].

2.5.2. Biochemical Reaction Processes

With respect to the biochemical reaction processes, we noted the presence of proteins responsible for the ketogenesis metabolic pathway, exemplified by the presence of oxoisovalerate dehydrogenase subunit alpha and acetyl-CoA acetyltransferase 1 (ACAT1) proteins [39]. Similarly, we identified aconitate hydratase, an enzyme involved in the isomerization of citrate to isocitrate within the citric acid cycle [40], and the transketolase b (TKT) enzyme that links the pentose phosphate pathway with the glycolytic pathway [40]. Also present was malate dehydrogenase (MDH), a protein responsible for the central oxidative pathway [41] and peroxiredoxin-1 (PRX1), which plays an antioxidant protective role in cells [42]. Somatolactin, which is a pituitary gland glycoprotein growth hormone involved in regulating acid-base, calcium and phosphate levels [43], was also present.

2.6. Proteins Linked to Physiological Processes

2.6.1. Brain Function

We noted the presence of proteins within the otoliths that are linked to various brain functions. These included 14-3-3 beta/alpha-1-like protein, which is involved in different brain functions and the nervous system of fish (e.g., neural signaling, neuronal development and neuroprotection) [44], as well as the alpha-2-HS-glycoprotein-like, which plays a critical role in brain development [45]. Likewise, we identified aspartate aminotransferase, which is responsible for synthesizing neurotransmitters [46].

2.6.2. Mediated Transport Processes

Proteins identified in cod otoliths that are linked to mediated transport processes included AP-3 complex subunit mu-2 (PA3), which is responsible for protein trafficking to lysosomes and specialized organelles [47], and the adaptor-related protein complex 3 subunit sigma 1, which is involved in clathrin-mediated vesicular transport from the trans-Golgi network (TGN) [48].

2.6.3. Mitochondrial Processes

Proteins identified in the otoliths that are linked to mitochondrial processes included ADP/ATP translocase, which belongs to the mitochondrial carrier family [49]. We also found the ATP-binding cassette sub-family B (MDR/TAP), which regulates apoptotic and non-apoptotic cell death [50]; the ATP synthase-coupling factor 6, which was reported to be essential for energy transduction [51]; and the ATP synthase subunits

alpha and beta that generate electron transport complexes for the respiratory chain [52]. Finally, we identified the voltage-dependent anion-selective channel 2 (VDAC2) protein, which is known to contribute to oxidative metabolism by facilitating solute transport across the outer mitochondrial membrane (OMM). VDAC2 also has a distinctive Ca^{2+} role in mediating the sarcoplasmic reticulum to mitochondria local transport in cardiomyocytes [53].

2.6.4. Cytoskeleton and Extracellular Matrices

Otolith proteins involved in the cytoskeleton and extracellular matrix formation included actin, beta protein and actin-related protein 2/3 complex subunit 5, all highly conserved major proteins involved in structure, the integrity of the contractile apparatus and non-muscle cytoskeletal actins that are ubiquitously expressed [54, 55]. We also identified chondroadherin-like b (CHADL) protein, which is responsible for creating the extracellular matrices, and the assembly of collagen fibrils, which are composed by the collagen-associated small leucine-rich proteins (SLRPS) family [56]. Also observed were choclin, an extracellular matrix (ECM) protein, which constitutes the main acellular microenvironment of cells in almost all tissues and organs [57]; decorin, also known as the small cellular or pericellular matrix proteoglycan (SLRP), the component of the connective tissues and stabilizing inter-fibrillar organization [29, 58]; and intermediate filament protein ON3-like (IFs) [59] and keratins [60], both proteins belonging to the cytoskeletal structural components. We also identified the F-actin-capping protein subunit beta complex, which binds in a calcium-independent way to the growing ends of actin filaments

(also called barbed end), blocking the exchange of subunits at these ends [55]. Additionally, we observed the presence of smoothelin a, an actin-binding protein that directs the functional contractility of the intestinal smooth muscle [61]. Finally, we observed the presence of the tubulin alpha-1A chain (TUBA 1A). This protein provides structural support and the pathway for transport and force generation in cell division, neuronal development and maturation [62].

2.6.5. Adhesion and Binding Processes

We observed the presence of proteins involved in the physiological processes of adhesion and binding, including annexin, which is a Ca^{2+} dependent phospholipid binding protein. This protein is implicated in a variety of pathophysiological processes, including cell proliferation, apoptosis, differentiation, metastasis and inflammatory response [63]. We also identified myelin basic protein (MBP), which is an abundant protein in the central nervous system. MBP acts as a membrane actin-binding protein, and is responsible for the adhesion of the cytosolic surfaces of multilayered compact myelin [64]. It is involved in several other functions, such as interacting with polyanionic proteins, including actin, tubulin, Ca^{2+}-calmodulin, clathrin and negatively charged lipids [65].

2.6.6. Cellular Signaling Processes

We identified several proteins involved in cellular signal processing in the two cod otoliths. Arrestin-domain containing protein 1 (Arrdc1) was identified and is known to have the ability to arrest or turn off the coupling of G-protein-coupled-Receptors (GPCRs)

and thereby inhibit signalling [66]. Similarly, we found calmodulin 2a phosphorylase kinase (CaMKII), which is involved in many signalling cascades and memory. It is well known that the divalent cation calcium (Ca^{2+}), which is vital to cellular physiology, is the most utilized second messenger in cellular signalling [67]. Due to its highly reactive nature, the low intracellular concentration of Ca^{2+} makes it a potent molecule for use in cellular signalling. Indeed, many of the secondary messenger effects of Ca^{2+} are mediated through the ubiquitous sensing protein calmodulin (CaM) [68]. We also identified the glypicans (Gpi) protein, which belongs to the heparan sulfate proteoglycans (HSPG) family. These are ubiquitous molecules playing essential functions in various biological processes. The Gpi-protein's main job is to anchor HSPGs directly to the cell surface and/or extracellular matrix, where they regulate growth factor signalling during development [69].

Similarly, we identified the presence of the glycoprotein tetraspanins, a membrane-spanning protein with a conserved structure that functions primarily as a tissue membrane protein organizer. All members of the tetraspanin family of proteins have four transmembrane domains, which contribute to creating a small (EC1) and large (EC2) extracellular loop. The large extracellular loop contains a conserved Cys-Cys-Gly amino acid motif (CCG motif). These four conserved cysteine residues within EC2 promote the formation of disulfide bridges [70]. Finally, we observed the presence of the Nucleobindin 1 (NUCB1) protein; it is a putative DNA- and calcium-binding protein which has a vital role in the central nervous system. NUCB1 was revealed to be present in the Golgi apparatus and can play an important role in the spatiotemporal calcium handling in signaling cells [71].

2.6.7. Cellular Immunological Processes

We identified two otolith proteins most commonly implicated in cellular immunological processes. The A20/AN1 zinc-finger protein's main role is to regulate the immune response. It also acts as a de-ubiquitinating enzyme and is involved in controlling fundamental cellular activities[72-74]. Pentraxin, which functions as a soluble pattern-recognition molecule, was also identified. Its main role is to induce host defense, primarily to induce the opsonization of the pathogens through activating the complement pathway and binding to Fc gamma receptors [75].

2.6.8. Physiological Nuclear Processes

For proteins associated with nuclear physiological processes, we found an otolith protein named the high mobility group (HMG) protein. The HMG is a superfamily of abundant and ubiquitous nuclear proteins that bind to DNA and nucleosomes and induce structural changes in the chromatin fiber. They are important in chromatin dynamics and influence the regulation of DNA-dependent processes such as transcription, replication, recombination, and DNA repair [76]. In addition, we found a histone protein that provides structural support for chromosomes containing an elongated molecule of DNA, which must acceptably fit into the cell nucleus. This allows DNA to wrap around complexes of histone proteins, allowing the chromosome to have a more compact shape [77].

2.6.9. Ion Transport Processes

We found two Na, K-ATPase proteins, the sodium/potassium-transporting ATPase subunit beta (NKA) and the sodium/potassium-transporting ATPase subunit alpha. Both proteins classically work as an ion pump that creates an electrochemical gradient across the plasma membrane [78]. This electrochemical gradient was created by pumping three molecules of Na^+ out of the cell in exchange for two molecules of K^+ entering the cell. This process is essential for transepithelial transport, nutrient uptake and membrane potential. In addition, Na, K-ATPase also functions as a receptor, a signal transducer and a cell adhesion molecule [78].

2.6.10. Sexual Differentiation

Our cod otoliths contained proteins related to sexual differentiation and gamete development. The SPATA6 protein identified in the male cod otolith is essential during the process of fertilization, during sperm–egg binding and fusion [79, 80]. In zebrafish, this sperm membrane protein is required for the formation of the segmented columns and the capitulum, two major structures of the sperm-connecting piece essential for linking the developing flagellum to the head during late spermiogenesis [81].

We also identified Vitellogenin-2-like. Vitellogenin (VTG) is a phospho-glyco-lipoprotein synthesized in the liver of oviparous animals in response to circulating estrogens [82]. The presence of the vitellogenin protein is specifically found in female blood serum during oocyte growth. It is generally accepted that vitellogenin protein, when hydrolyzed into a free amino acid pool, serves as the main nutritional source for the

developing embryo [82, 83]. These two identified otolith proteins could serve as major sexual differentiation biomarkers, supporting the idea that otoliths can store biological information about fish

2.7. Identification of Known Otolith Proteins

Some of the proteins that we identified had been previously documented in fish otoliths, although not necessarily for Atlantic cod. For example, we identified carbonic anhydrase (CA), an enzyme critical in acid-base homeostasis and bone remodeling. CA is produced in the brain and drives the neuronally guided bio-mineralization process. The CA protein is an enzyme secreted in the inner ear epithelium of the fish, where it regulates the provision of carbonate for calcium carbonate incorporation into the otolith [84]. We identified cochlin, which is one of the main known otolith constituents and is responsible for calcium carbonate crystalline formation. This otolith protein also regulates the immune response against infection, specifically innate immunity [85]. In addition, we identified myosin, another known constituent of otoliths. Myosins are motor proteins linking the actin-cytoskeleton with membrane phospholipids. The main roles of these proteins are to promote connections between the cytoskeleton and the plasma membrane. They are essential in cellular processes such as cell migration, vesicular trafficking and cytokinesis. Previous studies have implicated these molecules in cell functions, including endocytosis, exocytosis, the release of extracellular vesicles and the regulation of cell shape and membrane elasticity [86]. We also identified the important otogelin protein, a major constituent of the otoliths. The otogelin proteins are formed in the sensory maculae attached

to the otolithic membrane (a gelatinous extracellular matrix) that provides a physical coupling (tethering) between the otolith and the underlying sensory epithelium [87].

Otolin-1, a collagen-like protein which plays an important role in the growth of otoliths, was also identified. It has been proposed that it may serve as a template for the calcification of the otoliths [23]. We also found Na and K-ATPase proteins in our cod otoliths. These proteins serve as an ion pump that creates the electrochemical gradient across the plasma membrane. This gradient is essential for transepithelial transport, nutrient uptake and membrane potential [78]. Na and K-ATPase proteins can also function as receptors, signal transducers and cell adhesion molecules. The Na and K-ATPase proteins are also responsible for developing various physiological needs [78]. We identified the known secreted acidic cysteine-rich glycoprotein (Sparc), which plays an important role in otolith morphogenesis [88]. This secreted acidic cysteine-rich glycoprotein, which binds collagen and Ca^{2+}, is a precerebellin-like protein. It was suggested that it could associate with both collagenous otolin-1 and neuroserpin during framework assembly [88]. Another identified known otolith SERPIN domain-containing protein belongs to the serpins family, which is a broadly distributed family of protease inhibitors that can induce conformational change to inhibit target enzymes that are known to be central in controlling many important proteolytic cascades [88]. Serpins are conformationally labile, and pathogens can misfold them into inactive protein polymers [89]. Likewise, α-tectorin and β-tectorin proteins were also identified. These are glycoprotein components of the otolithic membrane and are essential in developing the teleost otolithic membrane at embryonic stages [86]. The last previously identified otolith protein that we detected in cod ololiths was the V-type proton

ATPase subunit G, which functions as a V-ATPase proton pump. This protein creates an acidic medium, which is necessary for the lysosome function and vesicular traffic. It is also essential for several developmental processes [90].

2.8. Conclusions and Future Directions

The qualitative preliminary shotgun proteomics approach used here revealed that cod otoliths contain thousands more proteins than previously documented. Most of these proteins are not implicated in the biomineralization of otoliths, raising the potential for the otolith proteome to help recreate details of fish life history at previously unrealized levels. Much work is still required, however, to fully understand the otolith proteome, the mechanisms by which proteins are incorporated into the otolith matrix and the linkages between otolith proteins and fish physiology. Efforts are underway to accurately quantify the proteins in the cod otolith proteome for the twelve fish examined here, which may be a first step to addressing some of these questions.

2.9. References

[1] A. N. Popper, and A. D. Hawkins, “The importance of particle motion to fishes and invertebrates,” *J. Acoust. Soc. Am.,* vol. 143, no. 1, pp. 470, Jan, 2018. DOI: https://doi.org/10.1121/1.5021594.

[2] O. Lowenstein, "7 The labyrinth," *Sensory systems and electric organs*, Fish Physiology W. S. Hoar and D. J. Randall, eds.Cambridge, MA, USA: Academic Press, 1971. pp. 207-240.

[3] F. Manning, “Hearing in the goldfish in relation to the structure of its ear,” *J. Exp. Zool.,* vol. 41, no. 1, pp. 5-20, 1924.

[4] L. Schnetz, C. Pfaff, E. Libowitzky, Z. Johanson, R. Stepanek, and J. Kriwet, “Morphology and evolutionary significance of phosphatic otoliths within the inner ears of cartilaginous fishes (Chondrichthyes),” *BMC Evol. Biol.,* vol. 19, no. 1, pp. 238, Dec, 2019. DOI: https://doi.org/10.1186/s12862-019-1568-z.

[5] R. R. Fay, “The goldfish ear codes the axis of acoustic particle motion in three dimensions,” *Science,* vol. 225, no. 4665, pp. 951-954, Aug, 1984. DOI: https://doi.org/10.1126/science.6474161.

[6] A. N. Popper, J. Ramcharitar, and S. E. Campana, “Why otoliths? Insights from inner ear physiology and fisheries biology,” *Mar. Freshw. Res.,* vol. 56, no. 5, pp. 497-504, May, 2005. DOI: https://doi.org/10.1071/mf04267.

[7] G. Panella, “Fish otoliths: Daily growth layers and periodical patterns,” *Science,* vol. 173, no. 4002, pp. 1124-1127, Sep, 1971. DOI: https://doi.org/10.1126/science.173.4002.1124.

[8] E. B. Brothers, C. P. P. Mathews, and R. Lasker, “Daily growth increments in otoliths from larval and adult fishes,” *Fish Bull.,* vol. 74, no. 1, pp. 1-8, 1976.

[9] D. Allemand, N. Mayer-Gostan, H. De Pontual, G. Boeuf, and P. Payan, "Fish otolith calcification in relation to endolymph chemistry," *Handbook of biomineralization: Biological aspects and structure formation*, E. Bäuerlein, ed.Weinheim, Germany: Wiley-VCH Verlag GmbH, 2007. pp. 291-308.

[10] S. E. Campana, and S. R. Thorrold, “Otoliths, increments, and elements: keys to a comprehensive understanding of fish populations?,” *Can. J. Fish. Aquat. Sci.,* vol. 58, no. 1, pp. 30-38, May, 2001.

[11] P. C. Daniel Ricard, A. Adamack, J. Burbank, A. D. Abby Daigle, T. L. Kim Emond, G. P. Andrea Perreault, K. Robertson, N. Rolland, M. Schofield, A. Smith, F.-É. Sylvain, and S. Wischniowski, “Proceedings of the technical expertise in Stock Assessment (TESA) national workshop on 'Best practices in age estimation', 31 January to 02 February 2023 in Moncton, New Brunswick,” *Can. J. Fish. Aquat. Sci.,* vol. 3609, pp. 3609: v + 3627 p, Oct, 2024.

[12] S. E. Campana, “How reliable are growth back-calculations based on otoliths?,” *Can. J. Fish. Aquat. Sci.,* vol. 47, no. 11, pp. 2219-2227, May, 1990.

[13] E. T. Degens, W. G. Deuser, and R. L. Haedrich, “Molecular structure and composition of fish otoliths,” *Mar. Biol.,* vol. 2, no. 2, pp. 105-113, 1969. DOI: https://doi.org/10.1007/bf00347005.

[14] S. E. Campana, “Chemistry and composition of fish otoliths:pathways, mechanisms and applications,” *Mar. Ecol. Prog. Ser.,* vol. 188, pp. 263-297, 1999. DOI: https://doi.org/10.3354/meps188263.

[15] P. Payan, H. De Pontual, G. Bœuf, and N. Mayer-Gostan, “Endolymph chemistry and otolith growth in fish,” *Comptes. Rendus. Palevol.,* vol. 3, no. 6-7, pp. 535-547, Oct, 2004. DOI: https://doi.org/10.1016/j.crpv.2004.07.013.

[16] C. Koppl, V. Wilms, I. J. Russell, and H. G. Nothwang, “Evolution of endolymph secretion and endolymphatic potential generation in the vertebrate inner ear,” *Brain*

Behav. Evol., vol. 92, no. 1-2, pp. 1-31, Nov, 2018. DOI: https://doi.org/10.1159/000494050.

[17] C. S. Romanek, and R. W. Gauldie, "A predictive model of otolith growth in fish based on the chemistry of the endolymph," *Comp. Biochem. Physiol. Part A Physiol.,* vol. 114, no. 1, pp. 71-79, May, 1996. DOI: https://doi.org/10.1016/0300-9629(95)02094-2.

[18] M. C. F. Disspain, S. Ulm, and B. M. Gillanders, "Otoliths in archaeology: Methods, applications and future prospects," *J. Archaeol. Sci. Rep.,* vol. 6, pp. 623-632, May, 2016. DOI: https://doi.org/10.1016/j.jasrep.2015.05.012.

[19] M. Yasuo, "Diurnal rhythm in otolith formation in the rainbow trout, Salmo gairdneri: Seasonal reversal of the rhythm in relation to plasma calcium concentrations," *Comp. Biochem. Physiol. Part A Physiol.,* vol. 78, no. 2, pp. 289-293, Jan, 1984. DOI: https://doi.org/10.1016/0300-9629(84)90149-x.

[20] O. R. B. Thomas, and S. E. Swearer, "Otolith biochemistry—A Review," *Rev. Fish. Sci. Aquac.,* vol. 27, no. 4, pp. 458-489, Jul, 2019. DOI: https://doi.org/10.1080/23308249.2019.1627285.

[21] T. N. Loewen, B. Carriere, J. D. Reist, N. M. Halden, and W. G. Anderson, "Linking physiology and biomineralization processes to ecological inferences on the life history of fishes," *Comp. Biochem. Physiol. Part A Mol. Integr. Physiol.,* vol. 202, pp. 123-140, Dec, 2016. DOI: https://doi.org/10.1016/j.cbpa.2016.06.017.

[22] G. Falini, S. Albeck, S. Weiner, and L. Addadi, “Control of aragonite or calcite polymorphism by Mollusk shell macromolecules,” *Science,* vol. 271, no. 5245, pp. 67-69, Oct, 1996. DOI: https://doi.org/10.1126/science.271.5245.67.

[23] E. Murayama, Y. Takagi, T. Ohira, J. G. Davis, M. I. Greene, and H. Nagasawa, “Fish otolith contains a unique structural protein, otolin-1,” *Eur. J. Biochem.,* vol. 269, no. 2, pp. 688-696, Jan, 2002. DOI: https://doi.org/10.1046/j.0014-2956.2001.02701.x.

[24] S. Huang, and S. Qian, “Advances in otolith-related protein research,” *Front. Neurosci.,* vol. 16, no. 7, pp. 956200, Jul, 2022. DOI: https://doi.org/10.3389/fnins.2022.956200.

[25] Y. W. Lundberg, Y. Xu, K. D. Thiessen, and K. L. Kramer, “Mechanisms of otoconia and otolith development,” *Dev. Dyn.,* vol. 244, no. 3, pp. 239-253, Sep, 2015. DOI: https://doi.org/10.1002/dvdy.24195.

[26] O. R. B. Thomas, S. E. Swearer, E. A. Kapp, P. Peng, G. Q. Tonkin-Hill, A. Papenfuss, A. Roberts, P. Bernard, and B. R. Roberts, “The inner ear proteome of fish,” *FEBS J.,* vol. 286, no. 1, pp. 66-81, Jan, 2019. DOI: https://doi.org/10.1111/febs.14715.

[27] E. Mulry, and K. Parham, “Inner ear proteins as potential biomarkers,” *Otol. Neurotol.,* vol. 41, no. 2, pp. 145-152, Feb, 2020. DOI: https://doi.org/10.1097/MAO.0000000000002466.

[28] E. Murayama, P. Herbomel, A. Kawakami, H. Takeda, and H. Nagasawa, “Otolith matrix proteins OMP-1 and Otolin-1 are necessary for normal otolith growth and

their correct anchoring onto the sensory maculae," *Mech. Dev.,* vol. 122, no. 6, pp. 791-803, Jun, 2005. DOI: https://doi.org/10.1016/j.mod.2005.03.002.

[29] M. B. Miller, A. M. Clough, J. N. Batson, and R. W. Vachet, "Transition metal binding to cod otolith proteins," *J. Exp. Mar. Biol. Ecol.,* vol. 329, no. 1, pp. 135-143, Feb, 2006. DOI: https://doi.org/10.1016/j.jembe.2005.08.016.

[30] M. L. Fournier, J. M. Gilmore, S. A. Martin-Brown, and M. P. Washburn, "Multidimensional separations-based shotgun proteomics," *Chem. Rev.,* vol. 107, no. 8, pp. 3654-3686, Aug, 2007. DOI: https://doi.org/10.1021/cr068279a.

[31] J. G. Meyer, "Qualitative and quantitative shotgun proteomics shotgun proteomics data analysis from data-dependent acquisition data-dependent acquisition (DDA) mass spectrometry," *Shotgun Proteomics: Methods and protocols*, M. Carrera and J. Mateos, eds.New York, NY: Springer US, 2021. pp. 297-308.

[32] H. Chen, *VennDiagram: Generate high-resolution venn and euler plots*, Available online: https://CRAN.R-project.org/package=VennDiagram, 2011.

[33] E. H. Dannevig, "Chemical composition of the zones in Cod otoliths," *ICES J. Mar. Sci.,* vol. 21, no. 2, pp. 156-159, 1956. DOI: https://doi.org/10.1093/icesjms/21.2.156.

[34] J. M. Peters, Z. Cejka, J. R. Harris, J. A. Kleinschmidt, and W. Baumeister, "Structural features of the 26 S proteasome complex," *J. Mol.Biol.,* vol. 234, no. 4, pp. 932-937, Dec, 1993. DOI: https://doi.org/10.1006/jmbi.1993.1646.

[35] F. Vanzi, S. Vladimirov, C. R. Knudsen, Y. E. Goldman, and B. S. Cooperman, "Protein synthesis by single ribosomes," *RNA,* vol. 9, no. 10, pp. 1174-1179, Oct, 2003. DOI: https://doi.org/10.1261/rna.5800303.

[36] G. Das, and U. Varshney, "Peptidyl-tRNA hydrolase and its critical role in protein biosynthesis," *Microbiology,* vol. 152, no. Pt 8, pp. 2191-2195, Aug, 2006. DOI: https://doi.org/10.1099/mic.0.29024-0.

[37] T. Osugi, Y. Ding, H. Tanaka, C. H. Kuo, E. Do, Y. Irie, and N. Miki, "Involvement of a single-stranded DNA binding protein, ssCRE-BP/Pur alpha, in morphine dependence," *FEBS Lett.,* vol. 391, no. 1-2, pp. 11-16, Aug, 1996. DOI: https://doi.org/10.1016/0014-5793(96)00696-5.

[38] E. G. Fey, G. Krochmalnic, and S. Penman, "The nonchromatin substructures of the nucleus: the ribonucleoprotein (RNP)-containing and RNP-depleted matrices analyzed by sequential fractionation and resinless section electron microscopy," *J. Cell. Biol.,* vol. 102, no. 5, pp. 1654-1665, May, 1986. DOI: https://doi.org/10.1083/jcb.102.5.1654.

[39] Q. Chen, J. Du, K. Cui, W. Fang, Z. Zhao, Q. Chen, K. Mai, and Q. Ai, "Acetyl-CoA derived from hepatic mitochondrial fatty acid beta-oxidation aggravates inflammation by enhancing p65 acetylation," *iScience,* vol. 24, no. 11, pp. 103244, Nov, 2021. DOI: https://doi.org/10.1016/j.isci.2021.103244.

[40] R. Waagbø, "Water-soluble vitamins in fish ontogeny," *Aquac. Res.,* vol. 41, no. 5, pp. 733-744, 2010. DOI: https://doi.org/10.1111/j.1365-2109.2009.02223.x.

[41] L. Panepucci, M. N. Fernandes, J. R. Sanches, and F. T. Rantin, "Changes in lactate dehydrogenase and malate dehydrogenase activities during hypoxia and after temperature acclimation in the armored fish, Rhinelepis strigosa (Siluriformes, Loricariidae)," *Rev. Bras. Biol.,* vol. 60, no. 2, pp. 353-360, May, 2000. DOI: https://doi.org/10.1590/s0034-71082000000200021.

[42] Y. Valero, F. J. Martinez-Morcillo, M. A. Esteban, E. Chaves-Pozo, and A. Cuesta, "Fish peroxiredoxins and their role in immunity," *Biology (Basel),* vol. 4, no. 4, pp. 860-880, Nov, 2015. DOI: https://doi.org/10.3390/biology4040860.

[43] M. Rand-Weaver, T. Noso, K. Muramoto, and H. Kawauchi, "Isolation and characterization of somatolactin, a new protein related to growth hormone and prolactin from Atlantic cod (*Gadus morhua*) pituitary glands," *Biochemistry,* vol. 30, no. 6, pp. 1509-1515, Feb, 1991. DOI: https://doi.org/10.1021/bi00220a010.

[44] Z. Liu, J. Zhang, A. Ma, X. Wang, Z. Sun, W. Cui, C. Yuan, and C. Zhu, "Molecular characterization, expression analysis of 14-3-3 beta/alpha and the effect of RNA interference on ion transporter protein Na+-K+-ATPase, Na+–H+-exchanger and CFTR in turbot (Scophthalmus maximus)," *Comp. Biochem. Physiol. Part B Biochem. Mol. Biol.,* vol. 246-247, no. November 2019, pp. 110458-110458, Aug-Sep, 2020. DOI: https://doi.org/10.1016/j.cbpb.2020.110458.

[45] S. A. Sower, W. A. Decatur, K. N. Hausken, T. J. Marquis, S. L. Barton, J. Gargan, M. Freamat, M. Wilmot, L. Hollander, J. A. Hall, M. Nozaki, M. Shpilman, and B. Levavi-Sivan, "Emergence of an ancestral glycoprotein hormone in the pituitary of

the sea lamprey, a basal vertebrate," *Endocrinology,* vol. 156, no. 8, pp. 3026-3037, Aug, 2015. DOI: https://doi.org/10.1210/en.2014-1797.

[46] B. Allah Abdulraheem, "Aspartate transaminase (AST) activity in selected tissues & organs of *Clarias Gariepinus* exposed to different levels of paraqua," *J. Environ. Anal. Toxicol.,* vol. 04, no. 03, Feb, 2014. DOI: https://doi.org/10.4172/2161-0525.1000214.

[47] L. A. Kimpler, N. L. Glosson, D. Downs, P. Gonyo, N. A. May, and A. W. Hudson, "Adaptor protein complexes AP-1 and AP-3 are required by the HHV-7 Immunoevasin U21 for rerouting of class I MHC molecules to the lysosomal compartment," *PLOS One,* vol. 9, no. 6, pp. e99139, Jun, 2014. DOI: https://doi.org/10.1371/journal.pone.0099139.

[48] J. Blumstein, V. Faundez, F. Nakatsu, T. Saito, H. Ohno, and R. B. Kelly, "The neuronal form of adaptor protein-3 is required for synaptic vesicle formation from endosomes," *J. Neurosci.,* vol. 21, no. 20, pp. 8034-8042, Oct, 2001. DOI: https://doi.org/10.1523/JNEUROSCI.21-20-08034.2001.

[49] R. Sugahara, A. Jouraku, T. Nakakura, T. Kusakabe, T. Yamamoto, Y. Shinohara, H. Miyoshi, and T. Shiotsuki, "Two adenine nucleotide translocase paralogues involved in cell proliferation and spermatogenesis in the silkworm Bombyx mori," *PLOS One,* vol. 10, no. 3, pp. e0119429, Mar, 2015. DOI: https://doi.org/10.1371/journal.pone.0119429.

[50] F. Bieczynski, J. C. Painefilu, A. Venturino, and C. M. Luquet, "Expression and function of ABC proteins in fish intestine," *Front. Physiol.,* vol. 12, no. December, pp. 791834, Feb, 2021. DOI: https://doi.org/10.3389/fphys.2021.791834.

[51] G. Katyal, B. Ebanks, M. Lucassen, C. Papetti, and L. Chakrabarti, "Sequence and structure comparison of ATP synthase F0 subunits 6 and 8 in notothenioid fish," *PLOS One,* vol. 16, no. 10, pp. e0245822, Oct, 2021. DOI: https://doi.org/10.1371/journal.pone.0245822.

[52] S. Ni, Y. Zhou, Y. Chen, X. Du, and S. Zhang, "Identification of ATP synthase alpha subunit as a new maternal factor capable of protecting zebrafish embryos from bacterial infection," *FASEB J.,* vol. 33, no. 11, pp. 12983-13001, Nov, 2019. DOI: https://doi.org/10.1096/fj.201901290R.

[53] S. Naghdi, and G. Hajnoczky, "VDAC2-specific cellular functions and the underlying structure," *Biochim. Biophys. Acta (BBA) Mol. Cell Res.,* vol. 1863, no. 10, pp. 2503-2514, Oct, 2016. DOI: https://doi.org/10.1016/j.bbamcr.2016.04.020.

[54] U. R. Acharya, S. Behera, S. Swain, M. K. Panda, A. R. Mistri, and B. Sahoo, "Sequence and structural analysis of β- actin protein of fishes, using bioinformatics tools and techniques," *Int. J. Biosci.*, pp. 249-256, Jun, 2014. DOI: https://doi.org/10.12692/ijb/4.11.249-256.

[55] C. G. dos Remedios, D. Chhabra, M. Kekic, I. V. Dedova, M. Tsubakihara, D. A. Berry, and N. J. Nosworthy, "Actin binding proteins: Regulation of cytoskeletal microfilaments," *Physiol. Rev.,* vol. 83, no. 2, pp. 433-473, Apr, 2003. DOI: https://doi.org/10.1152/physrev.00026.2002.

[56] V. Tillgren, J. C. Ho, P. Onnerfjord, and S. Kalamajski, "The novel small leucine-rich protein chondroadherin-like (CHADL) is expressed in cartilage and modulates chondrocyte differentiation," *J. Biol. Chem.,* vol. 290, no. 2, pp. 918-925, Jan, 2015. DOI: https://doi.org/10.1074/jbc.M114.593541.

[57] Y. J. Hsueh, D. H. Ma, K. S. Ma, T. K. Wang, C. H. Chou, C. C. Lin, M. C. Huang, L. J. Luo, J. Y. Lai, and H. C. Chen, "Extracellular matrix protein coating of processed fish scales improves human corneal endothelial cell adhesion and proliferation," *Transl. Vis. Sci. Technol.,* vol. 8, no. 3, pp. 27, May, 2019. DOI: https://doi.org/10.1167/tvst.8.3.27.

[58] J. J. Zoeller, W. Pimtong, H. Corby, S. Goldoni, A. E. Iozzo, R. T. Owens, S. Y. Ho, and R. V. Iozzo, "A central role for decorin during vertebrate convergent extension," *J. Biol. Chem.,* vol. 284, no. 17, pp. 11728-11737, Apr, 2009. DOI: https://doi.org/10.1074/jbc.M808991200.

[59] Y. Nishimura, K. Kasahara, and M. Inagaki, "Intermediate filaments and IF-associated proteins: from cell architecture to cell proliferation," *Proc. Jpn. Acad. Ser.,* vol. 95, no. 8, pp. 479-493, Jan, 2019. DOI: https://doi.org/10.2183/pjab.95.034.

[60] M. Schaffeld, and J. Markl, "Fish keratins," *Methods Cell Biol.,* vol. 78, pp. 627-671, 2004. DOI: https://doi.org/10.1016/s0091-679x(04)78022-x.

[61] F. T. van der Loop, G. Schaart, E. D. Timmer, F. C. Ramaekers, and G. J. van Eys, "Smoothelin, a novel cytoskeletal protein specific for smooth muscle cells," *J. Cell*

Biol., vol. 134, no. 2, pp. 401-411, Jul, 1996. DOI: https://doi.org/10.1083/jcb.134.2.401.

[62] H. W. Detrich, 3rd, T. J. Fitzgerald, J. H. Dinsmore, and S. P. Marchese-Ragona, "Brain and egg tubulins from antarctic fishes are functionally and structurally distinct," *J. Biol. Chem.,* vol. 267, no. 26, pp. 18766-18775, Sep, 1992.

[63] H. J. Hwang, C. H. Moon, H. G. Kim, J. Y. Kim, J. M. Lee, J. W. Park, and D. K. Chung, "Identification and functional analysis of salmon annexin 1 induced by a virus infection in a fish cell line," *J. Virol.,* vol. 81, no. 24, pp. 13816-13824, Dec, 2007. DOI: https://doi.org/10.1128/JVI.02822-06.

[64] S. Nawaz, J. Schweitzer, O. Jahn, and H. B. Werner, "Molecular evolution of myelin basic protein, an abundant structural myelin component," *Glia,* vol. 61, no. 8, pp. 1364-1377, Aug, 2013. DOI: https://doi.org/10.1002/glia.22520.

[65] J. M. Boggs, "Myelin basic protein: a multifunctional protein," *Cell. Mol. Life Sci.,* vol. 63, no. 17, pp. 1945-1961, Sep, 2006. DOI: https://doi.org/10.1007/s00018-006-6094-7.

[66] S. Anand, N. Foot, C. S. Ang, K. M. Gembus, S. Keerthikumar, C. G. Adda, S. Mathivanan, and S. Kumar, "Arrestin-domain containing protein 1 (ARRDC1) regulates the protein cargo and release of extracellular vesicles," *Proteomics,* vol. 18, no. 17, pp. e1800266, Sep, 2018. DOI: https://doi.org/10.1002/pmic.201800266.

[67] D. S. Kang, X. Tian, and J. L. Benovic, "Role of beta-arrestins and arrestin domain-containing proteins in G protein-coupled receptor trafficking," *Curr. Opin.*

Cell.Biol., vol. 27, pp. 63-71, Apr, 2014. DOI: https://doi.org/10.1016/j.ceb.2013.11.005.

[68] M. T. Swulius, and M. N. Waxham, "Ca(2+)/calmodulin-dependent protein kinases," *Cell. Mol. Life Sci.,* vol. 65, no. 17, pp. 2637-2657, Sep, 2008. DOI: https://doi.org/10.1007/s00018-008-8086-2.

[69] M. Gupta, and M. Brand, "Identification and expression analysis of zebrafish glypicans during embryonic development," *PLOS One,* vol. 8, no. 11, pp. e80824, Nov, 2013. DOI: https://doi.org/10.1371/journal.pone.0080824.

[70] C. M. Termini, and J. M. Gillette, "Tetraspanins function as regulators of cellular signaling," *Front. Cell. Dev. Biol.,* vol. 5, no. 4, pp. 34, Apr, 2017. DOI: https://doi.org/10.3389/fcell.2017.00034.

[71] S. Tulke, P. Williams, A. Hellysaz, E. Ilegems, M. Wendel, and C. Broberger, "Nucleobindin 1 (NUCB1) is a Golgi-resident marker of neurons," *Neuroscience,* vol. 314, pp. 179-188, Feb, 2016. DOI: https://doi.org/10.1016/j.neuroscience.2015.11.062.

[72] S. Vij, and A. K. Tyagi, "A20/AN1 zinc-finger domain-containing proteins in plants and animals represent common elements in stress response," *Funct. Integr. Genom.,* vol. 8, no. 3, pp. 301-307, Aug, 2008. DOI: https://doi.org/10.1007/s10142-008-0078-7.

[73] P. C. Evans, H. Ovaa, M. Hamon, P. J. Kilshaw, S. Hamm, S. Bauer, H. L. Ploegh, and T. S. Smith, "Zinc-finger protein A20, a regulator of inflammation and cell

survival, has de-ubiquitinating activity," *Biochem. J.,* vol. 378, no. Pt 3, pp. 727-734, Mar, 2004. DOI: https://doi.org/10.1042/BJ20031377.

[74] J. H. Jang, H. Kim, I. Y. Jung, and J. H. Cho, "A20 Inhibits LPS-induced inflammation by regulating TRAF6 polyubiquitination in *Rainbow Trout*," *Int. J. Mol. Sci.,* vol. 22, no. 18, pp. 9801-9801, Sep, 2021. DOI: https://doi.org/10.3390/ijms22189801.

[75] T. W. Du Clos, "Pentraxins: structure, function, and role in inflammation," *ISRN Inflamm.,* vol. 2013, pp. 379040, Sep, 2013. DOI: https://doi.org/10.1155/2013/379040.

[76] M. Bustin, and R. Reeves, "High-mobility-group chromosomal proteins: architectural components that facilitate chromatin function," *Prog. Nucleic Acid Res. Mol. Biol.,* vol. 54, pp. 35-100, Jan, 1996. DOI: https://doi.org/10.1016/s0079-6603(08)60360-8.

[77] R. DesJarlais, and P. J. Tummino, "Role of histone-modifying enzymes and their complexes in regulation of chromatin biology," *Biochemistry,* vol. 55, no. 11, pp. 1584-1599, Mar, 2016. DOI: https://doi.org/10.1021/acs.biochem.5b01210.

[78] Z. Li, and S. A. Langhans, "Transcriptional regulators of Na,K-ATPase subunits," *Front. Cell. Dev. Biol.,* vol. 3, no. OCT, pp. 66, Oct, 2015. DOI: https://doi.org/10.3389/fcell.2015.00066.

[79] M. I. Binner, A. Kogan, K. Panser, A. Schleiffer, V. E. Deneke, and A. Pauli, "The sperm protein Spaca6 is essential for fertilization in Zebrafish," *Front. cell dev.*

biol., vol. 9, no. 1, pp. 806982, Oct, 2021. DOI: https://doi.org/10.3389/fcell.2021.806982.

[80] S. Yuan, C. J. Stratton, J. Bao, H. Zheng, B. P. Bhetwal, R. Yanagimachi, and W. Yan, "Spata6 is required for normal assembly of the sperm connecting piece and tight head-tail conjunction," *Proc. Natl. Acad. Sci. USA,* vol. 112, no. 5, pp. E430-439, Feb, 2015. DOI: https://doi.org/10.1073/pnas.1424648112.

[81] M. S. Lehti, and A. Sironen, "Formation and function of sperm tail structures in association with sperm motility defects," *Biol. Reprod.,* vol. 97, no. 4, pp. 522-536, Oct, 2017. DOI: https://doi.org/10.1093/biolre/iox096.

[82] A. M. Cohen, A. A. H. Mansour, and J. H. Banoub, "'De novo' sequencing of Atlantic cod vitellogenin tryptic peptides by matrix-assisted laser desorption/ionization quadrupole time-of-flight tandem mass spectrometry: similarities with haddock vitellogenin," *Rapid Commun. Mass Spectrom.,* vol. 19, no. 17, pp. 2454-2460, Jul, 2005. DOI: https://doi.org/10.1002/rcm.2084.

[83] A. Hara, N. Hiramatsu, and T. Fujita, "Vitellogenesis and choriogenesis in fishes," *Fish. Sci.,* vol. 82, no. 2, pp. 187-202, Jan, 2016. DOI: https://doi.org/10.1007/s12562-015-0957-5.

[84] L. L. Hamm, N. Nakhoul, and K. S. Hering-Smith, "Acid-base homeostasis," *Clin. J. Am. Soc. Nephrol.,* vol. 10, no. 12, pp. 2232-2242, Dec, 2015. DOI: https://doi.org/10.2215/CJN.07400715.

[85] H. J. Rhyu, S. H. Bae, J. Jung, and Y. M. Hyun, "Cochlin-cleaved LCCL is a dual-armed regulator of the innate immune response in the cochlea during

inflammation," *BMB Rep.,* vol. 53, no. 9, pp. 449-452, Sep, 2020. DOI: https://doi.org/10.5483/BMBRep.2020.53.9.104.

[86] D. A. Giron-Perez, Z. L. Piedra-Quintero, and L. Santos-Argumedo, "Class I myosins: Highly versatile proteins with specific functions in the immune system," *J.Leukoc. Biol.,* vol. 105, no. 5, pp. 973-981, May, 2019. DOI: https://doi.org/10.1002/JLB.1MR0918-350RRR.

[87] G. A. Stooke-Vaughan, N. D. Obholzer, S. Baxendale, S. G. Megason, and T. T. Whitfield, "Otolith tethering in the zebrafish otic vesicle requires Otogelin and α-Tectorin," *Development,* vol. 142, no. 6, pp. 1137-1145, Jan, 2015.

[88] Y. J. Kang, A. K. Stevenson, P. M. Yau, and R. Kollmar, "Sparc protein is required for normal growth of zebrafish otoliths," *J. Assoc. Res. Otolaryngol.,* vol. 9, no. 4, pp. 436-451, Dec, 2008. DOI: https://doi.org/10.1007/s10162-008-0137-8.

[89] R. H. Law, Q. Zhang, S. McGowan, A. M. Buckle, G. A. Silverman, W. Wong, C. J. Rosado, C. G. Langendorf, R. N. Pike, P. I. Bird, and J. C. Whisstock, "An overview of the serpin superfamily," *Genome Biol.,* vol. 7, no. 5, pp. 216, May, 2006. DOI: https://doi.org/10.1186/gb-2006-7-5-216.

[90] J. L. Ramos-Balderas, S. Carrillo-Rosas, A. Guzman, R. E. Navarro, and E. Maldonado, "The zebrafish mutants for the V-ATPase subunits d, ac45, E, H and c and their variable pigment dilution phenotype," *BMC Res. Notes,* vol. 6, no. 1, pp. 39, Feb, 2013. DOI: https://doi.org/10.1186/1756-0500-6-39.

Chapter 3 Proteomic Blueprint of Atlantic Cod (*Gadus morhua*) Otoliths Revealing Environmental Stress Insights through Label-Free Quantitative Shotgun Proteomics

This Chapter is reproduced with permission from Trevena N. Youssef, Sherri L. Christian , Rick Rideout, Aaron Adamack, Pierre Thibault, Eric Bonneil, Travis D. Fridgen and Joseph Banoub "Proteomic blueprint of Atlantic Cod (*Gadus morhua*) otoliths revealing environmental stress insights through label-free quantitative shotgun proteomics," *BioChem,* vol. 4, no. 2, pp. 144-165, 2024; https://doi.org/10.3390/biochem4020008.

3.1. Abstract:

Otoliths of the fish's inner ear serve as a natural chronological recorder because of their continuous formation marked by daily, monthly, and annual increments. Despite their importance, the comprehensive protein content of otoliths remains not fully identified. Using the label-free shotgun proteomics method with one-dimensional liquid chromatography coupled to electrospray ionization-FAIMS-orbitrap tandem mass spectrometry, we quantified a broad range of proteins, with individual otoliths containing between 1341 and 1839 proteins. The identified proteins could potentially serve as a blueprint for fish growth from embryo to adult. We quantified eleven heat-shock proteins

(HSPs) in both sexes and several proteins impacted by endocrine disruptors, indicating the otolith's capacity to reflect environmental stress, potentially linked to climate change effects and altering of hormonal and neuroendocrine functions. Our bioinformatic ontology analysis confirmed the presence of proteins critical for various biological processes, including structural and enzymatic proteins. Protein–protein interaction (PPI) mapping also identified key interactions between the identified proteins. These findings significantly advance our understanding of otolith proteomics, offering a solid foundation for future work. Most of the identified proteins deposited daily and influenced by the environment were not implicated in the biomineralization of otolith, raising the potential for the otolith proteome to recreate details of fish life history at previously unrealized levels.

3.2. Introduction

Atlantic cod (*Gadus morhua*) fishing is a significant economic resource in Canada, impacted by both overfishing and climate change [1-3]. The cod's inner ear plays a crucial role in its balance and auditory functions. It consists of three semicircular canals that detect head movements and are essential for orientation; these canals are filled with endolymph fluid and contain a crista, which is a sensor for rotational and angular motions. Additionally, the inner ear includes three otolithic organs, the saccule, lagena, and utricle, each containing a unique otolith or ear stone (sagitta, lapillus, and asteriscus) vital for auditory and equilibrium processes [4-6].

Otoliths are composed of calcium carbonate ($CaCO_3$) embedded with organic molecules such as complex polysaccharides and proteins, and are metabolically inert. They

grow continuously through the daily accretion of concentric layers of the otolith matrix [7-9]. Otoliths are important tools in fisheries research, offering a window into the life history and ecological dynamics of fish species. Their multifaceted study includes macroscopic analyses, from shape and size, to microscopic examinations, such as growth increments and inorganic chemical composition, reflecting the fish's environment and behaviours [10]. The analysis of the otolith composition can reveal the existence of common environmental factors that influence fish growth, help uncover past climate conditions, and predict future environmental impacts on marine ecosystems [11, 12]. Fish growth is a complex biological process influenced by a combination of intrinsic and extrinsic factors. The intrinsic, such as ontogeny and sex, and extrinsic, such as abiotic conditions of the environment or intra-specific interactions, may complicate inferences about climatic impact [11].

A notable study created a century-long growth biochronology (1908–2014) for Atlantic Cod growth in Icelandic waters from otoliths, and demonstrated that temperature variations significantly influenced growth, with younger fish benefiting from warmer temperatures while older fish experienced negative growth effects under similar conditions [11].

The sagitta, the largest otolith, has garnered significant attention in research due to its size and detailed information about the fish's age and growth patterns. Larger otoliths provide clearer and more distinct growth rings, offering accurate inter-specific morphological diversity [13, 14].

Daily growth layers of otolith structures, formed by the gradual accumulation of new material, vary in thickness and composition depending on environmental conditions,

some associated with proteins and some with the $CaCO_3$ component. This continuous addition from hatching to death provides a valuable record of various aspects of fish life history, and serves as a potential environmental record [15, 16]. Proteins constitute a small portion of the otolith, estimated at around 2–3% [17, 18]. As most of these proteins are unlikely to be directly involved in biomineralization, it suggests that a diversity of proteins present in the endolymph are trapped in the otolith during increment formation [17]. This raises the intriguing possibility that the otolith is not only archiving elemental markers of environmental history, but also protein markers of development and physiological change over an individual's lifetime [17, 19]. Previous research has highlighted the significant roles of fifteen identified proteins in otolith formation and maintenance within vertebrates, focusing on three main groups: otolith matrix proteins, otolith anchoring proteins, and otolith regulatory proteins [15, 20, 21]. However, the comprehensive understanding of the otolith's whole protein composition has not yet been investigated.

The advancement in proteomics has been propelled by innovations in protein separation, mass spectrometry (MS) establishing the identification and analytical composition, and data analysis through bioinformatics. MS is central to extensive protein studies. The "bottom-up" approach dissects proteins into peptides via proteolysis for analysis, termed "shotgun proteomics", when applied to protein mixtures. This method assesses proteins indirectly by analyzing peptides from proteolytic digestion. In shotgun proteomics, peptides are fractionated, analyzed via LC-ESI-MS/MS, and identified by matching the characterized peptide sequences with the mass spectra against predicted spectra from a protein database [22-27].

We have recently demonstrated the feasibility of employing a shotgun proteomics approach to study the proteome of Atlantic Cod otolith key structures located in the fish's inner ears [17]. The data suggested that the otolith proteins could be used to discover the whole fish protein profile ranging from embryo to adult. We have shown that most of these proteins were not implicated in the biomineralization of otoliths, raising the potential for the otolith proteome to help recreate details of fish life history at previously unrealized levels [17]. This initial qualitative investigation of otolith proteins allowed the identification of two primary functional categories, significantly broadening our comprehension of their roles beyond mere biomineralization. The first category involved proteins integral to biochemical processes, primarily in synthesizing and degrading proteins. The second category included proteins that were instrumental in physiological processes. This data significantly broadened our understanding of the roles of otolith proteins beyond mere biomineralization. These recently identified proteins appear to have a significant influence on essential life processes, including but not limited to growth, development, metabolism, and the reproductive system within the otolith framework.

In this work, we present our current efforts to quantify the proteins of the cod otolith proteome from ten fish quantitatively, aiming to address the following objectives: (A) determine the quantity of either different, similar, or absent proteins present in the make-up of the otoliths obtained from both sexes, (B) establishment of the presence of indicators of heat stress present in the otoliths of both sexes, as a possible indicators of global warming of the Atlantic Ocean, and (C) establishment of the presence of endocrine disruptor protein

bioindicators that can indicate the alternation of the hormonal and neuroendocrine fish functions.

3.3. Materials and Methods

3.3.1. Otoliths

The archived otolith collection at the Northwest Atlantic Fisheries Centre (St. John's, NL, Canada) contains thousands of Atlantic cod otoliths collected over several decades. The methods used to collect otoliths can vary slightly with the individual technician, but in general, otoliths were exposed via a dorsal incision in the fish's skull and were removed using forceps. Otoliths were blotted dry with paper towels and stored in small paper envelopes. For this study, we selected ten otoliths (five males and five females) collected in 2019 from the northeast coast of Newfoundland, Canada. Otoliths were washed several times with deionized water before protein extraction, as previously described [17]. These otoliths are different from those used in the previous study **(Tables A2-1, Appendix: Supplementary Materials Excel sheet A2)** [17]. Finally, each individual otolith was ground in a mortar using a pestle and then added to a fine powder.

3.3.2. Chemicals and Standards

All standards, samples, and buffers were prepared using ultra-pure Milli-Q H_2O (18.2 MΩ·cm, Merck Millipore, Darmstadt, Germany). All chemicals were purchased from Sigma Aldrich (Castle Hill, NSW, Australia) and were of the highest available purity. Mass spectrometric grade trypsin was obtained from Promega (Madison, WI, USA). MS-grade

solvents for chromatography were obtained from Canadian Life Science (Peterborough, ON, Canada).

3.3.3. Otolith Protein Extraction

The sagitta otoliths were washed, cleaned, and dried as previously described [17]. Full powdered otoliths (2 mg) were suspended in 20% w/v trichloroacetic acid (TCA) (10 mL) and incubated overnight at room temperature. Samples were then centrifuged at 10,000× g for 10 min, and the supernatant was discarded. The crystals were washed with 100 µL of ice-cold acetone and recentrifuged. The supernatant and any remaining undissolved otolith were discarded, and the vacuum-dried pellet was processed for in-solution digestion. Briefly, 0.1 mg of the pellet was resuspended in denaturing buffer containing 8 M urea and 0.4 M ammonium bicarbonate (NH_4HCO_3). Then, 10 µL of 0.5 M dithiothreitol (DTT) was added and incubated for 30 min at 60 °C. After cooling for 5 min at room temperature, 20 µL of 0.7 M iodoacetamide ($IAcNH_2$) was added and incubated for 30 min. Next, the sample was diluted with 1.2 mL of H_2O followed by 10 µL of 0.1 M $CaCl_2$. For enzymatic digestion, 100 µL of 0.02 µg/µL trypsin (Promega Trypsin Gold, Mass Spectrometry Grade, Promega) prepared in 50 mM NH_4HCO_3 was added to each sample. The samples were incubated overnight at 37 °C in a shaker. The trypsin activity was inhibited by adding 1 µL of trifluoroacetic acid (TFA), and the samples were acidified to a pH below 3 with formic acid.

The samples were then desalted using Oasis HLB 3cc Extraction Cartridges (Waters, MA, USA) connected to a SuperlcoVisiprep DL manifold (Sigma-Aldrich,

Darmstadt, Germany). The column was conditioned using 0.5 mL methanol followed by 1 mL of an elution buffer containing 50% ACN and 0.1% TFA, and then with 2 mL wash buffer prepared with 0.1% TFA. After loading the sample, the column was washed with 5 mL of wash buffer and eluted twice with 0.5 mL of 50% acetonitrile-0.1% TFA and once with 0.5 mL of 80% ACN-0.1% TFA. The eluant was dried using a vacuum concentrator (SpeedVac Concentrator, Thermo Electron Corp., Waltham, MA, USA). The dried peptide was reconstituted in 12 µL of resuspension buffer containing 5% acetonitrile and 0.1% formic acid.

3.3.4. Shotgun Proteomics by LC-ESI-MS/MS

The LC separation was carried out using the Ultimate 3000RSLCnano system (Dionex/Thermo Fisher Scientific, Waltham, MA, USA). For analysis, 2 µL (1 mg/mL) of the sample was injected onto an in-house packed capillary column (50 cm × 75 µm, pulled tip, ESI source solutions) packed with Jupiter C18 4 µm chromatographic media (Phenomenex, Torrance, CA, USA) at a flow rate of 300 nL/min. Chromatographic separation was performed by a 120 min method using solvent A (0.1% formic acid in MS-grade water) and solvent B (0.1% formic acid in MS-grade acetonitrile) from 5% to 30% for 90 min, then increasing to 55% for the next 12 min, and then to 95% for 8 min before being reduced to 5% B for the remainder of the 120 min run. The column oven temperature was set at 40 ºC.

The ESI-MS and MS/MS spectra were obtained using an Orbitrap Fusion Lumos Tribrid Mass Spectrometer (ThermoScientific, Waltham, MA, USA) fitted with a

Nanospray Flex Ion source and a FAIMSpro source. The detailed acquisition parameters for mass spectrometry analysis were as follows: For ionization, the spray voltage was 1.8 kV, and the ion transfer tube temperature was 300 °C. The data were acquired in data-dependent acquisition (DDA) mode with a full scan using Orbitrap at a resolution of 120,000 over a mass range of 400–2000 m/z. The FAIMS source was operated at three different compensation voltages (CV = 40, 60 and 80). The auto gain control (AGC) was set in standard mode, and maximum injection time at Auto mode for each MS/MS, acquisition of peaks with intensities above 5.0 e^3 were performed using normalized HCD collision energy of 35%. The cycle time was set at 1 s. The isolation window for MS/MS was set at 1.6 Da. The AGC target was set at standard mode with the maximum injection time mode as Auto. The precursor ions with positive charges 2 to 5 were selected for MS/MS analysis. After every single MS/MS acquisition, the dynamic exclusion time was set at 60 s with a mass tolerance of ±10 ppm.

The MS/MS raw files were acquired using Thermo Scientific Xcalibur 4.5 and Tune 3.5 (Waltham, MA, USA) and searched against the *Gadus morhua* protein database (Taxon ID 8049) downloaded from Uniprot using Proteome Discoverer 2.5 (ThermoFisher, Waltham, MA, USA). The SequestHT search engine node was used for peptide and protein identification. Two missed cleavages for trypsin digestion were allowed with a 10 ppm precursor mass tolerance and fragment mass tolerance of 0.6 Da. Oxidation of methionine and N-terminal acetylation were set as dynamic modification, and carbamidomethyl cysteine was selected as a static modification.

3.3.5. Quantitative Analysis

This study was done using label-free proteomics quantification. The peptides are identified and searched against the *Gadus morhua* protein database (Taxon ID 8049) and searched for the MS/MS acquired during the DDA acquisition. The peptide quantification was performed by integrating the area under the curve of the MS^1 of the identified peptides using Proteome Discoverer 2.5 (ThermoFisher, Waltham, MA, USA). This was followed by populating the total area of all the identified peptides within a protein to derive protein abundances. The ratio of these abundances is then used to compare the different samples. This approach allows for relative quantitative analysis, comparing protein levels across samples (0.1 mg/mL), with careful standardization ensuring comparability despite not measuring absolute protein quantities. As a control, we used trypsin-digested bovine serum albumin (BSA) under the same experimental conditions.

To ensure precise comparisons in label-free proteomics quantification, this study implemented consistent protocols across all procedures, from sample prep to analysis.

3.3.5.1. Quantitative Expressed Protein Intensities Accuracy

The variance stabilization normalization (VSN) is a transformation technique employed in mass spectrometry data analysis to maintain consistent variance across the intensity spectrum [28]. VSN serves the dual purpose of background noise subtraction and data normalization, facilitating a clear relationship between MS peak intensity and variance. Consequently, this enhances the accuracy of the analytical results by stabilizing variance. The missing value imputes were performed by replacing missing values with

random values picked in the 5% lower end of the normal distribution of intensities. VSN was performed using Proteome Discoverer 2.5 (ThermoFisher, Waltham, MA, USA). Additionally, a p-value ≤ 0.05 was considered significant.

3.3.6. Statistical Analysis

The quantitative evaluation of the total number of protein expression differences between male and female groups was conducted using two-sample t-tests and then the calculation of 95% confidence intervals (CIs). The statistical analyses were carried out using various R software packages. These included tidyr [29], magrittr [30], plyr [31], dplyr [32], and ggplot2 [33], facilitating the creation of comparison tables to present the findings. Further normalization analysis, generation of heat maps, and creation of volcano plots (abundance ratio Adjusted *p*-Value: (Female)/(Male) by Benjamini-Hochberg procedure) were performed using Proteome Discoverer 2.5 (ThermoFsher, Waltham, MA, USA). A *p*-value ≤ 0.05 was considered significant.

3.3.7. Bioinformatics Analyses

Gene ontology (GO) functional analyses for the extracted otolith proteins from Atlantic cod (*Gadus morhua*) were performed using the ClueGO plugin (version 2.5.9) within Cytoscape software (version 3.9.1). Due to the absence of cod organisms in the ClueGO plugin program, Atlantic salmon (*Salmo Salar*) was used for analysis to obtain the conserved functional analysis with Atlantic cod (*Gadus morhua*). Biological functions, cellular components, immune system processes, molecular functions, and KEGG provide

specific gene annotations with their corresponding functions within identified biological pathways. Finally, the STRING database was used to visualize the PPI within Atlantic cod (*Gadus morhua*) (https://string-db.org/cgi/network?taskId=bybNmeXaeGFU&sessionId=boleulT8hMV6, accessed on 14 May 2024). To identify the top 20 proteins based on their degree of connectivity, the cytoHubba plugin was used.

3.4. Results and Discussion

The main purpose of this work was to provide a comprehensive analysis of the whole protein content of ten otoliths. As mentioned, we have formerly conducted a qualitative analysis of twelve otoliths [17], which helped us understand the composition of otolith proteins. We compared the total number of proteins identified in the previous study to those in the current study. We found differences in the total numbers; we speculate that this discrepancy is due to the ages of the samples or life histories. The previous study analyzed samples that were approximately 12 years old, while our current study includes samples ranging from 8 to 11 years old **(Figure 3-1)**. However, the eleven HSPs were identified in both studies.

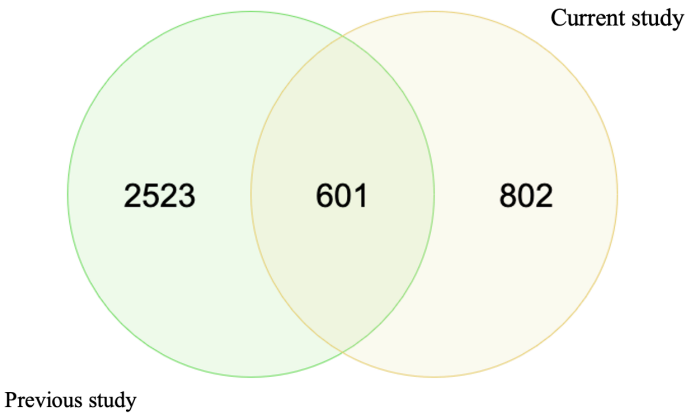

Figure 3-1. Comparison of the total number of otolith proteins between the current study and the previous one. This plot was generated by molbiotools online tools.

In the current research, we presented the quantitative results of the proteins identified in our previous qualitative study [17]. We focused on ten samples obtained from five males and five females collected in 2019 **(Tables A2-1, Appendix: Supplementary Materials Excel sheet A2)**, and we report interesting novel protein biomarkers obtained during this global quantitative analysis of either different, similar, or absent proteins in the make-up of the otoliths obtained from either sex. We highlight that the presence and variation of HSPs in marine organisms could potentially help predict how global climate change might impact species' metabolic costs [34]. Accordingly, in this manuscript, we suggest that the presence of HSPs in the otoliths of both sexes can be used as an indicator of global warming of the Atlantic Ocean. Furthermore, we quantified the proteins that could potentially be influenced by endocrine disruptors that can indicate alterations in the hormonal and neuroendocrine function of fish.

Analysis of our dataset revealed a range in the number of proteins per individual, varying from 1341 to 1839. Utilizing a two-sample t-test to compare the mean number of

proteins between males and females, we found that there was no significant difference in the total number of proteins **(Figure 3-2)**. This finding is supported by the 95% confidence intervals for females (1366.121, 1805.479) and for males (1327.221, 1700.779).

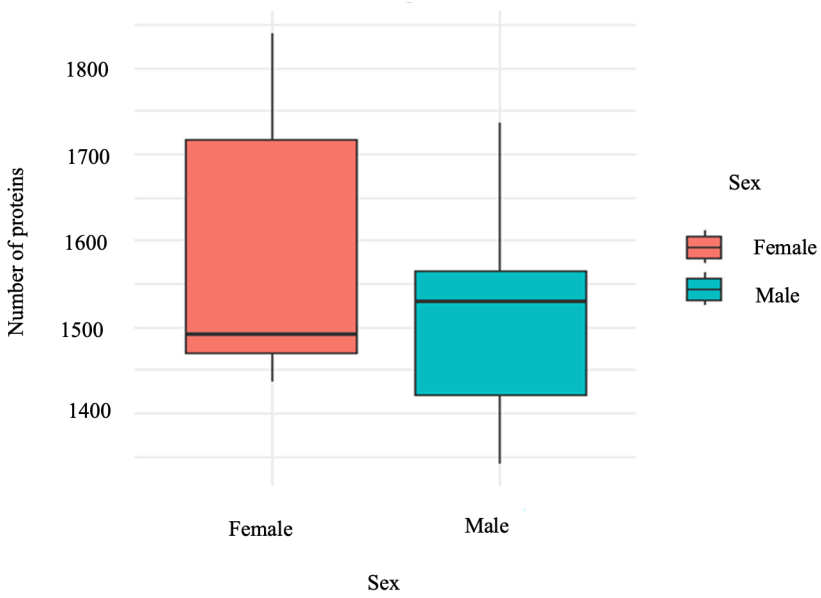

Figure 3-2. The total number of otolith proteins is similar between the sexes. This plot shows the distribution of protein counts for males and females. Despite apparent differences in medians and variability, a two-sample t-test determined that there is no statistically significant difference in the mean protein counts between sexes (p-value > 0.05). This plot was generated by R Studio using the package ggplot2 retrieved from [33].

In the following, we will describe the intensities of the protein blueprint of Atlantic cod otoliths that will reveal the different biological processes. It is out of the realm of possibility to discuss all of the quantified proteins in this rationale. For this reason, we shall deliberate about a few selected protein models that represent physiological, ontogenetic, evolutionary, and environmental processes.

3.4.1. Protein Expression Between Sexes

In our study employing ESI-MS/MS with DDA, we conducted a comprehensive proteomic analysis across ten individuals **(Tables A2-2, Appendix: Supplementary Materials Excel sheet A2)**. We identified significantly upregulated and downregulated proteins in females compared to males with an abundance ratio (Female/Male) range of 0.000911165–401.7070581 through the volcano plot visualization **(Figure 3-3 and Tables A2-3, Appendix: Supplementary Materials Excel sheet A2)**.

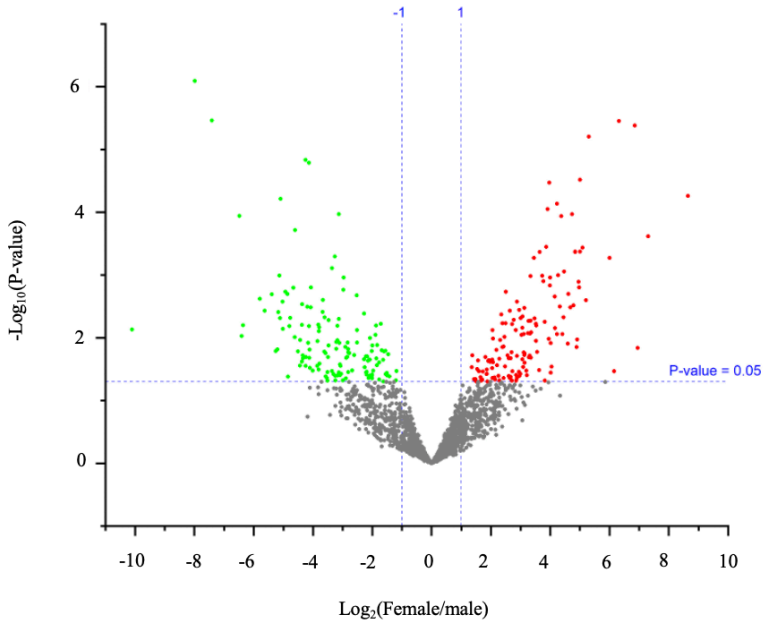

Figure 3-3. Protein expression is different between the sexes. Each dot expresses a specific protein. Proteins that appear in red are significantly upregulated in female samples, whereas those in green are significantly upregulated in male sexes at p-value < 0.05. This plot was generated by Proteome Discoverer 2.5.

Proteins with high abundance ratios (fold change > 2) and low adjusted p-values < 0.05 were considered significantly more abundant in females than males. A subset of these

proteins exhibiting sex-specific expression differences (differentially expressed proteins between sexes), as visualized in the heatmap **(Figure 3-4)**, which may have crucial roles in fish's physiological and reproductive processes.

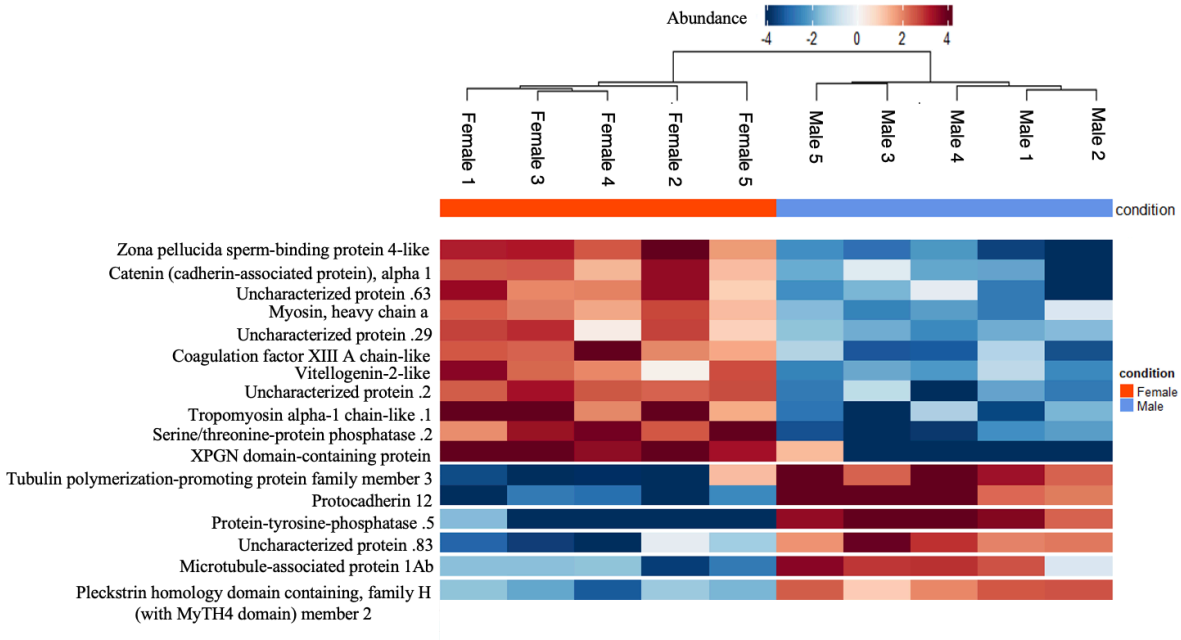

Figure 3-4. The differentially expressed proteins between sexes. The heatmap highlights proteins that showed the highest abundance between sexes with p-values ≤ 0.05. This visualization allows us to observe intensities of protein expression, with a colour gradient from blue lower expression to red representing higher expression levels. Each row corresponds to a protein, and each column to a sample, allowing us to compare the expression across our samples generated by Proteome Discoverer 2.5 software.

3.4.1.1. Otolith Proteins with Substantial Female-Biased Expression

Among the proteins with substantial female-biased expression in otoliths, zona pellucida sperm-binding protein 4-like was notable for its high log2 intensity, as visualized in the heatmap **(Figure 3-4)** that showed ≥ 2-fold change in abundance between sexes with p-values ≤ 0.05. There is evidence that this protein, which is essential in forming the egg

membrane and sperm-egg recognition, represents a key component of female fertilization [35]. In addition, the high presence of catenin (cadherin-associated protein), alpha 1, which is responsible for the conserved, calcium-dependent module crucial for cell–cell adhesion. Furthermore, it also plays a vital role in normal developmental processes and in maintaining tissue structure [36], which is likely related to its essential functions in reproductive processes.

Myosin heavy chain a is a key contractile protein of the muscular system, and its expression is often a reliable indicator of muscle development and growth. In Atlantic salmon, as in many other species, the mRNA expression levels of myosin heavy chain correlate with the muscle's ability to grow and accrue protein rather than just increase in size [37]. It is expressed with a higher intensity in female otoliths, possibly indicating differences in muscle physiology or energy demands between the sexes **(Figure 3-4)**. Tropomyosin alpha-1 chain-like is thought to be the master regulator of actin filament functions in the cytoskeleton. Coagulation factor XIII A chain-like protein **(Figure 3-4)** is important for blood coagulation and wound healing [38]. The vitellogenin-2-like proteins, a female marker, are phospho-glyco-lipoproteins synthesized in the livers of oviparous animals in response to circulating estrogens [17, 39]. Serine/threonine-protein phosphatase is one of the key enzymes responsible for dephosphorylation in vertebrates involved in various cellular processes, including the cell cycle and signal transduction [40]. It also displayed varying expression levels, indicating potential differences in cell regulation. The expression of the XPG N-terminal domain-containing protein is a critical part of the XPG

protein involved in DNA repair [41]. All these proteins display differential expression to support the unique physiological demands of females.

3.4.1.2. Otolith Proteins with Substantial Male-Biased Expression.

Among the proteins with substantial male-biased expression, we identified protocadherin and protein-tyrosine-phosphatase **(Figure 3-4)**. Protocadherins are cell adhesion molecules that belong to the cadherin superfamily and are expressed most prominently within the central nervous system, which suggests important neurobiological roles for these molecules [42]. A recent study suggested that genetic factors like protocadherins, which are expressed more in male cell lines, play a crucial role in the molecular basis of sex differences in the nervous system [43]. Protein-tyrosine-phosphatase is an enzyme that functions in a coordinated manner with protein tyrosine kinases to control signalling pathways that underlie a broad spectrum of fundamental physiological processes [44].

The Pleckstrin homology domain-containing protein, which is part of signal transduction in cells, exhibited a significant difference in expression, pointing to potential variances in cellular communication processes between sexes [45]. Tubulin polymerization-promoting protein family member 3 is an intrinsically unstructured protein that induces tubulin polymerization [46]. It has a role in microtubule stabilization, cell division, and developmental processes [47]. Microtubule-associated protein 1Ab, comprising distantly related protein complexes with heavy and light chains, is believed to be involved in the regulation of the neuronal cytoskeleton [48]. Pleckstrin homology

domain-containing family H (with MyTH4 Domain) member 2 is involved in crucial interactions with membranes and proteins, characterized by pleckstrin homology (PH) and MyTH4 domains crucial for cellular signalling. These domains aid in organizing the cytoskeleton, affecting cell shape, movement, and interactions between cell membranes and the cytoskeleton across various cellular activities [45]. These proteins' high expression reflects their importance in supporting the cellular processes specific to male Atlantic cod.

3.4.2. Quantitative Analysis of the Total Protein Profile

The comprehensive proteomic analysis across several individuals **(Tables A2-2, Appendix: Supplementary Materials Excel sheet A2)** yielded 802 proteins consistently found across all individuals **(Tables A2-4, Appendix: Supplementary Materials Excel sheet A2)**, 202 highly abundant that were more than 2-fold increased in females **(Tables A2-5, Appendix: Supplementary Materials Excel sheet A2),** and 90 proteins highly abundant that were more than 2-fold increased in males **(Tables A2-6, Appendix: Supplementary Materials Excel sheet A2)**, Furthermore, we also identified 81 proteins common only to males **(Tables A2-7, Appendix: Supplementary Materials Excel sheet A2)**, and 196 common only to females **(Tables A2-8, Appendix: Supplementary Materials Excel sheet A2)**, with 92 proteins exclusive to one individual, defined by sex **(Tables A2-9, Appendix: Supplementary Materials Excel sheet A2)**, which need further investigation, including genetic analysis, to understand the underlying reasons behind their expression. Therefore, we highlighted five proteins present within all males that were unique to males with high abundance **(Tables 3-1)**, and nine proteins unique to

females with high abundance **(Tables 3-2).** Lastly, our shotgun analysis also uncovered 214 uncharacterized proteins **(Tables A2-10, Appendix: Supplementary Materials excel sheet A2)**.

Table 3-1. Five proteins that are unique in males.

Description	Accession	Female Count [a]	Male Count [b]	Abundances (Average): Male [c]
Charged multivesicular body protein 2Ba OS=Gadus morhua OX=8049 GN=chmp2ba PE=3 SV=1	A0A8C4YUD6	0	5	261448.36432
DNA damage-binding protein 1 OS=Gadus morhua OX=8049 GN=ddb1 PE=3 SV=1	A0A8C5A9Z6	0	5	98004.482948
Fibroblast growth factor OS=Gadus morhua OX=8049 PE=3 SV=1	A0A8C4ZEA7	0	5	24,497.65508
Microtubule-associated protein 1Ab OS=Gadus morhua OX=8049 GN=map1ab PE=4 SV=1	A0A8C5CU29	0	5	3458736.85
Uncharacterized protein OS=Gadus morhua OX=8049 PE=3 SV=1	A0A8C5FA14	0	5	778547.8001

[a] Female count: the count of females associated with each protein entry.
[b] Male count: the count of males associated with each protein entry.
[c] Abundances (Average): Quantitative protein abundance measurements were averaged for all-female groups.

Table 3-2. Nine proteins that are unique in females

Description	Accession	Female count [a]	Male count [b]	Abundances (Average): Female [c]
Dihydrolipoamide acetyltransferase component of pyruvate dehydrogenase complex OS=Gadus morhua OX=8049 GN=dbt PE=3 SV=1	A0A8C5C1K4	5	0	108232.639474
Galectin OS=Gadus morhua OX=8049 GN=LOC115545324 PE=4 SV=1	A0A8C5ACJ8	5	0	489,972.337868
Heterogeneous nuclear ribonucleoprotein A/Ba OS=Gadus morhua OX=8049 GN=hnrnpaba PE=4 SV=1	A0A8C4YVY0	5	0	1301640.954998
Myosin light chain, phosphorylatable, fast skeletal muscle a OS=Gadus morhua OX=8049 GN=mylpfa PE=4 SV=1	A0A8C5B8E2	5	0	495851.125408
Nidogen 2a (osteonidogen) OS=Gadus morhua OX=8049 PE=4 SV=1	A0A8C5D3Y0	5	0	1349773.1182679997
Polypeptide N-acetylgalactosaminyltransferase OS=Gadus morhua OX=8049 GN=galnt6 PE=3 SV=1	A0A8C5BP60	5	0	42,686.3808994
SRSF protein kinase 2 OS=Gadus morhua OX=8049 GN=srpk2 PE=4 SV=1	A0A8C5CES3	5	0	20084.879869999997
Uncharacterized protein OS=Gadus morhua OX=8049 PE=4 SV=1	A0A8C5CCX7	5	0	211,271.979502

Vinculin OS=Gadus morhua OX=8049 PE=3 SV=1	A0A8C5A430	5	0	411,121.875006

[a] Female count: the count of females associated with each protein entry.
[b] Male count: the count of males associated with each protein entry.
[c] Abundances (Average): Quantitative protein abundance measurements were averaged for all-male groups.

3.4.2.1. Identified Otolith Protein Profile Common in Both Sexes

Some common abundant protein families were quantified in both sexes. In this study, among the proteins recognized, actins, were ubiquitous between sexes. α-actins are found in muscle tissues and are a significant constituent of the contractile apparatus. Developmental stage-specific muscle protein isoforms have also been reported for several fish species during the development [49-51]. Sixteen proteins related to the actin family were detected in this study **(Tables A2-11, Appendix: Supplementary Materials Excel sheet A2)**.

In addition, we quantified tropomyosins, which are actin-binding proteins that play a crucial role in regulating the actin cytoskeleton and muscle contraction [49, 52]. Six proteins (tropomyosin 1 (alpha), tropomyosin alpha-3 chain-like, tropomyosin 4a, tropomyosin alpha-1 chain-like, tropomyosin 3, tropomyosin 2 (beta)) were detected in this study **(Tables A2-12, Appendix: Supplementary Materials excel sheet A2)**.

We also detected that the tubulin proteins, which are the principal component of microtubules, are a heterodimer of two closely related proteins, α- and β-tubulin [49, 53]. α- and β-tubulin were detected in this study **(Tables A2-13, Appendix: Supplementary Materials Excel sheet A2)** .

Similarly, we detected that the tyrosine 3-monooxygenase/tryptophan activation protein β-polypeptide belongs to the 14–3–3 family and plays a critical role in signal transduction by attaching to proteins containing phosphoserine. These are involved in different cellular processes, including cell cycle progression, survival pathways, and metabolic regulation [49, 54, 55]. Three proteins (tyrosine 3-monooxygenase/tryptophan 5-monooxygenase activation protein, beta polypeptide a, tyrosine 3-monooxygenase/tryptophan 5-monooxygenase activation protein, eta polypeptide, and Tyrosine 3-monooxygenase/tryptophan 5-monooxygenase activation protein, theta polypeptide b) were detected in this study **(Tables A2-14, Appendix: Supplementary Materials Excel sheet A2)**.

The keratin proteins were consistently present across all individuals. Keratin proteins are ubiquitous and varied in their types between different age groups. Specifically, type II keratins were predominantly observed in the younger group, whereas type I keratins were more prevalent in the older group [49, 56-58]. Both types were detected in our data **(Tables A2-15, Appendix: Supplementary Materials Excel sheet A2)**.

3.4.2.2. Otolith Heat Shock Proteins

HSPs are expressed in response to various types of stress. This includes thermal, anoxia, acidosis, hypoxia, exposure to toxins, intense protein breakdown, and microbial infections [59, 60]. They are classified into five families based on molecular weight as well as domain structures and functions: Hsp110, Hsp90, Hsp70, Hsp60, Hsp40, Hsp10, and small HSP families [60, 61]. We identified and quantified eleven proteins belonging to the

Hsp90, Hsp70, Hsp60, and Hsp40 families, as shown in the heatmap **(Figure 3-5)** listed in **(Tables A2-16, Appendix: Supplementary Materials Excel sheet A2).**

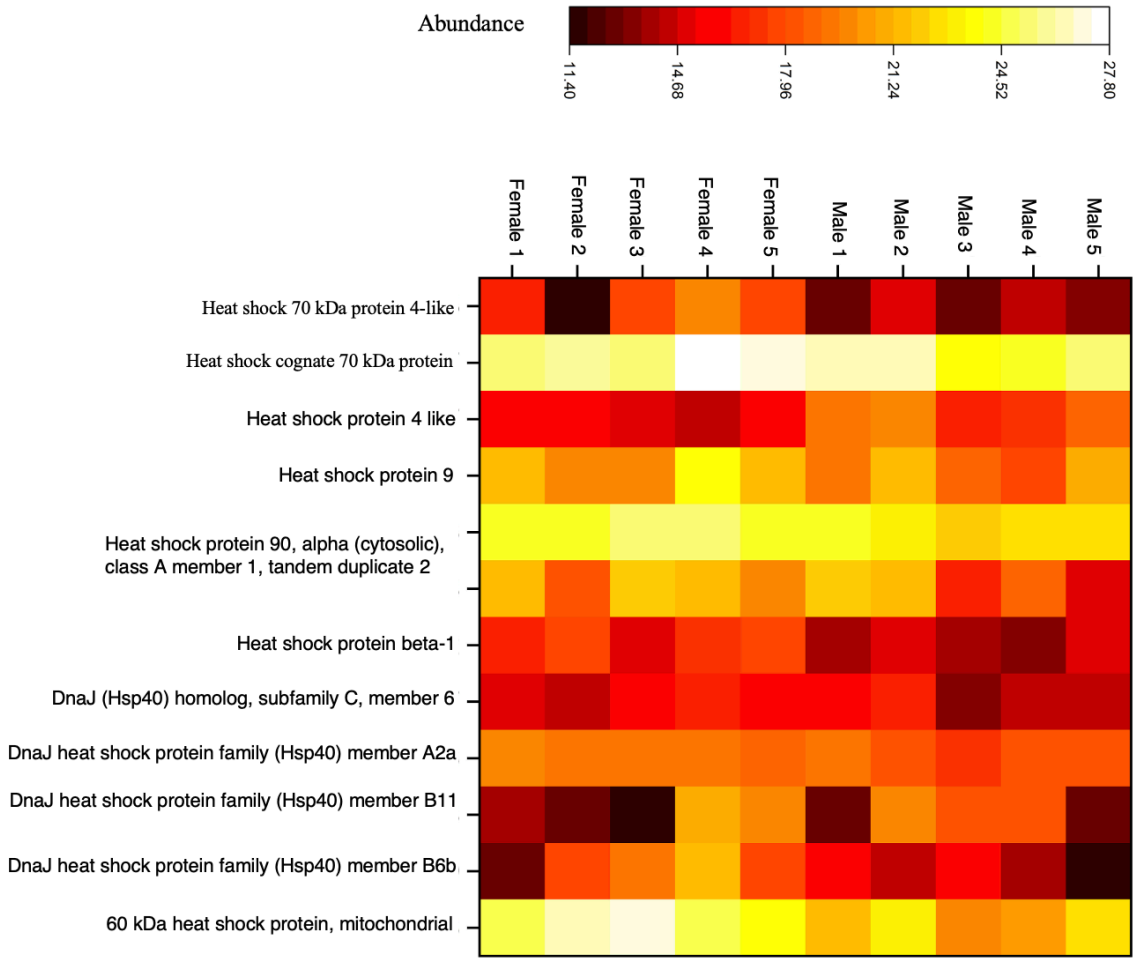

Figure 3-5. The expression of heat shock proteins within all individuals. Each column represents a sample, and each row corresponds to a specific protein, allowing us to compare the expressed protein absorbance across our samples. This figure was created by Proteome Discoverer 2.5 software.

Hsp90 can suppress thermal aggregation and facilitate protein folding by reducing misfolding via interactions with aggregation-prone unfolding intermediates [60, 62-64]. Hsp70 assists in folding newly synthesized polypeptides, refolding of misfolded proteins,

protein transport across organelles, and degradation of proteins. This protein is essential for maintaining cellular protein homeostasis, especially under stress conditions [65, 66]. HSP60 proteins play a critical role in regulating mitochondrial protein homeostasis. HSP60 has been primarily considered to reside in the mitochondria, where HSP60 and HSP10 form a complex and facilitate mitochondrial protein folding. Studies on channel catfish have shown that HSP60 is implicated in the immune response to bacterial infections, suggesting it may be crucial for disease defense in fish [60, 67]. Hsp40 proteins specifically interact with Hsp70, regulating its activity by stimulating ATP hydrolysis, which is essential for the chaperone's function in binding and releasing unfolded or misfolded protein substrates. This interaction is vital for maintaining cellular protein homeostasis, particularly under stress conditions that lead to protein damage [68].

As a result, HSPs are very crucial in maintaining cellular protein homeostasis through their chaperone functions. The presence of HSPs in both male and female fish reflects their fundamental role in cellular processes that are essential for the survival of all organisms, regardless of sex. These proteins are part of the cell's response to stress, assisting in protein folding, repair, and protection against damage caused by various stressors. Consequently, they play a crucial role in protecting the cod from the harmful effects of stress. [69-76]. Therefore, we predict that the presence of the eleven detected HSP chaperone proteins in our otolith samples could indicate climate change impacts.

3.4.2.3. Identification of Otolith Protein Bioindicators of Endocrine Disruptors

As mentioned in **Section 3.4.1**, a notable finding is the presence of vitellogenin-2-like protein, which directs egg development, showing a marked increase in abundance (193.2) in all female quantitative measurements [39]. However, its presence, albeit in lower abundance in males (38.1), indicates potential exposure to exogenous estrogens or estrogen mimics in aquatic environments [77-80]. This has been confirmed by previous studies of vitellogenin-2-like plasma levels in male vertebrates exposed to certain xenobiotic endocrine disruptors with estrogen-mimicking activity [81-84].

The zona pellucida sperm binding protein, which shows a focal role in the oocyte and gamete development, is the main predictor of fertilization capacity. Although the zona pellucida sperm binding protein-specific marker is present in higher abundance in females (192.4), it was also detected in males in low abundance (7.6) [79, 80]. We speculate that the presence of vitellogenin-2-like protein and the zona pellucida sperm-binding protein in males is due to exposure to endocrine disruptors.

3.4.3. Bioinformatics Analyses:

3.4.3.1. Gene Ontology (GO):

Next, we analyzed the proteins in both males and females based on annotated functions. Out of 1416 gene symbols, 328 genes had associated annotations from both sexes. We provide a conclusion chart **(Figure 3-6)**, showing the visualization representing the number of genes associated with specific terms and functional groups.

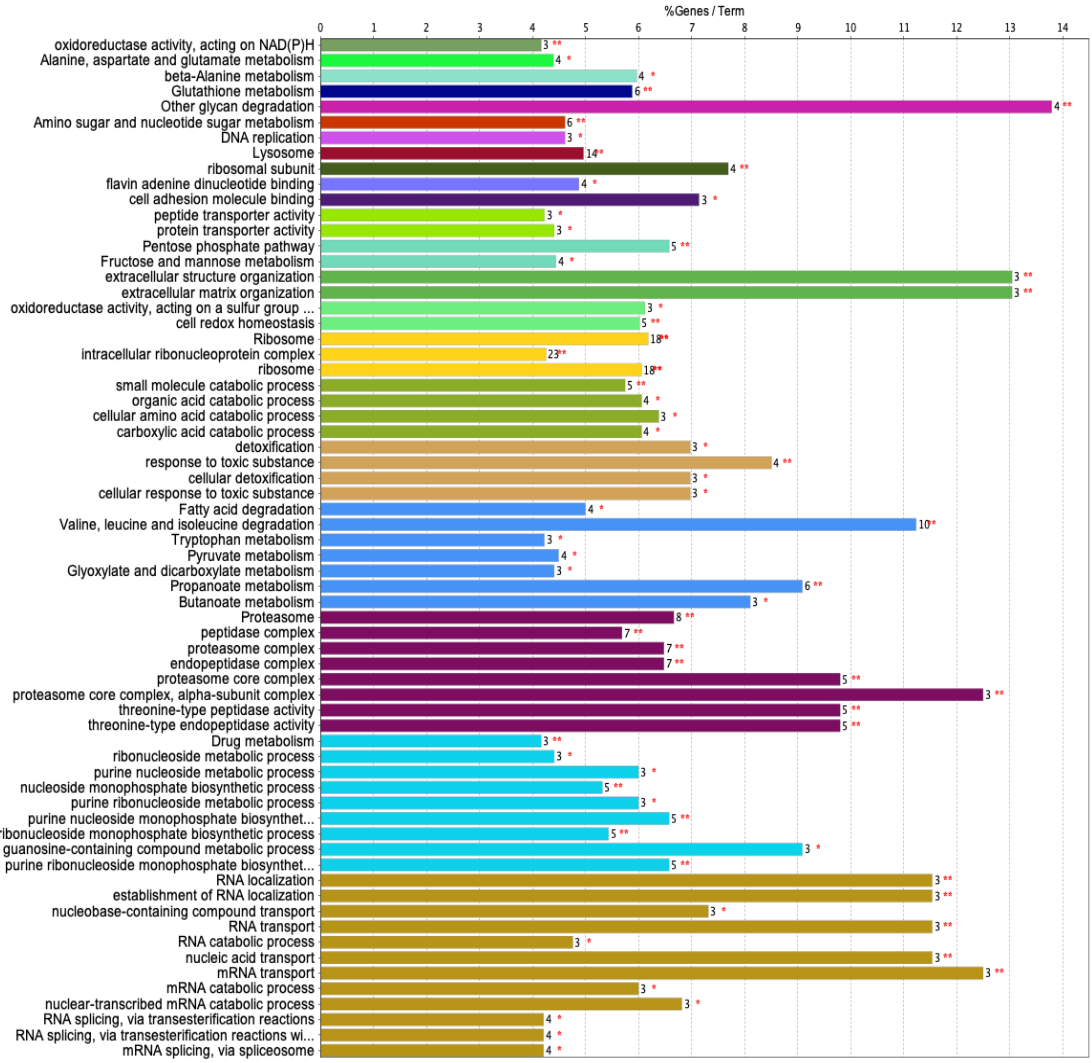

Figure 3-6. A conclusion chart provides a visualization representing the number of genes associated with specific terms and functional groups. Each bar represents a functional group, and the height of the bar corresponds to the number of genes related to the terms within that group. The label on each bar indicates the percentage of genes. * $p < 0.05$, ** $p < 0.01$.

A large portion of the biological function identified is mRNA transport (38.71%) **(Figure 3-7 A)** , [85]. The next most common biological process is the purine nucleoside monophosphate biosynthetic process (25.81%) [86].

A)

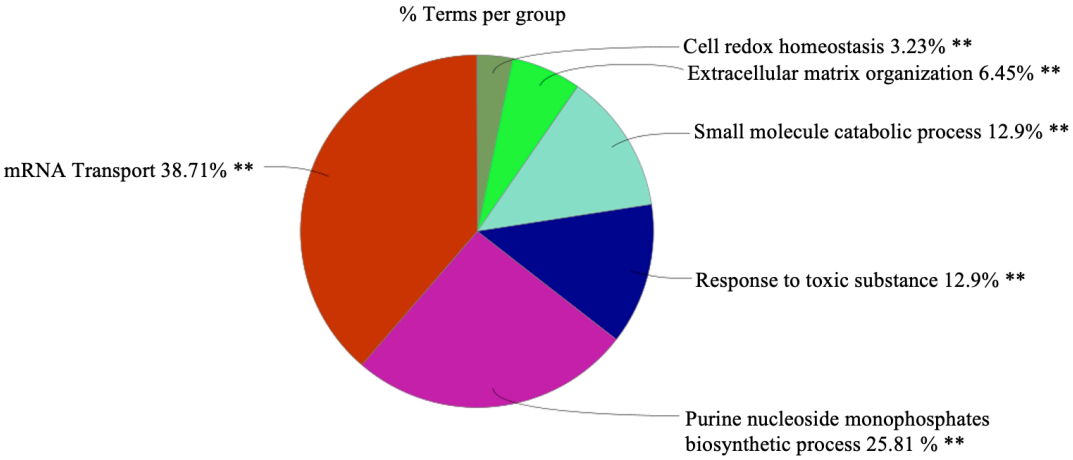
% Terms per group
Cell redox homeostasis 3.23% **
Extracellular matrix organization 6.45% **
Small molecule catabolic process 12.9% **
mRNA Transport 38.71% **
Response to toxic substance 12.9% **
Purine nucleoside monophosphates biosynthetic process 25.81 % **

B)

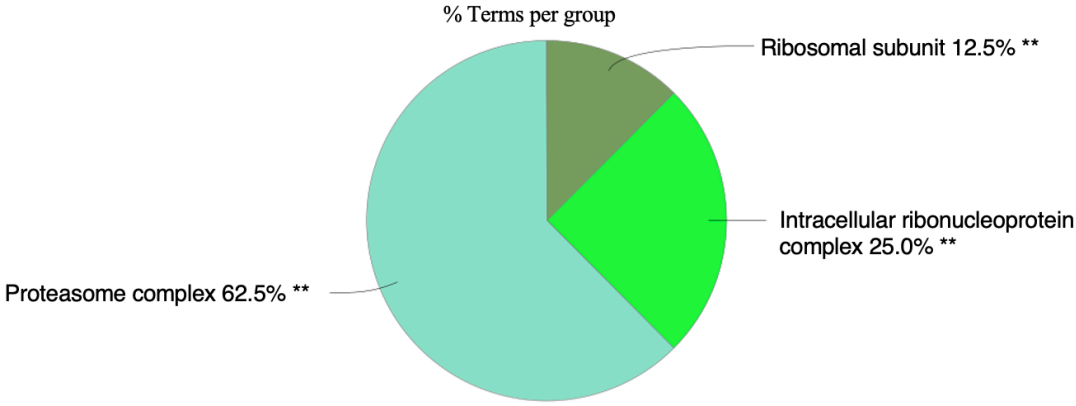
% Terms per group
Ribosomal subunit 12.5% **
Intracellular ribonucleoprotein complex 25.0% **
Proteasome complex 62.5% **

C)

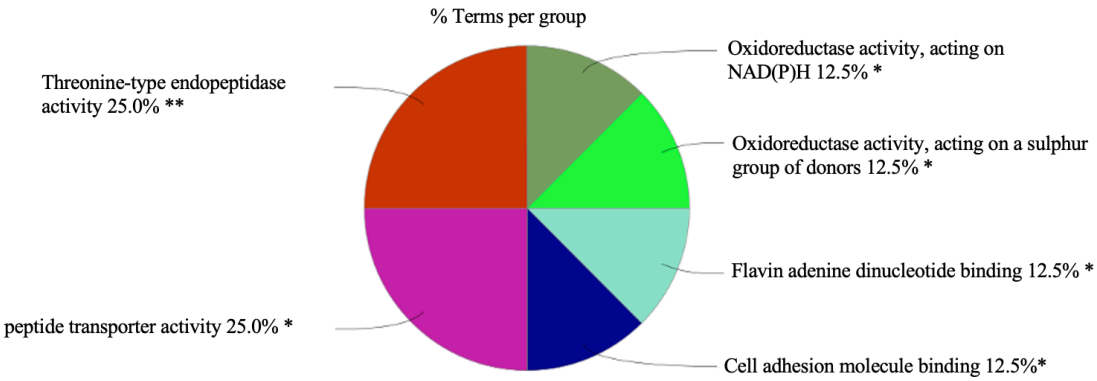

D)

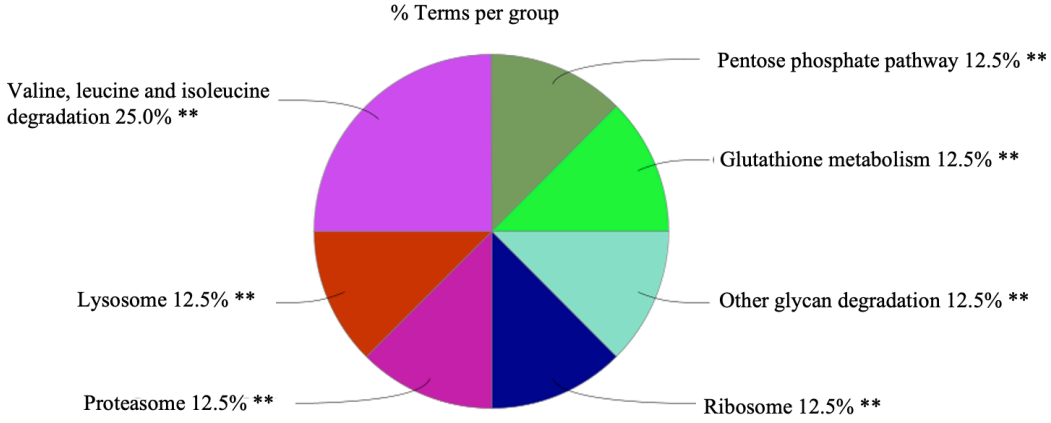

Figure 3-7. The distribution of identified genes across various functional groups. (A) This pie chart represents the distribution of genes across biological processes. (B) This pie chart represents the distribution of genes associated with specific cellular components. (C) This pie chart represents the distribution of identified genes across molecular functions. (D) This pie chart represents the distribution of identified genes categorized by their molecular functions, according to Kyoto Encyclopedia of Genes and Genomes (KEGG). The sizes of the slices are proportional to the number of genes involved in each process. Significant level of enrichment ** $p < 0.01$and * $p < 0.05$. This figure was created by Cytoscape software.

A large portion of the cellular components **(Figure 3-7 B)** is composed of genes that encode proteins associated with the proteasome complex (62.5%) [87] . Genes associated with the ribosomal subunits (12.5%) are critical for protein translation [88]. The

smallest slice shown represents genes linked to intracellular ribonucleoprotein complexes (2.5%), which are involved in gene transcription [89].

A significant portion of the molecular functions of the proteins **(Figure 3-7 C)** are associated with threonine-type endopeptidases (25.0%). Enzymes are vital in breaking down proteins by cutting internal peptide bonds in polypeptide chains. Another quarter of the genes is involved in the transport of peptides across cellular membranes. Oxidoreductase activity, acting on NAD(P)H (12.5%) and oxidoreductase activity, acting on a sulphur group of donors (12.5%); each category accounts for an equal proportion of the genes and indicates a significant role for oxidoreductase enzymes. Flavin adenine dinucleotide (FAD) binding (12.5%), this group of genes is associated with binding FAD, a cofactor involved in key metabolites for the maintenance of life and is involved in a wide range of physiological processes [90]. Cell adhesion molecule binding comprises 12.5%.

A significant proportion of proteins is involved in the catabolism of branched-chain amino acids (valine, leucine, and isoleucine) (25.0%) **(Figure 3-7 D)**, which not only act as building blocks for tissue protein (accounting for 35% of the essential amino acids in muscle), but also have other metabolic functions [91]. Lysosomes (12.5%), genes associated with lysosomal function, suggest involvement in degrading and recycling cellular waste, cellular signalling, and energy metabolism [92, 93]. Proteasome (12.5%) indicates a notable representation of genes involved in the proteasome pathway, which is critical for the cell cycle, cell survival, and cellular homeostasis [94]. Pentose phosphate pathway (12.5%), a significant number of genes are involved in this pathway, which is crucial for nucleotide synthesis and the generation of NADPH for reductive biosynthesis

[95]. Glutathione metabolism (12.5%) reflects genes involved in the synthesis and metabolism of glutathione, a major antioxidant that is critical in the regulation of the redox state of cells [96]. Glycan degradation (12.5%) genes are associated with the degradation of various glycans, complex carbohydrates that play major metabolic, structural, and physical roles in biological systems [97]. The ribosome comprises 2.5%, and a portion of the genes is related to the ribosome, indicating the importance of protein synthesis machinery in the cell [98].

3.4.3.2. Protein-Protein Interaction (PPI) Analysis

Our research used the STRING database to construct a comprehensive map of the PPI of the common otolith proteins within the *Gadus morhua*, listed in **(Tables A2-17, Appendix: Supplementary Materials Excel sheet A2)**. This network elucidates potential key proteins in Atlantic cod biological processes and predicted PPIs, substantiated by evidence such as genetic co-occurrence and experimental validations [99]. Due to the complexity of our dataset, this study will focus on the top 20 proteins with the highest score, suggesting robust evidence from multiple sources, including experimental data and literature support [100] **(Figure 3-8)**.

Key proteins identified include structural proteins such as actin and alpha cardiac and enzymatic proteins like citrate synthase and glyceraldehyde-3-phosphate dehydrogenase **(Tables A2-18, Appendix: Supplementary Materials Excel sheet A2)**. The category of ribosomal proteins includes ribosomal protein S14 and ribosomal protein L4. Additionally, signalling proteins like RAN binding protein 2 (RANBP2), and heat

shock proteins like Heat shock protein 9. Lastly, proteins such as the eukaryotic translation elongation factor 2 are involved in the translation process.

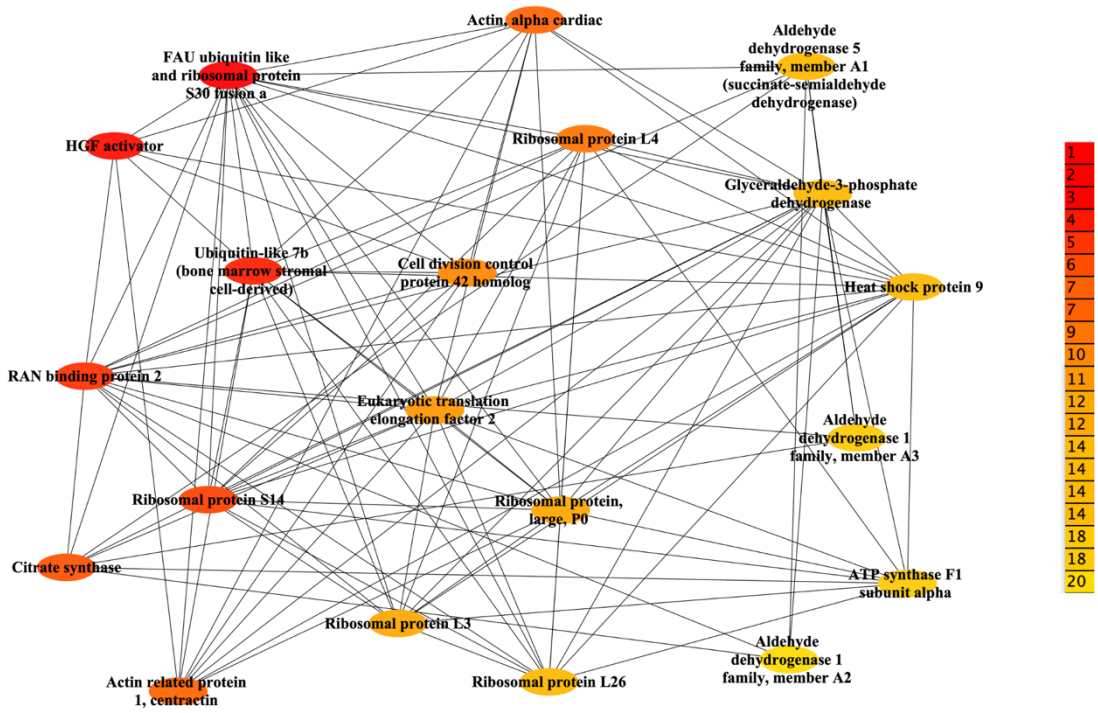

Figure 3-8. String network visualization of top 20 high-degree proteins in the otolith protein interaction map of Gadus morhua. This figure was created by Cytoscape software.

Focusing on the PPI network of the top 20 high-degree proteins reveals several key insights into cellular processes **(Figure 3-9 and Tables A2-19, Appendix: Supplementary Materials Excel sheet A2)**. Several notable interactions are supported by strong experimental evidence and co-expression data [101]. For example, the interaction between ribosomal proteins (L4, L3, S14, L26) and cell division control protein 42 homolog (CDC42) exhibit a high combined score of 1, with a co-expression value of approximately 0.935 and an experimental validation of approximately 0.987. Ribosomal

proteins are essential components of the ribosome, playing crucial roles in ribosome assembly and protein synthesis [102-105]. Meanwhile, CDC42, a small GTPase, plays a critical role in controlling cell division, polarity, and cytoskeleton organization [106]. This indicates a significant functional correlation between these proteins in maintaining cellular integrity, particularly in relation to protein synthesis and cell cycle regulation.

The connection between CDC42 and eukaryotic translation elongation factor 2 (EEF2) is notable, with a combined score of 1, a neighbourhood value of 0.146, a co-expression value of 0.939, and experimental support of 0.97. These proteins play complementary roles in cellular regulation and translation [106, 107]. EEF2 is crucial for the elongation step during translation, ensuring proper protein synthesis and contributing to overall cellular function [106, 107]. The high experimental and neighbourhood scores further suggest these proteins are central to the regulation of both cellular translation and division.

Additionally, the interaction between ATP synthase subunit alpha and citrate synthase has a combined score of 1, a co-expression value of 0.846, and database-curated evidence of 0.357. These proteins are pivotal in cellular energy production, with ATP synthase driving ATP synthesis in mitochondria and citrate synthase catalyzing the first step of the citric acid cycle [108, 109]. Their interaction highlights the importance of metabolic coordination in cellular energy homeostasis.

Furthermore, the interaction between RANBP2 and HSP9 shows strong experimental support, with a combined score of 1. The interaction is characterized by a neighbourhood score of 0.055, an experimental evidence score of 0.337, and a database

score of 0.944. This suggests that there is a strong database and experimental evidence supporting the functional interaction between RANBP2, involved in nuclear transport, gene expression, chromosome segregation during mitosis, chromatin regulation [110-112], and HSP9, which plays a key role in protein folding and stress response [113]. This interaction reflects an integrated cellular response to stress.

Overall, this analysis enriches functional proteomic research in *Gadus morhua* and illustrates the potential to chronicle the extensive protein interactions that underpin vital physiological processes. These high-confidence interactions, reflected by combined scores, experimental data, co-expression values, and neighbourhood scores, reveal an intricate regulatory network governing the cellular structure and function of the *Gadus morhua,* representing the fish's biology from the embryonic stage until death. This network integrates proteins involved in translation, metabolism, structural maintenance, stress response, and detoxification, each playing a crucial role in the biological processes essential for the fish's survival and adaptation.

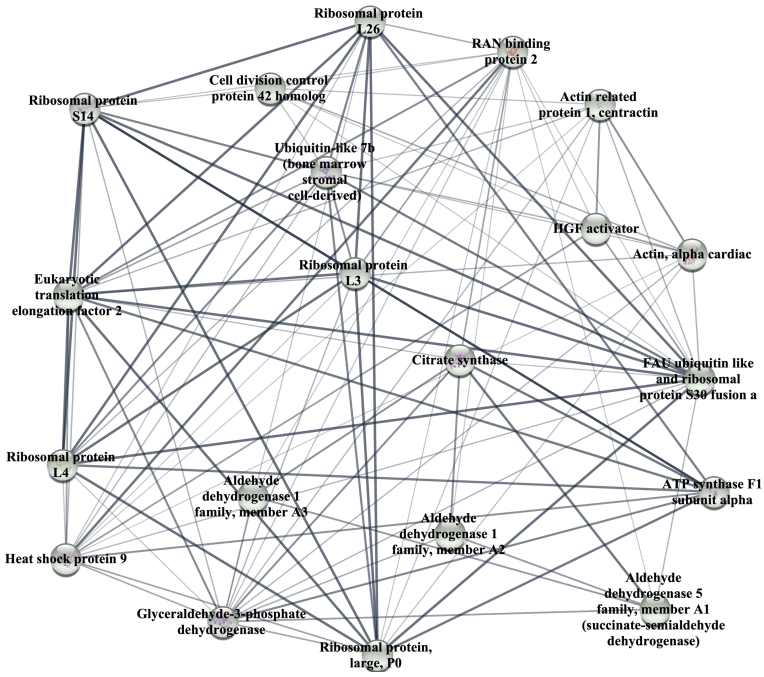

Figure 3-9. String PPI network visualization of top 20 high-degree proteins in the otolith of Gadus morhua. This figure was created by Cytoscape software.

3.5. Conclusions and Future Directions

We have shown in this study the presence of five proteins within all males that represent uniqueness to males and nine proteins unique to females. In addition, 802 proteins were consistently found across all individuals.

In 2019, the bottom temperatures in NAFO Subarea 3K were significantly above normal, reflecting the broader impacts of global warming. The fall bottom temperatures in Subarea 3K were recorded to be between +0.5 °C and +2.5 °C above the long-term average of around 4 °C, marking a return to warmer anomalies not seen since 2011 [114-116]. This warming trend is consistent with the global patterns of ocean warming due to climate change [117]. Temperature variations in aquaculture environments can be substantial and can approach the upper critical thermal limits of 8–12 °C for Atlantic cod, which are lethal.

These shifts can occur quickly, such as an ~8 °C increase in less than 12 h during thermocline inversions, particularly at depths where Atlantic cod tend to gather (≥5 m) [69, 70]. Fish are unable to escape temperature fluctuations, inevitably facing stressful environments completely. This thermal stress profoundly affects gene transcription, targeting genes linked to oxidative stress response, apoptosis, protein folding, energy metabolism, synthesis, membrane fluidity, and immune functions [69-76]. The proteins encoded by these genes include some of the elements that regulate both the organismal and cellular stress responses. As a result, HSPs play a crucial role in protecting the fish against the deleterious effects of stress [69-76]. This is why we predict that the eleven HSP chaperone proteins detected in otolith could be an indicator of climate change **(Tables A2-16, Appendix: Supplementary Materials Excel sheet A2)**; however, this needs to be empirically determined.

Recent studies have brought to light significant evidence regarding the stress conditions in fish, focusing on the impact of endocrine-disrupting chemicals (EDCs), treated sewage, and other environmental factors [77, 78]. This was discussed in the otolith's proteins of egg yolk precursors section. Although the zona pellucida sperm-binding protein-specific marker is present in higher abundance in females, it was also detected in males [79, 80]. Likewise, environmental effluence and exposure to EDCs and other contaminants can be likely factors contributing to these observations [77-80].

Further comprehensive research is needed to elucidate the full range of influences that are central to the alteration of sex markers in fish, ensuring that we consider all possible sources of stress, whether they are pollutants or other environmental variables. This

evidence collectively indicates a significant stress response in fish to environmental pollutants, warranting further investigation into the mechanisms of action and long-term consequences of these exposures on aquatic life. It is also vital to conduct further studies on the PPIs and their functional overlaps, to explore their evolutionary significance.

Finally, this study employs a quantitative shotgun proteomics approach and bioinformatic analysis to discover the unidentified proteins present in cod otoliths. Our results show that diverse proteins are stored in otolith that were accumulated, thereby enabling the discernment of both differences and similarities across protein profiles between sexes. We speculate that circulating proteins released by various cells in the body into the endolymph are captured by the otolith. In the future, we will explore the prospect of monitoring the growth of the fish by investigating the proteins present in each separate concentric layer of the otolith matrix.

In conclusion, this study suggests a broader applicative potential of otolith proteomics in marine research. By transcending traditional views of otoliths solely as chronometers, this study illuminates their capacity to provide invaluable insights into the proteomic profiles reflective of varying life stages and environmental interactions of cod. Despite these advances, our understanding of the otolith proteome remains nascent, with much terrain still to explore. Future endeavours will focus on comparing protein profiles of otoliths from different NAFO zones, trip, and depths. In the future, we plan to monitor the growth protein of the fish by investigating the presence of the protein concentric layers of the otolith matrix to follow the growth of the fish from embryo to adult. Such comparisons will be expected to substantially enrich our comprehension of the otolith

proteome, opening new avenues for research and offering profound implications for marine and environmental science.

3.6. References

[1] T. Norin, P. Canada, J. A. Bailey, and A. K. Gamperl, "Thermal biology and swimming performance of Atlantic cod (*Gadus morhua*) *and haddock* (*Melanogrammus aeglefinus*)," *PeerJ.,* vol. 7, pp. e7784, Oct, 2019. DOI: https://doi.org/10.7717/peerj.7784.

[2] A. T. Pinhorn, "Fishery and biology of Atlantic cod (*Gadus morhua*) off the Southwest Coast of Newfoundland," *J. Fish. Res. Board. Can.,* vol. 26, no. 12, pp. 3133-3164, 1969. DOI: https://doi.org/10.1139/f69-298.

[3] L. S. Meidell, A. K. Carvajal, T. Rustad, and E. Falch, "Upgrading marine oils from cod (*Gadus morhua*) on-board the deep-sea vessels-from waste to value," *Foods,* vol. 12, no. 8, Apr, 2023. DOI: https://doi.org/10.3390/foods12081659.

[4] A. D. Hawkins, and A. N. Popper, "Sound detection by Atlantic cod: An overview," *J. Acoust. Soc. Am.,* vol. 148, no. 5, pp. 3027, Nov, 2020. DOI: https://doi.org/10.1121/10.0002363.

[5] Y. Dauphin, and E. Dufour, "Composition and properties of the soluble organic matrix of the otolith of a marine fish: *Gadus morhua Linne*, 1758 (*Teleostei, Gadidae*)," *Comp. Biochem. Physiol. A Mol. Integr. Physiol.,* vol. 134, no. 3, pp. 551-561, Nov, 2003. DOI: https://doi.org/10.1016/S1095-6433(02)00358-6.

[6] E. Murayama, Y. Takagi, T. Ohira, J. G. Davis, M. I. Greene, and H. Nagasawa, "Fish otolith contains a unique structural protein, otolin-1," *Eur. J. Biochem.,* vol. 269, no. 2, pp. 688-696, Jan, 2002. DOI: https://doi.org/10.1046/j.0014-2956.2001.02701.x.

[7] L. S. Lewis, J. L. Huang, M. Willmes, R. A. Fichman, T.-C. Hung, L. T. Ellison, T. A. Stevenson, S. J. Teh, B. G. Hammock, A. A. Schultz, J. L. Grimsich, M. H. Huyskens, Q.-Z. Yin, L. M. Cavole, N. W. Botto, and J. A. Hobbs, "Visual, spectral, and microchemical quantification of crystalline anomalies in otoliths of wild and cultured delta smelt," *Sci. Rep.,* vol. 12, no. 1, Dec, 2022. DOI: https://doi.org/10.1038/s41598-022-22813-w.

[8] E. T. Degens, W. G. Deuser, and R. L. Haedrich, "Molecular structure and composition of fish otoliths," *Mar. Biol.,* vol. 2, no. 2, pp. 105-113, 1969. DOI: https://doi.org/10.1007/bf00347005.

[9] P. Payan, H. De Pontual, G. Bœuf, and N. Mayer-Gostan, "Endolymph chemistry and otolith growth in fish," *Comptes. Rendus. Palevol.,* vol. 3, no. 6-7, pp. 535-547, Oct, 2004. DOI: https://doi.org/10.1016/j.crpv.2004.07.013.

[10] J. Ferri, "Otoliths and their applications in fishery science," *Fishes,* vol. 8, no. 1, pp. 35, Jan, 2023. DOI: https://doi.org/10.3390/fishes8010035.

[11] S. Smolinski, J. Deplanque-Lasserre, E. Hjorleifsson, A. J. Geffen, J. A. Godiksen, and S. E. Campana, "Century-long cod otolith biochronology reveals individual growth plasticity in response to temperature," *Sci. Rep.,* vol. 10, no. 1, pp. 16708, Oct, 2020. DOI: https://doi.org/10.1038/s41598-020-73652-6.

[12] S. Smoliński, and Z. Mirny, “Otolith biochronology as an indicator of marine fish responses to hydroclimatic conditions and ecosystem regime shifts,” *Ecol. Indic.,* vol. 79, pp. 286-294, Aug, 2017. DOI: https://doi.org/10.1016/j.ecolind.2017.04.028.

[13] C. D'Iglio, M. Albano, S. Famulari, S. Savoca, G. Panarello, D. Di Paola, A. Perdichizzi, P. Rinelli, G. Lanteri, N. Spano, and G. Capillo, “Intra- and interspecific variability among congeneric Pagellus otoliths,” *Sci. Rep.,* vol. 11, no. 1, pp. 16315, Aug, 2021. DOI: https://doi.org/10.1038/s41598-021-95814-w.

[14] L. Santos, and A. M. Vaz-dos-Santos, “Insights of otoliths morphology to reveal patterns of Teleostean fishes in the southern Atlantic,” *Fishes,* vol. 8, no. 1, pp. 21, Dec, 2022. DOI: https://doi.org/10.3390/fishes8010021.

[15] Y. W. Lundberg, Y. Xu, K. D. Thiessen, and K. L. Kramer, “Mechanisms of otoconia and otolith development,” *Dev. Dyn.,* vol. 244, no. 3, pp. 239-253, Sep, 2015. DOI: https://doi.org/10.1002/dvdy.24195.

[16] S. H. Serre, K. E. Nielsen, T. B. Thomsen, and K. Hüssy, “Analysis of cod otolith microchemistry by continuous line transects using LA-ICP-MS,” *Geol. Surv. Den. Greenl. Bull.,* vol. 41, pp. 91–94, 2018. DOI: https://doi.org/10.34194/geusb.v41.4351.

[17] R. M. Rideout, T. N. Youssef, A. T. Adamack, R. John, A. M. Cohen, T. D. Fridgen, and J. H. Banoub, “Qualitative Shotgun proteomics strategy for protein expression profiling of fish otoliths,” *BioChem.,* vol. 3, no. 3, pp. 102-117, Jul, 2023. DOI: https://doi.org/10.3390/biochem3030008.

[18] S. E. Campana, “Chemistry and composition of fish otoliths:pathways, mechanisms and applications,” *Mar. Ecol. Prog. Ser.,* vol. 188, pp. 263-297, 1999. DOI: https://doi.org/10.3354/meps188263.

[19] O. R. B. Thomas, S. E. Swearer, E. A. Kapp, P. Peng, G. Q. Tonkin-Hill, A. Papenfuss, A. Roberts, P. Bernard, and B. R. Roberts, “The inner ear proteome of fish,” *FEBS J.,* vol. 286, no. 1, pp. 66-81, Jan, 2019. DOI: https://doi.org/10.1111/febs.14715.

[20] S. Huang, and S. Qian, “Advances in otolith-related protein research,” *Front. Neurosci.,* vol. 16, no. 7, pp. 956200, Jul, 2022. DOI: https://doi.org/10.3389/fnins.2022.956200.

[21] K. Bielak, D. Benkowska-Biernacka, M. Ptak, J. Stolarski, M. Kalka, A. Ozyhar, and P. Dobryszycki, “Otolin-1, an otolith- and otoconia-related protein, controls calcium carbonate bioinspired mineralization,” *Biochim. Biophys Acta. Gen. Subj.,* vol. 1867, no. 5, pp. 130327, May, 2023. DOI: https://doi.org/10.1016/j.bbagen.2023.130327.

[22] Y. Zhang, B. R. Fonslow, B. Shan, M. C. Baek, and J. R. Yates, 3rd, “Protein analysis by shotgun/bottom-up proteomics,” *Chem. Rev.,* vol. 113, no. 4, pp. 2343-2394, Apr, 2013. DOI: https://doi.org/10.1021/cr3003533.

[23] D. A. Wolters, M. P. Washburn, and J. R. Yates, 3rd, “An automated multidimensional protein identification technology for shotgun proteomics,” *Anal. Chem.,* vol. 73, no. 23, pp. 5683-5690, Dec, 2001. DOI: https://doi.org/10.1021/ac010617e.

[24] J. R. Yates, 3rd, “Mass spectral analysis in proteomics,” *Annu. Rev. Biophys. Biomol. Struct.,* vol. 33, pp. 297-316, 2004. DOI: https://doi.org/10.1146/annurev.biophys.33.111502.082538.

[25] A. J. Link, J. Eng, D. M. Schieltz, E. Carmack, G. J. Mize, D. R. Morris, B. M. Garvik, and J. R. Yates, 3rd, “Direct analysis of protein complexes using mass spectrometry,” *Nat. Biotechnol.,* vol. 17, no. 7, pp. 676-682, Jul, 1999. DOI: https://doi.org/10.1038/10890.

[26] J. R. Yates, 3rd, “Mass spectrometry and the age of the proteome,” *J. Mass Spectrom.,* vol. 33, no. 1, pp. 1-19, Jan, 1998.

[27] J. Banoub, T. Youssef, and A. Mikhael, “Proteomic technology applications for fisheries research,” *Tech. Report. Fish. Aquat. Sci.,* vol. 3465, pp. xi- 668, May, 2022.

[28] T. Valikangas, T. Suomi, and L. L. Elo, “A systematic evaluation of normalization methods in quantitative label-free proteomics,” *Brief Bioinform.,* vol. 19, no. 1, pp. 1-11, Jan, 2018. DOI: https://doi.org/10.1093/bib/bbw095.

[29] H. Wickham, and L. Henry, "tidyr: Tidy Messy Data. R package version 1.1.3. Retrieved from https://CRAN.R-project.org/package=tidyr)," 2021.

[30] S. M. Bache, and H. Wickham, "magrittr: A Forward-Pipe Operator for R. R package version 2.0.1. Retrieved from https://CRAN.R-project.org/package=magrittr," 2021.

[31] W. H, “The split-apply-combine strategy for data analysis,” *J. Stat. Softw.,* vol. 40, no. 1, pp. 1-29, 2011.

[32] Wickham H, François R, Henry L, Müller K, and V. D, "dplyr: A Grammar of Data Manipulation. R package version 1.1.4, https://github.com/tidyverse/dplyr, https://dplyr.tidyverse.org," 2023.

[33] W. H, *ggplot2: elegant graphics for data analysis*, Springer-Verlag New York, 2016.

[34] L. Tomanek, "Variation in the heat shock response and its implication for predicting the effect of global climate change on species' biogeographical distribution ranges and metabolic costs," *J. Exp. Biol.,* vol. 213, no. 6, pp. 971-979, Nov, 2010. DOI: https://doi.org/10.1242/jeb.038034.

[35] E. S. Litscher, and P. M. Wassarman, "The Fish Egg's Zona Pellucida," *Curr. Top. Dev. Biol.,* vol. 130, pp. 275-305, Apr, 2018. DOI: https://doi.org/10.1016/bs.ctdb.2018.01.002.

[36] D. Nathaniel Clarke, C. J. Lowe, and W. James Nelson, "The cadherin-catenin complex is necessary for cell adhesion and embryogenesis in Nematostella vectensis," *Dev. Biol.,* vol. 447, no. 2, pp. 170-181, Mar, 2019. DOI: https://doi.org/10.1016/j.ydbio.2019.01.007.

[37] E. M. Hevrøy, A. E. O. Jordal, I. Hordvik, M. Espe, G. I. Hemre, and P. A. Olsvik, "Myosin heavy chain mRNA expression correlates higher with muscle protein accretion than growth in Atlantic salmon, Salmo salar," *Aquaculture,* vol. 252, no. 2-4, pp. 453-461, Mar, 2006. DOI: https://doi.org/10.1016/j.aquaculture.2005.07.003.

[38] L. Casas, F. Saborido-Rey, T. Ryu, C. Michell, T. Ravasi, and X. Irigoien, “Sex change in clownfish: Molecular insights from transcriptome analysis,” *Sci. Rep.,* vol. 6, no. 1, pp. 35461, Oct, 2016. DOI: https://doi.org/10.1038/srep35461.

[39] A. M. Cohen, A. A. H. Mansour, and J. H. Banoub, “'De novo' sequencing of Atlantic cod vitellogenin tryptic peptides by matrix-assisted laser desorption/ionization quadrupole time-of-flight tandem mass spectrometry: similarities with haddock vitellogenin,” *Rapid Commun. Mass Spectrom.,* vol. 19, no. 17, pp. 2454-2460, Jul, 2005. DOI: https://doi.org/10.1002/rcm.2084.

[40] W. B. Liu, Q. Yan, F. Y. Liu, X. C. Tang, H. G. Chen, J. Liu, L. Nie, X. W. Zhang, W. K. Ji, X. H. Hu, W. F. Hu, Z. Woodward, K. L. Wu, M. X. Wu, X. L. Liu, L. X. Luo, M. B. Yu, Y. Z. Liu, S. J. Liu, and D. W. Li, “Protein serine/threonine phosphotase-1 is essential in governing normal development of vertebrate eye,” *Curr. Mol. Med.,* vol. 12, no. 10, pp. 1361-1371, Dec, 2012. DOI: https://doi.org/10.2174/156652412803833535.

[41] O. D. Schärer, "XPG: Its products and biological roles," *Molecular mechanisms of xeroderma pigmentosum*, Advances in Experimental Medicine and Biology Springer New York, 2009. pp. 83-92.

[42] A. Pancho, T. Aerts, M. D. Mitsogiannis, and E. Seuntjens, “Protocadherins at the crossroad of signaling pathways,” *Front. Mol. Neurosci.,* vol. 13, pp. 117, Jun, 2020. DOI: https://doi.org/10.3389/fnmol.2020.00117.

[43] P. Pottmeier, D. Nikolantonaki, F. Lanner, C. Peuckert, and E. Jazin, “Sex-biased gene expression during neural differentiation of human embryonic stem cells,”

Front. Cell. Dev. Biol., vol. 12, pp. 1341373, May, 2024. DOI: https://doi.org/10.3389/fcell.2024.1341373.

[44] N. K. Tonks, "Protein tyrosine phosphatases: From genes, to function, to disease," *Nat. Rev. Mol. Cell Biol.,* vol. 7, no. 11, pp. 833-846, Nov, 2006. DOI: https://doi.org/10.1038/nrm2039.

[45] M. Lenoir, I. Kufareva, R. Abagyan, and M. Overduin, "Membrane and protein interactions of the Pleckstrin homology domain superfamily," *Membr.,* vol. 5, no. 4, pp. 646-663, Oct, 2015. DOI: https://doi.org/10.3390/membranes5040646.

[46] J. A. Staverosky, B. A. Pryce, S. S. Watson, and R. Schweitzer, "Tubulin polymerization-promoting protein family member 3, Tppp3, is a specific marker of the differentiating tendon sheath and synovial joints," *Dev. Dyn.,* vol. 238, no. 3, pp. 685-692, Mar, 2009. DOI: https://doi.org/10.1002/dvdy.21865.

[47] F. Orosz, "On the tubulin polymerization promoting proteins of zebrafish," *Biochem. Biophys Res. Commun.,* vol. 457, no. 3, pp. 267-272, Feb, 2015. DOI: https://doi.org/10.1016/j.bbrc.2014.12.099.

[48] R. Noiges, R. Eichinger, W. Kutschera, I. Fischer, Z. Nemeth, G. Wiche, and F. Propst, "Microtubule-associated protein 1A (MAP1A) and MAP1B: light chains determine distinct functional properties," *J. Neurosci.,* vol. 22, no. 6, pp. 2106-2114, Mar, 2002. DOI: https://doi.org/10.1523/JNEUROSCI.22-06-02106.2002.

[49] H. Sveinsdottir, O. Vilhelmsson, and A. Gudmundsdottir, "Proteome analysis of abundant proteins in two age groups of early Atlantic cod (*Gadus morhua*) larvae,"

Comp. Biochem. Physiol. Part. D Genom. Proteom., vol. 3, no. 3, pp. 243-250, Sep, 2008. DOI: https://doi.org/10.1016/j.cbd.2008.06.001.

[50] B. Focant, F. Huriaux, E. Baras, and P. Vandewalle, "Expression of myofibrillar proteins and parvalbumin isoforms in white muscle of the developing Turbot Scophthalmus Maximus (*Pisces, Pleuronectiformes*)," *Basic. Appl. Myol.,* vol. 10, no. 6, pp. 269-278, 2000.

[51] F. Huriaux, E. Baras, P. Vandewalle, and B. Focant, "Expression of myofibrillar proteins and parvalbumin isoforms in white muscle of dorada during development," *J. Fish. Biol.,* vol. 62, no. 4, pp. 774-792, Jun, 2003. DOI: https://doi.org/10.1046/j.1095-8649.2003.00064.x.

[52] S. V. Perry, "Vertebrate tropomyosin: distribution, properties and function," *J. Muscle Res. Cell Motil.,* vol. 22, no. 1, pp. 5-49, Mar, 2001. DOI: https://doi.org/10.1023/a:1010303732441.

[53] V. D. Oehlmann, S. Berger, C. Sterner, and S. I. Korsching, "Zebrafish beta tubulin 1 expression is limited to the nervous system throughout development, and in the adult brain is restricted to a subset of proliferative regions," *Gene Expr. Patterns,* vol. 4, no. 2, pp. 191-198, Mar, 2004. DOI: https://doi.org/10.1016/j.modgep.2003.09.001.

[54] S. E. Meek, W. S. Lane, and H. Piwnica-Worms, "Comprehensive proteomic analysis of interphase and mitotic 14-3-3-binding proteins," *J. Biol. Chem.,* vol. 279, no. 31, pp. 32046-32054, Jul, 2004. DOI: https://doi.org/10.1074/jbc.M403044200.

[55] M. J. van Hemert, H. Y. Steensma, and G. P. van Heusden, “14-3-3 proteins: key regulators of cell division, signalling and apoptosis,” *Bioessays,* vol. 23, no. 10, pp. 936-946, Oct, 2001. DOI: https://doi.org/10.1002/bies.1134.

[56] K. Suzuki, K. Sato, K. Katsu, H. Hayashita, D. B. Kristensen, and K. Yoshizato, “Novel Rana keratin genes and their expression during larval to adult epidermal conversion in bullfrog tadpoles,” *Differentiation,* vol. 68, no. 1, pp. 44-54, Aug, 2001. DOI: https://doi.org/10.1046/j.1432-0436.2001.068001044.x.

[57] K. Suzuki, R. Utoh, K. Kotani, M. Obara, and K. Yoshizato, “Lineage of anuran epidermal basal cells and their differentiation potential in relation to metamorphic skin remodeling,” *Dev. Growth Differ.,* vol. 44, no. 3, pp. 225-238, Jun, 2002. DOI: https://doi.org/10.1046/j.1440-169x.2002.00637.x.

[58] Y. Ishida, K. Suzuki, R. Utoh, M. Obara, and K. Yoshizato, “Molecular identification of the skin transformation center of anuran larval skin using genes of Rana adult keratin (RAK) and SPARC as probes,” *Dev. Growth Differ.,* vol. 45, no. 5-6, pp. 515-526, Oct-Dec, 2003. DOI: https://doi.org/10.1111/j.1440-169x.2003.00719.x.

[59] S. Jeyachandran, H. Chellapandian, K. Park, and I.-S. Kwak, “A review on the involvement of heat shock proteins (Extrinsic Chaperones) in response to stress conditions in aquatic organisms,” *Antioxidants,* vol. 12, no. 7, pp. 1444, Jun, 2023. DOI: https://doi.org/10.3390/antiox12071444.

[60] Y. Xie, L. Song, Z. Weng, S. Liu, and Z. Liu, “Hsp90, Hsp60 and sHsp families of heat shock protein genes in channel catfish and their expression after bacterial

infections," *Fish Shellfish Immunol.,* vol. 44, no. 2, pp. 642-651, Jun, 2015. DOI: https://doi.org/10.1016/j.fsi.2015.03.027.

[61] L. Song, C. Li, Y. Xie, S. Liu, J. Zhang, J. Yao, C. Jiang, Y. Li, and Z. Liu, "Genome-wide identification of Hsp70 genes in channel catfish and their regulated expression after bacterial infection," *Fish Shellfish Immunol.,* vol. 49, pp. 154-162, Feb, 2016. DOI: https://doi.org/10.1016/j.fsi.2015.12.009.

[62] G. Chiosis, C. S. Digwal, J. B. Trepel, and L. Neckers, "Structural and functional complexity of HSP90 in cellular homeostasis and disease," *Nat. Rev. Mol. Cell Biol.,* vol. 24, no. 11, pp. 797-815, Nov, 2023. DOI: https://doi.org/10.1038/s41580-023-00640-9.

[63] T. Didenko, A. M. Duarte, G. E. Karagoz, and S. G. Rudiger, "Hsp90 structure and function studied by NMR spectroscopy," *Biochim. Biophys. Acta.,* vol. 1823, no. 3, pp. 636-647, Mar, 2012. DOI: https://doi.org/10.1016/j.bbamcr.2011.11.009.

[64] T. O. Street, L. A. Lavery, and D. A. Agard, "Substrate binding drives large-scale conformational changes in the Hsp90 molecular chaperone," *Mol. Cell,* vol. 42, no. 1, pp. 96-105, Apr, 2011. DOI: https://doi.org/10.1016/j.molcel.2011.01.029.

[65] R. Rosenzweig, N. B. Nillegoda, M. P. Mayer, and B. Bukau, "The Hsp70 chaperone network," *Nat. Rev. Mol. Cell Biol.,* vol. 20, no. 11, pp. 665-680, Nov, 2019. DOI: https://doi.org/10.1038/s41580-019-0133-3.

[66] R. J. Roberts, C. Agius, C. Saliba, P. Bossier, and Y. Y. Sung, "Heat shock proteins (chaperones) in fish and shellfish and their potential role in relation to fish health:

A review," *J. Fish. Dis.,* vol. 33, no. 10, pp. 789-801, Oct, 2010. DOI: https://doi.org/10.1111/j.1365-2761.2010.01183.x.

[67] Y. Duan, H. Tang, K. Mitchell-Silbaugh, X. Fang, Z. Han, and K. Ouyang, "Heat shock protein 60 in cardiovascular physiology and diseases," *Front. Mol. Biosci.,* vol. 7, pp. 73, Apr, 2020. DOI: https://doi.org/10.3389/fmolb.2020.00073.

[68] L. Song, J. Zhang, C. Li, J. Yao, C. Jiang, Y. Li, S. Liu, and Z. Liu, "Genome-wide identification of hsp40 genes in channel catfish and their regulated expression after bacterial infection," *PLoS One,* vol. 9, no. 12, pp. e115752, Feb, 2014. DOI: https://doi.org/10.1371/journal.pone.0115752.

[69] T. S. Hori, A. K. Gamperl, L. O. Afonso, S. C. Johnson, S. Hubert, J. Kimball, S. Bowman, and M. L. Rise, "Heat-shock responsive genes identified and validated in Atlantic cod (*Gadus morhua*) liver, head kidney and skeletal muscle using genomic techniques," *BMC Genom.,* vol. 11, no. 1, pp. 72, Jan, 2010. DOI: https://doi.org/10.1186/1471-2164-11-72.

[70] M. J. Gollock, S. Currie, L. H. Petersen, and A. K. Gamperl, "Cardiovascular and haematological responses of Atlantic cod (*Gadus morhua*) to acute temperature increase," *J. Exp. Biol.,* vol. 209, no. Pt 15, pp. 2961-2970, Aug, 2006. DOI: https://doi.org/10.1242/jeb.02319.

[71] J. C. Perez-Casanova, M. L. Rise, B. Dixon, L. O. Afonso, J. R. Hall, S. C. Johnson, and A. K. Gamperl, "The immune and stress responses of Atlantic cod to long-term increases in water temperature," *Fish Shellfish Immunol.,* vol. 24, no. 5, pp. 600-609, May, 2008. DOI: https://doi.org/10.1016/j.fsi.2008.01.012.

[72] K. S. Kassahn, M. J. Caley, A. C. Ward, A. R. Connolly, G. Stone, and R. H. Crozier, "Heterologous microarray experiments used to identify the early gene response to heat stress in a coral reef fish," *Mol. Ecol.,* vol. 16, no. 8, pp. 1749-1763, Apr, 2007. DOI: https://doi.org/10.1111/j.1365-294X.2006.03178.x.

[73] B. A. Buckley, A. Y. Gracey, and G. N. Somero, "The cellular response to heat stress in the gobyGillichthys mirabilis: a cDNA microarray and protein-level analysis," *J. Exp. Biol.,* vol. 209, no. 14, pp. 2660-2677, Apr, 2006. DOI: https://doi.org/10.1242/jeb.02292.

[74] J. E. Podrabsky, and G. N. Somero, "Changes in gene expression associated with acclimation to constant temperatures and fluctuating daily temperatures in an annual killifish Austrofundulus limnaeus," *J. Exp. Biol.,* vol. 207, no. Pt 13, pp. 2237-2254, Jun, 2004. DOI: https://doi.org/10.1242/jeb.01016.

[75] N. Basu, A. E. Todgham, P. A. Ackerman, M. R. Bibeau, K. Nakano, P. M. Schulte, and G. K. Iwama, "Heat shock protein genes and their functional significance in fish," *Gene,* vol. 295, no. 2, pp. 173-183, Aug, 2002. DOI: https://doi.org/10.1016/s0378-1119(02)00687-x.

[76] M. Yiangou, E. Paraskeva, C. C. Hsieh, E. Markou, P. Victoratos, Z. Scouras, and J. Papaconstantinou, "Induction of a subgroup of acute phase protein genes in mouse liver by hyperthermia," *Biochim. Biophys. Acta,* vol. 1396, no. 2, pp. 191-206, Mar, 1998. DOI: https://doi.org/10.1016/s0167-4781(97)00188-7.

[77] M. Y. Gross-Sorokin, S. D. Roast, and G. C. Brighty, "Assessment of feminization of male fish in English rivers by the Environment Agency of England and Wales,"

Environ. Health Perspect., vol. 114 Suppl 1, no. Suppl 1, pp. 147-151, Apr, 2006. DOI: https://doi.org/10.1289/ehp.8068.

[78] L. J. Mills, R. E. Gutjahr-Gobell, D. B. Horowitz, N. D. Denslow, M. C. Chow, and G. E. Zaroogian, "Relationship between reproductive success and male plasma vitellogenin concentrations in cunner, Tautogolabrus adspersus," *Env. Health Perspect,* vol. 111, no. 1, pp. 93-100, Jan, 2003. DOI: https://doi.org/10.1289/ehp.5531.

[79] M. Soffker, and C. R. Tyler, "Endocrine disrupting chemicals and sexual behaviors in fish-a critical review on effects and possible consequences," *Crit. Rev. Toxicol.,* vol. 42, no. 8, pp. 653-668, Sep, 2012. DOI: https://doi.org/10.3109/10408444.2012.692114.

[80] D. Montjean, A. S. Neyroud, M. G. Yefimova, M. Benkhalifa, R. Cabry, and C. Ravel, "Impact of endocrine disruptors upon non-genetic inheritance," *Int. J. Mol. Sci.,* vol. 23, no. 6, Mar, 2022. DOI: https://doi.org/10.3390/ijms23063350.

[81] A. M. Cohen, A. A. Mansour, and J. H. Banoub, "Absolute quantification of Atlantic salmon and rainbow trout vitellogenin by the 'signature peptide' approach using electrospray ionization QqToF tandem mass spectrometry," *J. Mass Spectrom.,* vol. 41, no. 5, pp. 646-658, May, 2006. DOI: https://doi.org/10.1002/jms.1023.

[82] A. M. Cohen, F. Jahouh, S. Sioud, R. M. Rideout, M. J. Morgan, and J. H. Banoub, "Quantification of Greenland halibut serum vitellogenin: a trip from the deep sea

to the mass spectrometer," *Rapid Commun. Mass Spectrom.,* vol. 23, no. 7, pp. 1049-1060, Jan, 2009. DOI: https://doi.org/10.1002/rcm.3966.

[83] J. Banoub, P. Thibault, A. Mansour, A. Cohen, D. H. Heeley, and D. Jackman, "Characterisation of the intact rainbow trout vitellogenin protein and analysis of its derived tryptic and cyanogen bromide peptides by matrix-assisted laser desorption/ionisation time-of-flight-mass spectrometry and electrospray ionisation quadrupole/time-of-flight mass spectrometry," *Eur. J. Mass. Spectrom.,* vol. 9, no. 5, pp. 509-524, 2003. DOI: https://doi.org/10.1255/ejms.572.

[84] A. M. Cohen, and J. H. Banoub, "Application of Mass Spectrometry for the Analysis of Vitellogenin, a Unique Biomarker for Xenobiotic Compounds," *NATO Sci. Peace Secur. Ser. A: Chem. Biol.,* vol. 301-318, Oct, 2010. DOI: https://doi.org/10.1007/978-90-481-9815-3_19.

[85] J. Katahira, "Nuclear export of messenger RNA," *Genes,* vol. 6, no. 2, pp. 163-184, Mar, 2015. DOI: https://doi.org/10.3390/genes6020163.

[86] H. Zhao, C. R. Chiaro, L. Zhang, P. B. Smith, C. Y. Chan, A. M. Pedley, R. J. Pugh, J. B. French, A. D. Patterson, and S. J. Benkovic, "Quantitative analysis of purine nucleotides indicates that purinosomes increase de novo purine biosynthesis," *J. Biol. Chem.,* vol. 290, no. 11, pp. 6705-6713, Mar, 2015. DOI: https://doi.org/10.1074/jbc.M114.628701.

[87] K. Tanaka, "The proteasome: overview of structure and functions," *Proc. Jpn. Acad. Ser. B Phys. Biol. Sci.,* vol. 85, no. 1, pp. 12-36, 2009. DOI: https://doi.org/10.2183/pjab.85.12.

[88] B. Gregory, N. Rahman, A. Bommakanti, M. Shamsuzzaman, M. Thapa, A. Lescure, J. M. Zengel, and L. Lindahl, “The small and large ribosomal subunits depend on each other for stability and accumulation,” *Life Sci. Alliance,* vol. 2, no. 2, pp. e201800150, Apr, 2019. DOI: https://doi.org/10.26508/lsa.201800150.

[89] G. Dreyfuss, L. Philipson, and I. W. Mattaj, “Ribonucleoprotein particles in cellular processes,” *J. Cell Biol.,* vol. 106, no. 5, pp. 1419-1425, May, 1988. DOI: https://doi.org/10.1083/jcb.106.5.1419.

[90] A. Moreno, V. Taleb, M. Sebastian, E. Anoz-Carbonell, M. Martinez-Julvez, and M. Medina, “Cofactors and pathogens: Flavin mononucleotide and flavin adenine dinucleotide (FAD) biosynthesis by the FAD synthase from Brucella ovis,” *IUBMB Life,* vol. 74, no. 7, pp. 655-671, Jul, 2022. DOI: https://doi.org/10.1002/iub.2576.

[91] S. Zhang, X. Zeng, M. Ren, X. Mao, and S. Qiao, “Novel metabolic and physiological functions of branched chain amino acids: a review,” *J. Anim. Sci. Biotechnol.,* vol. 8, pp. 10, Dec, 2017. DOI: https://doi.org/10.1186/s40104-016-0139-z.

[92] M. N. Moore, A. Koehler, D. Lowe, and A. Viarengo, "Chapter thirty-three lysosomes and autophagy in aquatic animals," *Methods Enzymol.*, Academic Press, 2008. pp. 581-620.

[93] S. R. Bonam, F. Wang, and S. Muller, “Lysosomes as a therapeutic target,” *Nat. Rev. Drug Discov.,* vol. 18, no. 12, pp. 923-948, Dec, 2019. DOI: https://doi.org/10.1038/s41573-019-0036-1.

[94] G. Hu, Y. Shu, P. Luan, T. Zhang, F. Chen, and X. Zheng, "Genomic analysis of the proteasome subunit gene family and their response to high density and saline-alkali stresses in grass carp," *Fishes,* vol. 7, no. 6, pp. 350, Nov, 2022. DOI: https://doi.org/10.3390/fishes7060350.

[95] T. D. Sharkey, "Pentose phosphate pathway reactions in photosynthesizing cells," *Cells,* vol. 10, no. 6, pp. 1547, Jun, 2021. DOI: https://doi.org/10.3390/cells10061547.

[96] S. Li, Y. Liu, B. Li, L. Ding, X. Wei, P. Wang, Z. Chen, S. Han, T. Huang, B. Wang, and Y. Sun, "Physiological responses to heat stress in the liver of rainbow trout (*Oncorhynchus mykiss*) revealed by UPLC-QTOF-MS metabolomics and biochemical assays," *Ecotoxicol. Environ. Saf.,* vol. 242, pp. 113949, Sep, 2022. DOI: https://doi.org/10.1016/j.ecoenv.2022.113949.

[97] A. Varki, "Biological roles of glycans," *Glycobiology,* vol. 27, no. 1, pp. 3-49, Jan, 2017. DOI: https://doi.org/10.1093/glycob/cww086.

[98] W. Wang, S. Nag, X. Zhang, M. H. Wang, H. Wang, J. Zhou, and R. Zhang, "Ribosomal proteins and human diseases: pathogenesis, molecular mechanisms, and therapeutic implications," *Med. Res. Rev.,* vol. 35, no. 2, pp. 225-285, Mar, 2015. DOI: https://doi.org/10.1002/med.21327.

[99] K. A. Pattin, and J. H. Moore, "Role for protein-protein interaction databases in human genetics," *Expert. Rev. Proteom.,* vol. 6, no. 6, pp. 647-659, Dec, 2009. DOI: https://doi.org/10.1586/epr.09.86.

[100] S. S. Wimalagunasekara, J. Weeraman, S. Tirimanne, and P. C. Fernando, “Protein-protein interaction (PPI) network analysis reveals important hub proteins and sub-network modules for root development in rice (Oryza sativa),” *J. Genet Eng. Biotechnol.,* vol. 21, no. 1, pp. 69, May, 2023. DOI: https://doi.org/10.1186/s43141-023-00515-8.

[101] D. Szklarczyk, R. Kirsch, M. Koutrouli, K. Nastou, F. Mehryary, R. Hachilif, A. L. Gable, T. Fang, N. T. Doncheva, S. Pyysalo, P. Bork, L. J. Jensen, and C. von Mering, “The STRING database in 2023: protein-protein association networks and functional enrichment analyses for any sequenced genome of interest,” *Nucleic Acids Res.,* vol. 51, no. D1, pp. D638-D646, Jan, 2023. DOI: https://doi.org/10.1093/nar/gkac1000.

[102] X. Xu, X. Xiong, and Y. Sun, “The role of ribosomal proteins in the regulation of cell proliferation, tumorigenesis, and genomic integrity,” *Sci. China Life Sci.,* vol. 59, no. 7, pp. 656-672, Jul, 2016. DOI: https://doi.org/10.1007/s11427-016-0018-0.

[103] A. Meskauskas, and J. D. Dinman, “Ribosomal protein L3: gatekeeper to the A site,” *Mol. Cell,* vol. 25, no. 6, pp. 877-888, Mar, 2007. DOI: https://doi.org/10.1016/j.molcel.2007.02.015.

[104] A. Petrov, A. Meskauskas, and J. D. Dinman, “Ribosomal protein L3: influence on ribosome structure and function,” *RNA Biol.,* vol. 1, no. 1, pp. 59-65, May, 2004. DOI: https://doi.org/10.4161/rna.1.1.957.

[105] A. Meskauskas, and J. D. Dinman, “Ribosomal protein L3 functions as a 'rocker switch' to aid in coordinating of large subunit-associated functions in eukaryotes and Archaea,” *Nucleic Acids Res.,* vol. 36, no. 19, pp. 6175-6186, Nov, 2008. DOI: https://doi.org/10.1093/nar/gkn642.

[106] F. Pichaud, R. F. Walther, and F. Nunes de Almeida, “Regulation of Cdc42 and its effectors in epithelial morphogenesis,” *J. Cell Sci.,* vol. 132, no. 10, pp. jcs217869, May, 2019. DOI: https://doi.org/10.1242/jcs.217869.

[107] B. S. Negrutskii, and A. V. El’skaya, "Eukaryotic translation elongation factor 1α: Structure, expression, functions, and possible role in aminoacyl-trna channeling," *Progress in nucleic acid research and molecular biology*, K. Moldave, ed. Academic Press, 1998. pp. 47-78.

[108] S. Ni, Y. Zhou, Y. Chen, X. Du, and S. Zhang, “Identification of ATP synthase alpha subunit as a new maternal factor capable of protecting zebrafish embryos from bacterial infection,” *FASEB J.,* vol. 33, no. 11, pp. 12983-13001, Nov, 2019. DOI: https://doi.org/10.1096/fj.201901290R.

[109] P. D. J. Weitzman, and M. J. Danson, "Citrate Synthase," *Current topics in cellular regulation*, B. L. Horecker and E. R. Stadtman, eds. Academic Press, 1976. pp. 161-204.

[110] C. Dingwall, S. Kandels-Lewis, and B. Seraphin, “A family of Ran binding proteins that includes nucleoporins,” *Proc. Natl. Acad. Sci. USA,* vol. 92, no. 16, pp. 7525-7529, Aug, 1995. DOI: https://doi.org/10.1073/pnas.92.16.7525.

[111] U. Kutay, R. Juhlen, and W. Antonin, “Mitotic disassembly and reassembly of nuclear pore complexes,” *Trends Cell Biol.,* vol. 31, no. 12, pp. 1019-1033, Dec, 2021. DOI: https://doi.org/10.1016/j.tcb.2021.06.011.

[112] X. Yu, H. Wu, Z. Wu, Y. Lan, W. Chen, B. Wu, Y. Deng, and J. Liu, “Nuclear pore complex protein RANBP2 and related SUMOylation in solid malignancies,” *Genes & Diseases*, Jun, 2024. DOI: https://doi.org/10.1016/j.gendis.2024.101407.

[113] F. Tian, X.-L. Hu, T. Yao, X. Yang, J.-G. Chen, M.-Z. Lu, and J. Zhang, “Recent advances in the roles of HSFs and HSPs in heat stress response in woody plants,” *Front. Plant Sci.,* vol. 12, Jul, 2021. DOI: https://doi.org/10.3389/fpls.2021.704905.

[114] F. Cyr, E. Colbourne, J. Holden, Snook, S., G. Han, N. Chen, W. Bailey, J. Higdon, S. Lewis, B. Pye, and D. Senciall, “Physical Oceanographic conditions on the Newfoundland and Labrador shelf during 2017,” *DFO Can. Sci. Advis. Sec. Res.*, pp. iv + 58, Sep, 2019.

[115] F. Cyr, S. Snook, C. Bishop, P. S. Galbraith, N. Chen, and G. Han, “Physical Oceanographic conditions on the Newfoundland and Labrador shelf during 2021,” *DFO Can. Sci. Advis. Sec. Res.*, pp. iv + 48, Jun, 2022.

[116] F. Cyr, and P. S. Galbraith, “A climate index for the Newfoundland and Labrador shelf,” *Earth Syst. Sci. Data,* vol. 13, no. 5, pp. 1807-1828, Dec, 2021. DOI: https://doi.org/10.5194/essd-13-1807-2021.

[117] M. A. Alexander, S.-i. Shin, J. D. Scott, E. Curchitser, and C. Stock, “The response of the Northwest Atlantic Ocean to climate change,” *J. Clim.,* vol. 33, no. 2, pp. 405-428, Sep, 2020. DOI: https://doi.org/10.1175/jcli-d-19-0117.1.

Chapter 4 Structural Diversity in Lipid A of Gram-Negative Bacteria *Aeromonas hydrophila SJ-26*

This Chapter is reproduced with permission from Trevena N.Youssef, Abanoub Mikhael, David R. Goodlett, and Joseph Banoub. This research is currently submitted for publication in the journal Rapid Commun. Mass Spectrom.

4.1. Abstract

The chemical structure of lipid A, isolated from the lipopolysaccharide of a wild strain of *Aeromonas hydrophila* (*A. hydrophila SJ-26*), was investigated using electrospray ionization with field asymmetric wave ion mobility-Orbitrap mass spectrometry (ESI-FAIMS-MS), high energy collision-induced dissociation tandem mass spectrometry (HCD-MS/MS), and Kendrick mass defect (KMD) plots, revealing significant heterogeneity in the isolated Lipid A mixture. FAIMS allowed the fractionation of Lipid A ions into three main types: di-phosphorylated Lipid A (DPLA, M_{1-3}), mono-phosphorylated Lipid A (MPLA, M_{4-6}), and Lipid A adducts and/or aggregated dimers. Major precursor anions of each Lipid A fraction were elucidated by tandem mass spectrometry. Additionally, heterogeneity in each Lipid A fraction was investigated using KMD plots. The combination of tandem MS and Kendrick analysis MS enabled the elucidation of the complex molecular architecture of lipid A of this *Aeromonadaceae* family.

4.2. Introduction

Mass spectrometry (MS) has become an indispensable tool for analyzing biomolecules by accurately identifying molecular masses [1-3]. MS/MS analysis has been transformative in enabling researchers to identify the complex structures of biomolecules, including lipid A [1-3]. Lipid A is a key component of the lipopolysaccharides (LPS) that form the outer membrane of Gram-negative bacteria, contributing to the bacterial virulence and immunogenicity [4-6].

Gram-negative bacteria are well-known to cause many serious diseases in humans and animals, including food-borne illnesses, respiratory and urinary tract infections, and even sexually transmitted diseases [7-11]. In some cases, Gram-negative bacterial infections can trigger highly aggressive immune responses, which can prove fatal without prompt and proper treatment. One distinguishing feature of Gram-negative bacteria is their cell envelope, which consists of a thin peptidoglycan layer sandwiched between an inner cytoplasmic membrane and an outer membrane rich in LPS [2, 10-13].

LPS is a structurally complex amphiphilic molecule composed of three covalently linked regions: a hydrophilic non-repeating core oligosaccharide, a distal O-polysaccharide (or O-antigen), and a hydrophobic domain known as lipid A. Lipid A serves as the anchoring component that embeds LPS into the bacterial outer membrane, while the polysaccharide portion interacts with the external environment, including the host immune defense mechanisms. Importantly, lipid A is responsible for the strong immune-stimulatory properties of LPS and is considered the most toxic component [4]. The highly conserved biosynthetic pathway of lipid A has been well-characterized in model organisms like

Escherichia coli and *Salmonella typhimurium* [5, 13-18]. The structural variations in lipid A can lead to differences in bacterial virulence. Lipid A consists of a β-D- Gl*cp*N-(1→6)-α-D-Gl*cp*N disaccharide backbone, which is acylated with varying numbers and lengths of fatty acid chains [19].

The genus *Aeromonas*, originally ranked in the *Vibrionaceae* family, has been reclassified based on molecular genetic evidence. Ribosomal RNA sequence studies have shown it has a distinct evolutionary path, warranting its own family, *Aeromonadaceae* [20]. The genus *Aeromonas*, which includes the pathogen *A hydrophila*, has been extensively studied due to its clinical relevance and role in aquatic ecosystems [7, 21-25]. *A. hydrophila* is a Gram-negative bacterium with heterotrophic, aerobic, and anaerobic metabolic capabilities, making it highly adaptable to various environments. It is particularly notorious for causing motile Aeromonas septicemia (MAS), hemorrhagic septicemia, and ulcer disease (also known as red-sore disease) in fish [26]. In humans, *A. hydrophila* is an opportunistic pathogen linked to gastroenteritis and wound infections [26, 27].

The amphiphilic nature of lipid A presents challenges for separation and ionization, but advances in ESI negative-ion mode MS have made it possible to study lipid A species with greater precision [1-3].

KMD plots have emerged as essential tools for the classification and visualization of structurally related ions in complex mixtures [28-33]. These plots enable the systematic grouping of ions with similar structural characteristics into recognizable patterns. Structurally related ions are organized along horizontal lines, referred to as KMD families, which reveal their relationships in a clear and interpretable manner. By using tandem mass

spectrometry (MS/MS) to identify one anion within a KMD family, it is possible to deduce the structural information of all other ions in the same series. This approach significantly reduces the number of spectra required for thorough structural analysis, making KMD plots highly effective for elucidating and profiling lipid A molecules in detail [28]. This work showcases the benefits of FAIMS and KMD plots in the characterization of *A. hydrophila SJ-26.*

The structural elucidation studies pave the way for the development and identification of specific fatty acid modifications and acylation patterns that are unique to certain bacterial strains. Such structural differences are crucial in understanding the varying immune responses elicited by different lipid A variants and developing targeted vaccines and antibiotics [5]. Also, the structural characterization of lipid A in Gram-negative bacteria *A. hydrophila* is essential for understanding bacterial virulence and developing new therapeutic strategies to combat infections. *A. hydrophila* is essential for understanding bacterial virulence and developing new therapeutic strategies to combat infections [5].

Here, we report the structural elucidation by ESI-FAIMS-MS, HCD-MS/MS, and KMD plots of a heterogeneous mixture of lipid As isolated from the LPS of *A. hydrophila*, the Gram-negative bacteria, SJ-26.

4.3. Materials and Methods

4.3.1. Bacterial Culture

The original strain of *A. hydrophila* was obtained from Dr. H. N. Atkinson (The South Australian School of Technology Oceans, Australia). It was initially isolated from Sockeye salmon. This strain was added to the Northwest Atlantic Fisheries Center, St. John's collection (SJ-26). The cultures were grown to medium-to-late stationary phase in Trypticase Soy Broth without added glucose (Baltimore Biological Laboratories Inc.) for approximately 20 hours at 25 °C with aeration at 20 L/min in a New Brunswick MF-128S fermentor. They were then killed by the addition of 0.3% formalin with continuous agitation for 16 hours at room temperature. Cells were subsequently collected by centrifugation at 44,720 ×g in a Sorvall SS-34 rotor, washed with 0.15 M NaCl, lyophilized, and stored at -50 °C until required.

4.3.2. Purification of the Lipopolysaccharide

LPS was extracted using the hot-phenol method and subsequently freeze-dried. Stored cells (10 g) were suspended in 175 mL of deionized water and heated to 70 °C. An equal volume of 90% heated phenol was added, followed by 20 minutes of stirring at 70 °C. After cooling on ice, the mixture was centrifuged at 1,371 ×g in a Sorvall SS-34 rotor. The aqueous layer was isolated, and the extraction was repeated twice. The combined aqueous layers were dialyzed, reduced under vacuum, and centrifuged at 169,570 ×g for 3 hours. The resulting LPS pellet was resuspended in water, centrifuged twice more, and lyophilized. LPS was further purified with polymyxin-coated Affi-Prep beads, suspended in PBS (pH 7.4), washed with 0.1 M NaOH, and incubated overnight

with agitation at 251 ×g . After centrifugation at 698 ×g for 10 minutes, the supernatant was collected and the supernatants were combined, dialyzed, and lyophilized.

4.3.3. Hydrolysis of the Lipopolysaccharide

LPS (100 mg) was hydrolyzed with 1% acetic acid for 90 minutes at 100 °C. The hydrolysate was then centrifuged at 1,790 ×g for 30 minutes, resulting in the precipitation of lipid A, while the polysaccharide remained in the aqueous phase. The lipid A was carefully removed and subsequently washed with water.

4.3.4. ESI- FAIMS-MS, HCD-MS/MS and Kendrick Mass Defect

Negative ion mode ESI-MS was performed with an Orbitrap Fusion™ Lumos™ Tribrid™ Mass Spectrometer with a FAIMS pro interface (Thermo Scientific, Waltham, MA, USA), as described previously [28]. The lipid A mixture of the Gram-negative bacteria *Aeromonas hydrophila* SJ-26 was dissolved in chloroform: methanol: water: triethyl ammonium acetate (TEAA, pH = 7) (1:1:0.02: 0.002) at a concentration of 1 μg/μL and directly infused into the ESI-FAIMS source at a flow rate of 2 μL/min. The spray voltage was set to 2.8 kV, capillary temperature to 275 °C, and sheath and auxiliary gas to 2 a.u. The FAIMS separation was accomplished with the following settings: inner electrode temperature = 100 °C, outer electrode temperature = 100 °C, FAIMS N_2 carrier gas flow = 1.2 L/min, asymmetric waveform with dispersion voltages (DV) = +5000 V. Compensation voltages (CV) were scanned from 0 to 70 V with a step size of 1 volt at 120 K resolution, 250– 2000 *m/z* range, 60% RF lens, 100% normalized automatic gain control (AGC) target,

and 100 ms Maximum injection time (IT). Tandem MS was performed at specific CVs that maximize the signal-to-noise ratio (S/N) of the selected precursor ions. Normalized HCD in the range of 10-40% was used for tandem MS. Data were visualized using Freestyle software 1.8 SP1 (Thermo Scientific). Tandem MS interpretation was done manually using ChemDraw Prime (version 23.1.1.3). The mass list of each Lipid A fraction separated by FAIMS at different compensation voltages was exported and used for Kendrick analysis. The Kendrick mass defect (KMD) plots were visualized on the constellation website (https://constellation.chemie.hu-berlin.de/). Different fractional KMD base units of $CH_2/2$ (14.01565/2= 7.007825), $CH_2/5$ (14.01565/5= 2.80313), and C14:0/11 (210.198365/11= 19.10894227) were used with a ceiling rounding function (i.e. 7.007825 was rounded up to a nominal of 8.000000, etc.). Different fractional base units was used to enhance the separation of related isotopologues (same isotopic envelope) and facilitate the visualization of structural relationships [34].

4.4. Results and Discussion

4.4.1. ESI-FAIMS-Orbitrap-MS Analysis

The lipid A structures of *Aeromonas* Gram-negative bacteria SJ-26 were investigated using negative ion mode ESI-FAIMS-Orbitrap-MS. This analysis revealed the presence of three different types of Lipid A anions: MPLA detected mainly in the CV range of 0-22 V, lipid A adducts or aggregate dimers at the CV range of 23-43 volts, and DPLA at the CV range of 44 to 70 volts. The most abundant lipid A anions detected across different CV were four DPLA doubly charged anions $[M - 2H]^{2-}$ at *m/z* 897.6064, 883.5891,

and 792.5054, and their corresponding singly charged MPLA anions $[M - H]^-$ at *m/z* 1716.2488, 1688.2198, and 1506.0510 **(Figure 4-1)**.

Structural elucidation was achieved through a combination of ESI-MS and HCD-MS/MS analysis conducted with a FAIMS interface. FAIMS is a gas-phase ion separation technique in conjunction with mass spectrometry based on the separation of the ions based on their mobility differences in a strong electric field compared to a weak electric field [35]. This technique offers enhanced selectivity and sensitivity, particularly for complex mixtures, by reducing chemical noise and increasing the separation of each distinct anion [35, 36].

It is well established that the competitive hydrolysis of the primary and/or secondary fatty acid esters on the β-D-Glc*p*N-(1→6)-α-D-Glc*p*N disaccharide backbone of lipid A occurs stepwise. Notably, the ester-linked fatty acid groups at O-3 and O-3′ are more susceptible to hydrolysis compared to the fatty acyl amide groups located at N-2 and N-2′. This increased resistance is attributed to the greater stability of the fatty acyl amide groups [3]. We speculate that the observed Lipid A heterogeneity reflects variations in the hydrolysis patterns of these lipid A structures that can occur during the hot phenol extraction procedure [37, 38]. To confirm these speculations, further structural elucidation will be performed using HCD-MS/MS analysis.

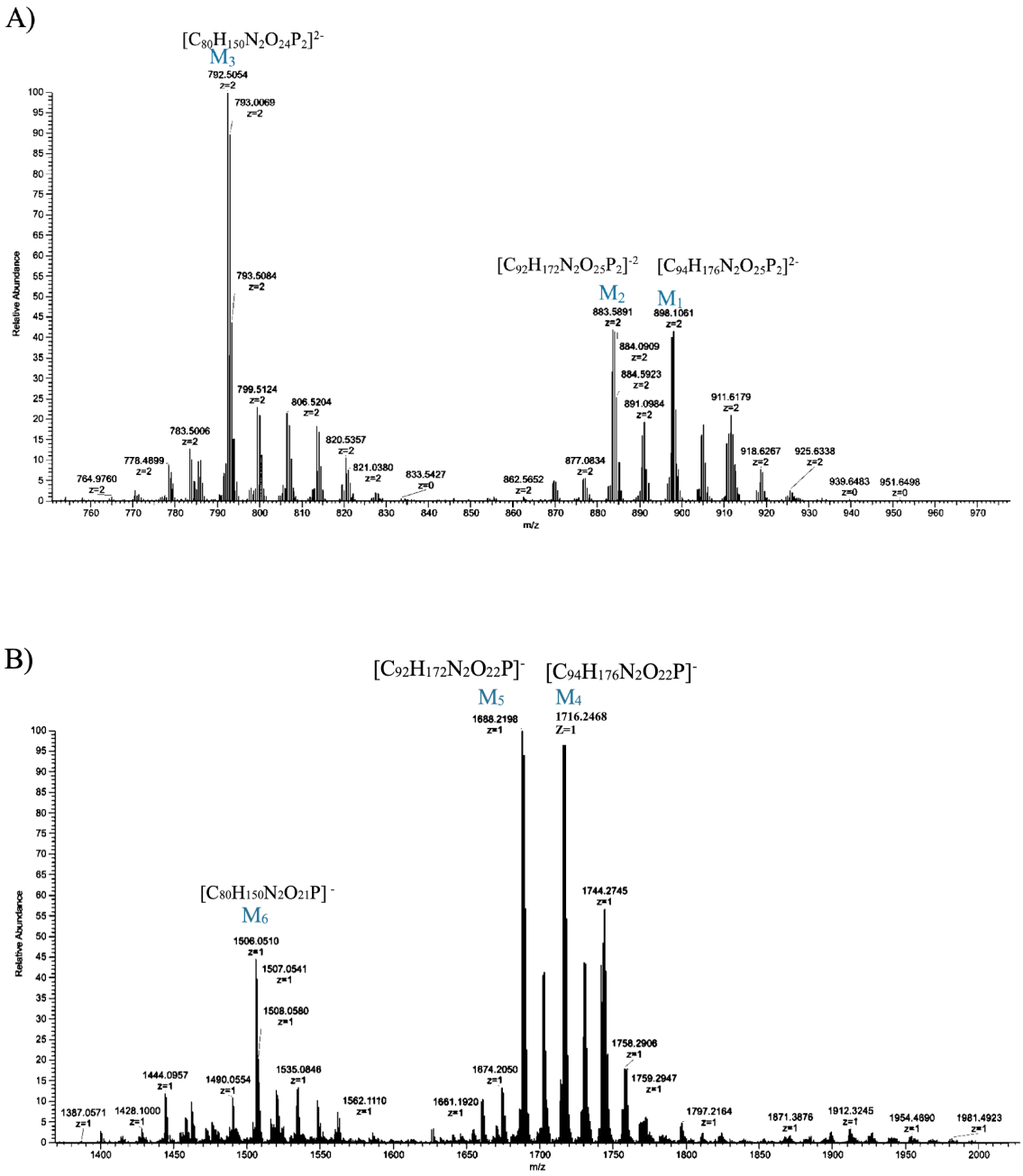

Figure 4-1. Negative ion ESI-FAIMS-Orbitrap-MS spectra of the native lipid A extract from *A. hydrophila*: A) DPLA with CV = 52, and B) MPLA detected at FAIMS-MS with CV = 15.

The three major doubly charged DPLA anions $[M_n - 2H]^{2-}$ (n = 1-3) and their three corresponding MPLA singly charged anions $[M_n - H]^-$ (n=4-6) indicated a preliminary

heterogeneity in the lipid A phosphorylation degree, as shown in **Figures 4-1 and 4-2, and Table 4-1**. These major anions (n=1-6, **Table 4-1)** were further selected for HCD-MS/MS analysis, as elaborated in subsequent sections. Detailed HCD-MS/MS analysis allowed the assignment of anion chemical compositions and the determination of primary and secondary acyl chain types in the lipid A chemical structure. In analyzing the molecular formula of organic molecules, the degree of unsaturation (DU) is a calculation that determines the total number of rings and π bonds .

The $[M_1 - 2H]^{2-}$ ion at *m/z* 897.6046 was assigned as the deprotonated DPLA hexa-acylated lipid A anion form, containing four (C14:0(3-OH)), with two substituted by Myristic acid (C14:0) and Lauric acid (C12:0), creating Cl4:0(3-O-14:0) and Cl4:0(3-O-12:0). The $[M_4 - H]^-$ ion at *m/z* 1716.2488 represented its MPLA form **(Figure 4-2 and Table 4-1).**

The $[M_2 - 2H]^{2-}$ ion at *m/z* 833.5891 was assigned as the deprotonated DPLA hexa-acylated lipid anion form, incorporating four (C14:0(3-OH)) with two substituted by two Lauric acid (C12:0), creating two (Cl4:0(3-O-12:0). The $[M_5 - H]^-$ ion at *m/z* 1688.2198 represented its MPLA form **(Figure 4-2 and Table 4-1).**

Furthermore, the $[M_3 - 2H]^{2-}$ ion at *m/z* 792.5054 was assigned as a deprotonated, DPLA penta-acylated lipid A anion form, which consisted of incorporating four (C14:0(3-OH)) with one substituted by Lauric acid (C12:0), creating Cl4:0(3'-O-12:0). The MPLA penta-acylated lipid A anion form $[M_6 - H]^-$ ion at *m/z* 1506.0510 **(Figure 4-2 and Table 4-1)**.

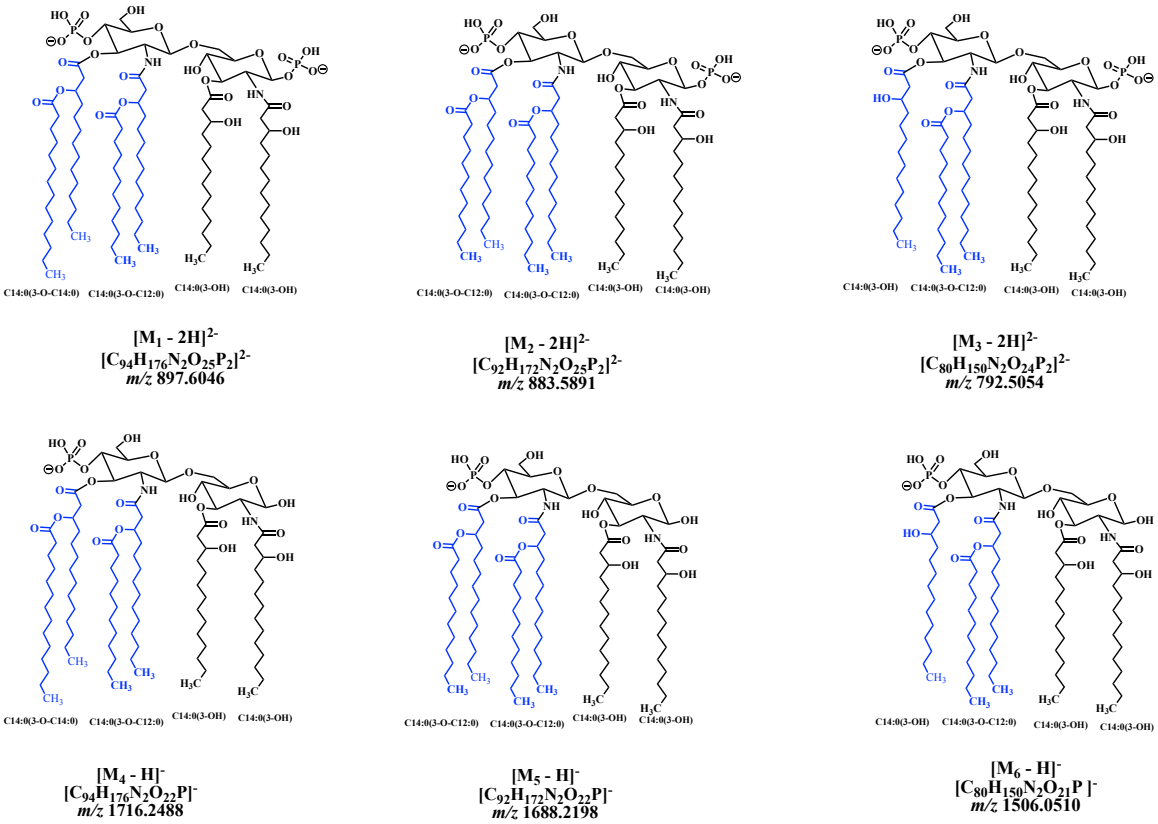

Figure 4-2. Schematic representation of suggested structures of the molecular anions of the lipid As mixture extracted from *A. hydrophila* SJ-26. The DPLA ($[M_n - 2H]^{2-}$ (n = 1-3)) and MPLA ($[M_n - H]^-$ (n=4-6)).

Table 4-1. Assignments of the deprotonated mono-phosphorylated DPLA and MPLA molecules observed in ESI-MS analysis of a native mixture of lipid A extracted from the *A. hydrophila* SJ-26.

Ion in KMD plots[a]	Diagnostic ion	Empirical formula	*m/z* Observed	*m/z* Calculated	*m/z* Error (ppm)	DU[b]
	DPLA					
1	$[M_1 - 2H]^{2-}$	$[C_{94}H_{176}N_2O_{25}P_2]^{2-}$	897.6046	1795.2048/2= 897.6024	2.4	10
2	$[M_2 - 2H]^{2-}$	$[C_{92}H_{172}N_2O_{25}P_2]^{2-}$	883.5891	1767.1735/2= 883.5868	2.6	10
3	$[M_3 - 2H]^{2-}$	$[C_{80}H_{150}N_2O_{24}P_2]^-$	792.5054	1585.0065/2 = 792.5033	2.6	9
	MPLA					
4	$[M_4 - H]^-$	$[C_{94}H_{176}N_2O_{22}P]^-$	1716.2468	1716.2458	0.5	9

5	$[M_5 - H]^-$	$[C_{92}H_{172}N_2O_{22}P]^-$	1688.2198	1688.2145	3.1	9
6	$[M_6 - H]^-$	$[C_{80}H_{150}N_2O_{21}P]^-$	1506.0510	1506.0474	2.3	8

[a]Simplified ion numbers 1-6 will be used later in the Kendrick mass defect analysis (Section 4.4.4).
[b]The degree of unsaturation (DU) is a calculation that determines the total number of rings and π bonds. The calculation was performed using the corresponding neutral molecular formulas

The proposed structures were confirmed through a detailed analysis of the HCD-MS/MS spectra of selected $[M_n - 2H]^{2-}$ and $[M_n - H]^-$ anions, as elaborated in subsequent sections.

4.4.2. ESI-FAIMS-Orbitrap-MS/MS Analysis

The assignment of the three DPLA anions at *m/z* 897.6046, 833.5891, and 792.5054, as well as their corresponding three MPLA anions at *m/z* 1716.2488, 1688.2198, and 1506.0510, respectively, **(Figure 4-1)** observed in the single-stage high-resolution MS analysis confirmed solely the exact anion *m/z* values. Therefore, MS/MS enabled the identification of diagnostic product ions, confirming their proposed molecular structures [39]. The application of high-energy dissociation HCD-MS/MS further facilitates detailed structural elucidation by generating product ions that reveal the connectivity and composition of molecules, contributing to a comprehensive understanding of the molecule's structure and fragmentation pathways [3, 40].

We employed the combined nomenclature systems of Domon and Costello [41], along with and Morrison *et al.* [42], which specifically addresses MS/MS fragmentation patterns for carbohydrates and lipid A, respectively [11].

Scheme 4-1 illustrates the HCD-MS/MS fragmentation pathways of the β-D-Gl*cp*N-(1→6)-α-D-Gl*cp*N disaccharide, characterized by the sequential loss of acyl chains [42]. For example, the most common losses occur on the primary and secondary acyl chains at the O-3′ position, which results in fragments assigned as the 3'ζ, 3'ε, 3'α, and 3'β positions. This is followed by the loss of the primary chain at the O-3 position and subsequent 2'ζ fission at the N-2′ amido group, as depicted in **Scheme 4-1.** Additionally, $^{0,4}A_2$ cross-ring cleavages were observed, along with the cleavage of the β-(1→6) -glycosidic linkage, leading to the formation of Y_1 and C_1 fragments. Further fragmentation involves the elimination of the PO_3 group located at the O-1 position, producing the [C2 - H]$^-$ product anion through the release of HPO_3 [2, 42].

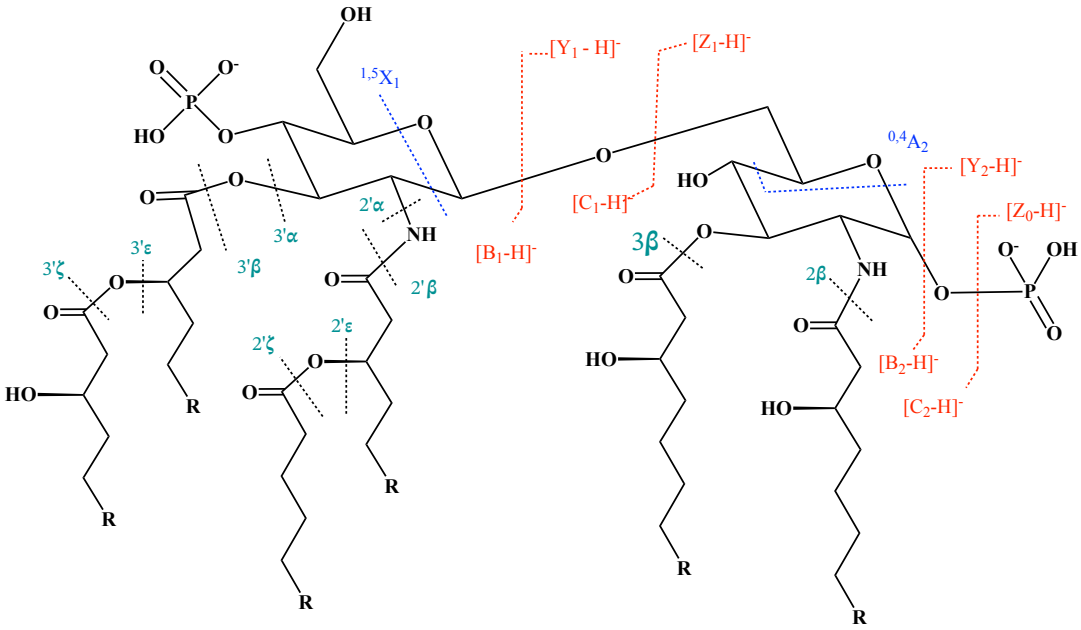

Scheme 4-1. Proposed fragmentation of the HCD-MS/MS fragmentation patterns of the molecular anion of lipid A.

4.4.2.1. HCD-MS/MS Analysis of the Lipid As $M_{1\&4}$

The mass spectra revealed a DPLA doubly charged ion at *m/z* 898.1061 and its corresponding MPLA singly charged species at *m/z* 1716.2488 annotated as $[M_1 - 2H]^{2-}$ and $[M_4 - H]^-$, respectively (**Figure 4-3).**

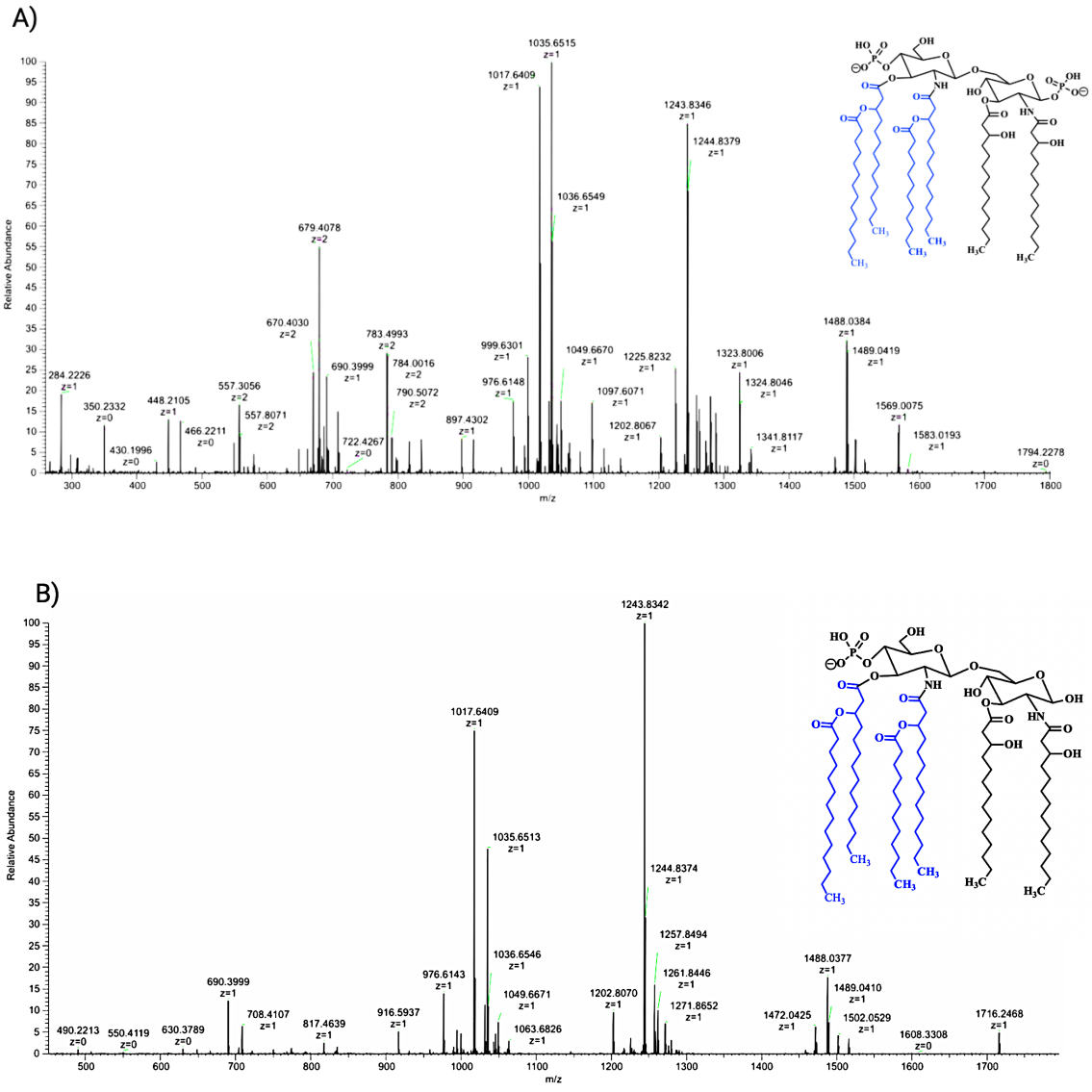

Figure 4-3. HCD-MS/MS of DPLA and MPLA anions extract from *A. hydrophila.* (A) The doubly charged DPLA $[M_1 - 2H]^{2-}$ anion at *m/z* 898.1061 and (B) The singly charged MLPA $[M_4 - H]^-$ anion at *m/z* 1716.2488.

We proposed this heterogeneous lipid A mixture $[M_1 - 2H]^{2-}$ and $[M_4 - H]^-$ corresponded to the DPLA and MPLA forms of the β-D- Gl*cp*N-(1→6)-α-D-Gl*cp*N disaccharide backbone in which the O- 3' and N-3' positions were substituted by (C14:0(3-O(14:0))) and (C14:0(3-O(12:0))) groups, respectively, at the non-reducing end sugar, whereas the O-3 and N-3 positions on the reducing sugar moiety were both substituted with a 3-OH-myristic acid chain (C14:0(3-OH)). Illustrated in **Figure 4-3**, **Scheme 4-2** and **Table 4-2**.

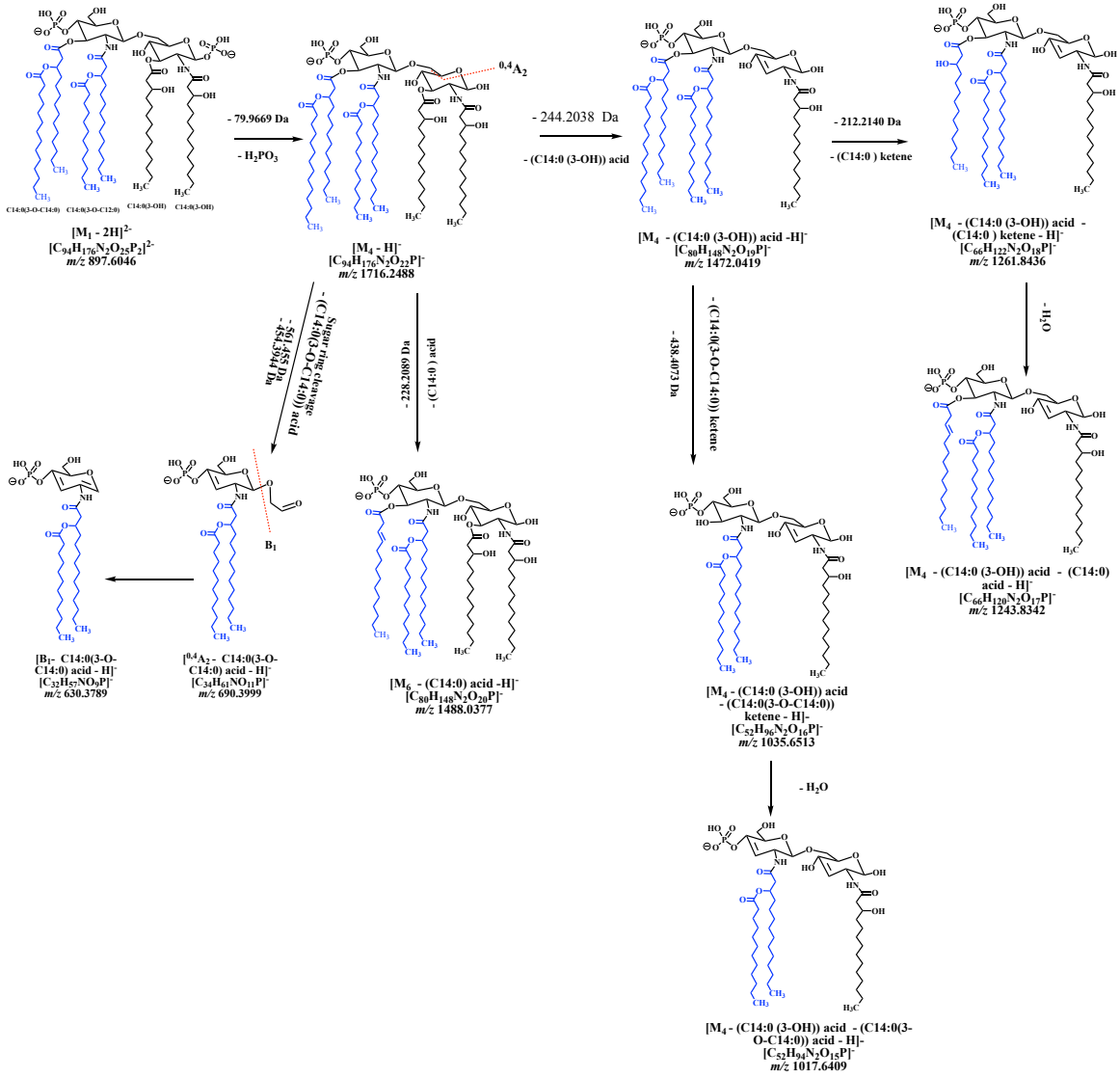

Scheme 4-2. Proposed fragmentation pathways of the selected precursor anions, $[M_1 - 2H]^{2-}$ and $[M_4 - H]^-$ anions at *m/z* 897.6046 and 1716.2468, respectively.

Table 4-2. Assignments of the diagnostic product anions in HCD-MS/MS analysis of the $[M_1 - 2H]^{2-}$ and $[M_4 - H]^-$ anions at *m/z* 897.6046, 1716.2468 respectively.

Diagnostic ion	Empirical formula	*m/z* Observed	*m/z* Calculated	*m/z* Error (ppm)
$[M_4$ - (C14:0) acid- H$]^-$	$[C_{80}H_{148}N_2O_{20}P]^-$	1488.0377	1488.0369	0.5
$[M_4$ - (C14:0 (3-OH)) acid- H$]^-$	$[C_{80}H_{148}N_2O_{19}P]^-$	1472.0425	1472.0419	0.4
$[M_4$ - (C14:0 (3-OH)) acid - (C14:0) ketene - H$]^-$	$[C_{66}H_{122}N_2O_{18}P]^-$	1261.8436	1261.8436	0
$[M_4$ - (C14:0 (3-OH)) acid - (C14:0) acid- H$]^-$	$[C_{66}H_{122}N_2O_{18}P]^-$	1243.8342	1243.8330	0.9
$[M_4$ - (C14:0 (3-OH)) acid - (C14:0(3-O-C14:0)) ketene - H$]^-$	$[C_{52}H_{96}N_2O_{16}P]^-$	1035.6513	1035.6503	0.9
$[M_4$ - (C14:0 (3-OH)) acid - (C14:0(3-O-C14:0)) acid- H$]^-$	$[C_{52}H_{94}N_2O_{15}P]^-$	1017.6409	1017.6397	1.1
$[^{0,4}A_2$ - C14:0(3-O-C14:0) acid - H$]^-$	$[C_{34}H_{61}NO_{11}P]^-$	690.3999	690.3988	1.5
$[B_1$ - C14:0(3-O-C14:0) acid - H$]^-$	$[C_{32}H_{57}NO_9P]^-$	630.3789	630.3776	2.0

HCD-MS/MS of both $[M_1 - 2H]^-$ and $[M_4 - H]^-$ produced product anions at *m/z* 1488.0377, 1472.0425, 1261.8436, 1243.8342, 1035.6513, 1017.6409, 690.3999, and 630.3789 illustrated in **Figure 4-3**, **Scheme 4-2** and **Table 4-2**.

The product anion at *m/z* 1488.0377 was attributed to the loss of a (C14:0) acid group (228.2089 Da) from the branched (C14:0(3-O-C14:0)) fatty acid at O-3' position and assigned as the $[M_4$ - (C14:0 (3-OH)) acid -H$]^-$. The product anion at *m/z* 1472.0425 was assigned as the $[M_4$ - (C14:0 (3-OH)) acid -H$]^-$, formed by the elimination of (C14:0 (3-OH)) acid group (244.2038 Da) attached to the O-3 position of the lipid A disaccharide backbone. The chemical structure of the latter ion at *m/z* 1472.0425 confirmed the presence of (C14:0 (3-OH)) groups.

This latter anion at *m/z* 1472.0425 underwent further fragmentation, losing a (C14:0(3-O-C14:0)) ketene group (438.4073 Da) at the O-3' position, forming the product

anion at *m/z* 1035.6513, assigned as [M_4 - (C14:0 (3-OH)) acid - (C14:0(3-O-C14:0)) ketene - H]$^-$. This was followed by the elimination of H_2O from the hydroxyl groups at O-3' position, forming the secondary product anion at *m/z* 1017.6409, assigned as [M_4 - (C14:0 (3-OH)) acid - (C14:0(3-O-C14:0)) acid- H]$^-$.

Further fragmentation of the anion at *m/z* 1472.0425 involved the elimination of (C14:0) ketene group (212.2140 Da) from (C14:0(3-O-C14:0)) branched in position O-3', resulting in the formation of product anion at *m/z m/z* 1261.8436, assigned as [M_4 - (C14:0 (3-OH)) acid - (C14:0) ketene - H]$^-$. This was followed by the removal of H_2O from the hydroxyl groups from C14:0(3-OH) at O-3' position, forming the secondary product anion at *m/z* 1243.8342, assigned as [M_4 - (C14:0 (3-OH)) acid - (C14:0) acid - H]$^-$. This supported the presence of the branched (C14:0(3-O-C14:0)) group in position O-3'. These fragmentations confirmed the presence of a branched (C14:0(3-O-C14:0)) group.

The product anion at *m/z* 690.3999 generated through cyclic cleavage ($^{0,4}A_2$) at the reducing sugar (561.455 Da) followed by loss of (C14:0(3-O-C14:0)) acid (454.3944 Da) from O-3' position to produce *m/z* 690.3999, which was assigned [$^{0,2}A_2$ - (C14:0(3-O-C14:0)) acid - H]$^-$. Likewise, product anion at *m/z* 630.3789 was assigned as [B_1 - (C14:0(3-O-C14:0)) acid - H]$^-$, formed by glycosidic cleavages of the β-D-Glc*p*N-(1→6)-α-D-Glc*p*N disaccharide backbone leading to the formation of the non-reducing D-Glc*p*N-H_2PO_4 species.

The [M_1 - 2H]$^{2-}$ ion represented a DPLA form of [M_4 - H]$^-$ ion, and by losing a phosphate group, both species shared the same *m/z* values (**Figure 4-3)**. These MS/MS studies support the suggested structural assignment of the [M_4 - H]$^-$ molecule, where the

H_2PO_3 group is located at the O-4' position of the non-reducing end of the disaccharide backbone. The results also confirmed the presence of two the presence of two molecules of 3-hydroxy-myristic acid at positions O-3 and N-2 of the reducing end of the disaccharide backbone. Additionally, the branched (C14:0(3-O-C14:0) and (C14:0(3-O-C12:0) fatty acids were located on the O-3′ and N-2′ positions of the non-reducing end of the β-D-Glc*p*N-(1→6)-α-D-Glc*p*N disaccharide backbone of $[M_4 - H]^-$ lipid A.

4.4.2.2. HCD-MS/MS Analysis of the Lipid As $M_{2\&5}$

The mass spectra contained doubly charged ions, and the corresponding minor singly charged anion at *m/z* 883.5891and 1688.2198, respectively, were assigned as $[M_2 - 2H]^{2-}$ and $[M_5 - H]^-$ were shown in **Figure 4-4 A** and **Figure 4-4 B**, respectively and illustrated in **Scheme 4-3** and **Table 4-3**.

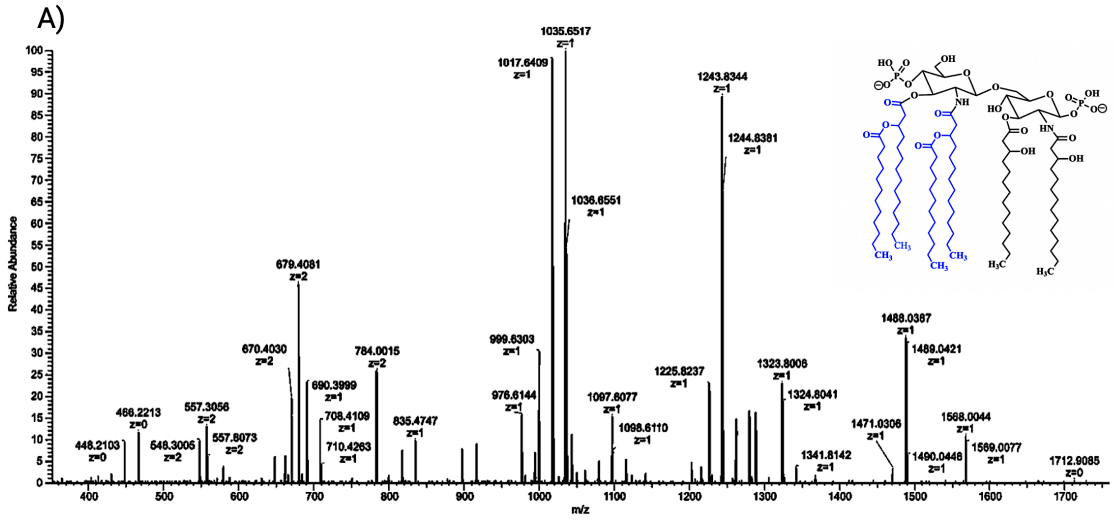

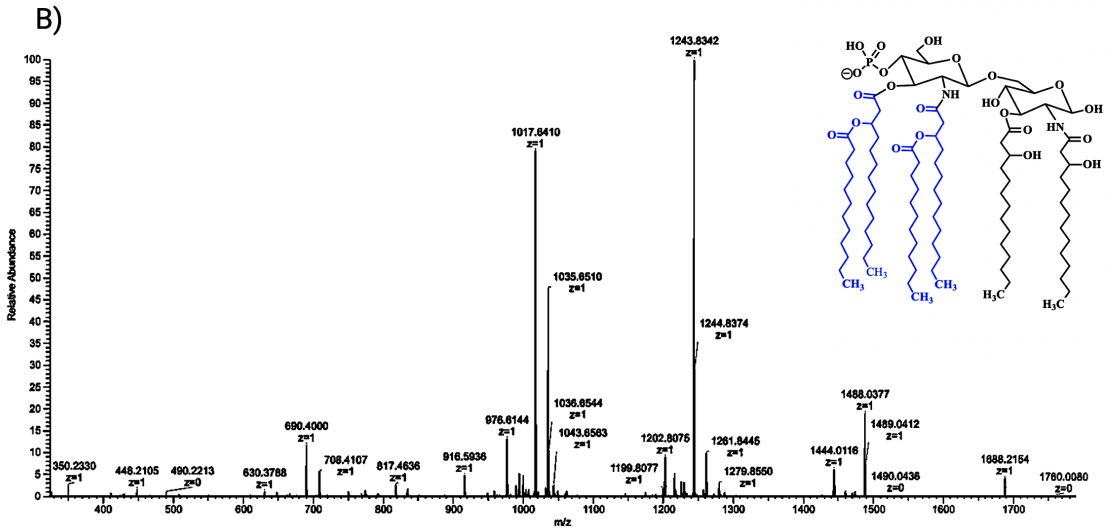

Figure 4-4. HCD-MS/MS of DPLA and MPLA anions extract from *A. hydrophila.* (A) The doubly charged DPLA $[M_2 - 2H]^{2-}$ ion at *m/z* 883.5891 and (B) The singly charged MPLA $[M_5 –H]^-$ ion at *m/z* 1688.2198.

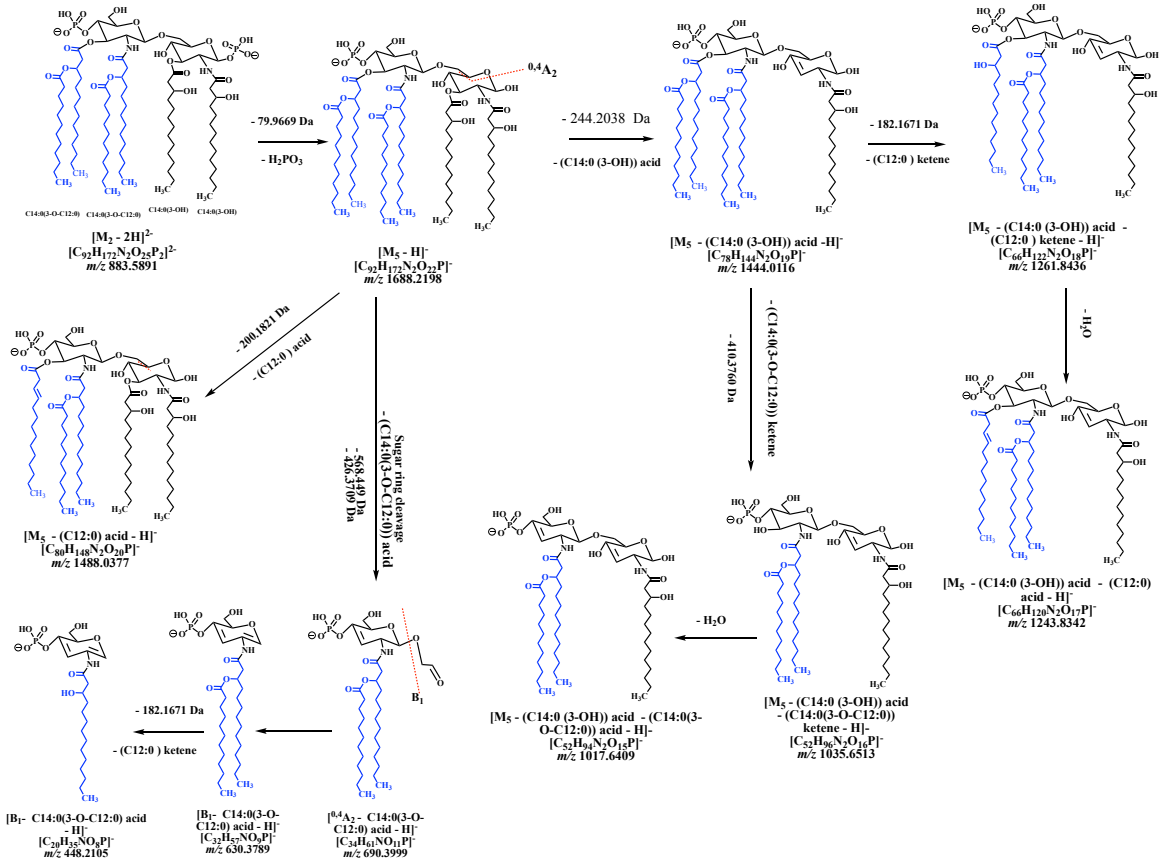

Scheme 4-3. Proposed fragmentation pathways of the selected precursor anions, $[M_2 - 2H]^{2-}$ and $[M_5 - H]^-$ anions at *m/z* 883.5891 and 1688.2198, respectively.

Table 4-3. Assignments of the diagnostic product anions in HCD-MS/MS analysis of $[M_2 - 2H]^{2-}$ and $[M_5 - H]^-$ anions at *m/z* 883.5891 and 1688.2198, respectively.

Diagnostic ion	**Empirical formula**	***m/z* Observed**	***m/z* Calculated**	***m/z* Error (ppm)**
$[M_5$ - (C12:0) acid -H$]^-$	$[C_{80}H_{148}N_2O_{20}P]^-$	1488.0377	1488.0369	0.5
$[M_5$- (C14:0(3-OH)) acid - H$]^-$	$[C_{78}H_{144}N_2O_{19}P]^-$	1444.0116	1444.0106	0.6
$[M_5$ - (C14:0(3-OH)) acid - (C12:0) ketene - H$]^-$	$[C_{66}H_{122}N_2O_{18}P]^-$	1261.8445	1261.8436	0.7
$[M_5$ - (C14:0(3-OH)) acid - (C12:0) acid - H$]^-$	$[C_{66}H_{120}N_2O_{17}P]^-$	1243.8342	1243.8330	0.9
$[M_5$ - (C14:0(3-OH)) acid - (C14:0(3-O-C12:0)) ketene - H$]^-$	$[C_{52}H_{96}N_2O_{16}P]^-$	1035.6510	1035.6503	0.6
$[M_5$ - (C14:0(3-OH)) acid - (C14:0(3-O-C12:0)) acid - H$]^-$	$[C_{52}H_{94}N_2O_{15}P]^-$	1017.6410	1017.6397	1.2
$[^{0,4}A_2$ - C14:0(3-O-C12:0) acid - H$]^-$	$[C_{34}H_{61}NO_{11}P]^-$	690.4000	690.3988	1.7
$[B_1$ - C14:0(3-O-C12:0) acid - H$]^-$	$[C_{32}H_{57}NO_9P]^-$	630.3788	630.3776	1.9
$[B_1$ - C14:0(3-O-C12:0) acid - (C12:0) ketene - H$]^-$	$[C_{20}H_{35}NO_8P]^-$	448.2105	448.2106	- 0.2

HCD-MS/MS of both $[M_2 - 2H]^-$ and $[M_5 - H]^-$ produced product anions at *m/z* 1488.0377, 1444.0116, 1261.8445, 1243.8342, 1035.6510, 1017.6410, 690.4000, 630.3788, and 448.2105 (**Scheme 4-3** and **Table 4-3)**.

The product anion at *m/z* 1488.0377 was identified as $[M_5$ - (C12:0) acid -H$]^-$, formed by the elimination of the (C12:0) acid group (200.1821Da) from the branched (Cl4:0(3-O-12:0)) fatty acid at the O-3' position of the lipid A disaccharide backbone. These product anions supported the presence of the (C12:0) groups attached to the O-3 position of the lipid A disaccharide.

The same product anion at *m/z* 1488.0377 also underwent loss of a (C14:0(3-OH)) acid group (244.2038 Da) located at O-3 position, resulting in the product anion at *m/z* 1444.0116, assigned as $[M_5$ - (C14:0(3-OH)) acid - H$]^-$. Further fragmentation resulted in the elimination of the (C12:0) ketene groups (182.1671 Da), producing the product anion at *m/z* 1261.8445, assigned as $[M_5$ - (C14:0(3-OH)) acid - (C12:0) ketene - H$]^-$. Subsequently, water loss of water from hydroxyl groups at C14:0(3-OH) localized at O-3' position, forming the secondary product anion at *m/z* 1243.8342, assigned as $[M_5$ - (C14:0 (3-OH)) acid - (C12:0) acid - H$]^-$. These fragmentations confirmed the presence of the branched (C14:0(3-O-C12:0)) fatty acid group.

Additionally, the product anion at *m/z* 1444.0116 underwent elimination of a (C14:0(3-O-C12:0)) ketene group (410.3760 Da), resulting in the product anion at *m/z* 1035.6510*,* assigned as $[M_5$ - (C14:0(3-OH)) acid - (C14:0(3-O-C12:0)) ketene - H$]^-$. That was followed by the elimination of the water group from the hydroxyl groups from the O-3' position, creating an anion at *m/z* 1017.6410, assigned as $[M_5$ - (C14:0(3-O-C12:0)) acid - (C14:0(3-OH)) acid - H$]^-$.

The product anions at *m/z* 690.4000 and 448.2105 were generated via glycosidic cleavage of the β-D-Glc*p*N-(1→6)-α-D-Glc*p*N disaccharide backbone, resulting in the non-reducing D-GlcpN-PO_3 species. Cyclic cleavage ($^{0,4}A_2$) at the reducing sugar (568.449 Da) with subsequent loss of a (C14:0(3-O-C12:0)) acid group (426.3709 Da) from O-3' position yielded the ion at*m/z* 690.3999, assigned as [$^{0,2}A_2$ - (C14:0(3-O-C14:0)) acid - H$]^-$. Similarly, product anion at *m/z* 630.3789 was attributed to [B_1 - (C14:0(3-O-C14:0)) acid - H$]^-$, formed through glycosidic cleavage, leading to the formation of the non-

reducing D-Glc*p*N-H_2PO_4 species. Further elimination of a C12:0 ketene group from (C14:0(3'-O-C12:0)) branched at the 3'-O position, produced the anion at *m/z* 448.2105, assigned as $[B_1$ - (C14:0(3-O-C14:0)) acid - (C12:0) ketene - $H]^-$.

The $[M_2 - 2H]^{2-}$ ion represented a di-phosphorylated form of $[M_5 - H]^-$ ion, and by losing a phosphate group, both species shared the same *m/z* values (**Figure 4-4)**. These MS/MS studies support the suggested structural assignment of the $[M_5 - H]^-$ molecule, where the H_2PO_3 group is located at the O-4' position of the non-reducing end of the disaccharide backbone. The results also confirmed the presence of two molecules of 3-hydroxy-myristic acid at positions O-3 and N-2 of the reducing end of the disaccharide backbone. Additionally, the two branched (C14:0(3-O-C12:0) fatty acids were located on the O-3′ and N-2′ positions of the non-reducing end of the β-D-Glc*p*N-(1→6)-α-D-Glc*p*N disaccharide backbone of $[M_5 - H]^-$ lipid A.

4.4.2.3. HCD-MS/MS Analysis of the Lipid As $M_{3\&6}$

The mass spectra contained a doubly charged ion and the corresponding minor ion for the singly charged species at *m/z* 792.5054 and 1506.0510, respectively. These ions were assigned as the $[M_3 - 2H]^{2-}$ and $[M_6 - H]^-$ and were shown in **Figure 4-5 A** and **Figure 4-5 B**, respectively. Illustrated in **Scheme 4-4** and **Table 4-4**.

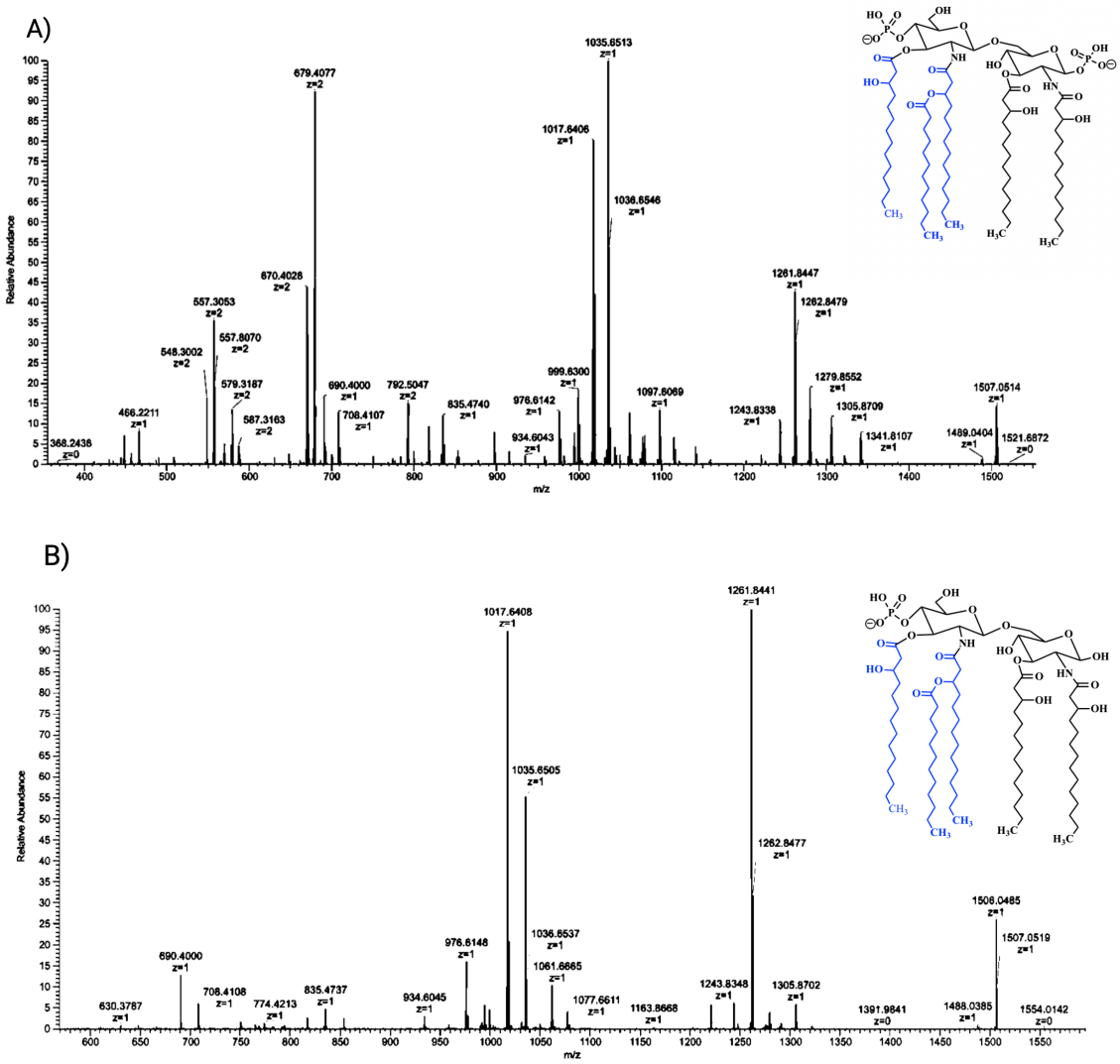

Figure 4-5. HCD-MS/MS of DPLA and MPLA anions extract from *A. hydrophila* (A) The doubly charged DPLA $[M_3 - 2H]^{2-}$ ion at *m/z* 792.5054 and (B) The singly charged MPLA $[M_6 - H]^-$ ion at *m/z* 1506.0510.

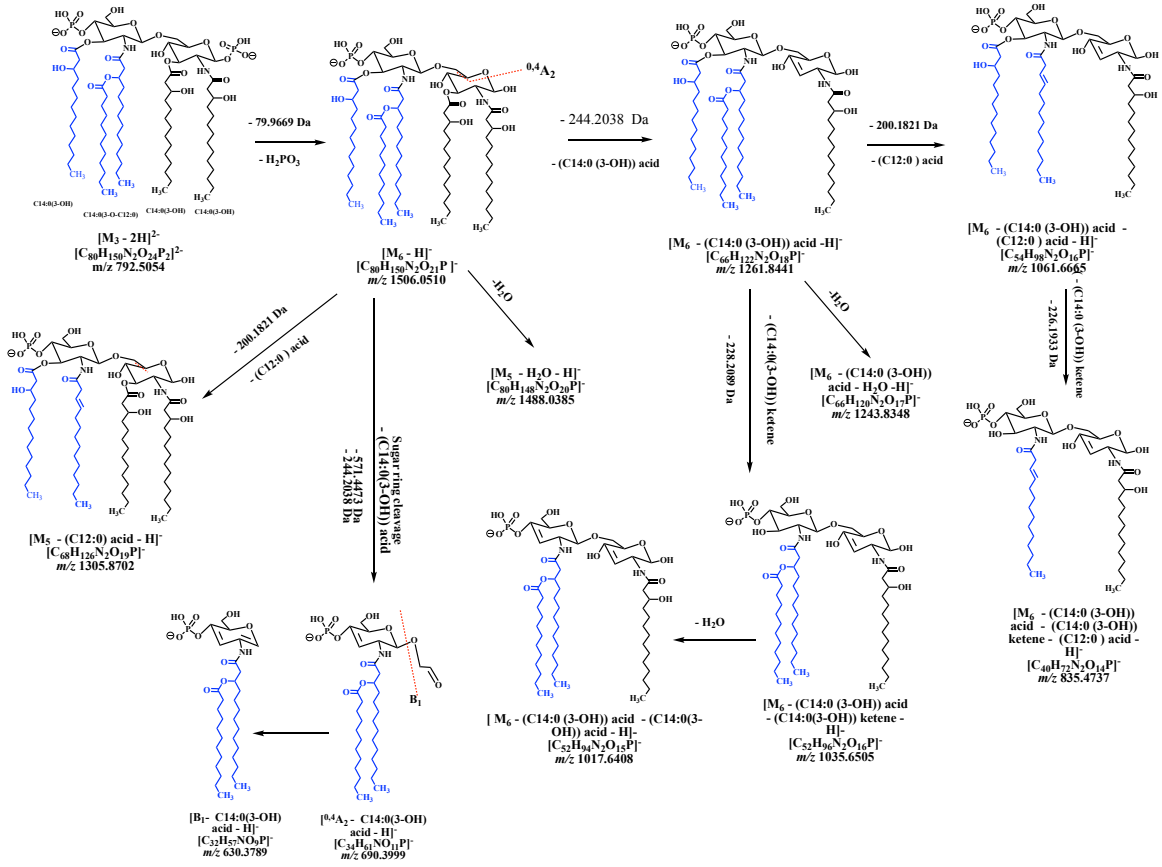

Scheme 4-4. Proposed fragmentation pathways of the selected precursor anions, $[M_3 - 2H]^{2-}$ and $[M_6 - H]^-$ anions at *m/z* 792.5054 and 1506.0510, respectively.

Table 4-4. Assignments of the diagnostic product anions in HCD-MS/MS analysis of the $[M_3 - 2H]^{2-}$ and $[M_6 - H]^-$ anions at *m/z* 792.5054, 1506.0510.

Diagnostic ion	Empirical formula	*m/z* Observed	*m/z* Calculated	*m/z* Error (ppm)
$[M_6 - H_2O - H]^-$	$[C_{80}H_{148}N_2O_{20}P]^-$	1488.0385	1488.0369	1.0
$[M_6 - (C12:0)$ acid $- H]^-$	$[C_{68}H_{126}N_2O_{19}P]^-$	1305.8702	1305.8698	0.3
$[M_6 - (C14:0$ (3-OH)) acid $- H]^-$	$[C_{66}H_{122}N_2O_{18}P]^-$	1261.8441	1261.8436	0.3
$[M_6 - (C14:0$ (3-OH)) acid $- H_2O - H]^-$	$[C_{66}H_{120}N_2O_{17}P]^-$	1243.8348	1243.8330	1.4
$[M_6 - (C14:0$ (3-OH)) acid - (C12:0) acid $- H]^-$	$[C_{54}H_{98}N_2O_{16}P]^-$	1061.6665	1061.6659	0.5
$[M_6 - (C14:0$ (3-OH)) acid- (C14:0 (3-OH)) ketene) $- H]^-$	$[C_{52}H_{96}N_2O_{16}P]^-$	1035.6505	1035.6503	0.1
$[M_6 - (C14:0$ (3-OH)) acid- (C14:0 (3-OH)) ketene $- H_2O - H]^-$	$[C_{52}H_{94}N_2O_{15}P]^-$	1017.6408	1017.6397	1.0

$[^{0,4}A_2$ - C14:0(3-OH) acid - H]$^-$	$[C_{34}H_{61}NO_{11}P]^-$	690.4000	690.3988	1.7
$[B_1$ - C14:0(3-OH) acid - H]$^-$	$[C_{32}H_{57}NO_9P]^-$	630.3788	630.3776	- 1.9
$[M_6$ - (C14:0 (3-OH)) acid - (C14:0 (3-OH)) ketene - (C12:0) acid - H]$^-$	$[C_{40}H_{72}N_2O_{14}P]^-$	835.4737	835.4727	1.1

HCD-MS/MS of both $[M_3 - 2H]^-$ and $[M_6 - H]^-$ created product anions at *m/* 1488.0385, 1305.8702, 1261.8441, 1243.8348, 1061.6665, 1035.6505, 1017.6408, 690.4000, 630.3788, and 835.4737 (**Scheme 4-4** and **Table 4-4)**.

The product anion at *m/z* 1488.0385 was assigned as $[M_6 - H_2O - H]^-$, formed by eliminating a water molecule from the hydroxyl group located at the O-3 position of the lipid A disaccharide backbone. The product anion at *m/z* 1305.8702 was identified as $[M_6$ - (C12:0) acid -H]$^-$, resulting from the loss of the (C12:0) acid group (200.1821 Da) from the branched (Cl4:0(3-O-12:0)) fatty acid at the N-2' position. This confirmed the attachment of a (C12:0) acid.

The product anion at *m/z* 1261.8441 was assigned as $[M_6$ - (C14:0(3-OH)) acid - H]$^-$, which was formed by the elimination of a (C14:0(3-OH)) acid group (244 Da) located at O-3 position. This anion underwent further fragmentation, resulting in the loss of a hydroxyl group from (C14:0(3-OH)) located at O-3', generating the product anion at*m/z* 1243.8348, identified as $[M_6$ - (C14:0(3-OH)) acid - H_2O - H]$^-$. Additionally, the ion at *m/z* 1261.8441 underwent further fragmentation, eliminating the (C14:0(3-OH)) ketene group (228.089 Da), to produce the product anion at *m/z* 1035.6510, assigned as $[M_6$ - (C14:0(3-OH)) acid - (C14:0(3-OH)) ketene - H]$^-$. That also was followed by the elimination of the hydroxyl group from the O-3' position to produce anion at *m/z* 1017.6410, which was

assigned as $[M_6$ - (C14:0(3-OH)) acid - (C14:0(3'-OH)) acid - $H]^-$. These fragmentations validated the presence of a (C14:0(3-OH)) acid group.

Another fragmentation pathway of anion at *m/z* 1261.8441 involved the loss of the (C12:0) acid group (200.1821 Da) from the branched (Cl4:0(3-O-12:0)) fatty acid at the N-2' position, producing the product anion at *m/z* 1061.6665, assigned as $[M_6$ - (C14:0(3-OH)) acid - (C12:0) acid - $H]^-$. That was followed by the elimination of the (C14:0(3-OH)) ketene group (226.1933 Da) located at O-3' to produce anion at *m/z* 835.4737, assigned as $[M_6$ - (C14:0(3-OH)) acid - (C14:0(3-OH)) ketene - (C12:0) acid - $H]^-$.

The product anion at *m/z* 690.4000 was formed by glycosidic cleavage of the β-D-Glc*p*N-(1→6)-α-D-Glc*p*N disaccharide backbone, resulting in the non-reducing D-GlcpN-PO_3 species. This cleavage involved a cyclic cleavage ($^{0,4}A_2$) at the reducing sugar (571.4473 Da) followed by the loss of (C14:0(3-OH)) acid group (255.2038 Da) from O-3' position to produce *m/z* 690.3999, which was assigned $[^{0,2}A_2$ - (C14:0(3-OH)) acid - $H]^-$. Likewise, product anion at *m/z* 630.3789 was assigned as $[B_1$ - (C14:0(3-OH)) acid - $H]^-$, formed through glycosidic cleavage of the β-D-Glc*p*N-(1→6)-α-D-Glc*p*N disaccharide backbone leading to the formation of the non-reducing D-Glc*p*N-H_2PO_4 species.

The $[M_3 - 2H]^{2-}$ ion represented a di-phosphorylated form of $[M_6 - H]^-$ ion, and by losing a phosphate group, both species shared the same *m/z* values (**Figure 4-5)**. These MS/MS studies support the suggested structural assignment of the $[M_6 - H]^-$ molecule, where the H_2PO_3 group is located at the O-4' position of the non-reducing end of the disaccharide backbone. The results also confirmed the presence of three molecules of 3-hydroxy-myristic acid at positions O-3, N-2 and O-3' of the disaccharide backbone.

Additionally, one branched (C14:0(3-O-C12:0) fatty acid was located on the N-2′ position of the non-reducing end of the β-D-Glc*p*N-(1→6)-α-D-Glc*p*N disaccharide backbone of $[M_6 - H]^-$ lipid A.

4.4.3. Separation of Lipid A Aggregate Dimers and/or Adducts by FAIMS

One of the challenges in lipid analysis by ESI-MS is the ability of lipids to form aggregates that add more complexity to the profile spectrum and data interpretation [43]. The extent of lipid aggregation usually depends on their chemical structures, concentration and the ESI-MS solvent composition. In this work, although triethyl ammonium acetate buffer (TEAA) was added to the ESI solvent to disaggregate any expected Lipid A micelles [44], several dimers of MPLA were detected as doubly charged ions in the CV range of 23-43 volts **(Figure 4-6)**. It should be noted that further studies are needed in the future to investigate the effect of concentration and ESI-MS solvent composition on the formation of these Lipid A aggregates.

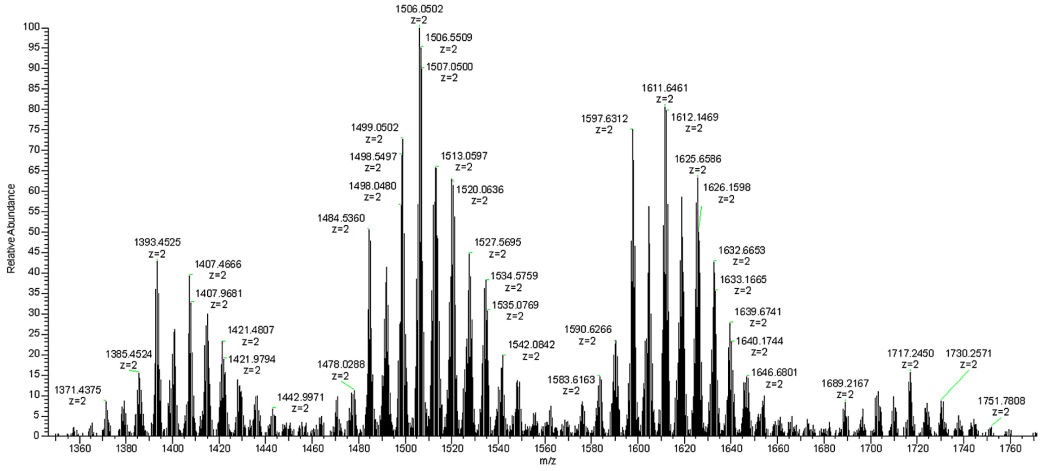

Figure 4-6. Negative ion ESI-FAIMS-Orbitrap-MS spectra of the native lipid A extract from *A. hydrophila* with CV = 28 forming adduct of singly charged ions.

The FAIMS successfully separated these MPLA dimers from their corresponding monomeric MPLA, thus avoiding intermixing between this Lipid A species and complicating the MS and MS/MS analysis and/or interpretation. For example, the doubly charged ion at *m/z* 1506.05 (Z = -2) detected in the CV range of 23-43 V was expected to be composed of two MPLA monomeric ions that were detected at *m/z* 1506.05 (Z = -1) in the lower CV range (0-23 V). However, MS/MS of this doubly charged dimeric lipid A **(Figure 4-7)** revealed that it is a mixture of at least four isomeric Lipid A dimers: two penta-acylated MPLA (2x 1506.05/2 = 1506.05) $[2M_6 - 2H]^{2-}$, hexa-tetra acylated lipid A (1732.24+1279.86/2 = 1506.05), hexa-tetra acylated lipid A (1688.22 + 1323.88/2= 1506.5), hepta-tri acylated Lipid A (1914.41 +1097.68/2 = 1506.05). This clearly indicates the complexity of the composition of these adduct ions. The ability of the FAIMS to isolate such kind of complicated adducts from monomeric MPLA or DPLA greatly facilitated the analysis and avoided complicated MS/MS spectrum if both monomeric and dimeric MPLA of identical *m/z* value and different charge states were fragmented together. Additionally, FAIMS gas phase fractionation allowed the Kendrick analyses of each faction separately and avoided complications from these adduct formations in the data interpretation.

The doubly charged nature of this adduct was due to the presence of two phosphates on two different Lipid A molecules, which facilitated the binding and charge sharing between the ions [45]. The resulting adducts appeared as a distinct peak in the mass spectrum, reflecting the transition from singly charged to doubly charged species. It should be noted that several types of biologically relevant lipids are known to form aggregates/micelles/bilayers in the aqueous environment of the human body. Thus, the

study of these kinds of lipid A aggregates may provide insight into how lipid A may aggregate in real biological systems.

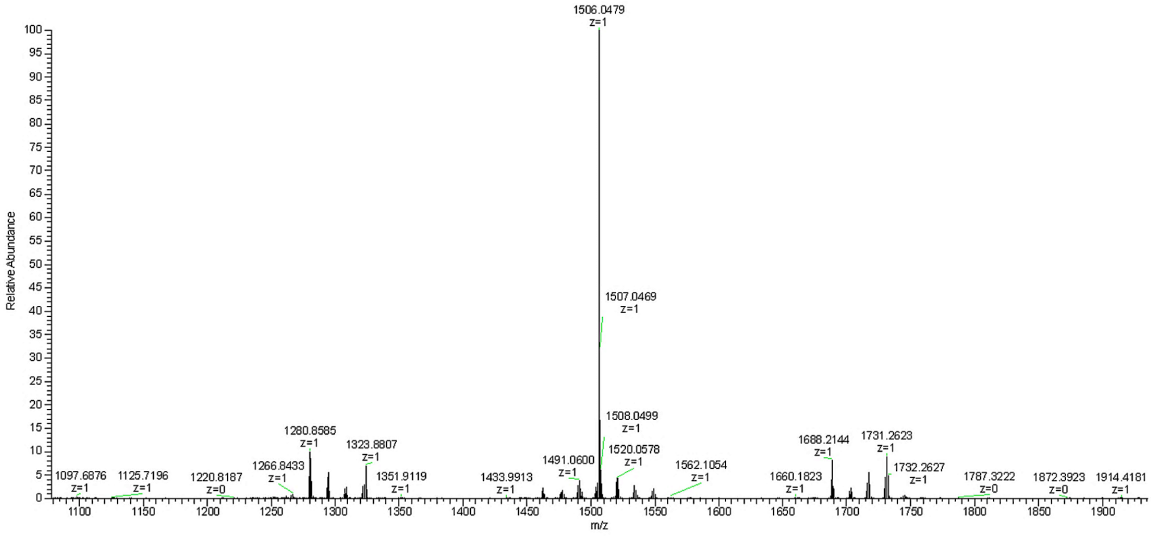

Figure 4-7. HCD-MS/MS of doubly charged adduct anion at *m/z* 1506.05 showing at least four possible dimeric Lipid A with the same *m/z* value (isomers).

4.4.4. Kendrick Analysis of Lipid A Fractions Separated by FAIMS

4.4.4.1. Kendrick Analysis of DPLA Anions

To better understand the complexity of the analyzed Lipid A mixture, we performed analysis using the non-deconvoluted mass list. The Kendrick analysis of the DPLA doubly charged anions detected from CV 44 to 60 was performed using a fractional base unit of $CH_2/2$ (**Figure 4-8)**. Anions *1,2,* and *3* **(Table 4-1)** were previously characterized using tandem MS, providing a basis for identifying related species. The Kendrick plot (**Figure 4-8)** includes red lines representing anions differing by 14.01 Da, suggesting the presence of unusual Lipid A species with an odd number of carbons.

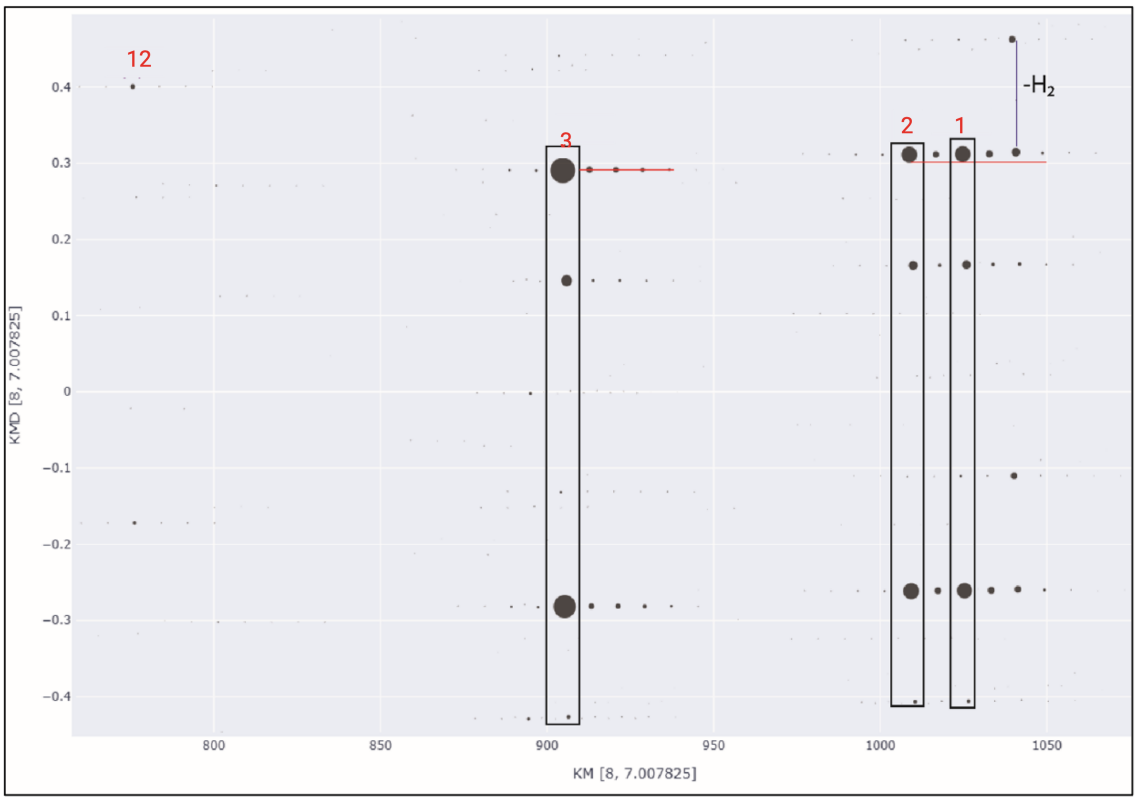

Figure 4-8. Kendrick analysis of DPLA singly charged ions detected from CV 44-60 using CH_2/2 base unit, allowing the vertical expansion of isotopologues.

In the Kendrick Mass Defect plot, isotopologues belonging to the same isotopic envelope tend to align vertically (indicated by ions enclosed in black boxes, **Figure 4-8**). Additionally, vertical differences in the KMD plot by H_2 can show variability in the number of double bonds (**Figure 4-8**). Lastly, low-abundant ions (*12) at m/z* 657.39 (Z = -2) showed the elimination of the C12-OH group (198.162 Da) and C_2H_4 group (28.03 Da) with respect to anion *3*. This shows the usefulness of KMD plot relationships and/or networks in predicting the chemical composition of low-abundant ions that cannot be characterized adequately by tandem mass spectrometry.

4.4.4.2. Kendrick Analysis of MPLA Anions

Further, KMD analysis focused on MPLA anions with a single charge and detected CV= 0 to 22 was performed using a CH_2/5 fractional base unit. The Kendrick plot (**Figure 4-9)** Shows the anions annotated from *5* to *10.* Anions *5* and *6* were previously characterized and studied using tandem MS, which provided more detailed information about their structure (**Table 4-1)**. Anions *5* and *6* anions served as reference points for identifying the related composition of anions without the need to perform and interpret additional tandem MS spectra.

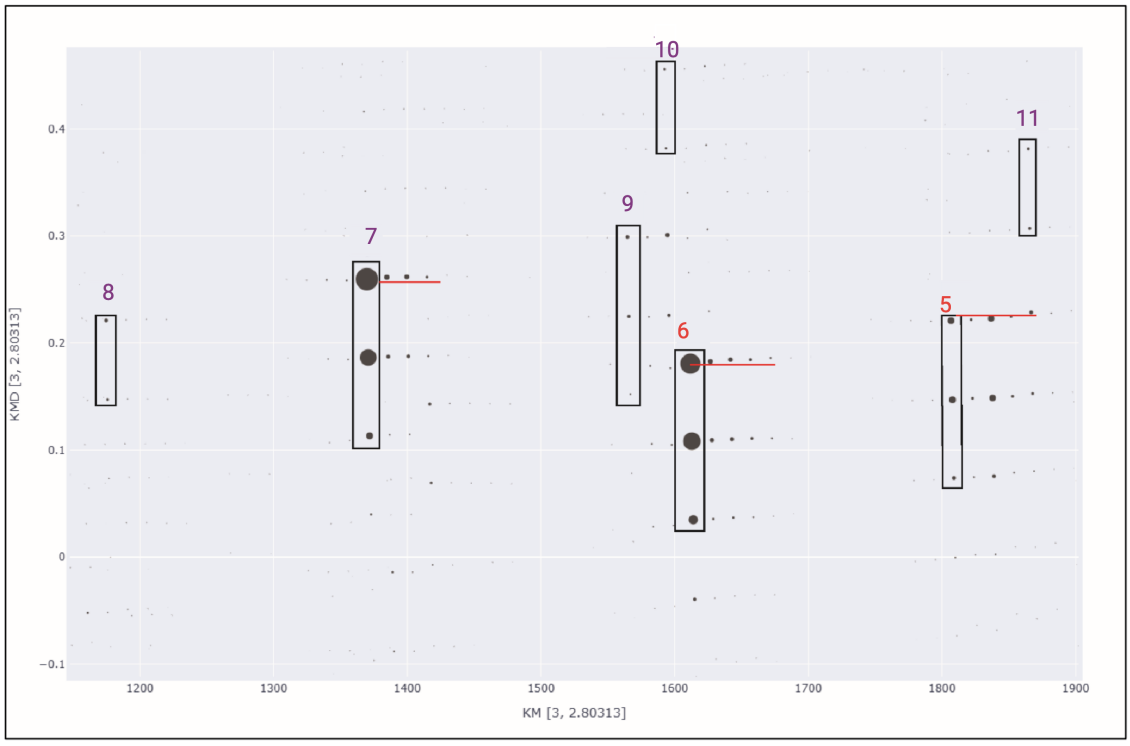

Figure 4-9. Kendrick analysis of MPLA singly charged ions detected from CV 0 to 22 using CH_2/5 base unit.

In the KMD plot, anions with the same chemical composition but differing in the number of CH_2 will have the same KMD and will align on the horizontal line in the KMD plot [28]. The red lines (**Figure 4-9**) connect ions that differ by 14.01565 Da, corresponding to a CH_2 group. Similar to the DPLA fraction, the 14.01565 difference suggests the presence of unusual Lipid A molecules with an odd number of carbons. For example, *anion 6* at *m/z* 1506.0510 is followed by an anion at *m/z* 1520.0601 (1506.0510 + 14.01565), indicating an odd number of carbons in one of the Lipid A acyl chains.

The tandem MS characterized penta-acylated lipid A anion at *m/z* 1506.0510 was found to have an extra 226.1976 Da with respect to Anion *7* at *m/z* 1279.8534, indicating the loss of a C12:0-OH group (198.1620 Da) along with a C_2H_4 group (28.0313 Da). Therefore, Anion *7* at *m/z* 1279.8534 is identified as a tetra-acylated lipid. Additionally, anion *7* was found to have an additional 182.1674 Da with respect to Anion *8 at m/z* 1097.6860, indicating the elimination of the C12:0 group (182.1667 Da). Therefore, Anion *8* is identified as a tri-acylated lipid.

Furthermore, Anion *9* at *m/z* 1462.0201 showed an extra 182.1667 Da with respect to Anion *7*, indicating the addition of the C12:0 group (182.1667 Da). So, Anion *9* is identified as a tetra-acylated lipid. Additionally, anion 10 at *m/z* 1488.0361 was found to have an extra 26.0160 Da with respect to Anion *9*, indicating the addition of the C_2H_4 group (28.0313 Da) and removal of H_2 (2.0157). Finally, anion *11* at *m/z* 1742.2562 was found to have an additional 54.0438 Da with respect to Anion *5*, indicating the addition of two (C_2H_4) groups (2 x 28.0313 Da) and elimination of H_2 (2.0156), thus showing the sequential

mass differences between anions and providing insights into the structural diversity of Lipid A.

In the Kendrick Mass Defect plot, isotopologues belonging to the same isotopic envelope tend to align vertically (indicated by boxes, **Figure 4-9**). These anions share a similar molecular structure but differ in their exact mass due to isotopic substitution. The vertical expansion of isotopologues across the Kendrick plot range (+0.5 to -0.5) facilitated the visualization of these anion relationships, providing a clearer understanding of isotopic patterns and structural similarities.

This Kendrick analysis highlights the series of mass differences between anions, providing important insights into the structural variations within the Lipid A mixture, such as differences in the number of acyl groups and carbon chain lengths.

4.4.4.3. Kendrick Analysis of Lipid A Adducts

Kendrick analysis was also performed on doubly charged Lipid A adducts detected across a compensation voltage range from CV 23 to CV 48. The red lines connect ions horizontally in the Kendrick plot (**Figure 4-10)**, with a difference of 42.04 Da, indicating trimethylation and suggesting the presence of Lipid A species with an odd number of fatty acids as previously determined in DPLA and MPLA factions.

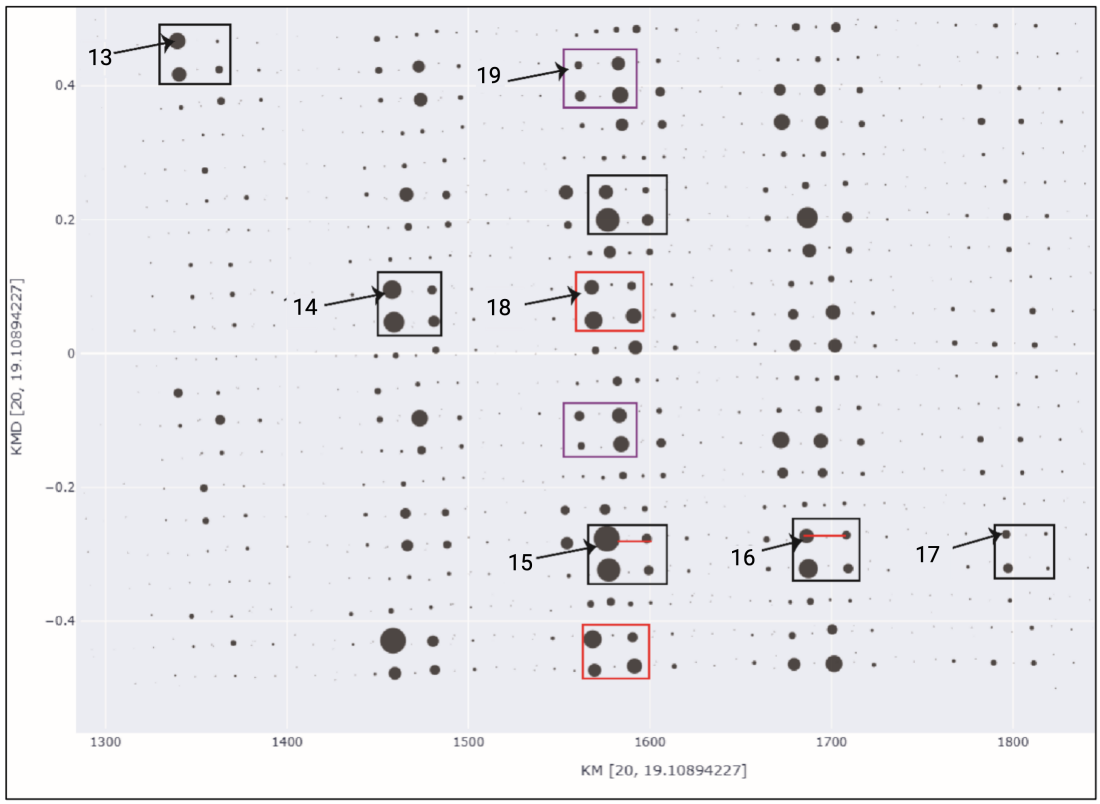

Figure 4-10. Kendrick analysis of lipid A adducts detected in the CV range 23 to 43 using C14:0/11 fractional base unit.

Ion *13* at *m/z* 1279.8531 (z = -2) was identified as a dimer of two tetra-acylated Lipid A molecules (2 x 1279.8531 / 2 = 1279.8531). It should be noted that the monomeric ion at *m/z* 1279.8531 is anion *7* in the KMD plot of the MPLA fraction (2 x anion 7, **Figure 4-10**). Ion *14* at *m/z* 1392.9509 (z = -2) represents a tetra-acylated adducted with a penta-acylated MPLA (1279.8531+ 1506.048/2 = *m/z* 1392.95). Anion *15* at *m/z* 1506.048 (z = -2) corresponds to a mainly penta-acylated Lipid A dimer (2 x 1506.048 / 2 = 1506.048)) as proved by tandem MS (**Figure 4-7**). The relationships between ions 13-15 are an example of structural variations that occur diagonally across the KMD plot.

Anion *16* at *m/z* 1611.1445 (z = -2) is an adduct of a penta-acylated and a hexa-acylated MPLA (1506.048 + 1716.2411/ 2 = 1611.1445). Anion 17 at *m/z* 1716.2411 (z = -2) corresponds to a dimer of two hexa-acylated Lipid A molecules (2 x 1716.2411/ 2 = 1716.2411). The relationships between anions 15-17 exemplify horizontal structural variations across the KMD plots.

Moreover, anion *18* at *m/z* 1498.046 (z = -2) was predicted to have one less oxygen atom with respect to anion *15* (*m/z* 1506.048 (z = -2)), while Anion *19* at *m/z* 1491.0414 (z was predicted to have one less oxygen and CH_2 group with respect to anion 15. Anions *18* and *19* illustrate examples of structural variations that are observed vertically across the KMD plot with respect to anion 15, providing insights into some lipid A modifications involving oxygen and CH_2 units loss **(Figure 4-10**). It should be noted that the divisors for the Lipid A related chemical units (CH_2 and C14:0) used in this Kendrick analysis were selected by trial and error. Different divisors were tested to find the best visual ion arrangements and/or separations, thus facilitating relationship predictions of ions. This opens a way for developing a platform for the Kendrick analysis of such complex biological mixtures that needs lots of manual visualization of ions relationships and the chemical knowledge about the possible structural variations.

4.5. Conclusions and Future Directions

The analysis of the lipid A mixture, conducted using ESI-MS in negative ion mode, revealed a heterogeneous composition of lipid A molecules that bind to polymyxin-coated Affi-Prep. HCD-MS/MS experiments further confirmed the identities of these molecules,

providing detailed insights into their molecular features. The application of FAIMS demonstrated that changes in CV significantly influenced ion formation and adduct generation, aiding the identification of compounds within the lipid A mixture of SJ-26.

This comprehensive MS/MS analysis enabled the precise characterization of lipid A molecules, verifying the presence of DPLA and MPLA forms with distinct fatty acid substitutions, including myristyl-oxy-myristic acid and 3-hydroxy-myristic acid. To further understand the complexity of the lipid A mixture, KMD analysis was performed using the mass list of doubly, singly, and adduct-charged anions from MS^1. This analysis uncovered structural patterns and relationships among the anions in the mixture. KMD plots proved instrumental in classifying and organizing structurally related ions, offering a clearer understanding of lipid A's composition and facilitating a systematic exploration of its molecular diversity.

Structural similarities were observed with lipid A from other strains and families, such as *Aeromonas liquefaciens* SJ-19a [46] and *Yersinia pestis (Yersiniaceae)* [47], respectively. These findings lay the groundwork for investigating the potential immunological responses and functional roles of lipid A in host-pathogen interactions, paving the way for therapeutic development targeting diverse Gram-negative bacterial infections. Understanding the structural diversity of lipid A will contribute to developing improved vaccines and therapeutics targeting these pathogens [48, 49].

Future research will focus on exploring lipid A structures in other species of the *Aeromonadaceae* family, a group known for pathogenic members associated with diseases

in fish, amphibians, reptiles, and humans. These pathogens possess virulence factors such as toxins, hemolysins, and enzymes that facilitate host tissue invasion [50].

Finally, this study demonstrated that high-energy HCD-MS/MS, coupled with FAIMS, is a reproducible and powerful tool for elucidating the structures of lipid molecules. This approach enhances our ability to analyze lipid A and related molecules, providing valuable insights for future studies.

4.6. References

[1] M. Caroff, and D. Karibian, "Structure of bacterial lipopolysaccharides," *Carbohydr. Res.,* vol. 338, no. 23, pp. 2431-2447, Nov, 2003. DOI: https://doi.org/10.1016/j.carres.2003.07.010.

[2] M. Almostafa, T. D. Fridgen, and J. H. Banoub, "Structural investigation by tandem mass spectrometry analysis of a heterogeneous mixture of Lipid A(n) isolated from the lipopolysaccharide of Aeromonas hydrophila SJ-55Ra," *Rapid Commun. Mass Spectrom.,* vol. 32, no. 3, pp. 167-183, Feb, 2018. DOI: https://doi.org/10.1002/rcm.8017.

[3] A. El-Aneed, and J. Banoub, "Elucidation of the molecular structure of lipid A isolated from both a rough mutant and a wild strain of *Aeromonas salmonicida* lipopolysaccharides using electrospray ionization quadrupole time-of-flight tandem mass spectrometry," *Rapid Commun. Mass Spectrom.,* vol. 19, no. 12, pp. 1683-1695, Apr, 2005. DOI: https://doi.org/10.1002/rcm.1971.

[4] G. Larrouy-Maumus, A. Clements, A. Filloux, R. R. McCarthy, and S. Mostowy, "Direct detection of lipid A on intact Gram-negative bacteria by MALDI-TOF mass spectrometry," *J. Microbiol. Methods,* vol. 120, pp. 68-71, Jan, 2016. DOI: https://doi.org/10.1016/j.mimet.2015.12.004.

[5] K. Kawahara, "Variation, modification and engineering of lipid A in endotoxin of Gram-negative bacteria," *Int. J. Mol. Sci.,* vol. 22, no. 5, pp. 1-15, Feb, 2021. DOI: https://doi.org/10.3390/ijms22052281.

[6] F. Di Lorenzo, F. Crisafi, V. La Cono, M. M. Yakimov, A. Molinaro, and A. Silipo, "The structure of the lipid A of Gram-negative cold-adapted bacteria isolated from Antarctic environments," *Mar. Drugs,* vol. 18, no. 12, Nov, 2020. DOI: https://doi.org/10.3390/md18120592.

[7] K. Bush, "Investigational agents for the treatment of Gram-negative bacterial infections: A reality check," *ACS Infect. Dis.,* vol. 1, no. 11, pp. 509-511, Nov, 2015. DOI: https://doi.org/10.1021/acsinfecdis.5b00100.

[8] S. K. Bouchillon, R. E. Badal, D. J. Hoban, and S. P. Hawser, "Antimicrobial susceptibility of inpatient urinary tract isolates of Gram-negative bacilli in the United States: results from the study for monitoring antimicrobial resistance trends (SMART) program: 2009-2011," *Clin. Ther.,* vol. 35, no. 6, pp. 872-877, Jun, 2013. DOI: https://doi.org/10.1016/j.clinthera.2013.03.022.

[9] K. S. Kaye, and J. M. Pogue, "Infections caused by resistant Gram-negative bacteria: epidemiology and management," *Pharmacotherapy,* vol. 35, no. 10, pp. 949-962, Oct, 2015. DOI: https://doi.org/10.1002/phar.1636.

[10] M. Caroff, D. Karibian, J. M. Cavaillon, and N. Haeffner-Cavaillon, "Structural and functional analyses of bacterial lipopolysaccharides," *Microbes Infect.,* vol. 4, no. 9, pp. 915-926, Jul, 2002. DOI: https://doi.org/10.1016/s1286-4579(02)01612-x.

[11] C. M. Crittenden, L. D. Akin, L. J. Morrison, M. S. Trent, and J. S. Brodbelt, "Characterization of lipid A variants by energy-resolved mass spectrometry: Impact of acyl chains," *J. Am. Soc. Mass Spectrom.,* vol. 28, no. 6, pp. 1118-1126, Jun, 2017. DOI: https://doi.org/10.1007/s13361-016-1542-6.

[12] A. Kilar, A. Dornyei, and B. Kocsis, "Structural characterization of bacterial lipopolysaccharides with mass spectrometry and on- and off-line separation techniques," *Mass Spectrom. Rev.,* vol. 32, no. 2, pp. 90-117, Mar-Apr, 2013. DOI: https://doi.org/10.1002/mas.21352.

[13] C. R. Raetz, and C. Whitfield, "Lipopolysaccharide endotoxins," *Annu. Rev. Biochem.,* vol. 71, pp. 635-700, Nov, 2002. DOI: https://doi.org/10.1146/annurev.biochem.71.110601.135414.

[14] A. C. Casabuono, F. Sisti, J. Fernandez, D. Hozbor, and A. S. Couto, "Bordetella bronchiseptica Glycosyltransferase Core Mutants Trigger Changes in Lipid A Structure," *J. Am. Soc. Mass Spectrom.,* vol. 30, no. 9, pp. 1679-1689, Sep, 2019. DOI: https://doi.org/10.1007/s13361-019-02233-3.

[15] C. R. Raetz, "Biochemistry of endotoxins," *Annu. Rev. Biochem.,* vol. 59, pp. 129-170, 1990. DOI: https://doi.org/10.1146/annurev.bi.59.070190.001021.

[16] X. Wang, P. J. Quinn, and A. Yan, “Kdo2 -lipid A: structural diversity and impact on immunopharmacology,” *Biol. Rev. Camb. Philos Soc.,* vol. 90, no. 2, pp. 408-427, May, 2015. DOI: https://doi.org/10.1111/brv.12114.

[17] H. Petrosova, A. Mikhael, S. Culos, A. Giraud-Gatineau, A. M. Gomez, M. E. Sherman, R. K. Ernst, C. E. Cameron, M. Picardeau, and D. R. Goodlett, “Lipid A structural diversity among members of the genus Leptospira,” *Front. Microbiol.,* vol. 14, pp. 1181034, May, 2023. DOI: https://doi.org/10.3389/fmicb.2023.1181034.

[18] A. Mikhael, H. Petrosova, D. Smith, R. K. Ernst, and D. R. Goodlett, “Lipid A double bond position determination using ozone and laser-induced dissociation,” *Rapid Commun. Mass Spectrom.,* vol. 38, no. 16, pp. e9854, Aug, 2024. DOI: https://doi.org/10.1002/rcm.9854.

[19] A. Silipo, and A. Molinaro, "Lipid A structure," *Bacterial lipopolysaccharides*, Springer Vienna, 2011. pp. 1-20.

[20] R. R. Colwell, M. T. Macdonell, and J. De Ley, “Proposal to Recognize the Family *Aeromonadaceae* fam. nov,” *Int. J. Syst. Evol. Microbiol.,* vol. 36, no. 3, pp. 473-477, Jul, 1986. DOI: https://doi.org/10.1099/00207713-36-3-473.

[21] G. Pieretti, S. Carillo, R. Lanzetta, M. Parrilli, S. Merino, J. M. Tomas, and M. M. Corsaro, “Structural determination of the O-specific polysaccharide from Aeromonas hydrophila strain A19 (serogroup O:14) with S-layer,” *Carbohydr. Res.,* vol. 346, no. 15, pp. 2519-2522, Nov, 2011. DOI: https://doi.org/10.1016/j.carres.2011.08.003.

[22] J. H. Banoub, and D. H. Shaw, "Structural investigations on the core oligosaccharide of *Aeromonas hydrophila* (chemotype III) lipopolysaccharide," *Carbohydr. Res.,* vol. 98, no. 1, pp. 93-103, Dec, 1981. DOI: https://doi.org/10.1016/s0008-6215(00)87145-1.

[23] J. H. Banoub, Y. M. Choy, F. Michon, and D. H. Shaw, "Structural investigations on the core oligosaccharide of *Aeromonas hydrophila* (Chemotype II) lipopolysaccharide," *Carbohydr. Res.,* vol. 114, no. 2, pp. 267-276, Apr, 1983. DOI: https://doi.org/10.1016/0008-6215(83)88193-2.

[24] F. Michon, D. H. Shaw, and J. H. Banoub, "Structure of the lipopolysaccharide core isolated from a human strain of *Aeromonas hydrophila*," *Eur. J. Biochem.,* vol. 145, no. 1, pp. 107-114, Nov, 1984. DOI: https://doi.org/10.1111/j.1432-1033.1984.tb08528.x.

[25] J. M. Janda, and S. L. Abbott, "The genus Aeromonas: taxonomy, pathogenicity, and infection," *Clin. Microbiol. Rev.,* vol. 23, no. 1, pp. 35-73, Jan, 2010. DOI: https://doi.org/10.1128/CMR.00039-09.

[26] A. Semwal, A. Kumar, and N. Kumar, "A review on pathogenicity of *Aeromonas hydrophila* and their mitigation through medicinal herbs in aquaculture," *Heliyon,* vol. 9, no. 3, pp. e14088, Mar, 2023. DOI: https://doi.org/10.1016/j.heliyon.2023.e14088.

[27] F. Matyar, A. Kaya, and S. Dinçer, "Distribution and antibacterial drug resistance of *Aeromonas* spp. from fresh and brackish waters in Southern Turkey," *Annals. of*

Microbiol., vol. 57, no. 3, pp. 443-447, Jun, 2007. DOI: https://doi.org/10.1007/bf03175087.

[28] A. Mikhael, D. Hardie, D. Smith, H. Petrosova, R. K. Ernst, and D. R. Goodlett, "Structural elucidation of intact rough-type lipopolysaccharides using field asymmetric ion mobility spectrometry and Kendrick mass defect plots," *Analy. Chem.,* vol. 95, no. 46, pp. 16796–16800, Jul, 2023. DOI: https://doi.org/10.1021/acs.analchem.3c02947.

[29] C. A. Hughey, C. L. Hendrickson, R. P. Rodgers, A. G. Marshall, and K. Qian, "Kendrick mass defect spectrum: a compact visual analysis for ultrahigh-resolution broadband mass spectra," *Anal. Chem.,* vol. 73, no. 19, pp. 4676-4681, Oct, 2001. DOI: https://doi.org/10.1021/ac010560w.

[30] G. Gaiffe, R. B. Cole, A. Sonnette, N. Floch, and M. C. Bridoux, "Identification of postblast residues by DART-high resolution mass spectrometry combined with multivariate statistical analysis of the Kendrick mass defect," *Anal. Chem.,* vol. 91, no. 13, pp. 8093-8100, Jul, 2019. DOI: https://doi.org/10.1021/acs.analchem.9b00137.

[31] X. Ortiz, K. J. Jobst, E. J. Reiner, S. M. Backus, K. M. Peru, D. W. McMartin, G. O'Sullivan, V. Y. Taguchi, and J. V. Headley, "Characterization of naphthenic acids by gas chromatography-Fourier transform ion cyclotron resonance mass spectrometry," *Anal. Chem.,* vol. 86, no. 15, pp. 7666-7673, Aug, 2014. DOI: https://doi.org/10.1021/ac501549p.

[32] M. W. Alton, H. J. Stark, M. R. Canagaratna, and E. C. Browne, “Generalized Kendrick analysis for improved visualization of atmospheric mass spectral data,” *Atmos. Meas. Tech.,* vol. 16, no. 12, pp. 3273-3282, Dec, 2023. DOI: https://doi.org/10.5194/amt-16-3273-2023.

[33] T. R. Rosa, G. S. Folli, W. L. S. Pacheco, M. P. Castro, W. Romao, and P. R. Filgueiras, “DropMS: Petroleomics data treatment based in a web server for high-resolution mass spectrometry,” *J. Am. Soc. Mass Spectrom.,* vol. 31, no. 7, pp. 1483-1490, Jul, 2020. DOI: https://doi.org/10.1021/jasms.0c00109.

[34] T. Fouquet, and H. Sato, “Improving the resolution of Kendrick mass defect analysis for polymer ions with fractional base units,” *Mass Spectrom.,* vol. 6, no. 1, pp. A0055, Feb, 2017. DOI: https://doi.org/10.5702/massspectrometry.A0055.

[35] R. Guevremont, G. Thekkadath, and C. K. Hilton, “Compensation voltage (CV) peak shapes using a domed FAIMS with the inner electrode translated to various longitudinal positions,” *J. Am. Soc. Mass Spectrom.,* vol. 16, no. 6, pp. 948-956, Jun, 2005. DOI: https://doi.org/10.1016/j.jasms.2005.03.001.

[36] M. A. Ewing, M. S. Glover, and D. E. Clemmer, “Hybrid ion mobility and mass spectrometry as a separation tool,” *J. Chromatogr. A,* vol. 1439, pp. 3-25, Mar, 2016. DOI: https://doi.org/10.1016/j.chroma.2015.10.080.

[37] J. C. Tsang, C. S. Wang, and P. Alaupovic, “Degradative effect of phenol on endotoxin and lipopolysaccharide preparations from *Serratia marcescens*,” *J. Bacteriol.,* vol. 117, no. 2, pp. 786-795, Feb, 1974. 10.1128/jb.117.2.786-795.1974.

[38] S. Okuda, M. Sato, H. Uchiyama, and H. Takahashi, “Degradation of lipopolysaccharide of *Escherichia Coli* by a hot phenol extraction,” *J. Gen. Appl. Microbiol.,* vol. 21, no. 3, pp. 169-184, 1975. DOI: https://doi.org/10.2323/jgam.21.169.

[39] C. Dass, *Fundamentals of contemporary mass spectrometry*, 1 ed., Wiley-Interscience, 2007.

[40] P. J. Amorim Madeira, and M. Helena, "Applications of tandem mass spectrometry: From structural analysis to fundamental studies," InTech, 2012. pp. 2-33.

[41] B. Domon, and C. E. Costello, “A systematic nomenclature for carbohydrate fragmentations in FAB-MS/MS spectra of glycoconjugates,” *Glycoconjugate J.,* vol. 5, no. 4, pp. 397-409, Aug, 1988. DOI: https://doi.org/10.1007/BF01049915.

[42] L. J. Morrison, W. R. Parker, D. D. Holden, J. C. Henderson, J. M. Boll, M. S. Trent, and J. S. Brodbelt, “UVliPiD: A UVPD-based hierarchical approach for de novo characterization of Lipid A structures,” *Anal. Chem.,* vol. 88, no. 3, pp. 1812-1820, Feb, 2016. DOI: https://doi.org/10.1021/acs.analchem.5b04098.

[43] K. Yang, and X. Han, “Accurate quantification of lipid species by electrospray ionization mass spectrometry — meets a key challenge in lipidomics,” *Metabolites,* vol. 1, no. 1, pp. 21-40, 2011. DOI: https://doi.org/10.3390/metabo1010021.

[44] A. Apffel, J. A. Chakel, S. Fischer, K. Lichtenwalter, and W. S. Hancock, “analysis of oligonucleotides by HPLC-electrospray ionization mass spectrometry,” *Anal. Chem.,* vol. 69, no. 7, pp. 1320-1325, Apr, 1997. DOI: https://doi.org/10.1021/ac960916h.

[45] A. Steimle, I. B. Autenrieth, and J. S. Frick, "Structure and function: Lipid A modifications in commensals and pathogens," *Int. J Med. Microbiol.,* vol. 306, no. 5, pp. 290-301, Aug, 2016. DOI: https://doi.org/10.1016/j.ijmm.2016.03.001.

[46] M. Almostafa, B. Allehyane, S. Egli, C. Bottaro, T. D. Fridgen, and J. Banoub, "Tandem mass spectrometry determination of the putative structure of a heterogeneous mixture of Lipid As isolated from the lipopolysaccharide of the Gram-negative bacteria *Aeromonas liquefaciens* SJ-19a," *Rapid Commun. Mass Spectrom.,* vol. 30, no. 8, pp. 1043-1058, Apr, 2016. DOI: https://doi.org/10.1002/rcm.7540.

[47] J. W. Jones, I. E. Cohen, F. Turecek, D. R. Goodlett, and R. K. Ernst, "Comprehensive structure characterization of lipid A extracted from Yersinia pestis for determination of its phosphorylation configuration," *J. Am. Soc. Mass Spectrom.,* vol. 21, no. 5, pp. 785-799, May, 2010. DOI: https://doi.org/10.1016/j.jasms.2010.01.008.

[48] M. Matsuura, "Structural modifications of bacterial lipopolysaccharide that facilitate Gram-negative bacteria evasion of host innate immunity," *Front. Immunol.,* vol. 4, pp. 109, May, 2013. DOI: https://doi.org/10.3389/fimmu.2013.00109.

[49] Y. Torres-Corral, A. Girons, O. Gonzalez-Barreiro, R. Seoane, A. Riaza, and Y. Santos, "Effect of bivalent Vaccines against *Vibrio anguillarum* and *Aeromonas salmonicida* Subspecie achromogenes on health and survival of Turbot," *Vaccines*

(Basel), vol. 9, no. 8, pp. 906, Aug, 2021. DOI: https://doi.org/10.3390/vaccines9080906.

[50] A. N. Schuetz, "Emerging agents of gastroenteritis: *Aeromonas, Plesiomonas, and the diarrheagenic* pathotypes of Escherichia coli," *Semin Diagn. Pathol.,* vol. 36, no. 3, pp. 187-192, May, 2019. DOI: https://doi.org/10.1053/j.semdp.2019.04.012.

Chapter 5 Structural Elucidation of a Novel Unique Mixture Of Lipid As Obtained from the Phenol-Phase Soluble Lipopolysaccharide Of *Vibrio Anguillarum Serovar SJ-41*

This Chapter is reproduced with permission from Trevena N. Abanoub Mikhael, David R. Goodlett, Travis Fridgen, and Joseph Banoub. This research is currently submitted for publication in the journal Rapid Commun. Mass Spectrom.

5.1. Abstract

In this study, we investigated a unique lipid A derived from the phenol-phase soluble lipopolysaccharide (LPS) of *Vibrio anguillarum* serovar SJ-41, a virulent marine and freshwater pathogen. In order to elucidate the lipid A molecular structure, we have used electrospray ionization with field asymmetric wave ion mobility-Orbitrap mass spectrometry (ESI-FAIMS-MS). The conventional ESI- FAIMS- spectrum indicated that the obtained lipid A consisted of a heterogeneous mixture of compounds. Tandem mass spectrometry using high collision dissociation tandem mass spectrometry (HCD-MS/MS) allowed us to propose the chemical structure of this heterogeneous lipid A mixture. Kendrick Mass Defect (KMD) architecture of lipid A of *V. anguillarum* strain SJ-41 from the *Vibrionaceae family*. Structural analysis revealed significant deviations from conventional lipid A, including the presence of a phospho-glycerol moiety at the O-1

anomeric position of the lipid A glucosamine-reducing end. As far as we know, this is the first report of lipid A structures substituted with the phospho-glycerol D-glucosamine at the O-1). Kendrick plots were employed to further classify structurally diverse lipid A molecules. These findings provide new insights into the lipid A composition of *V. anguillarum* strain SJ-41 and underscore the need for further studies to explore its biological implications, potentially reshaping our understanding of lipid A and its role in host-pathogen interactions.

5.2. Introduction

The family Vibrionaceae comprises seven genera of Gram-negative bacteria, including *Vibrio*, *Photobacterium*, *Allomonas*, *Listonella*, *Enhydrobacter*, *Allomonanas*, *Salinivibrio*, and *Enterovibrio*, with the genus Vibrio containing the largest number of species [1]. Species of the genus Vibrio are widespread in coastal ecosystems and are ubiquitous in marine, estuarine, and freshwater environments worldwide [1-3]. There are 48 recognized species in the genus *Vibrio*, ten of which are known human pathogens [1]. *Vibrio anguillarum* is highly pathogenic to both freshwater and saltwater fish, causing hemorrhagic septicemia vibriosis, which leads to significant losses in aquaculture [4-6]. As a result, aquaculture has increasingly relied on vaccination for disease control [7]. Although various immunization methods have been explored and *Vibrio* vaccines have shown success, most vaccine production has focused on crude empirical approaches, with limited attention to the antigenic properties of *Vibrio* cells at the molecular level their high antigenic variability [6, 8-12].

Some *Vibrio* species exhibit multiple lifestyles, including a free-swimming planktonic state and attachment to zooplankton, shellfish, and fish [13]. *V. anguillarum* strains consist of a variety of serotypes, making them superficially indistinguishable from *Aeromonas* [14]. Gram-negative bacteria are usually surrounded by a three-layer envelope formed by the inner membrane (IM), also known as the cytoplasmic membrane, a thin layer of peptidoglycan (PG), and an outer membrane (OM). The OM is an asymmetric bilayer, with phospholipids populating the inner leaflet and lipopolysaccharide (LPSs) predominating in the outer leaflet, known as "Endotoxin." These LPSs are assembled by *O*-specific polysaccharides, core oligosaccharides and lipid A [6, 15-17].

It is widely expected that lipid A is essential for the viability of the Gram-negative bacteria, although the O-antigen and the core oligosaccharide are always expendable. Some exceptions to this rule are species with a dual membrane system but naturally lack lipid A, such as *Sphingomona*s *spp*. and *Treponema pallidum* [18-21]. A growing number of novel lipid A variants have been structurally characterized due to advancements in extraction, purification, and GC- and LC of hard and soft MS ionization techniques, along with significant improvements in mass spectrometric instrumentation. Many bacterial species have lipid A structures substituted with diverse fatty acid chain lengths and linkages at N-2, O-3, N-2', and O-3' positions of β-D-Glc*p*N-(1→ 6)-α-D- Glc*p*N disaccharides. In some bacteria, lipid A contains a single type of 3-hydroxy fatty acid, while in others, ester- and amide-linked acyl chains differ in length [21-24].

Lipid A plays a crucial role in bacterial bioactivity, including its interaction with and activation of immune system receptors, which is highly dependent on its primary

structure. There are numerous structural variations of lipid A across different Gram-negative bacterial species [21]. Lipid A is essential for bacterial viability and is responsible for the endotoxic properties of LPS. It acts as a potent stimulator of the innate immune system through toll-like receptor 4 (TLR4), often leading to a range of biological effects, from enhancing resistance to infection to triggering uncontrolled immune responses, such as sepsis or septic shock [24-28]. In many species, the presence of O-1- and O-4'-phosphate groups of lipids A increases susceptibility to cationic antimicrobial peptides (CAMPs) [29].

Over the past few decades, significant effort has been made to elucidate the molecular structure of LPS in *V. anguillaru*m, focusing primarily on the specificities of *O*-antigenic determinants across various serotypes. However, the structural components of lipid A have remained undefined [6, 15-17].

In this investigation, we have used ESI-FAIMS coupled to an orbitrap mass spectrometer and benefited from the high collision dissociation tandem mass spectrometry (HCD-MS/MS) to propose and confirm the putative molecular and chemical structures of this heterogenous lipid A mixture.

Furthermore, we have availed of the KMD plots, which have proven to be tools for classifying and visualizing structurally related ions within complex heterogeneous mixtures [30-35]. These plots rely on aligning ions with similar structural features into distinct patterns, enabling systematic categorization. Structurally related ions align along horizontal lines (KMD families), allowing their relationships to be readily interpreted. The identification of a single anion within a KMD family through tandem mass spectrometry (MS/MS) facilitates the characterization of all ions within the series. This significantly

reduces the number of spectra required for comprehensive structural analysis, making KMD plots particularly effective for the structural elucidation of the profiling of lipid A molecules [30].

This work showcases the benefits of FAIMS and KMD plots in characterizing *V. anguillarum* SJ-41. These findings aim to enhance the understanding of novel lipid A structures within this important pathogen and their potential impact on immunogenicity.

5.3. Materials and Methods

5.3.1. Bacterial Culture

The original strain of *V. anguillarum* was isolated from sockeye salmon. It was kindly supplied by Dr. T. P. Evelyn (Department of Fisheries and Oceans, Nanaimo, British Columbia, Canada). This strain was added to the Northwest Atlantic Fisheries Center, St. John's collection as (SJ-41). The cultures were grown to medium-to-late stationary phase in Trypticase Soy Broth without added glucose (Baltimore Biological Laboratories Inc.) for approximately 20 hours at 25 °C with aeration at 20 L/min in a New Brunswick MF-128S fermenter. They were then killed by the addition of 0.3% formalin with continuous agitation for 16 hours at room temperature. Cells were subsequently collected by centrifugation at 44,720 ×g in a Sorvall SS-34 rotor, washed with 0.15 M NaCl, lyophilized, and stored at -50 °C until required.

5.3.2. Purification of the Lipopolysaccharides

LPS was extracted using the hot-phenol method and subsequently freeze-dried. Stored cells (10 g) were suspended in 175 mL of deionized water and heated to 70 °C [36]. An equal volume of 90% heated phenol was added, followed by 20 minutes of stirring at 70 °C. After cooling on ice, the mixture was centrifuged at 1370 ×g in a Sorvall SS-34 rotor. The phenol layer was isolated, and the extraction was repeated twice. The combined phenol layers were dialyzed, reduced under vacuum, and centrifuged at 169,570 ×g for 3 hours. The resulting LPS pellet was resuspended in water, centrifuged twice more, and lyophilized. LPS was further purified with polymyxin-coated Affi-Prep beads, suspended in PBS (pH 7.4), washed with 0.1 M NaOH, and incubated overnight with agitation at 251 ×g . After centrifugation at 698 ×g for 10 minutes, the supernatant was collected, and the supernatants were combined, dialyzed, and lyophilized.

5.3.3. Hydrolysis of the Lipopolysaccharides

LPS (100 mg) was hydrolyzed with 1% acetic acid for 90 minutes at 100 °C. The hydrolysate was then centrifuged at 1,790 ×g for 30 minutes, resulting in the precipitation of lipid A, while the polysaccharide remained in the aqueous phase. The lipid A was carefully removed and subsequently washed with water.

5.3.4. ESI- FAIMS-MS, HCD-MS/MS, and Kendrick Mass Defect Plot

Negative ion mode ESI-MS was performed on an Orbitrap Fusion™ Lumos™ Tribrid™ Mass Spectrometer with a FAIMS pro interface (Thermo Scientific, Waltham,

MA, USA)[30]. The lipid A mixture of the Gram-negative bacteria A. *Vibrio anguillarum serovar* SJ-41 was dissolved in chloroform: methanol: water: triethyl ammonium acetate (TEAA, pH =7) (1:1:0.02:0.002) at a concentration of 1 μg/μL and directly infused into the ESI- FAIMS source at a flow rate of 3 μL/min. The spray voltage was set to 2.5 kV, capillary temperature to 275 °C, and sheath and auxiliary gas to 2 a.u. The FAIMS separation was accomplished with the following settings: inner electrode temperature = 100 °C, outer electrode temperature = 100 °C, FAIMS N_2 carrier gas flow = 1.2 L/min, asymmetric waveform with dispersion voltages (DV) = +5000 V. Compensation voltages (CV) were scanned from 30 to 80 V with a step size of one volt at 120 K resolution, 250 – 2000 *m/z* range, 60% RF lens, 100% normalized automatic gain control (AGC) target, and 100 ms Maximum injection time (IT). Tandem MS was performed at specific CVs that maximize the signal-to-noise ratio (S/N) of selected doubly charged precursor ions. Stepped high-energy collision-induced dissociation (HCD) with three normalized HCD energies from the 30-50% range was used for tandem MS. Data were recalibrated using RecalOffline 4.1.2 using the palmitate background ion (theoretical *m/z* 281.23295) and visualized using Freestyle software 1.8 SP1 (Thermo Scientific). Tandem MS interpretation was done manually using ChemDraw Prime (version 23.1.1.3). The mass list of the detected doubly charged (500-1500 *m/z*) was exported and used for Kendrick analysis. The Kendrick mass defect (KMD) plots were visualized on the constellation website (https://constellation.chemie.hu-berlin.de/). A fractional KMD base unit of $CH_2/2$ (14.01565/2= 7.007825) with a ceiling rounding function (i.e. 7.007825 was rounded up to

a nominal of 8.000000). A fractional base unit was used to enhance the separation of related isotopologues and facilitate the visualization of structural relationships [37].

5.4. Results and Discussion

Lipid A consists of a disaccharide composed of two glucosamine sugars linked by a β-D-(1→6) linkage, in which the fatty acid chains normally acetylated at the O-3 and N-2 of the non-reducing end and O-3', N-2'. It also can contain a phosphate group at C-1 and C-4' of this disaccharide. The Kdo core sugar is attached to OH-6' [38]. Lipid A structures differ in their number of fatty acid substitutions, chain length, and types of modifications. Additionally, the lipid A disaccharide substitutions at the O-1 and O-4' positions contribute to its structural diversity. Despite extensive research, many lipid A structures remain uncharacterized [21, 39].

In this study, we characterized the lipid A structure obtained from the hydrolysis of phenol-soluble LPS of *Vibrio anguillarum* serovar SJ-41 strain using negative ion mode ESI-FAIMS-MS and HCD-MS/MS, revealing a spectrum indicative of a complex heterogeneous mixture (**Figure 5-1)**.

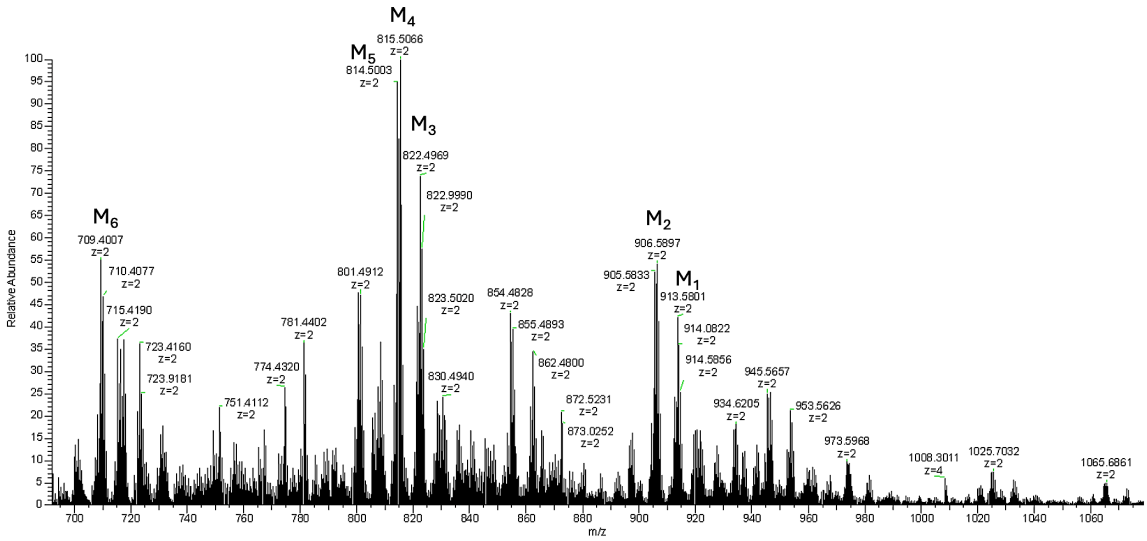

Figure 5-1. Average ESI-FAIMS-MS (CV=30 TO CV=80) of the lipid As mixture extracted from the *V.anguillarum serovar* SJ-41.

This present study of lipid A benefited from the charge-based anions separation offered by FAIMS. Using FAIMS enhances the detection of multi-charged ions usually suppressed by the singly charged ones [30]. This allowed the detection of various doubly charged ions, mainly in the 700-1000 *m/z* range.

We have chosen *inter alia* only six doubly charged deprotonated anions $[M_n - 2H]^{2-}$ (where n = 1-6) from this micro-heterogenic mixture for a follow-up accomplished by HCD tandem MS/MS analysis. The molecular structures and compositions of these six doubly protonated molecules are shown in (**Figures 5-1 and 5-2)**. The assignment of this series of doubly charged anions is indicated in **Table 5-1**.

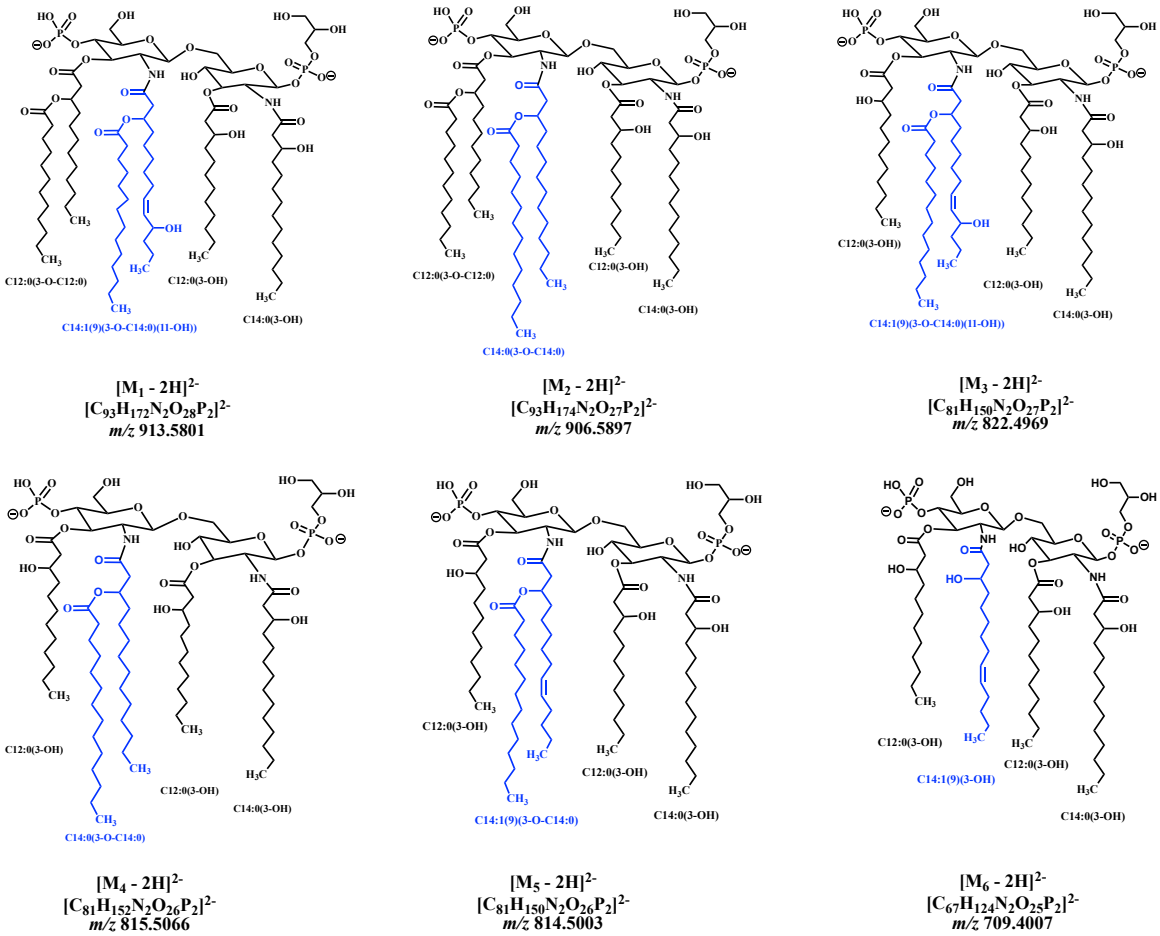

Figure 5-2. Schematic representation of suggested structures of the molecular anions of the lipid As mixture extracted from the *Vibrio anguillarum serovar* SJ-41.

To establish the chemical structures of this series of $[M_n - 2H]^{2-}$ precursor anions, we have calculated the degree of unsaturation (DU). The calculated DU was a convincing and valuable tool in determining lipid A molecular structures of the SJ-41 strain, deducing confirmatory proof of structure determination by mass spectrometry. It provided a numerical value corresponding to a molecule's number of multiple bonds (double or triple) or rings. The degree of unsaturation was calculated depending on the following equation:(1

+ [2C – H + N + (3 x P)] / 2), in which C, H, N., and P, are the exact numbers of atoms in the precursor ion (**Table 5-1**) [40, 41].

Table 5-1. Assignments of the deprotonated lipid As molecules observed in ESI-MS analysis extracted from the *V. anguillarum serovar* SJ-41.

Ion numbers for Kendrick analysis[a]	Diagnostic ion	Empirical formula	*m/z* Observed	*m/z* Calculated	*m/z* Error (ppm)	DU[b]
1	$[M_1 - 2H]^{2-}$	$[C_{93}H_{172}N_2O_{28}P_2]^{2-}$	913.5801	913.5792	- 0.98	11
2	$[M_2 - 2H]^{2-}$	$[C_{93}H_{174}N_2O_{27}P_2]^{2-}$	906.5897	906.5894	- 0.33	10
3	$[M_3 - 2H]^{2-}$	$[C_{81}H_{150}N_2O_{27}P_2]^{2-}$	822.4969	822.4956	+1.58	10
4	$[M_4 - 2H]^{2-}$	$[C_{81}H_{152}N_2O_{26}P_2]^{2-}$	815.5066	815.5060	+0.73	9
5	$[M_5 - 2H]^{2-}$	$[C_{81}H_{150}N_2O_{26}P_2]^{2-}$	814.5003	814.4982	+2.57	10
6	$[M_6 - 2H]^{2-}$	$[C_{67}H_{124}N_2O_{25}P_2]^{2-}$	709.4007	1418.7979/2= 709.3989	+2.53	9

[a]Simplified ion numbers 1-6 will be used later in the Kendrick mass defect analysis.
[b]The degree of unsaturation (DU) is a calculation that determines the total number of rings and π bonds.

It was proposed that all these lipid As contained di-phosphorylated acylated located at the O-1 anomeric position reducing end and O-4' of the non-reducing end of these series of D-glucosamine disaccharide backbones, with one glycerol phosphate group at the O-1 position, as shown in (**Figures 5-2)**. To our knowledge, this is the first report of lipid A structures that was ever reported that contain phospho-glycerol at the O-1 anomeric position of the glucosamine-reducing end of this series M_1-M_6 molecules.

The proposed structures of these series of lipids were established by performing HCD-MS/MS analysis of their respective deprotonated molecules. We elucidate the MS/MS fragmentation in the following sections.

5.4.1.1. HCD-MS/MS of the Precursor Anion $[M_1 - 2H]^{-2}$ *at m/z* 913.5801

HCD-MS/MS of the precursor anion *1* at *m/z* 913.5801, which was assigned as the doubly charged deprotonated anion having a formula $[C_{93}H_{172}N_2O_{28}P_2]^{2-}$, which corresponded to a neutral molecular mass of 1829.1728 Da, as shown in the **Figures 5-3**.

In **Figures 5-3 B,** the low mass region of the spectrum highlighted a consistent of peak at *m/z* 171, corresponding to the assigned phospho-glycerol region, corresponding to its location on the O-1 position of the disscacharide glucosamine backbone. This peak appeared uniformly across all different precursor ions in the MS/MS spectrum and fragmentation routes of the main backbone of the acylated β-D-Glc*p*N-(1→6)-α-D-Glc*p*N disaccharide. Since this peak is identical across the different spectra, it was omitted from further figures to avoid redundancy.

A)

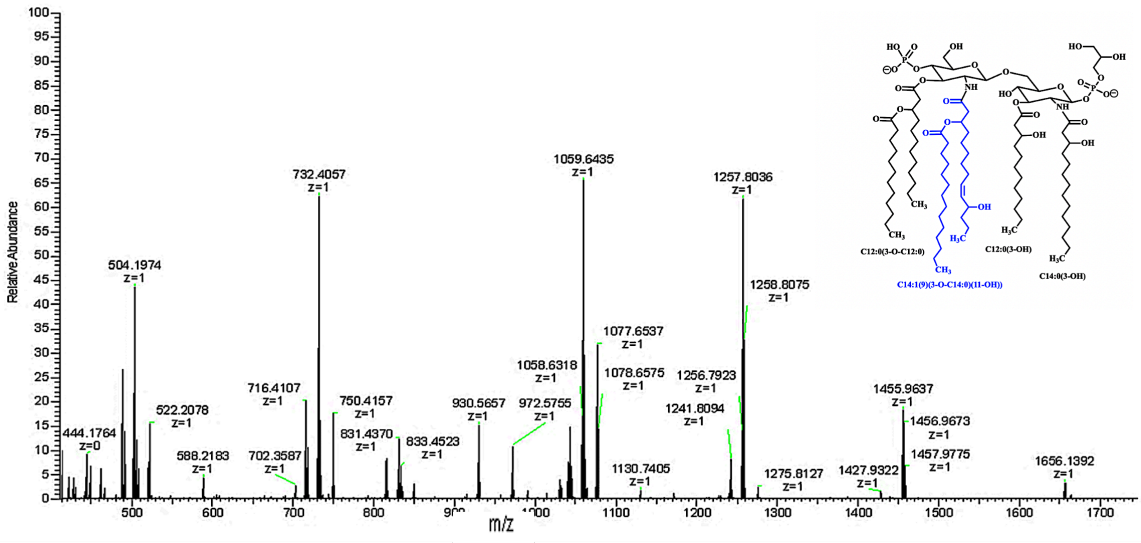

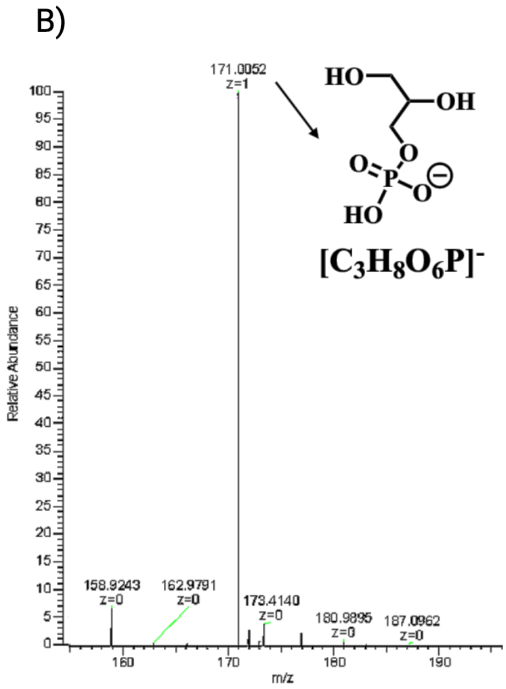

Figure 5-3. HCD-MS/MS of lipid A $[M_1 - 2H]^{2-}$ anion at *m/z* 913.5801extract from *V. anguillarum* serovar SJ-41 with B) The low mass region at *m/z* 171.0052, indicating the presence of glycerol phosphate moiety.

The HCD-MS/MS analysis of the precursor anion $[M_1 - 2H]^{-2}$ anion at *m/z* 913.5801 produced inter alia a series of singly charged product ions observed at *m/z* values of 1656.1392, 1455.9637, 1257.8036, 1059.6435, 972.5755, 930.5657, 831.4370, 732.4057, 588.2183, 504.1974, 444.1764, and 171.0052. These fragmentation routes were detailed in **Scheme 5-1 and Table 5-2**.

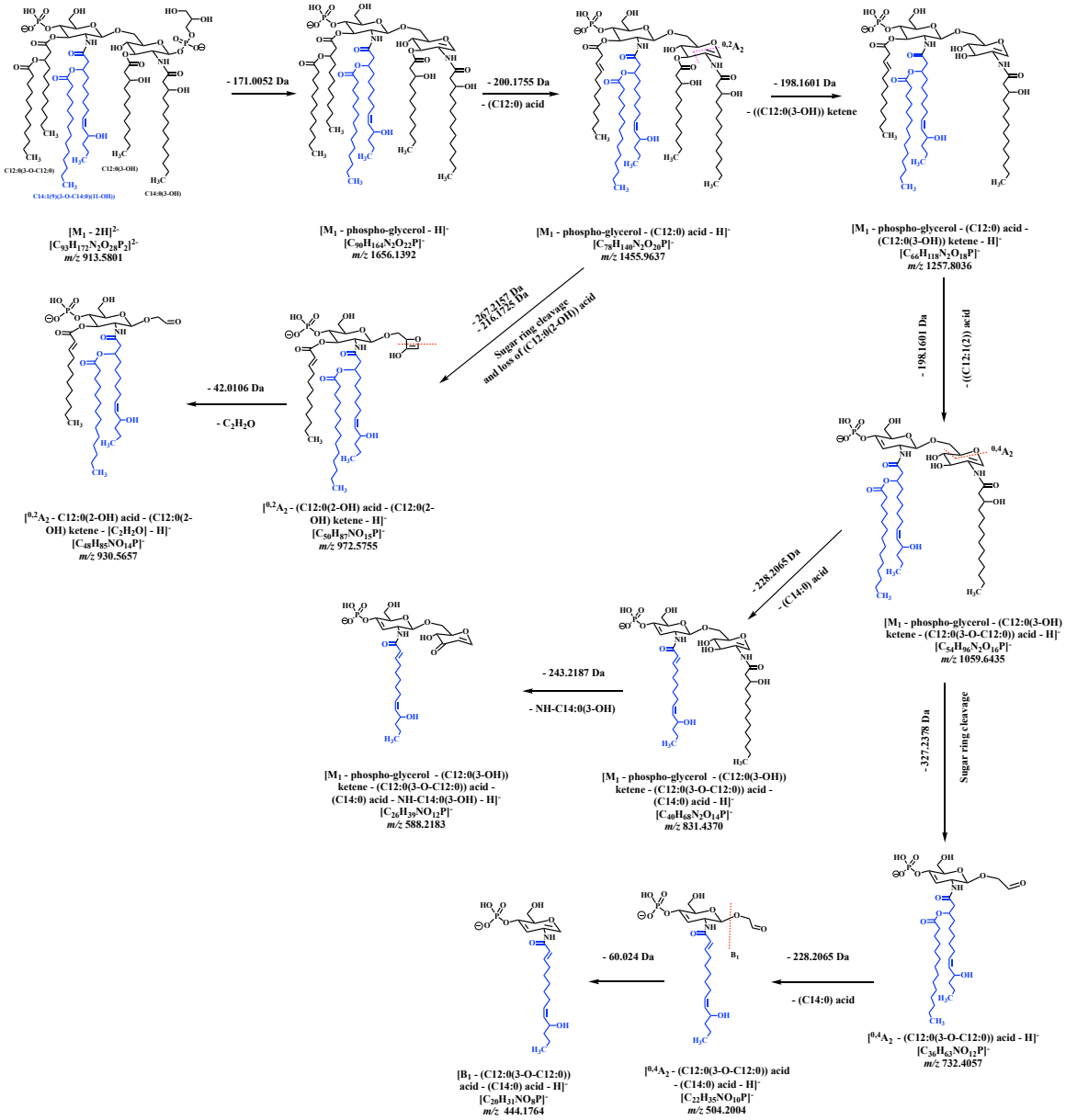

Scheme 5-1. Proposed fragmentation pathways of the selected precursor anion $[M_1 - 2H]^{2-}$ at *m/z* 913.5801 in HCD-MS/MS analysis.

Table 5-2. The assignments of the diagnostic product ions in HCD-MS/MS analysis of the $[M_1 - 2H]^{2-}$ anion at *m/z* 913.5801.

Diagnostic ion	Empirical formula	*m/z* Observed	*m/z* Calculated	*m/z* Error (ppm)
$[M_1$ - phospho-glycerol - $H]^-$	$[C_{90}H_{164}N_2O_{22}P]^-$	1656.1392	1656.1519	-7.6
$[M_1$ - phospho-glycerol - (C12:0) acid - $H]^-$	$[C_{78}H_{140}N_2O_{20}P]^-$	1455.9637	1455.9743	-7.2
$[M_1$ - phospho-glycerol - (C12:0) acid - (C12:0(2-OH)) ketene - $H]^-$	$[C_{66}H_{118}N_2O_{18}P]^-$	1257.8036	1257.8123	-6.9
$[M_1$ - phospho-glycerol - (C12:0(3-OH)) ketene - (C12:0(3-O-C12:0)) acid- $H]^-$	$[C_{54}H_{96}N_2O_{16}P]^-$	1059.6435	1059.6503	-6.4
$[^{0,2}A_2$ - (C12:0(3-O-C12:0)) acid- (C12:0(3-O-C12:0)) ketene - $H]^-$	$[C_{50}H_{87}NO_{15}P]^-$	972.5755	972.5819	-6.5
$[^{0,2}A_2$ - (C12:0(3-O-C12:0)) acid- (C12:0(3-O-C12:0)) ketene -$[C_2H_2O]$ - $H]^-$	$[C_{48}H_{85}NO_{14}P]^-$	930.5657	930.5713	-6.0
$[M_1$ - phospho-glycerol - (C12:0(3-OH)) ketene - (C12:0(3-O-C12:0)) acid - (C14:0) acid - $H]^-$	$[C_{40}H_{68}N_2O_{14}P]^-$	831.437	831.4414	-5.2
$[^{0,4}A_2$ - (C12:0(3-O-C12:0)) acid - $H]^-$	$[C_{36}H_{63}NO_{12}P]^-$	732.4057	732.4093	-4.9
$[M_1$ - phospho-glycerol - (C12:0(3-OH)) ketene - (C12:0(3-O-C12:0)) acid - (C14:0) acid - NH-C14:0(3-OH) - $H]^-$	$[C_{26}H_{39}NO_{12}P]^-$	588.2183	588.2215	-5.4
$[^{0,4}A_2$ - (C12:0(3-O-C12:0)) acid - (C14:0) acid - $H]^-$	$[C_{22}H_{35}NO_{10}P]^-$	504.1974	504.2004	-5.9
$[B_1$ - (C12:0(3-O-C12:0)) acid - (C14:0) acid - $H]^-$	$[C_{20}H_{31}NO_8P]^-$	444.1764	444.1793	-6.5
phospho-glycerol group	$[C_3H_8O_6P]^-$	171.0052	171.0064	-7.0

The first product anion at *m/z* 1656.1392 was formed by losing a phospho-glycerol group (171.0064 Da) from the O-1 position of the lipid A disaccharide anion. This loss resulted in the ion being assigned as $[M_1$ - phospho-glycerol - $H]^-$. The subsequent loss of a (C12:0) acid (200.1755 Da) located at the O-3' position generated the product anion at *m/z* 1455.9637, assigned as $[M_1$ - phospho-glycerol - (C12:0) acid - $H]^-$. Further fragmentation of this ion involved cyclic cleavage ($^{0,2}A_2$) at the reducing sugar (267.2157

Da) followed by loss of (C12:0(3-OH)) acid (216.1725 Da) from O-3 position to produce *m/z* 972.5755, which was assigned [$^{0,2}A_2$ - (C12:0(3-OH)) acid - (C12:0(3-OH)) ketene - H]$^-$. A secondary cyclic cleavage (42.0106 Da) led to the formation of an anion at *m/z* 930.5657, which was designated as [$^{0,2}A_2$ - (C12:0(3-OH)) acid - (C12:0(3-OH)) ketene - [C_2H_2O] - H]$^-$.

Additional fragmentation of the anion at *m/z* 1455.9637 included the loss of a (C12:0(3-OH)) ketene (198.1601 Da) located at O-3 position to produce *m/z* 1257.8036 anions, which was assigned as [M_1 - phospho-glycerol - (C12:0) acid - (C12:0(3-OH)) ketene - H]$^-$. The subsequent elimination of (C12:1(2)) acid (198.1601 Da) at O-3' position, resulting in the formation of a product anion at *m/z* 1059.6435, designated as [M_1 - phospho-glycerol - (C12:0(3-OH) ketene - (C12:0(3-O-C12:0)) acid- H]$^-$. Further loss of a (C14:0) acid located at the N-2' position generated a product anion at *m/z* 831.4370, which was denoted as [M_1 - phospho-glycerol - (C12:0(3-OH) ketene - (C12:0(3-O-C12:0)) acid - (C14:0) acid - H]$^-$. The removal of an (NH-C14:0(3-OH)) group (243.2187 Da) from the reducing sugar part at the N-2 position generated the at *m/z* 588.2183, which was assigned as [phospho-glycerol - (C12:0(3-OH) ketene - (C12:0(3-O-C12:0)) acid - (C14:0) acid - NH-C14:0(3-OH) - H]$^-$.

The anion at *m/z* 1059.6435 also underwent sugar ring cleavage ($^{0,4}A_2$) of the reducing sugar part (327.2378 Da) position to form anion at *m/z* 732.4057, which was assigned as [$^{0,4}A_2$ - (C12:0(3-O-C12:0)) acid - H]$^-$. Further elimination of a (C14:0) acid (228.2065 Da) from the branched fatty acid located at the N-2' position of this latter anion led to the formation of anion at *m/z* 504.1974, which was assigned as [$^{0,4}A_2$ - (C12:0(3-O-

C12:0)) acid - (C14:0) acid - H]$^-$. Glycosidic cleavage of the β-D-Glc*p*N-(1→6)-α-D-Glc*p*N disaccharide backbone produced anion at *m/z* 444.1764, which was assigned as [B_1 (C12:0(3-O-C12:0)) acid - (C14:0) acid - H]$^-$. The chemical structure of the latter ion at *m/z* 444.1764 clearly confirms the presence of the dihydroxy C14:1 fatty acid.

From the HCD-MS/MS fragmentation routes, we speculated that the doubly charged anion, [M_1 - 2H]$^{2-}$ at *m/z* 913.5801 (DU = 11), was attributed as a deprotonated lipid of a hexa-acylated β-D-Glc*p*N-(1→6)-α-D-Glc*p*N disaccharide, where the N-2 and O-3 free positions of the reducing sugar were substituted with 3-hydroxy-myristic acid (C14:0(3-OH)) and 3-hydroxy-lauric acid (C12:0(3-OH), respectively. Additionally, the N-2' and O-3'-free positions of the non-reducing sugar were substituted with 11-hydroxy myristoic acid-3-oxy-lauryl group (C14:1(9)) (3-O-C14:0((11-OH)) and lauric acid-3-oxy-lauroyl group (C12:0(3-O-C12:0)), respectively. It should be noted that the two hydroxyl groups on myristoleic acid were putatively added to carbon 3 and carbon 11. Similarly, lauryl hydroxyl group can be either on C-2 or C-3. Further studies are needed to confirm the positions of double bonds and hydroxyl groups in all proposed structures described in this manuscript.

5.4.1.2. HCD-MS/MS of the Precursor Anion [M_2 - 2H]$^{-2}$ *at m/z* 906.5897

HCD-MS/MS of the precursor ion *2* at *m/z* 906.5897 has a formula [$C_{93}H_{174}N_2O_{29}P_2$]$^{-2}$, was attributed to a neutral molecular mass of 1815.1936 Da, as shown in the **Figures 5-4**.

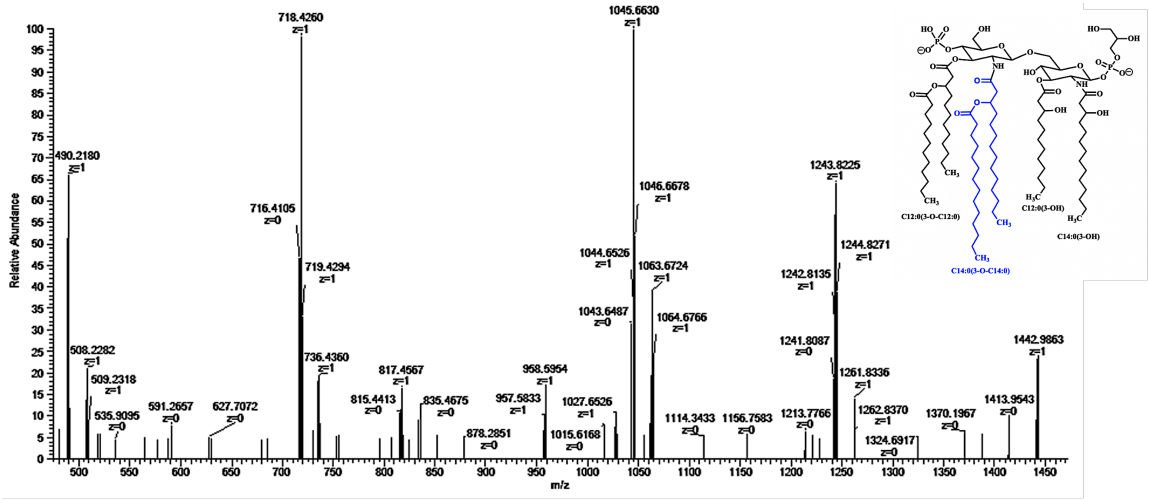

Figure 5-4. HCD-MS/MS of lipid A $[M_2 - 2H]^{2-}$ anion at *m/z* 906.5897 extract from *V. anguillarum serovar SJ*-41.

Proposed fragmentation pathways of the selected doubly charged precursor ion in HCD-MS/MS analysis of the $[M_2 - 2H]^{2-}$ at *m/z* 906.5897, which produced a series of singly charged product ions observed at *m/z* values of 1642.1722, 1441.9863, 1243.8225, 1045.663, 958.5954, 835.4675, 736.436, 718.4301, 591.2657, 490.2179, and 430.197, as shown in **Scheme 5-2** and detailed in **Table 5-3**.

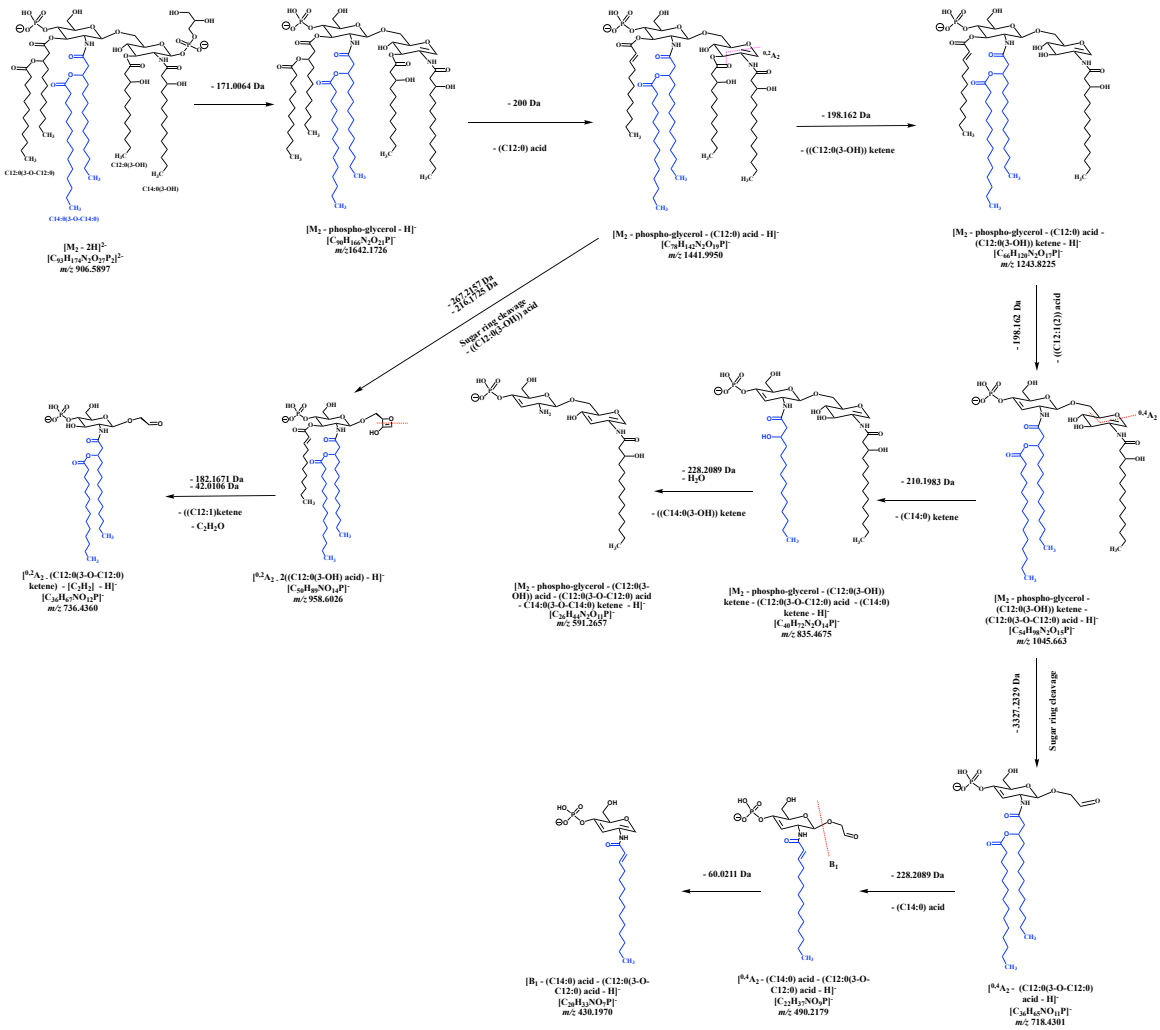

Scheme 5-2. Proposed fragmentation pathways of the selected precursor anion $[M_2 - 2H]^{2-}$ at *m/z* 906.5897in HCD-MS/MS analysis.

Table 5-3.The assignments of the diagnostic product anions in HCD-MS/MS analysis of the $[M_2 - 2H]^{2-}$ anion at *m/z* 906.5897.

Diagnostic ion	Empirical formula	*m/z* Observed	*m/z* Calculated	*m/z* Error (ppm)
$[M_2$ - phospho-glycerol - $H]^-$	$[C_{90}H_{166}N_2O_{21}P]^-$	1642.1722	1642.1726	-0.2
$[M_2$ - phospho-glycerol - (C12:0) acid - $H]^-$	$[C_{78}H_{142}N_2O_{19}P]^-$	1441.9863	1441.995	-6.0
$[M_2$ - phospho-glycerol - (C12:0) acid - (C12:0(3-OH)) ketene - $H]^-$	$[C_{66}H_{120}N_2O_{17}P]^-$	1243.8225	1243.833	-8.4

[M_2 - phospho-glycerol - (C12:0(3-OH) ketene - (C12:0 (3-O-C12:0) acid - H]$^-$	[$C_{54}H_{98}N_2O_{15}P$]$^-$	1045.663	1045.671	-7.6
[$^{0,2}A_2$ - 2((C12:0(3-OH) acid) - H]$^-$	[$C_{50}H_{89}NO_{14}P$]$^-$	958.5954	958.6026	-7.5
[M_2 - phospho-glycerol - (C12:0(3-OH)) ketene - (C12:0 (3-O-C12:0) acid - (C14:0) ketene - H]$^-$	[$C_{40}H_{72}N_2O_{14}P$]$^-$	835.4675	835.4727	-6.2
[$^{0,2}A_2$ - (C12:0(3-O-C12:0) ketene - [C_2H_2O] - H]$^-$	[$C_{36}H_{67}NO_{12}P$]$^-$	736.436	736.4406	-6.2
[$^{0,4}A_2$ - C12:0(3-O-C12:0) acid - H]$^-$	[$C_{36}H_{65}NO_{11}P$]$^-$	718.4301	718.4301	0
[M_2 - phospho-glycerol - (C12:0(3-OH) acid - (C12:0 (3-O-C12:0) acid - (C14:0(3-O-C14:0) ketene - H]$^-$	[$C_{26}H_{44}N_2O_{11}P$]$^-$	591.2657	591.2688	-5.2
[$^{0,4}A_2$ - (C14:0) acid- C12:0(3-O-C12:0) acid - H]$^-$	[$C_{22}H_{37}NO_9P$]$^-$	490.2179	490.2211	-6.5
[B_1 - (C14:0) acid- C12:0(3-O-C12:0)) acid - H]$^-$	[$C_{20}H_{33}NO_7P$]$^-$	430.197	430.2	-6.9
phospho-glycerol group	[$C_3H_8O_6P$]$^-$	171.0052	171.0064	-7.0

The precursor anion, [M_2 - 2H]$^{2-}$, at *m/z* 906.5897, underwent multiple fragmentation pathways, revealing detailed structural insights. The first product anion at *m/z* 1642.1722 was formed by losing a phospho-glycerol group (171.0064 Da) from the O-1 position of the lipid A disaccharide anion. This loss resulted in the ion being assigned as [M_2 - phospho-glycerol - H]$^-$. Further fragmentation of this anion led to the loss of a loss of a (C12:0) acid (200.1755 Da) located at the O-3' position, forming the product anion at *m/z* 1441.9950, assigned as [M_2 - phospho-glycerol - (C12:0) acid - H]$^-$. This latter anion then underwent cyclic cleavage ($^{0,2}A_2$) at the reducing sugar (267.2157 Da) followed by loss of ((C12:0(3-OH)) acid (216.1725 Da) from O-3 position to produce *m/z* 958.6026, which was assigned [$^{0,2}A_2$ - 2((C12:0(3-OH) acid) - H]$^-$. This was further followed by secondary cyclic cleavage (42.0106 Da) and elimination of (C12:1) ketene from the O-3' position, which led to the production of an anion at *m/z* 736.436, which was assigned as [$^{0,2}A_2$ - (C12:0(3-O-C12:0) ketene - [C_2H_2O] - H]$^-$.

Additional fragmentation of the anion at *m/z* 1441.9950 involved the loss (C12:0(3-OH)) ketene (198.1601 Da) located at O-3 position to produce *m/z* 1243.8225 anions, which was assigned as $[M_2$ - phospho-glycerol - (C12:0) acid - (C12:0(3-OH)) ketene - $H]^-$. Following this initial ketene loss, an additional (C12:1(2)) acid (198.1601 Da) was lost located at O-3' position, resulting in the formation of a product anion at *m/z* 1045.6630, designated as $[M_2$ - phospho-glycerol - (C12:0(3-OH)) ketene - (C12:0 (3-O-C12:0(3-OH)) acid - $H]^-$. Further fragmentation by the loss of an additional (C14:0) ketene (210.1983 Da) located at the N-2' position, generating a product anion at *m/z* 835.4675, which was denoted as $[M_2$ - phospho-glycerol - (C12:0(3-OH)) ketene - (C12:0 (3-O-C12:0) acid - (C14:0) ketene - $H]^{-\cdot}$ Further loss involving the removal of a (C14:0(3-OH)) ketene (228.2089 Da) from the N-2' position and water molecule from the hydroxyl group at O-3 position, resulting in an anion at *m/z* 591.2657, which was assigned as $[M_2$ - phospho-glycerol - C12:0(3-OH) acid -C12:0(3-O-C12:0) acid - C14:0(3-O-C14:0) ketene - $H]^-$.

The anion at *m/z* 1045.6630 also underwent sugar ring cleavage ($^{0,4}A_2$) of the reducing sugar part (3327.2329 Da) to form anion at *m/z* 718.4301, which was assigned as $[^{0,4}A_2$ - (C12:0(3-O- C12:0) acid - $H]^-$. Further loss of (C14:0) acid (228.2065 Da) located at the N-3' position of this latter anion led to the formation of anion at *m/z* 490.2179, which was assigned as $[^{0,4}A_2$ - (C14:0) acid - (C12:0(3-O- C12:0) acid - $H]^-$. The product anion at *m/z* 430.1970 was formed by glycosidic cleavages of the β-D-Glc*p*N-(1→6)-α-D-Glc*p*N disaccharide backbone, resulting in the non-reducing D-Glc*p*N-H_2PO_4 species, which was assigned as $[B_1$ - (C14:0) acid - (C12:0(3-O- C12:0) acid - $H]^-$.

This anion at *m/z* 430.1970 was less than the diagnostic *m/z* 444.1764 detected in the MS/MS of the previous ion at *m/z* 913.5801 by 13.98 Da (minus oxygen plus $H_{2\,=}$ - 15.99 + 2.01=13.98 Da). This clearly confirmed that *m/z* 906.5897 did not have an extra hydroxyl group and/or a double bond on the fatty acyl chain at the N-3' position as in the case of *m/z* 913.5725. For this reason, the chemical composition of the anion at *m/z* 906.582 was also less than that at *m/z* 913.5801 by 13.98 Da (-O plus H_2). This clearly explained that it was important to overlay the MS/MS spectrum of different precursor anions in order to figure out the structural difference that led to the mass shift of some diagnostic ions, such as the case of *m/z* 430.1970 and *m/z* 444.1764 originated from the precursor ions at *m/z* 906.5897 and *m/z* 913.5801 respectively.

From the HCD-MS/MS fragmentation routes, we speculated that the doubly charged anion, $[M_2 - 2H]^{2-}$ at *m/z* 906.5897 (DU = 10), was assigned as a deprotonated lipid of a hexa-acylated β-D-Glc*p*N-(1→6)-α-D-Glc*p*N disaccharide, where the N-2 and O-3 free positions of the reducing sugar were substituted with C14:0(3-OH) and C12:0(3-OH), respectively. Additionally, the N-2' and O-3'-free positions of the non-reducing sugar were substituted with myristic acid-3-oxy-myristoyl group (C14:0 (3-O-C14:0) and (C12:0(3-O-C12:0), respectively.

5.4.1.3. HCD-MS/MS of the Precursor Anion $[M_3 - 2H]^{-2}$ *at m/z* 822.4969

HCD-MS/MS of the precursor ion *3* at *m/z* 822.4969 has a formula $[C_{81}H_{150}N_2O_{27}P_2]^{-2}$, which corresponded to a neutral molecular mass of 1647.0058 Da, as shown in the **Figures 5-5**.

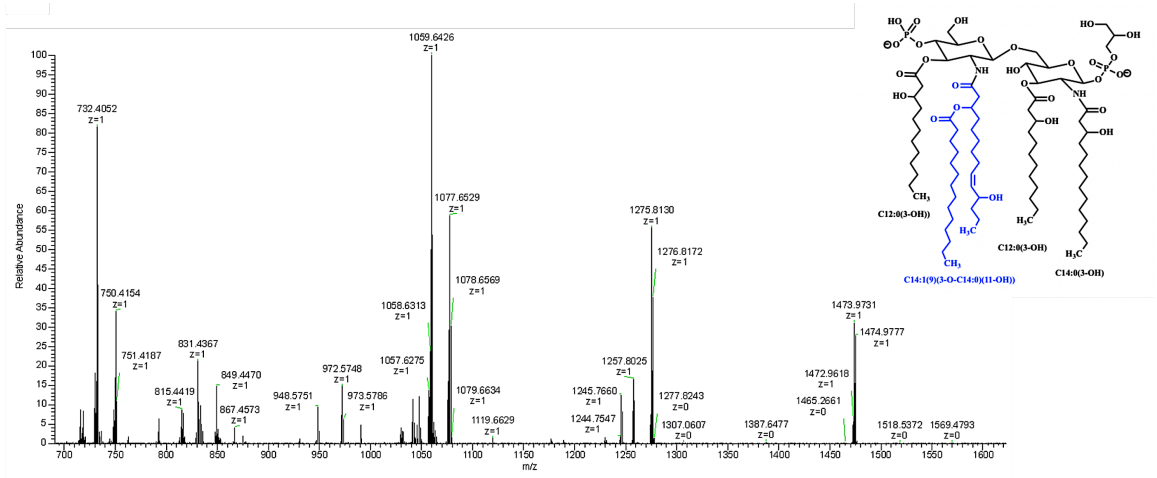

Figure 5-5. HCD-MS/MS of lipid A $[M_3 - 2H]^{2-}$ ions at *m/z* 822.4969 extract from *V. anguillarum serovar* SJ-41.

Proposed fragmentation pathways of the selected precursor doubly charged anion in HCD-MS/MS analysis of the $[M_3 - 2H]^{2-}$ at *m/z* 822.4969, which produced singly charged series of product ions observed at *m/z* values of 1473.9731, 1275.813, 1077.6529, 1059.6526, 972.5748, 849.447, 831.4367, 732.4052, 588.2181, 504.1972, 444.1762, and 171.0052, as shown in **Scheme 5-3** and detailed in **Table 5-4**.

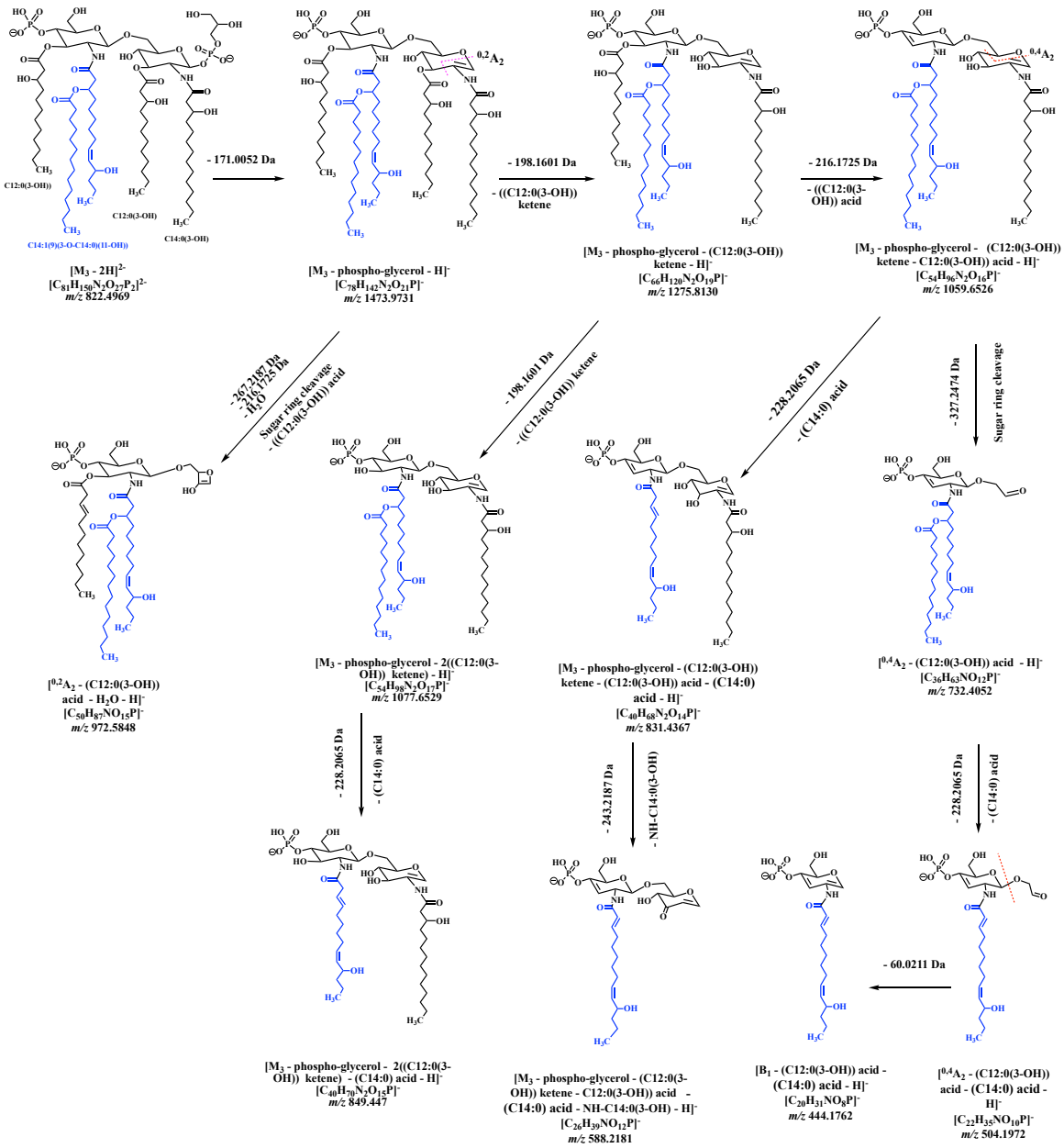

Scheme 5-3. Proposed fragmentation pathways of the selected precursor anion $[M_3 - 2H]^{2-}$ at *m/z* 822.4969 in HCD-MS/MS analysis.

Table 5-4. The assignments of the diagnostic product anions in HCD-MS/MS analysis of the $[M_3 - 2H]^{2-}$ anion at *m/z* 822.4969.

Diagnostic ion	Empirical formula	*m/z* Observed	*m/z* Calculated	*m/z* Error (ppm)
$[M_3$ - phospho-glycerol - $H]^-$	$[C_{78}H_{142}N_2O_{21}P]^{2-}$	1473.9731	1473.9848	-7.9
$[M_3$ - phospho-glycerol - (C12:0(3-OH)) ketene - $H]^-$	$[C_{66}H_{120}N_2O_{19}P]^-$	1275.813	1275.8228	-7.6
$[M_3$ - phospho-glycerol - 2((C12:0(3-OH)) ketene) - $H]^-$	$[C_{54}H_{98}N_2O_{17}P]^-$	1077.6529	1077.6609	-7.4
$[M_3$ - phospho-glycerol - (C12:0(3-OH)) ketene- (C12:0(3-OH)) acid - $H]^-$	$[C_{54}H_{96}N_2O_{16}P]^-$	1059.6526	1059.6503	2.1
$[^{0,2}A_2$ - ((C12:0(3-OH)) acid - H_2O - $H]^-$	$[C_{50}H_{87}NO_{15}P]^-$	972.5748	972.5819	-7.3
$[M_3$ - phospho-glycerol - 2((C12:0(3-OH)) ketene) - (C14:0) acid - $H]^-$	$[C_{40}H_{70}N_2O_{15}P]^-$	849.447	849.4519	-5.7
$[M_3$ - phospho-glycerol - (C12:0(3-OH)) ketene - (C12:0(3-OH)) acid - (C14:0) acid - $H]^-$	$[C_{40}H_{68}N_2O_{14}P]^-$	831.4367	831.4414	-5.6
$[^{0,4}A_2$ - (C12:0(3-OH)) acid - $H]^-$	$[C_{36}H_{63}NO_{12}P]^-$	732.4052	732.4093	-5.6
$[M_3$ - phospho-glycerol - (C12:0(3-OH)) ketene - (C12:0(3-OH)) acid - NH-C14:0(3-OH) - $H]^-$	$[C_{26}H_{39}NO_{12}P]^-$	588.2181	588.2215	-5.7
$[^{0,4}A_2$ - (C12:0(3-OH)) acid - (C14:0) acid - $H]^-$	$[C_{22}H_{35}NO_{10}P]^-$	504.1972	504.2004	-6.35
$[B_1$ - (C12:0(3-OH)) acid - (C14:0) acid - $H]^-$	$[C_{20}H_{31}NO_8P]^-$	444.1762	444.1793	-6.98
phospho-glycerol group	$[C_3H_8O_6P]^-$	171.0052	171.0064	-7.02

The precursor anion $[M_3 - 2H]^{2-}$ at *m/z* 822.4969 underwent multiple fragmentation pathways. The first product anion at *m/z* 1473.9731 was formed by losing a phospho-glycerol group (171.0064 Da) from the O-1 position of the lipid A disaccharide anion, resulting in the assignment $[M_3$ - phospho-glycerol - $H]^-$. This anion then underwent cyclic cleavage ($^{0,2}A_2$) at the reducing sugar (267.2157 Da), followed by the loss of a water molecule from the hydroxyl group at the O-3' position and loss of (C12:0(3-OH)) acid

(216.1725 Da) from O-3 position, which form 2H-oxet-4-ol to produce *m/z* 972.5755, which was assigned $[^{0,2}A_2$ - (C12:0(3-OH)) acid - H_2O - H]$^-$.

Additional fragmentation of the anion at *m/z* 1473.9731 included the loss of (C12:0(3-OH)) ketene (198.1601 Da) at O-3 position to produce *m/z* 1257.8130 anion, which was assigned as [M_3 - phospho-glycerol - (C12:0(3-OH)) ketene - H]$^-$. Subsequently, the latter anion lost an additional ((C12:0(3-OH)) ketene (198.1601 Da) from the O-3' position, resulting in the formation of a product anion at *m/z* 1077.6529, designated as [M_3 - phospho-glycerol - 2((C12:0(3-OH) ketene) - H]$^-$. Further fragmentation included the loss of an additional (C14:0) acid from the branched fatty acid located at the N-2' position, generating a product anion at *m/z* 849.447, which was denoted as [M_3 - phospho-glycerol - 2((C12:0(3-OH)) ketene) - (C14:0) acid - H]$^-$.

The anion at *m/z* 1275.8130 also underwent loss of a (C12:0(3-OH)) acid (216.1725 Da) from O-3' position, resulting in the formation of a product anion at *m/z* 1059.6526, designated as [M_3 - phospho-glycerol - (C12:0(3-OH)) ketene - (C12:0(3-OH)) acid - H]$^-$. Further loss of a (C14:0) acid from the branched fatty acid located at the N-2' position, generating a product anion at *m/z* 831.4367, which was denoted as [M_3 - phospho-glycerol - (C12:0(3-OH)) ketene - (C12:0(3-OH)) acid - (C14:0) acid - H]$^-$. An additional loss of an (NH-C14:0(3-OH)) group (243.2187 Da) from the reducing sugar part at the N-2' position generated the product anion at *m/z* 588.2181, assigned as [M_3 - phospho-glycerol - (C12:0(3-OH)) ketene - (C12:0(3-OH)) acid - (C14:0) acid - NH-C14:0(3-OH) - H]$^-$.

The anion at *m/z* 1059.6435 also underwent sugar ring cleavage ($^{0,4}A_2$) of the reducing sugar part (327.2474 Da) to form an anion at *m/z* 732.4052, which was assigned

as $[^{0,4}A_2$ - (C12:0(3-OH)) acid - H]$^-$. Further elimination of a (C14:0) acid (228.2065 Da) located at the N-2' position of this latter anion led to the formation of anion at *m/z* 504.1972, which was assigned as $[^{0,4}A_2$ - (C12:0(3-OH)) acid - (C14:0) acid - H]$^-$. Glycosidic cleavage of the the β-D-Glc*p*N-(1→6)-α-D-Glc*p*N disaccharide backbone produced anion at *m/z* 444, identified as [B_1 - (C12:0(3-OH)) acid - (C14:0) acid - H]$^-$, representing the non-reducing D-Glc*p*N-H_2PO_4 species.

From the HCD-MS/MS fragmentation routes, we speculated that the doubly charged anion, $[M_3 - 2H]^{2-}$ at *m/z* 822.4969 (DU = 10), was assigned as a deprotonated lipid of a penta-acylated β-D-Glc*p*N-(1→6)-α-D-Glc*p*N disaccharide, where the N-2 and O-3 free position of the reducing sugar was substituted with C14:0(3-OH) and C12:0(3-OH). Additionally, the N-2' and O-3'-free positions of the non-reducing sugar were substituted with (C14:1(9)(3-O-C14:0)(11-OH) and C12:0(3-OH), respectively.

5.4.1.4. HCD-MS/MS of the Precursor Anion $[M_4 - 2H]^{-2}$ at *m/z* 815.5066

HCD-MS/MS of the precursor ion *4* at *m/z* 815.5066 has a formula $[C_{81}H_{152}N_2O_{26}P_2]^{-2}$, which corresponded to a neutral molecular mass of 1633.0265 Da, as shown in the **Figures 5-6**.

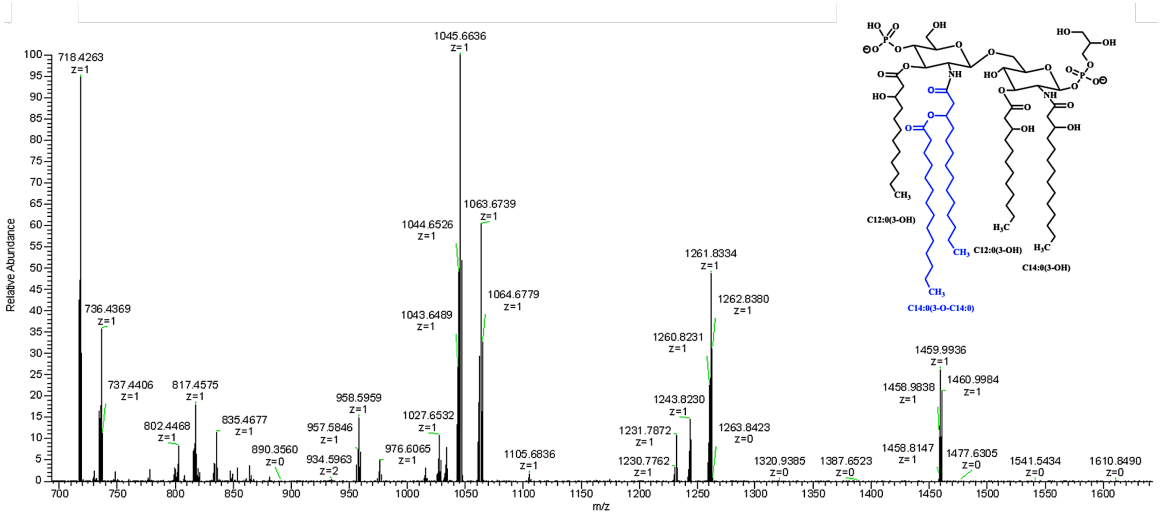

Figure 5-6. HCD-MS/MS of lipid A $[M_4 - 2H]^{2-}$ anion at *m/z* 815.5066 extract from *V. anguillarum serovar* SJ-41.

Proposed fragmentation pathways of selected doubly charged precursor ion in HCD-MS/MS analysis of the $[M_4 - 2H]^{2-}$ at *m/z* 815.5066, which produced singly charged series of product ions observed at *m/z* values of 1459.9936, 1261.8334, 1063.6739, 1045.6636, 976.6065, 958.5959, 835.4677, 718.4263, 490.2181, 430.1971, and 171.0052, as shown in **Scheme 5-4** and detailed in **Table 5-5**.

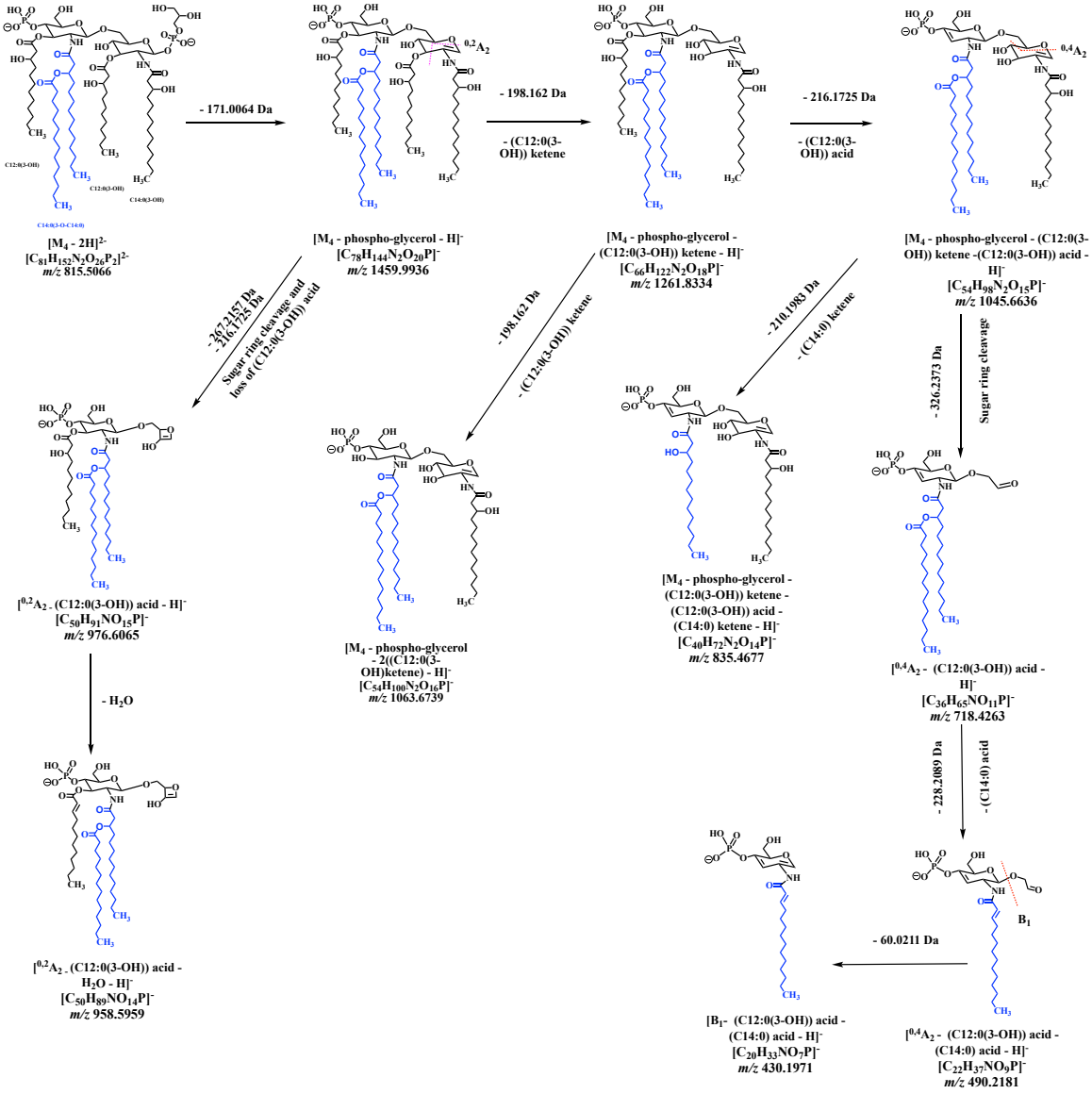

Scheme 5-4. Proposed fragmentation pathways of the selected precursor anion $[M_4 - 2H]^{2-}$ at *m/z* 815.5066 in HCD-MS/MS analysis.

Table 5-5. Assignments of the diagnostic product ions in HCD-MS/MS analysis of the $[M_4 - 2H]^{2-}$ anion at *m/z* 815.5066.

Diagnostic ion	Empirical formula	*m/z* Observed	*m/z* Calculated	*m/z* Error (ppm)
$[M_4$ - phospho-glycerol - $H]^-$	$[C_{78}H_{144}N_2O_{20}P]^-$	1459.9936	1460.0056	-8.2
$[M_4$ - phospho-glycerol - (C12:0(3-OH)) ketene - $H]^-$	$[C_{66}H_{122}N_2O_{18}P]^-$	1261.8334	1261.8436	-8.0
$[M_4$ - phospho-glycerol - 2((C12:0(3-OH)) ketene) - $H]^-$	$[C_{54}H_{100}N_2O_{16}P]^-$	1063.6739	1063.6816	-7.2
$[M_4$ - phospho-glycerol - (C12:0(3-OH)) ketene - (C12:0(3-OH)) acid - $H]^-$	$[C_{54}H_{98}N_2O_{15}P]^-$	1045.6636	1045.671	-7.0
$[^{0,2}A_2$ - (C12:0(3-OH)) acid - $H]^-$	$[C_{50}H_{91}NO_{15}P]^-$	976.6065	976.6132	-6.8
$[^{0,2}A_2$ - (C12:0(3-OH)) acid - H_2O - $H]^-$	$[C_{50}H_{89}NO_{14}P]^-$	958.5959	958.6026	-6.9
$[M_4$ - phospho-glycerol - (C12:0(3-OH)) ketene - (C12:0(3-OH)) acid - (C14:0) ketene - $H]^-$	$[C_{40}H_{72}N_2O_{14}P]^-$	835.4677	835.4727	-5.9
$[^{0,4}A_2$ - (C12:0(3-OH)) acid - $H]^-$	$[C_{36}H_{65}NO_{11}P]^-$	718.4263	718.4301	-5.2
$[^{0,4}A_2$ - (C12:0(3-OH)) acid - (C14:0) acid - $H]^-$	$[C_{22}H_{37}NO_9P]^-$	490.2181	490.2211	-6.1
$[B_1$ - (C12:0(3-OH)) acid - (C14:0) acid - $H]^-$	$[C_{20}H_{33}NO_7P]^-$	430.1971	430.2	-6.7
phospho-glycerol group	$[C_3H_8O_6P]$-	171.0052	171.0064	-7.0

The precursor anion $[M_4 - 2H]^{2-}$ at *m/z* 815.5066 underwent multiple fragmentation pathways. The first product anion at *m/z* 1459.9936 was formed by losing a phospho-glycerol group (171.0064 Da) from the O-1 position of the lipid A disaccharide anion. This loss resulted in the ion being assigned as $[M_4$ - phospho-glycerol - $H]^-$. This anion then underwent cyclic cleavage ($^{0,2}A_2$) at the reducing sugar (267.2157 Da) followed by loss of (C12:0(3-OH)) acid (216.1725 Da) from O-3 position, which formed 2H-oxet-4-ol to produce *m/z* 976.6065, which was assigned as $[^{0,2}A_2$ - (C12:0(3-OH)) acid - $H]^-$. This was followed by the elimination of water molecule from the hydroxyl group at (C12:0(3-OH)

fatty acid at O-3' position, which led to the production of an anion at *m/z* 958.5959, which was assigned as $[^{0,2}A_2$ - (C12:0(3-OH)) acid - H_2O - H]$^-$.

Additional fragmentation of the anion at *m/z* 1459.9936 involved the elimination of a (C12:0(3-OH) ketene (198.162 Da) located at the O-3 position of the previous product anion to form *m/z* 1261.8334, which was assigned as [M_4 - phospho-glycerol - (C12:0(3-OH) ketene - H]$^-$. Further fragmentation included elimination of (C12:0(3-OH) ketene (198.162 Da) located at the O-3' position led to form *m/z* 1063.6739, which was assigned as [M_4 - phospho-glycerol - 2((C12:0(3-OH)) ketene) - H]$^-$.

Moreover, the anion at *m/z* 1261.8443 also underwent the elimination of (C12:0) (3-OH) acid (216.1725 Da) located at the O-3' position led to the form *m/z* 1045.6636, which was assigned as [M_4 - phospho-glycerol - (C12:0(3-OH) ketene - (C12:0(3-OH) acid - H]$^-$. Further fragmentation involved the loss of a (C14:0) ketene (210.1983 Da) from the branched located at the N-2' position, generating a product anion at *m/z* 835.4677, which was denoted as [M_4 - phospho-glycerol - (C12:0(3-OH) ketene - (C12:0(3-OH) acid - (C14:0) ketene - H]$^-$.

The anion at *m/z* 1045.6636 also underwent sugar ring cleavage ($^{0,4}A_2$) of the reducing sugar part (326.2373 Da) to form anion at *m/z* 718.4263, which was assigned as [$^{0,4}A_2$ - (C12:0(3-OH)) acid - H]$^-$. Further loss of (C14:0) acid (228.2065 Da) the branched located at the N-2' position of this latter anion led to the formation of anion at *m/z* 490.2181, which was assigned as [$^{0,4}A_2$ - (C12:0(3-OH) acid - (C14:0) acid - H]$^-$. Glycosidic cleavages of the β-D-Glc*p*N-(1→6)-α-D-Glc*p*N disaccharide backbone produced the

product anion at *m/z* 430.1971, which was assigned as [B_1 - (C12:0(3-OH) acid - (C14:0) acid - H]$^-$, corresponding to the non-reducing D-Glc*p*N-H_2PO_4 species.

From the HCD-MS/MS fragmentation routes, we speculated that the doubly charged anion, [M_4 - 2H]$^{2-}$ at *m/z* 815.5066 (DU = 9), was assigned as a deprotonated lipid of a penta-acylated β-D-Glc*p*N-(1→6)-α-D-Glc*p*N disaccharide, where the N-2 and O-3 free positions of the reducing sugar were substituted with C14:0(3-OH), C12:0(3-OH), respectively. Additionally, the N-2' and O-3'-free positions of the non-reducing sugar were substituted with C14:0(3-O-14:0) and C12:0(3-OH), respectively.

5.4.1.5. HCD-MS/MS of the Precursor Anion [M_5 - 2H]$^{-2}$ at *m/z* 814.5003

HCD-MS/MS of the precursor ion *5* at *m/z* 814.5003 has a formula [$C_{81}H_{150}N_2O_{26}P_2$]$^{-2}$, which corresponded to a neutral molecular mass of 1631.0109 Da, as shown in the **Figures 5-7**.

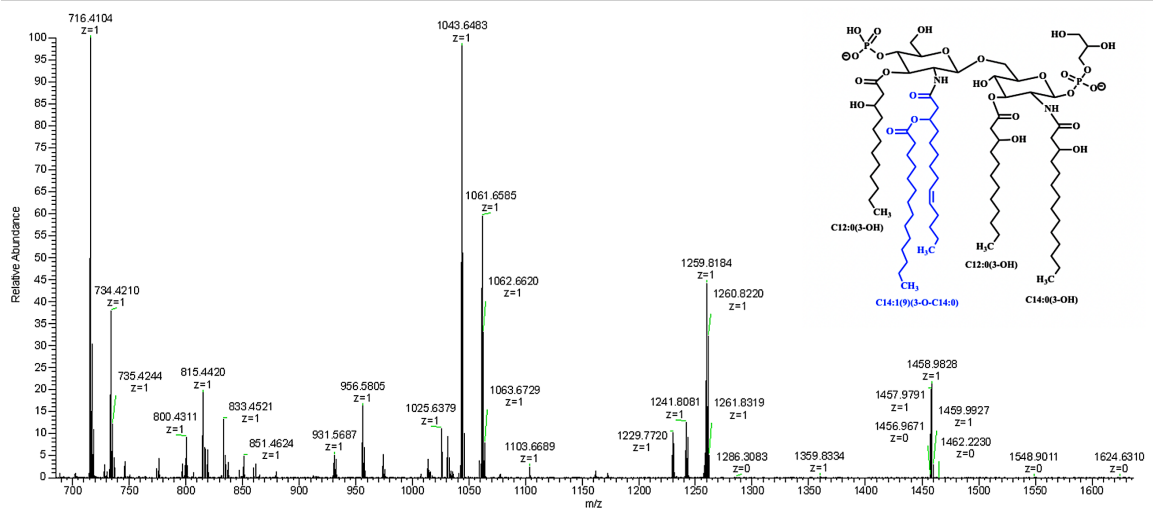

Figure 5-7. HCD-MS/MS of lipid A [M_5 - 2H]$^{2-}$ anion at *m/z* 814.5003 extract from *V. anguillarum serovar* SJ-41.

Proposed fragmentation pathways of the selected precursor anions $[M_5 - 2H]^{2-}$ at *m/z* 814.5003, which produced singly charged series of product ions observed at *m/z* values of 1457.9791, 1259.8184, 1229.772, 1061.6585, 1043.6483, 956.5805, 833.4521, 716.4104, 488.2023, 428.1813, and 171.0053, as shown in **Scheme 5-5** and detailed in **Table 5-6**.

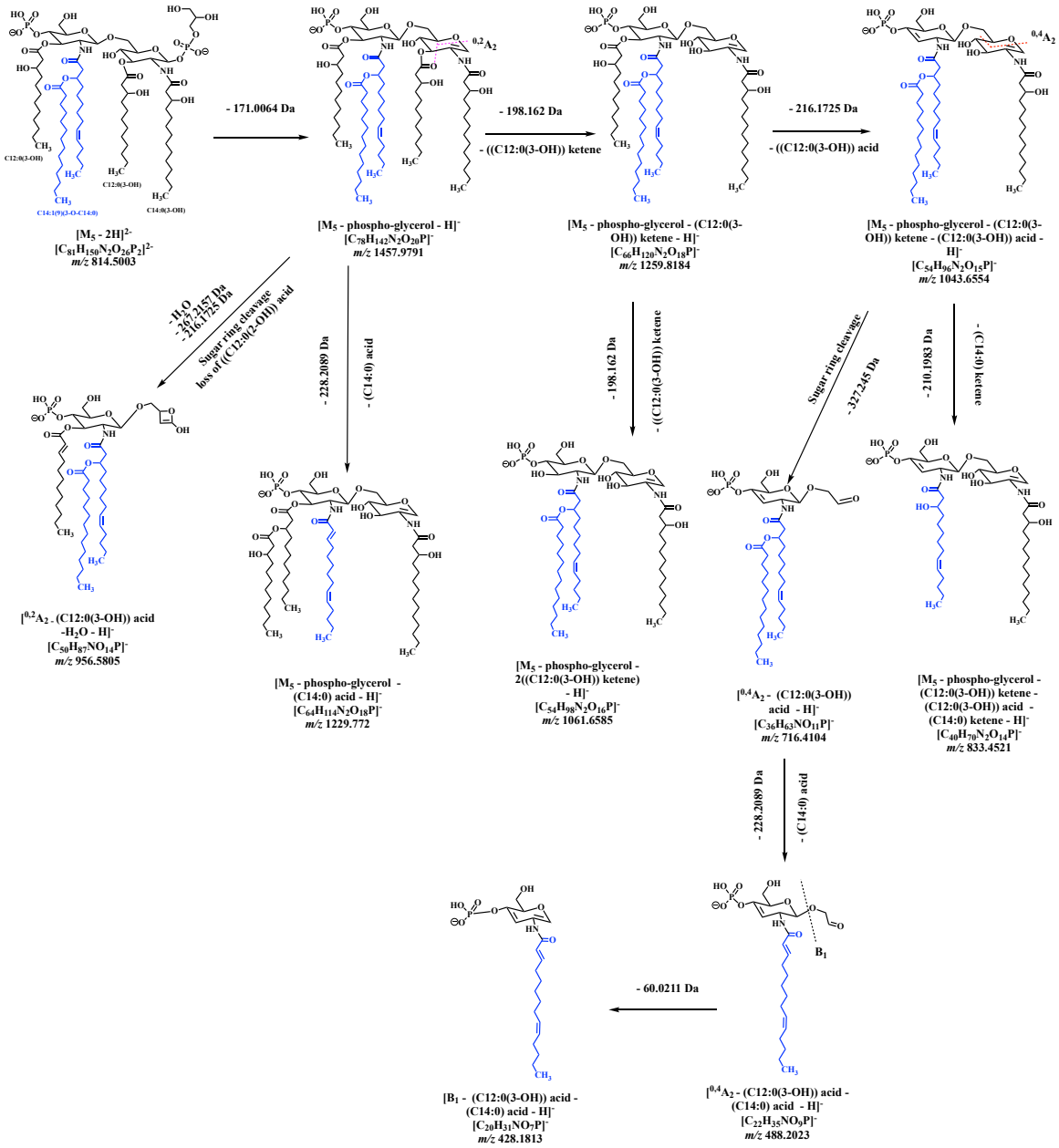

Scheme 5-5. Proposed fragmentation pathways of the selected precursor anion $[M_5 - 2H]^{2-}$ at *m/z* 814.5003 in HCD-MS/MS analysis.

Table 5-6. Assignments of the diagnostic product anions in HCD-MS/MS analysis of the $[M_5 - 2H]^{2-}$ anion at *m/z* 814.5003.

Diagnostic ion	Empirical formula	*m/z* Observed	*m/z* Calculated	*m/z* Error (ppm)
$[M_5$ - phospho-glycerol - H$]^-$	$[C_{78}H_{142}N_2O_{20}P]^-$	1457.9791	1457.9899	-7.4
$[M_5$ - phospho-glycerol - (C12:0(3-OH)) ketene - H$]^-$	$[C_{66}H_{120}N_2O_{18}P]^-$	1259.8184	1259.8279	-7.5
$[M_5$ - phospho-glycerol - (C14:0) acid - H$]^-$	$[C_{64}H_{114}N_2O_{18}P]^-$	1229.772	1229.781	-7.3
$[M_5$ - phospho-glycerol - 2((C12:0(3-OH)) ketene) - H$]^-$	$[C_{54}H_{98}N_2O_{16}P]^-$	1061.6585	1061.6659	-6.9
$[M_5$ - phospho-glycerol - (C12:0(3-OH)) ketene - (C12:0(3-OH)) acid - H$]^-$	$[C_{54}H_{96}N_2O_{15}P]^-$	1043.6483	1043.6554	-6.8
$[^{0,2}A_2$ - ((C12:0(3-OH)) acid - H_2O - H$]^-$	$[C_{50}H_{87}NO_{14}P]^-$	956.5805	956.587	-6.7
$[M_5$ - phospho-glycerol - (C12:0(3-OH)) ketene - (C12:0(3-OH)) acid - ((C14:0) ketene - H$]^-$	$[C_{40}H_{70}N_2O_{14}P]^-$	833.4521	833.457	-5.8
$[^{0,4}A_2$ - (C12:0(3-OH)) acid - H$]^-$	$[C_{36}H_{63}NO_{11}P]^-$	716.4104	716.4144	-5.5
$[^{0,4}A_2$ - (C12:0(3-OH)) acid - (C14:0) acid - H$]^-$	$[C_{22}H_{35}NO_9P]^-$	488.2023	488.2055	-6.5
$[B_1$ - (C12:0(3-OH)) acid - (C14:0) acid - H$]^-$	$[C_{20}H_{31}NO_7P]^-$	428.1813	428.1844	-7.2
phospho-glycerol group	$[C_3H_8O_6P]$-	171.0053	171.0064	-6.4

The precursor anion $[M_5 - 2H]^{2-}$ at *m/z* 814.5003 underwent multiple fragmentation pathways. The first product anion at *m/z* 1457.9691 was formed by losing a phospho-glycerol group (171.0064 Da) from the O-1 position of the lipid A disaccharide anion. This loss resulted in the ion being assigned as $[M_5$ - phospho-glycerol - H$]^-$. This anion then underwent cyclic cleavage ($^{0,2}A_2$) at the reducing sugar (267.2157 Da), followed by the loss of a water molecule from the hydroxyl group at the O-3' position. Furthermore, loss of

(C12:0(3-OH)) acid (216.1725 Da) from position O-3 to produce *m/z* 956.5805, which was assigned as $[^{0,2}A_2$ - (C12:0(3-OH)) acid - H_2O - $H]^-$.

Additional fragmentation of the anion at *m/z* 1457.9791 involved the loss of the (C14:0) acid (228.2089 Da) from the branched fatty acid at the N-2' position, forming the product anion at *m/z* 1229.772, which was assigned as $[M_5$ - phospho-glycerol - (C14:0) acid - $H]^-$. Another fragmentation pathway the anion at *m/z* 1457.9791 included the elimination of (C12:0(3-OH) ketene (198.162 Da) located at the O-3 position led to the form *m/z* 1259.8184, which was assigned as $[M_5$ - phospho-glycerol - (C12:0(3-OH)) ketene - $H]^-$. Following this initial ketene loss, an additional ((C12:0(3-OH)) ketene (198.1601 Da) was lost from O-3' position, resulting in the formation of a product anion at *m/z* 1061.6585, which was assigned as $[M_5$ - phospho-glycerol - 2((C12:0 (3-OH)) ketene) - $H]^-$. Furthermore, the anion at *m/z* 1259.8184 lost ((C12:0(3-OH)) acid (216.1725 Da) was lost from O-3' position, producing product anion at *m/z* 1043.6554, which was assigned as $[M_5$ - phospho-glycerol - (C12:0 (3-OH)) ketene - (C12:0 (3-OH)) acid - $H]^-$.

The anion at *m/z* 1043.6554 also underwent sugar ring cleavage ($^{0,4}A_2$) of the reducing sugar part (327.245 Da) to form anion at *m/z* 716.4104, which was assigned as $[^{0,4}A_2$ - (C12:0 (3-OH)) acid - $H]^-$. Further fragmentation included the loss of (C14:0) acid (228.2065 Da) located at the N-2' position, led to the formation of anion at *m/z* 488.2023, which was assigned as $[^{0,4}A_2$ - (C12:0 (3-OH)) acid - (C14:0) acid - $H]^-$. The product anion at *m/z* 428.1813 was formed by glycosidic cleavages of the β-D-Glc*p*N-(1→6)-α-D-Glc*p*N disaccharide backbone, resulting in the non-reducing D-Glc*p*N-H_2PO_4 species, which was assigned as $[B_1$ - (C12:0 (3-OH)) acid - (C14:0) acid - $H]^-$.

From the HCD-MS/MS fragmentation routes, we speculated that the doubly charged anion, $[M_5 - 2H]^{2-}$ at *m/z* 814.5003 (DU = 10), was assigned as a deprotonated lipid of a penta-acylated β-D-Glc*p*N-(1→6)-α-D-Glc*p*N disaccharide, where the N-2 and O-3-free positions of the reducing sugar were substituted with C14:0(3-OH) and C12:0(3-OH), respectively. Additionally, the N-2' and O-3'-free positions of the non-reducing sugar were substituted with (C14:1(9)(3-O-C14:0) and C12:0(3-OH), respectively.

5.4.1.6. HCD-MS/MS of the Precursor Anion $[M_6 - 2H]^{-2}$ at *m/z* 709.4007

HCD-MS/MS of the precursor ion *6* at *m/z* 709.4007 has a formula $[C_{67}H_{124}N_2O_{25}P_2]^{-2}$, which corresponded to a neutral molecular mass of 1420.8125 Da, as shown in the **Figures 5-8**.

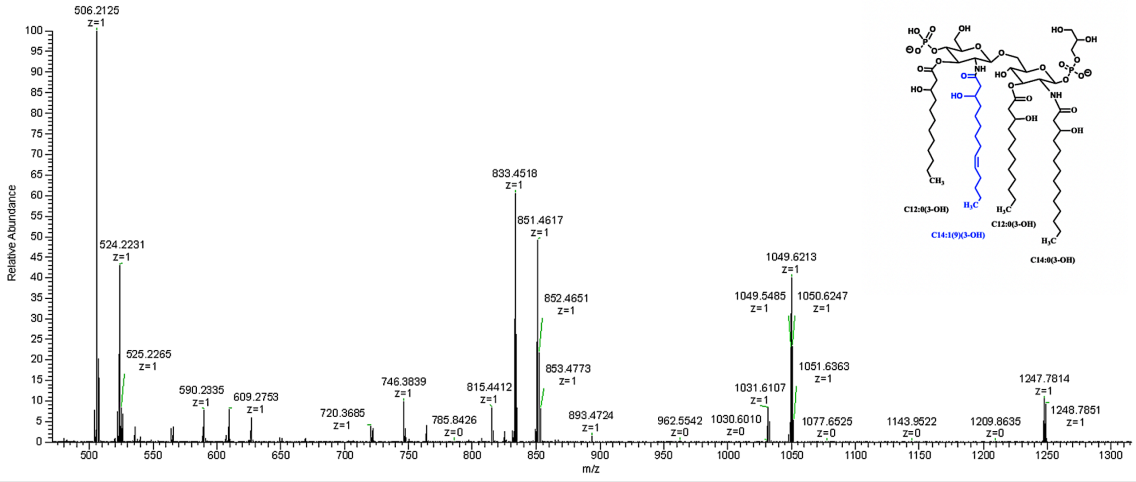

Figure 5-8. HCD-MS/MS of lipid A $[M_6 - 2H]^{2-}$ anion at *m/z* 709.4007 extract from *V. anguillarum serovar* SJ-41.

Proposed fragmentation pathways of the selected doubly charged precursor ion in HCD-MS/MS analysis of the $[M_6 - 2H]^{2-}$ at *m/z* 709.4007, which produced singly charged

series of product ions observed at *m/z* values of 1247.7814, 1049.6213, 1031.6107, 851.4412, 833.4518, 815.4412, 746.3839, 524.2231, 506.2125, 428.1813, and 171.0052, as shown in **Scheme 5-6** and detailed in **Table 5-7**.

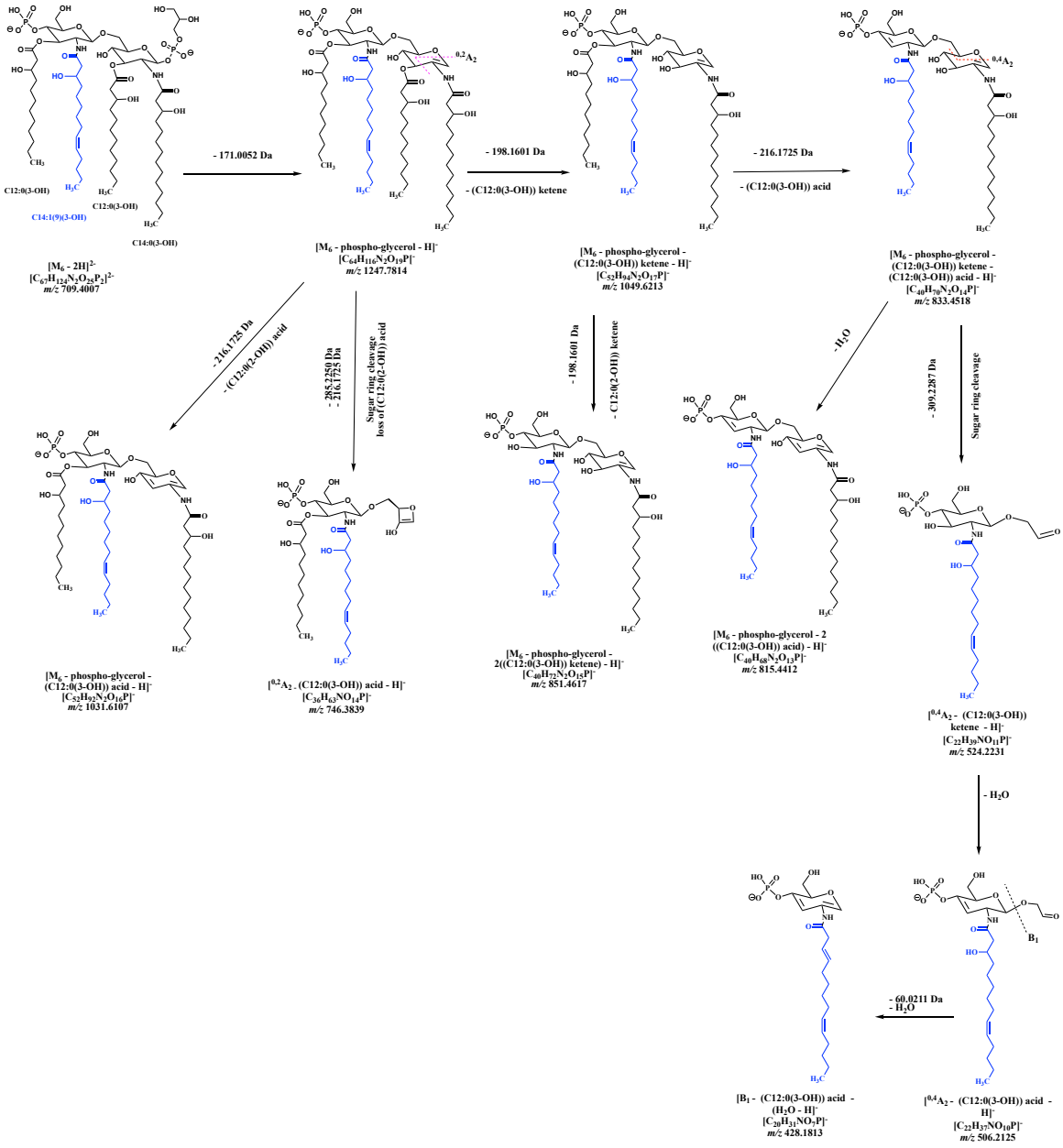

Scheme 5-6. Proposed fragmentation pathways of the selected precursor anion $[M_6 - 2H]^{2-}$ at *m/z* 709.4007 in HCD-MS/MS analysis.

Table 5-7. The Assignments of the diagnostic product ions in HCD-MS/MS analysis of the $[M_6 - 2H]^{2-}$ anion at *m/z* 709.4007.

Diagnostic ion	Empirical formula	*m/z* Observed	*m/z* Calculated	*m/z* Error (ppm)
$[M_6$ - phospho-glycerol - $H]^-$	$[C_{64}H_{116}N_2O_{19}P]^-$	1247.7814	1247.7915	-8.0
$[M_6$ - phospho-glycerol - C12:0(3-OH)) ketene - $H]^-$	$[C_{52}H_{94}N_2O_{17}P]^-$	1049.6213	1049.6296	-7.9
$[M_6$ - phospho-glycerol - (C12:0(3-OH)) acid - $H]^-$	$[C_{52}H_{92}N_2O_{16}P]^-$	1031.6107	1031.619	-8.0
$[M_6$ - phospho-glycerol - 2((C12:0(3-OH)) ketene) - $H]^-$	$[C_{40}H_{68}N_2O_{13}P]^-$	851.4412	851.4465	-6.2
$[M_6$ - phospho-glycerol - (C12:0(3-OH)) ketene - (C12:0 (3-OH)) acid - $H]^-$	$[C_{40}H_{70}N_2O_{14}P]^-$	833.4518	833.457	-6.2
$[M_6$ - phospho-glycerol - 2((C12:0(3-OH)) acid) - $H]^-$	$[C_{40}H_{72}N_2O_{15}P]^-$	815.4412	815.4465	-6.5
$[^{0,2}A_2$ - (C12:0(3-OH)) acid - $H]^-$	$[C_{36}H_{63}NO_{14}P]^-$	746.3839	746.3992	-20
$[^{0,4}A_2$ - (C12:0(3-OH)) ketene - $H]^-$	$[C_{22}H_{39}NO_{11}P]^-$	524.2231	524.2266	-6.6
$[^{0,4}A_2$ - (C12:0(3-OH)) acid - $H]^-$	$[C_{22}H_{37}NO_{10}P]^-$	506.2125	506.2161	-7.1
$[B_1$ - (C12:0(3-OH)) acid - H_2O - $H]^-$	$[C_{20}H_{31}NO_7P]^-$	428.1813	428.1844	-7.2
phospho-glycerol group	$[C_3H_8O_6P]$-	171.0052	171.0064	-7.0

The precursor anion $[M_6 - 2H]^{2-}$ at *m/z* 709.4007 underwent multiple fragmentation pathways. The first product anion at *m/z* 1247.7814 was formed by losing a phospho-glycerol group (171.0064 Da) from the O-1 position of the lipid A disaccharide anion. This loss resulted in the ion being assigned as $[M_6$ - phospho-glycerol - $H]^-$. This latter anion then underwent cyclic cleavage ($^{0,2}A_2$) at the (41.027 Da) followed by loss of (C12:0(3-OH)) acid (216.1725 Da) from position O-3 to produce *m/z* 746.3839, which was assigned as $[^{0,2}A_2$ - (C12:0(3-OH)) acid - $H]^-$.

Additional fragmentation of the anion at *m/z* 1247.7814 involved the loss of a (C12:0(3-OH) acid (216.1725 Da) located at the O-3 position of the previous product anion

to form *m/z* 1031.6107, which was assigned as [M_6 - phospho-glycerol - (C12:0(3-OH) acid - H]$^-$. Another fragmentation pathway anion at *m/z* 1247.7814 involved the loss of a (C12:0(3-OH) ketene (198.162 Da) located at the O-3 position, led to the form *m/z* 1049.6213, designated as [M_6 - phospho-glycerol - (C12:0(3-OH)) ketene - H]$^-$. Following this initial ketene loss, an additional ((C12:0(3-OH)) ketene (198.1601 Da) was lost from branched fatty acid located at O-3' position, resulting in the formation of a product anion at *m/z* 851.4617, which was assigned as [M_6 - phospho-glycerol - 2(C12:0(3-OH)) ketene - H]$^-$.

The anion at *m/z* 1049.6213 also underwent the loss of a ((C12:0(3-OH)) acid (216.1725 Da) at O-3' position, resulting in the formation of a product anion at *m/z* 833.4518, which was assigned as [M_6 - phospho-glycerol - (C12:0(3-OH)) ketene - (C12:0(3-OH)) acid - H]$^-$. This was followed by the loss of water molecule from the hydroxyl group at O-3 to form *m/z* 815.4412, which was assigned as [M_6 - phospho-glycerol - 2((C12:0(3-OH)) acid) - H]$^-$.

The anion at *m/z* 833.4518 underwent sugar ring cleavage ($^{0,4}A_2$) of the reducing sugar part (309.2287 Da) to form anion at *m/z* 524.2231, which was assigned as [$^{0,4}A_2$ - (C12:0(3-OH)) ketene - H]$^-$. Further loss of water molecule from O-3' position to produce *m/z* 506.2125, which was assigned as [$^{0,4}A_2$ - (C12:0(3-OH)) acid - H]$^-$.

The product anion at *m/z* 428.1813 was formed by glycosidic cleavages of the β-D-Glc*p*N-(1→6)-α-D-Glc*p*N disaccharide backbone followed by loss water molecule from the hydroxyl of C14:1 fatty acid at N=2', resulting in the non-reducing D-Glc*p*N-H_2PO_4 species, which was assigned as [B_1 - (C12:0(3-OH)) acid - H_2O - H]$^-$.

From the HCD-MS/MS fragmentation routes, we speculated that the doubly charged anion, $[M_6 - 2H]^{2-}$ at *m/z* 709.4007 (DU = 9), was assigned as a deprotonated lipid of a tetra-acylated β-D-Glc*p*N-(1→6)-α-D-Glc*p*N disaccharide, where the N-2 and O-3-free positions of the reducing sugar were substituted with (C14:0(3-OH)), (C12:0(3-OH)), respectively. In addition, the N-2' and O-3'-free positions of the non-reducing sugar were substituted with (C14:1(9)(3-OH) and (C12:0(3-OH)), respectively.

5.5. Kendrick Analysis Using a Fractional Base Unit of $CH_2/2$

In order to view the complexity of the analyzed lipid A mixture, the doubly charged anions mass list was used for Kendrick analysis. A fractional base unit of $CH_2/2$ allowed the expansion of isotopologues (same isotopic envelope) vertically across the Kendrick mass defect plot range (+0.5 to -0.5), thus facilitating the visualization of ion relationships (**Figure 5-9**). Isotopologues that belong to the same isotopic envelope have similar patterns of arrangement on the KMD plot (anions enclosed by the same colour, **Figure 5-9**). Moreover, many anions are arranged on the same horizontal line, indicating the extreme variability in the number of CH_2 units across the different lipid A species. Furthermore, many ion clusters across the KMD plot share the same arrangement pattern. Thus, structural relationships between these ion clusters can be deduced.

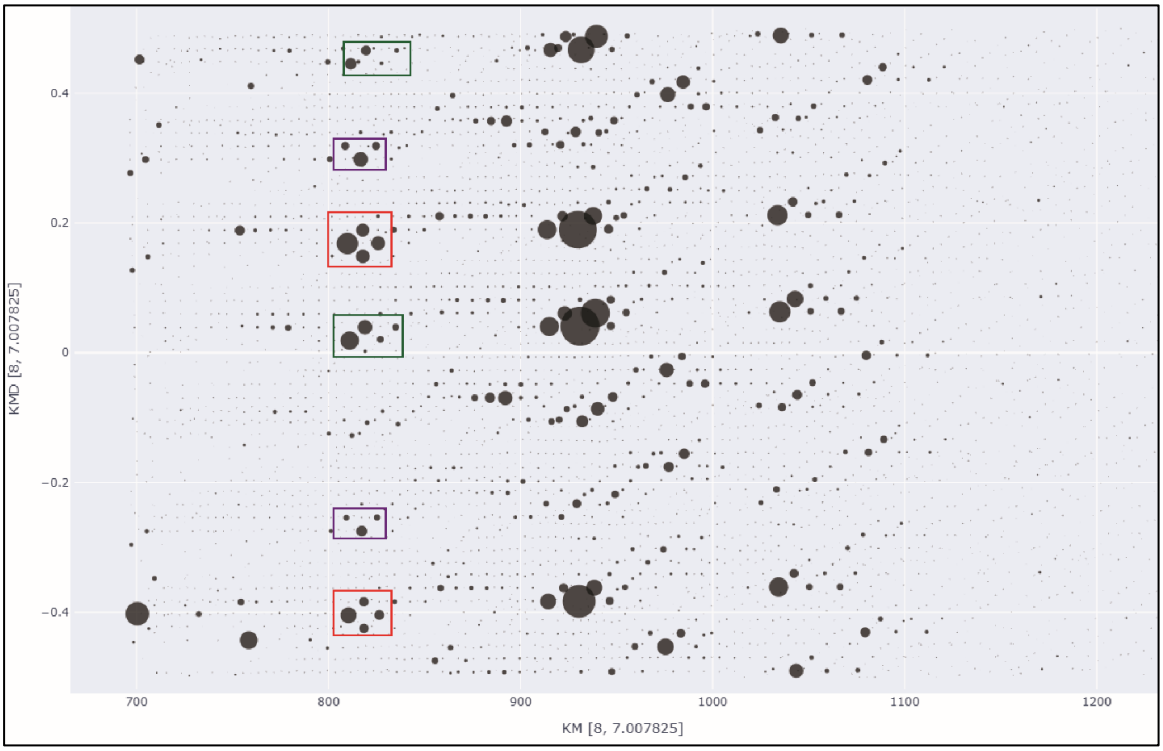

Figure 5-9. KMD analysis using $CH_2/2$ allowed the vertical expansion of isotopologues. Isotopologues that belong to the same isotopic envelope have the same pattern of arrangement on the KMD plot and are enclosed in the same colour.

Various anion relationships can be deduced from the Kendrick analysis; however, for the sake of brevity, a few examples will be explained herein, highlighting the importance of KMD plots in analyzing complex bio-extracts such as lipid A. For example, **Figure 5-10** shows that anions annotated as 6,7,8,9 are organized in a rhombus-like pattern. Thus, the relationships between these anion clusters can be easily investigated. Anion *6* at *m/z* 709.4007 was already characterized by tandem mass spectrometry, and it was deduced to have the chemical composition of $[C_{67}H_{124}N_2O_{25}P_2]^{-2}$. Thus, it can be used as a reference chemical composition to deduce the composition of nearby anions. Anion *7* at *m/z* 716.3905 was found to have an extra 13.98 Da with respect to anion *6,* indicating the

addition of an oxygen atom (+15.99) and removal of H_2 (-2.0157); thus, 15.99 - 2.01 creates a difference of 13.98 Da. On the other hand, Anion *8* at *m/z* 716.2459 was found to have an extra 14.05 Da with respect to anion *6,* indicating the addition of C_2H_4 (28.0313) and H_2 (2.0157) and the removal of an oxygen atom (-15.99), thus 28.03 +2.01-15.99=14.05 Da. Lastly, anion *9* at *m/z* 723.4160 has an extra 28.0313 Da (C_2H_4) with respect to Anion *6*. This clearly explains that the arrangement of these anion clusters (*6-9*) in a rhombus-like shape facilitates the prediction of their chemical composition without needing tandem MS on each ion in that cluster.

Moreover, some low-abundant anions, such as anions *10* and *11,* can be deduced from their mass difference from the highly abundant MS/MS characterized anions *2* and *6*, respectively. Anion *10* at *m/z* 1025.7032 was deduced to have two extra C_2H_4 units (2 x 28.0313 Da) plus an extra C12:0 residue (+182.1727 Da) with respect to anion *2* (*m/z* 906.5897), indicating that anion *10* is a hepta-acylated lipid A. On the other hand, anion *11* (*m/z 618.3161*) was less than anion *6 (m/z* 709.4007) by 182.17 Da, indicating that anion *11* is a tri-acylated lipid A. This shows that KMD plots can be easily used to find the chemical composition of low-abundant anions/lipid A species (*10* and *11*) by comparing it to well-characterized anions (*2* and *6*) by tandem mass spectrometry (**Table 5-1**). These examples clearly show the power of KMD plots in characterizing complex bio-extracts. Although the use of KMD plots in analyzing complex biological mixtures is still in its infancy due to the extreme mixture variability and endless ion relationships that can be deduced, it is an excellent tool to dig deeper and view the complexity of biological systems at the molecular level.

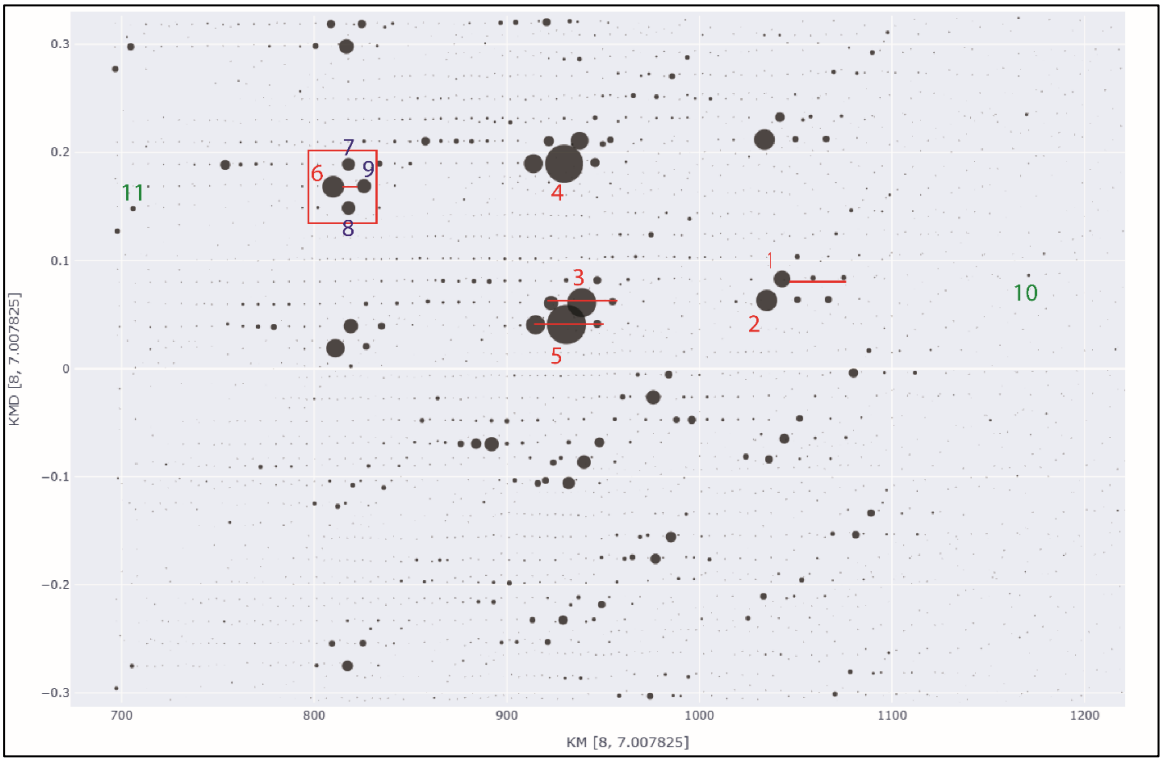

Figure 5-10. Expanded region of KMD plot using $CH_2/2$ showing some ions structural relationships. Ions 1-6 are the ions investigated by tandem mass spectrometry. Red lines are connecting ions that differ by 28.03 Da (C_2H_4 units). Relationships between ions 6, 7, 8, and 9 arranged in a rhombus-like shape can be easily investigated. Also, low-abundant ions 10 and 11 can be easily identified from their relationships with ions 2 and 6, previously identified and confirmed by tandem mass spectrometry.

5.6. Conclusions and Future Directions

Our findings represent a pivotal step forward in identifying the structural diversity of new lipid A within Gram-negative marine. These lipid A molecules were only extracted from the phenol layer of Westphal and Jan LPS extraction [36]. The lipid A of *Vibrio anguillarum* SJ-41 exhibited unique characteristics, with each member of this heterogeneous mixture containing an O-1 phospho-glycerol unit at the reducing end of β-D- Glc*p*N-(1→ 6)-α-D-Glc*p*N disaccharides. According to our knowledge, this new

finding has never been reported in the literature. The biosynthetic pathways involved in the phosphorylation of this strain need further studies.

Interestingly, sn-1-phosphoglycerol has previously been identified in membrane-derived oligosaccharides (MDO), which are composed of 8–10 units of D-glucose residues linked by β-D-(1→2) and β-D-(1→6) bonds. These oligosaccharides are typically localized in the periplasmic space between the inner and outer bacterial membranes. MDO structures are often modified by succinyl ester residues and sn-1-phosphoglycerol groups derived from membrane phospholipids [42]. Additionally, the sn-1-phospho-glycerol group has been reported in *Vibrio fischeri*, a bioluminescent Gram-negative marine bacterium. The lipid A of *Vibrio fischeri* includes unique modifications at the secondary acylation site of the 3-O-position of C12:0, notably involving sn-1-phospho-glycerol, lysophosphatidic acid, and phosphatidic acid moieties. These modifications result in a micro-heterogeneous mixture that includes mono-, di-, and tri-phosphorylated lipid A derivatives [43].

Furthermore, the presence of di-hydroxy fatty acids in *Vibrio anguillarum* highlights the complexity of these molecules. This study specifically identified C14:0 and/or C14:1 as di-hydroxy fatty acids, similar to previously observed compounds such as ipurolic acid (3,11-dihydroxy myristoic acid), a hydrophobic molecule practically insoluble in water [44]. However, further research is required to accurately determine the positions of the double bonds and hydroxyl groups within these fatty acids [45]. This suggests that structural variability may play an essential role in the pathogen's adaptation strategies, potentially allowing it to evade immune responses that typically recognize conventional lipid A. This discovery underscores the flexibility and evolutionary

innovation within bacterial lipid structures, especially in pathogenic adaptation in marine environments. The forthcoming study will analyze the remaining peaks of the microheterogeneity obtained from SJ-41-lipid A (phenol soluble) LPS with ESI-FAIMS-MS and HCD-MS/MS. In addition, the Kendrick analysis of the extreme complexity of the Lipid A mixture. Furthermore, understanding how these lipid A differ in their immunogenic profiles can guide the development of new therapeutic strategies that target non-traditional lipid A structures, potentially aiding in the design of treatments for infections caused by *Vibrio* species and similar pathogens. Our results pave the way for future investigations into how structural variations in lipid A contribute to diverse bacterial pathogens' survival, virulence, and immune evasion.

5.7. References

[1] G. B. Nair, S. M. Faruque, and D. A. Sack, "Vibrios," *Emerging foodborne pathogens*, 2006. pp. 332-372.

[2] B. Gomez-Gil, C. C. Thompson, Y. Matsumura, T. Sawabe, T. Iida, R. Christen, F. Thompson, and T. Sawabe, "The famlily *Vibrionaceae*," *The prokaryotes*, 2014. pp. 659-747.

[3] R. Guerrero-Ferreira, C. Gorman, A. A. Chavez, S. Willie, and M. K. Nishiguchi, “Characterization of the bacterial diversity in Indo-West Pacific loliginid and sepiolid squid light organs,” *Microb. Ecol.,* vol. 65, no. 1, pp. 214-226, Jan, 2013. DOI: https://doi.org/10.1007/s00248-012-0099-6.

[4] I. Frans, C. W. Michiels, P. Bossier, K. A. Willems, B. Lievens, and H. Rediers, "*Vibrio anguillarum* as a fish pathogen: virulence factors, diagnosis and prevention," *J. Fish. Dis.,* vol. 34, no. 9, pp. 643-661, Sep, 2011. DOI: https://doi.org/10.1111/j.1365-2761.2011.01279.x.

[5] G. M. M. Sanches-Fernandes, I. Sa-Correia, and R. Costa, "Vibriosis outbreaks in Aquaculture: Addressing environmental and public health concerns and preventive therapies using gilthead seabream farming as a model system," *Front. Microbiol.,* vol. 13, no. July, pp. 904815, Jul, 2022. DOI: https://doi.org/10.3389/fmicb.2022.904815.

[6] J. H. Banoub, F. Michon, and H. J. Hodder, "Structural elucidation of the O-specific polysaccharide of the phenol-phase soluble lipopolysaccharide of *Vibrio anguillarum*," *Biochem. Cell Biol.,* vol. 65, no. 1, pp. 19-26, Jan, 1987. DOI: https://doi.org/10.1139/o87-003.

[7] A. Radhakrishnan, B. Vaseeharan, P. Ramasamy, and S. Jeyachandran, "Oral vaccination for sustainable disease prevention in aquaculture-an encapsulation approach," *Aquac. Int.,* vol. 31, no. 2, pp. 867-891, Oct, 2023. DOI: https://doi.org/10.1007/s10499-022-01004-4.

[8] Q. Ji, S. Wang, J. Ma, and Q. Liu, "A review: Progress in the development of fish *Vibrio spp.* vaccines," *Immunol. Lett.,* vol. 226, pp. 46-54, Oct, 2020. DOI: https://doi.org/10.1016/j.imlet.2020.07.002.

[9] D. Sepulveda, M. J. Hansen, I. Dalsgaard, J. Skov, and N. Lorenzen, "Antigenic variability of *Vibrio anguillarum* serotype O2a: A hurdle for vaccine efficacy

against vibriosis in rainbow trout (Oncorhynchus mykiss)," *Fish Shellfish Immunol.,* vol. 131, pp. 300-311, Dec, 2022. DOI: https://doi.org/10.1016/j.fsi.2022.09.072.

[10] K. L. Seib, G. Dougan, and R. Rappuoli, "The key role of genomics in modern vaccine and drug design for emerging infectious diseases," *PLoS Genet.,* vol. 5, no. 10, pp. e1000612, Oct, 2009. DOI: https://doi.org/10.1371/journal.pgen.1000612.

[11] J. Xing, H. Xu, Y. Wang, X. Tang, X. Sheng, and W. Zhan, "Identification of immunogenic proteins and evaluation of four recombinant proteins as potential vaccine antigens from *Vibrio anguillarum* in flounder (Paralichthys olivaceus)," *Vaccine,* vol. 35, no. 24, pp. 3196-3203, May, 2017. DOI: https://doi.org/10.1016/j.vaccine.2017.04.071.

[12] D. E. S. Stewart-Tull, C. R. Bleakley, and T. S. Galloway, "Characteristics of Vibrio cholerae proteinases: potential, candidate vaccine antigens," *Vaccine,* vol. 22, no. 23, pp. 3026-3034, Aug, 2004. DOI: https://doi.org/10.1016/j.vaccine.2004.02.012.

[13] L. McCarter, "The multiple identities of Vibrio parahaemolyticus," *J. Mol. Microbiol. Biotechnol.,* vol. 1, no. 1, pp. 51-57, Aug, 1999.

[14] E. B. Shotts, "Diagnostic approaches for fish diseases," *Diagnostic procedure in veterinary bacteriology and mycology*, 1990. pp. 507-517.

[15] J. H. Banoub, F. Michon, and F. Cooper, "Occurrence of 3-acetamido-3,6-dideoxy-4-O-miethyl-L-glucose in the O-polysaccharide of *Vibrio anguillarum*," *Can. J. Biochem. Cell Biol.,* vol. 63, no. 12, pp. 1265-1267, Jun, 1985. DOI: https://doi.org/10.1139/o85-159.

[16] J. H. Banoub, and D. H. Shaw, “Isolation and characterization of 3-acetamido-3,6-dideoxy-L-glucose from the core oligosaccharides obtained from the aquatic Gram-negative bacteria *Aeromonas hydrophila* and *Vibrio anguillarum*,” *Can. J. Biochem. Cell Biol.,* vol. 59, no. 11-12, pp. 877-879, Jun, 1981. DOI: https://doi.org/10.1139/o81-122.

[17] I. Sadovskaya, J. R. Brisson, E. Altman, and L. M. Mutharia, “Structural studies of the lipopolysaccharide O-antigen and capsular polysaccharide of *Vibrio anguillarum* serotype O:2,” *Carbohydr. Res.,* vol. 283, pp. 111-127, Mar, 1996. DOI: https://doi.org/10.1016/0008-6215(95)00398-3.

[18] K. Kawahara, U. Seydel, M. Matsuura, H. Danbara, E. T. Rietschel, and U. Zahringer, “Chemical structure of glycosphingolipids isolated from *Sphingomonas paucimobilis*,” *FEBS Lett.,* vol. 292, no. 1-2, pp. 107-110, Nov, 1991. DOI: https://doi.org/10.1016/0014-5793(91)80845-t.

[19] S. Kawasaki, R. Moriguchi, K. Sekiya, T. Nakai, E. Ono, K. Kume, and K. Kawahara, “The cell envelope structure of the lipopolysaccharide-lacking Gram-negative bacterium *Sphingomonas paucimobilis*,” *J. Bacteriol.,* vol. 176, no. 2, pp. 284-290, Jan, 1994. DOI: https://doi.org/10.1128/jb.176.2.284-290.1994.

[20] P. H. Hardy, Jr., and J. Levin, “Lack of endotoxin in *Borrelia hispanica* and *Treponema pallidum*,” *Proc. Soc. Exp. Biol. Med.,* vol. 174, no. 1, pp. 47-52, Oct, 1983. DOI: https://doi.org/10.3181/00379727-174-41702.

[21] Y. A. Knirel, and M. A. Valvano, *Bacterial lipopolysaccharides*, 1 ed., Springer Vienna, 2011.

[22] A. El-Aneed, and J. Banoub, “Elucidation of the molecular structure of lipid A isolated from both a rough mutant and a wild strain of *Aeromonas salmonicida* lipopolysaccharides using electrospray ionization quadrupole time-of-flight tandem mass spectrometry,” *Rapid Commun. Mass Spectrom.,* vol. 19, no. 12, pp. 1683-1695, Apr, 2005. DOI: https://doi.org/10.1002/rcm.1971.

[23] M. Almostafa, T. D. Fridgen, and J. H. Banoub, “Structural investigation by tandem mass spectrometry analysis of a heterogeneous mixture of Lipid A(n) isolated from the lipopolysaccharide of Aeromonas hydrophila SJ-55Ra,” *Rapid Commun. Mass Spectrom.,* vol. 32, no. 3, pp. 167-183, Feb, 2018. DOI: https://doi.org/10.1002/rcm.8017.

[24] M. Almostafa, B. Allehyane, S. Egli, C. Bottaro, T. D. Fridgen, and J. Banoub, “Tandem mass spectrometry determination of the putative structure of a heterogeneous mixture of Lipid As isolated from the lipopolysaccharide of the Gram-negative bacteria *Aeromonas liquefaciens* SJ-19a,” *Rapid Commun. Mass Spectrom.,* vol. 30, no. 8, pp. 1043-1058, Apr, 2016. DOI: https://doi.org/10.1002/rcm.7540.

[25] A. Farhana, and Y. S. Khan, "Biochemistry, lipopolysaccharide," *StatPearls*, Treasure Island (FL): StatPearls Publishing, 2024.

[26] A. Steimle, I. B. Autenrieth, and J. S. Frick, “Structure and function: Lipid A modifications in commensals and pathogens,” *Int. J Med. Microbiol.,* vol. 306, no. 5, pp. 290-301, Aug, 2016. DOI: https://doi.org/10.1016/j.ijmm.2016.03.001.

[27] H. Heine, and A. Zamyatina, “Therapeutic targeting of TLR4 for inflammation, infection, and cancer: A perspective for disaccharide lipid A mimetics,” *Pharmaceuticals (Basel),* vol. 16, no. 1, pp. 23, Dec, 2022. DOI: https://doi.org/10.3390/ph16010023.

[28] A. Shimoyama, and K. Fukase, “Lipid A-mediated bacterial-host chemical ecology: Synthetic research of bacterial lipid As and their development as adjuvants,” *Molecules,* vol. 26, no. 20, pp. 6294-6294, Oct, 2021. DOI: https://doi.org/10.3390/molecules26206294.

[29] J. J. Zik, S. H. Yoon, Z. Guan, G. Stankeviciute Skidmore, R. R. Gudoor, K. M. Davies, A. M. Deutschbauer, D. R. Goodlett, E. A. Klein, and K. R. Ryan, “Caulobacter lipid A is conditionally dispensable in the absence of fur and in the presence of anionic sphingolipids,” *Cell. Rep.,* vol. 39, no. 9, pp. 110888, May, 2022. DOI: https://doi.org/10.1016/j.celrep.2022.110888.

[30] A. Mikhael, D. Hardie, D. Smith, H. Petrosova, R. K. Ernst, and D. R. Goodlett, “Structural elucidation of intact rough-type lipopolysaccharides using field asymmetric ion mobility spectrometry and Kendrick mass defect plots,” *Analy. Chem.,* vol. 95, no. 46, pp. 16796–16800, Jul, 2023. DOI: https://doi.org/10.1021/acs.analchem.3c02947.

[31] C. A. Hughey, C. L. Hendrickson, R. P. Rodgers, A. G. Marshall, and K. Qian, “Kendrick mass defect spectrum: a compact visual analysis for ultrahigh-resolution broadband mass spectra,” *Anal. Chem.,* vol. 73, no. 19, pp. 4676-4681, Oct, 2001. DOI: https://doi.org/10.1021/ac010560w.

[32] G. Gaiffe, R. B. Cole, A. Sonnette, N. Floch, and M. C. Bridoux, “Identification of postblast residues by DART-high resolution mass spectrometry combined with multivariate statistical analysis of the Kendrick mass defect,” *Anal. Chem.,* vol. 91, no. 13, pp. 8093-8100, Jul, 2019. DOI: https://doi.org/10.1021/acs.analchem.9b00137.

[33] X. Ortiz, K. J. Jobst, E. J. Reiner, S. M. Backus, K. M. Peru, D. W. McMartin, G. O'Sullivan, V. Y. Taguchi, and J. V. Headley, “Characterization of naphthenic acids by gas chromatography-Fourier transform ion cyclotron resonance mass spectrometry,” *Anal. Chem.,* vol. 86, no. 15, pp. 7666-7673, Aug, 2014. DOI: https://doi.org/10.1021/ac501549p.

[34] M. W. Alton, H. J. Stark, M. R. Canagaratna, and E. C. Browne, “Generalized Kendrick analysis for improved visualization of atmospheric mass spectral data,” *Atmos. Meas. Tech.,* vol. 16, no. 12, pp. 3273-3282, Dec, 2023. DOI: https://doi.org/10.5194/amt-16-3273-2023.

[35] T. R. Rosa, G. S. Folli, W. L. S. Pacheco, M. P. Castro, W. Romao, and P. R. Filgueiras, “DropMS: Petroleomics data treatment based in a web server for high-resolution mass spectrometry,” *J. Am. Soc. Mass Spectrom.,* vol. 31, no. 7, pp. 1483-1490, Jul, 2020. DOI: https://doi.org/10.1021/jasms.0c00109.

[36] C. Galanos, O. Luderitz, and O. Westphal, “A new method for the extraction of R lipopolysaccharides,” *Eur. J. Biochem.,* vol. 9, no. 2, pp. 245-249, Jun, 1969. DOI: https://doi.org/10.1111/j.1432-1033.1969.tb00601.x.

[37] T. Fouquet, and H. Sato, “Improving the resolution of Kendrick mass defect analysis for polymer ions with fractional base units,” *Mass Spectrom.,* vol. 6, no. 1, pp. A0055, Feb, 2017. DOI: https://doi.org/10.5702/massspectrometry.A0055.

[38] A. Silipo, and A. Molinaro, "Lipid A structure," *Bacterial lipopolysaccharides*, Springer Vienna, 2011. pp. 1-20.

[39] K. Kawahara, “Variation, modification and engineering of lipid A in endotoxin of Gram-negative bacteria,” *Int. J. Mol. Sci.,* vol. 22, no. 5, pp. 1-15, Feb, 2021. DOI: https://doi.org/10.3390/ijms22052281.

[40] "Rings and double bond equivalents," https://www.crawfordscientific.com/chromatography-blog/post/rdb-rule-rings-and-double-bond-equivalents.

[41] M. Badertscher, K. Bischofberger, M. E. Munk, and E. Pretsch, “A novel formalism to characterize the degree of unsaturation of organic molecules,” *J. Chem. Inf. Comput. Sci.,* vol. 41, no. 4, pp. 889-893, Jul-Aug, 2001. 10.1021/ci000135o.

[42] D. E. Goldberg, M. K. Rumley, and E. P. Kennedy, “Biosynthesis of membrane-derived oligosaccharides: a periplasmic phosphoglyceroltransferase,” *Proc. Natl. Acad Sci. USA.,* vol. 78, no. 9, pp. 5513-5517, Sep, 1981. DOI: https://doi.org/10.1073/pnas.78.9.5513.

[43] N. J. Phillips, D. M. Adin, E. V. Stabb, M. J. McFall-Ngai, M. A. Apicella, and B. W. Gibson, “The lipid A from *Vibrio fischeri* lipopolysaccharide: A unique structure bearing a phosphoglycerol moiety,” *J. Biol. Chem.,* vol. 286, no. 24, pp. 21203-21219, Jun, 2011. DOI: https://doi.org/10.1074/jbc.M111.239475.

[44] A. Swizdor, A. Panek, N. Milecka-Tronina, and T. Kolek, “Biotransformations utilizing beta-oxidation cycle reactions in the synthesis of natural compounds and medicines,” *Int. J. Mol. Sci.,* vol. 13, no. 12, pp. 16514-16543, Dec, 2012. DOI: https://doi.org/10.3390/ijms131216514.

[45] A. Mikhael, H. Petrosova, D. Smith, R. K. Ernst, and D. R. Goodlett, “Lipid A double bond position determination using ozone and laser-induced dissociation,” *Rapid Commun. Mass Spectrom.,* vol. 38, no. 16, pp. e9854, Aug, 2024. DOI: https://doi.org/10.1002/rcm.9854.

Chapter 6 Conclusions and Future Work

6.1. Conclusions

This work provides significant insights into the molecular biology of marine organisms, focusing on the proteomic composition of Atlantic cod otoliths and the structural elucidation of lipid A from pathogenic marine bacteria. Through an in-depth proteomic analysis, we revealed a previously unrecognized diversity of proteins in Atlantic cod otolith, demonstrating that the otoliths serve as reservoirs of complex physiological information beyond their known role as biochronological markers [1].

Using high-resolution mass spectrometry (ESI-FAIMS-Orbitrap MS and HCD-MS/MS), we generated a comprehensive protein profile, marking the first such detailed study for this species. This analysis identified thousands of proteins, including those involved in calcium binding and crystal nucleation, underscoring the otolith's potential as a tool for examining fish physiology and life history.

We used the state-of-the-art Orbitrap Fusion™ Lumos™ Tribrid™ Mass Spectrometer (Thermo Scientific, Waltham, MA, USA), which combines a quadrupole mass filter, a linear ion trap, and an Orbitrap mass analyzer. This instrument was selected for our study due to its high sensitivity **(Figure 1-19)** [2]. In addition, we employed Field Asymmetric Waveform Ion Mobility Spectrometry (FAIMS), which separates gas-phase ions based on their mobility in alternating strong and weak electric fields. By adjusting the compensation voltage (CV), FAIMS can separate ions according to their shape and size in asymnetric electric fields [3, 4].

In Chapter 2, we presented the first qualitative proteomic study of Atlantic cod otoliths, uncovering over 2000 proteins, including somatolactin, F-actin-capping protein, and annexin, which play roles in calcium ion binding and contribute to crystal formation. This methodology lays the groundwork for using otolith proteomics to understand fish biology thoroughly. We identified sex-related biomarkers for males (SPATA6 protein) and females (Vitellogenin-2-like protein) and other proteins related to biochemical and physiological processes, which supported our hypothesis that otoliths record the biological information of cod fish (**Table 2-1**). In addition, this represented a proof-of-concept study.

In Chapter 3, we quantified a range of otolith proteins, identifying key stress and endocrine-responsive proteins, including eleven heat shock proteins (HSPs), which underscore the otolith's ability to record environmental and physiological changes.

In this chapter, we examined different samples than those in the previous chapter, collected from the same area; however, they differ in age or possibly life history, which may account for the differences in the total number of identified proteins, as shown in **Figure 3-1**. Nevertheless, eleven HSPs were consistently identified in both studies. Additionally, in this study, the total number of otolith proteins was similar between sexes, as shown in **Figure 3-2**. Furthermore, several proteins exhibited sex-specific expression differences, as visualized in the volcano plot **(Figure 3-3)** and the heatmap **(Figure 3-4).**

Lastly, we conducted bioinformatics analyses, including Gene Ontology (**Figures 3-6 and 3-7**) and protein–protein interaction analysis (**Figure 3-8**). Altogether, these results provide further support for the idea that otolith proteins offer valuable insight into

the biology of the fish itself. These findings offer a proteomic baseline for Atlantic cod that can serve as a reference for assessing the impacts of climate change and pollutants on marine species.

Chapters 4 and 5 shifted focus to lipid A structural analysis in *Aeromonas hydrophila* and *Vibrio anguillarum*. Lipid A is a key component of lipopolysaccharides (LPS) that form the outer membrane of Gram-negative bacteria, contributing to bacterial virulence and immunogenicity [5-7]. Lipid A is a glycolipid typically composed of mono or di-phosphorylated glucosamine disaccharide core with variable numbers and types of fatty acyl chains [5-7]. Lipid A acts as a potent stimulator of the innate immune system through recognition by the Toll-like receptor TLR4 [8-10]. Several studies have focused on modifying the structure of lipid A in various Gram-negative bacterial species, such as *Escherichia coli* and *Salmonella*, to reduce its toxicity while preserving its immunostimulatory properties. This has been achieved by altering acylation patterns and developing synthetic analogs [11, 12]. As a result, lipid A has become a key target for the development of adjuvants, such as monophosphoryl lipid A (MPLA), which retains immune-activating properties with significantly reduced endotoxicity and is now widely used in licensed vaccines [12].

Using ESI-FAIMS-Orbitrap MS and HCD-MS/MS, along with Kendrick mass defect (KMD) analysis, we characterized lipid A derivatives with unique structural features. KMD plots are particularly valuable for classifying and organizing structurally related ions within complex mixtures [13-18]. In a KMD plot, the relationship between the Kendrick mass defect and the nominal Kendrick mass is visually represented. Ions whose

elemental compositions differ by one or more base units share the same KMD value and therefore align horizontally in the plot **(Figure 1-25)** [13]. In contrast, ions with different KMD values align vertically, reflecting variations in double bond equivalents (DBE) or heteroatom content higher DBE or greater numbers of heteroatoms result in larger mass defects [13].

In Chapter 4, the complex lipid A architecture of *A. hydrophila* revealed distinctive β-D-Glc*p*N-(1→6)-α-D-Glc*p*N disaccharide cores and specialized acyl chain linkages, as shown in **(Figure 4-2 and Table 4-1)**. To the best of our knowledge, this is the first report on the structural characterization by FAIMS-MS and KMD plots. Lipid A extracted from the *Aeromonas* Gram-negative strain SJ-26 was analyzed in negative ion mode using ESI-FAIMS-Orbitrap-MS/MS. This analysis revealed presence of three main Lipid A fractions: Mono-phosphorylated Lipid A (MPLA) at CV = 0 - 22 V, MPLA adduct/aggregate dimers at CV= 23 - 43 volts, and di-phosphorylated Lipid A (DPLA) at CV = 44 - 70 volts. The ability of FAIMS to isolate dimeric MPLA aggregates from monomeric MPLA avoided complications in tandem MS analysis.

For example, doubly charged ion at *m/z* 1506.05 (z= -2) was expected to be composed of two MPLA monomeric singly charged ions of m/z 1506.05 (z = -1). However, MS/MS of this dimeric MPLA revealed that it is a mixture of at least four isomeric dimers: two penta-acylated MPLA (2 x 1506.05 / 2 = 1506.05), hexa-tetra acylated MPLA (1732.24 + 1279.86 / 2 = 1506.05), hexa-tetra MPLA (1688.22 + 1323.88 / 2 = 1506.5), hepta-tri acylated MPLA (1914.41 + 1097.68 / 2 = 1506.05). his clearly demonstrates the compositional complexity of lipid A *A. hydrophila*.

Chapter 5 identified a lipid A mixture from *V. anguillarum* with novel structures, diverging from the phospho-glycerol substituted at O-1 position, as shown in **(Figure 5-1 and Table 5-1)**. Furthermore, the presence of di-hydroxylated acyl chains at the N-2' in highlights the complexity of lipid A in *Vibrio anguillarum*. This unexpected finding challenges current paradigms and suggests unique immunogenic properties that may be relevant to host-pathogen interactions in marine environments. This suggests that structural variability plays an essential role in the pathogen's adaptation strategies, allowing it to evade immune responses that typically recognize conventional lipid A structures.

The identification of these novel lipid A derivatives (Chapters 4 and 5) enhances our understanding of bacterial pathogenicity in marine ecosystems and paves pathways for developing targeted vaccines. Collectively, this work establishes a framework for exploring marine organism physiology and pathogen interactions at the molecular level, with implications for innovations in fisheries science, environmental monitoring, and aquaculture health management.

6.2. Future Work

6.2.1. Otolith Proteins

This thesis has highlighted the complex protein composition within Atlantic cod otoliths, unrevealing roles in fish physiology, stress response, and adaptation. To deepen our understanding, future research should focus on specific protein families, such as heat shock proteins (HSPs), as they play critical roles in thermal adaptation and resilience [19-22].

HSPs are molecular chaperones that facilitate protein folding, stabilize proteins under stress, and play an essential role in cellular protection and repair [19-22]. Different HSPs are expressed in response to thermal and other environmental stressors, making them promising biomarkers for studying adaptation in Atlantic cod. Future research on HSPs could include analyzing HSP expression from archived otolith samples collected across various years, seasons, and regions within Canadian waters. The high-resolution mass spectrometry, could be used to quantify and compare HSP expression levels across timeframes, providing a unique opportunity to observe changes in stress response over years or even decades.

By correlating HSP levels with historical environmental data, we could evaluate whether cod's stress response reveals trends linked to climate shifts. Such findings could assess whether cod stocks have developed resilience to gradually warming ocean temperatures. Identifying specific HSPs or patterns that correlate with temperature resilience could yield valuable biomarkers for climate adaptation. This approach could provide fisheries managers with crucial information to support the most resilient stocks, promoting the stability and long-term sustainability of Atlantic cod populations.

6.2.2. Bacterial Lipid A Research

This work also has highlighted the molecular structure of unique lipid A structures of pathogenic marine bacteria, including *Vibrio anguillarum* and *Aeromonas hydrophila*. Future work should explore how changes in the composition of lipid A are influenced by environmental factors, particularly variations in temperature and interactions with immune systems, such as bacteriophages [8, 23, 24].

Environmental factors, such as temperature, influence lipid A biosynthesis and structural modifications, affecting bacterial pathogenicity [8, 23]. Culturing *Vibrio anguillarum* and other pathogens under varied temperature conditions and analyzing lipid A structure, help in determine how thermal changes impact lipid A composition. High-energy CID-MS/MS could reveal structural adaptations in response to temperature, informing our understanding of bacterial resilience to environmental stress.

Furthermore, we should examine how these distinct lipid A molecules interact with fish immune systems, which could provide insights into how bacterial lipid A adapt to evade host defenses. Immunogenic assays would help identify lipid A variants with unique immune-modulating properties relevant to host-pathogen interactions. Characterizing other unknown lipid A structures could aid in developing vaccines for different species, advancing aquaculture health management [11, 25, 26].

6.3. References

[1] S. Smolinski, J. Deplanque-Lasserre, E. Hjorleifsson, A. J. Geffen, J. A. Godiksen, and S. E. Campana, “Century-long cod otolith biochronology reveals individual growth plasticity in response to temperature,” *Sci. Rep.,* vol. 10, no. 1, pp. 16708, Oct, 2020. DOI: https://doi.org/10.1038/s41598-020-73652-6.

[2] "Orbitrap Tribrid Mass Spectrometer," https://www.thermofisher.com/ca/en/home/industrial/mass-spectrometry/liquid-chromatography-mass-spectrometry-lc-ms/lc-ms-systems/orbitrap-lc-ms/orbitrap-tribrid-mass-spectrometers.html.

[3] B. M. Kolakowski, and Z. Mester, “Review of applications of high-field asymmetric waveform ion mobility spectrometry (FAIMS) and differential mobility spectrometry (DMS),” *Analyst,* vol. 132, no. 9, pp. 842-864, Sep, 2007. DOI: https://doi.org/10.1039/b706039d.

[4] K. Hohenwallner, L. M. Lamp, L. Peng, M. Nuske, J. Hartler, G. E. Reid, and E. Rampler, “FAIMS Shotgun lipidomics for enhanced HILIC-like separation and automated annotation of gangliosides,” *ChemRxiv*, 2024. 10.26434/chemrxiv-2024-qht6q.

[5] G. Larrouy-Maumus, A. Clements, A. Filloux, R. R. McCarthy, and S. Mostowy, “Direct detection of lipid A on intact Gram-negative bacteria by MALDI-TOF mass spectrometry,” *J. Microbiol. Methods,* vol. 120, pp. 68-71, Jan, 2016. DOI: https://doi.org/10.1016/j.mimet.2015.12.004.

[6] K. Kawahara, “Variation, modification and engineering of lipid A in endotoxin of Gram-negative bacteria,” *Int. J. Mol. Sci.,* vol. 22, no. 5, pp. 1-15, Feb, 2021. DOI: https://doi.org/10.3390/ijms22052281.

[7] F. Di Lorenzo, F. Crisafi, V. La Cono, M. M. Yakimov, A. Molinaro, and A. Silipo, “The structure of the lipid A of Gram-negative cold-adapted bacteria isolated from Antarctic environments,” *Mar. Drugs,* vol. 18, no. 12, Nov, 2020. DOI: https://doi.org/10.3390/md18120592.

[8] Y. A. Knirel, and M. A. Valvano, *Bacterial lipopolysaccharides*, 1 ed., Springer Vienna, 2011.

[9] C. W. Cluff, "Monophosphoryl lipid A (MPL) as an adjuvant for anti-cancer vaccines: clinical results," Springer New York, 2009. pp. 111-123.

[10] S. Kim, Dhilon S. Patel, S. Park, J. Slusky, Jeffery B. Klauda, G. Widmalm, and W. Im, "Bilayer properties of lipid a from various Gram-negative bacteria," *Biophys. J.,* vol. 111, no. 8, pp. 1750-1760, Jun, 2016. DOI: https://doi.org/10.1016/j.bpj.2016.09.001.

[11] A. Shimoyama, and K. Fukase, "Lipid A-mediated bacterial-host chemical ecology: Synthetic research of bacterial lipid As and their development as adjuvants," *Molecules,* vol. 26, no. 20, pp. 6294-6294, Oct, 2021. DOI: https://doi.org/10.3390/molecules26206294.

[12] A. Zamyatina, and S. Strobl, "Synthesis of bioactive lipid A and analogs," *Recent trends in carbohydrate chemistry*, Elsevier Inc., 2020. pp. 51-102.

[13] A. Mikhael, D. Hardie, D. Smith, H. Petrosova, R. K. Ernst, and D. R. Goodlett, "Structural elucidation of intact rough-type lipopolysaccharides using field asymmetric ion mobility spectrometry and Kendrick mass defect plots," *Analy. Chem.,* vol. 95, no. 46, pp. 16796–16800, Jul, 2023. DOI: https://doi.org/10.1021/acs.analchem.3c02947.

[14] C. A. Hughey, C. L. Hendrickson, R. P. Rodgers, A. G. Marshall, and K. Qian, "Kendrick mass defect spectrum: a compact visual analysis for ultrahigh-resolution broadband mass spectra," *Anal. Chem.,* vol. 73, no. 19, pp. 4676-4681, Oct, 2001. DOI: https://doi.org/10.1021/ac010560w.

[15] G. Gaiffe, R. B. Cole, A. Sonnette, N. Floch, and M. C. Bridoux, “Identification of postblast residues by DART-high resolution mass spectrometry combined with multivariate statistical analysis of the Kendrick mass defect,” *Anal. Chem.,* vol. 91, no. 13, pp. 8093-8100, Jul, 2019. DOI: https://doi.org/10.1021/acs.analchem.9b00137.

[16] X. Ortiz, K. J. Jobst, E. J. Reiner, S. M. Backus, K. M. Peru, D. W. McMartin, G. O'Sullivan, V. Y. Taguchi, and J. V. Headley, “Characterization of naphthenic acids by gas chromatography-Fourier transform ion cyclotron resonance mass spectrometry,” *Anal. Chem.,* vol. 86, no. 15, pp. 7666-7673, Aug, 2014. DOI: https://doi.org/10.1021/ac501549p.

[17] M. W. Alton, H. J. Stark, M. R. Canagaratna, and E. C. Browne, “Generalized Kendrick analysis for improved visualization of atmospheric mass spectral data,” *Atmos. Meas. Tech.,* vol. 16, no. 12, pp. 3273-3282, Dec, 2023. DOI: https://doi.org/10.5194/amt-16-3273-2023.

[18] T. R. Rosa, G. S. Folli, W. L. S. Pacheco, M. P. Castro, W. Romao, and P. R. Filgueiras, “DropMS: Petroleomics data treatment based in a web server for high-resolution mass spectrometry,” *J. Am. Soc. Mass Spectrom.,* vol. 31, no. 7, pp. 1483-1490, Jul, 2020. DOI: https://doi.org/10.1021/jasms.0c00109.

[19] F. Tian, X.-L. Hu, T. Yao, X. Yang, J.-G. Chen, M.-Z. Lu, and J. Zhang, “Recent advances in the roles of HSFs and HSPs in heat stress response in woody plants,” *Front. Plant Sci.,* vol. 12, Jul, 2021. DOI: https://doi.org/10.3389/fpls.2021.704905.

[20] T. O. Street, L. A. Lavery, and D. A. Agard, "Substrate binding drives large-scale conformational changes in the Hsp90 molecular chaperone," *Mol. Cell,* vol. 42, no. 1, pp. 96-105, Apr, 2011. DOI: https://doi.org/10.1016/j.molcel.2011.01.029.

[21] T. Didenko, A. M. Duarte, G. E. Karagoz, and S. G. Rudiger, "Hsp90 structure and function studied by NMR spectroscopy," *Biochim. Biophys. Acta.,* vol. 1823, no. 3, pp. 636-647, Mar, 2012. DOI: https://doi.org/10.1016/j.bbamcr.2011.11.009.

[22] G. Chiosis, C. S. Digwal, J. B. Trepel, and L. Neckers, "Structural and functional complexity of HSP90 in cellular homeostasis and disease," *Nat. Rev. Mol. Cell Biol.,* vol. 24, no. 11, pp. 797-815, Nov, 2023. DOI: https://doi.org/10.1038/s41580-023-00640-9.

[23] M. Matsuura, "Structural modifications of bacterial lipopolysaccharide that facilitate Gram-negative bacteria evasion of host innate immunity," *Front. Immunol.,* vol. 4, pp. 109, May, 2013. DOI: https://doi.org/10.3389/fimmu.2013.00109.

[24] M. Almostafa, B. Allehyane, S. Egli, C. Bottaro, T. D. Fridgen, and J. Banoub, "Tandem mass spectrometry determination of the putative structure of a heterogeneous mixture of Lipid As isolated from the lipopolysaccharide of the Gram-negative bacteria *Aeromonas liquefaciens* SJ-19a," *Rapid Commun. Mass Spectrom.,* vol. 30, no. 8, pp. 1043-1058, Apr, 2016. DOI: https://doi.org/10.1002/rcm.7540.

[25] D. H. Persing, R. N. Coler, M. J. Lacy, D. A. Johnson, J. R. Baldridge, R. M. Hershberg, and S. G. Reed, "Taking toll: lipid A mimetics as adjuvants and

immunomodulators," *Trends Microbiol.,* vol. 10, no. 10 Suppl, pp. S32-37, Oct, 2002. DOI: https://doi.org/10.1016/s0966-842x(02)02426-5.

[26] J. Arenas, E. Pupo, C. Phielix, D. David, A. Zariri, A. Zamyatina, J. Tommassen, and P. van der Ley, "Shortening the Lipid A Acyl chains of *Bordetella pertussis* enables depletion of lipopolysaccharide endotoxic activity," *Vaccines (Basel),* vol. 8, no. 4, Oct, 2020. DOI: https://doi.org/10.3390/vaccines8040594.

Appendix

Appendix A1. Supporting Information for Chapter 2

All tables from Appendix A1 are provided in the Supplementary Materials Excel sheet A1.

Table A1-1. Results of the shotgun proteomics analysis of male Atlantic Cod (*Gadus morhua*) proteins.

Table A1-2. Results of the shotgun proteomics analysis of female Atlantic Cod (*Gadus morhua*) proteins.

Table A1-3. The full list of the 302 most abundant proteins identified from male Atlantic Cod (*Gadus morhua*).

Table A1-4. The full list of the 247 most abundant proteins identified from female Atlantic Cod (Gadus morhua).

Table A1-5. According to the complete details of the protein description, there are 143 otolith core proteins, common between male and female Atlantic Cod (Gadus morhua) proteins.

Table A1-6. According to the complete details of the protein description, the male Atlantic Cod (Gadus morhua) has 138 unique.

Table A1-7. According to the complete details of the protein description, the female Atlantic Cod (Gadus morhua) has 67 unique.

Appendix A2. Supporting Information for Chapter 3

All tables from Appendix A2 are provided in the Supplementary Materials Excel sheet A2.

Table A2- 1. Overview of sample used in the current study.

Table A2- 2 (1).10 Otolith protein; Table A2 -2 (2). 10 Otolith protein with protein sequences (Full data).

Table A2- 3.Volcano Plot.

Table A2- 4. 802 Proteins are always common between individuals.

Table A2- 5. 202 Highly abundance proteins for female.

Table A2- 6. 90 Highly abundance proteins for males.

Table A2- 7. 81 Proteins Present in ≥X Males and zero females.

Table A2- 8. 196 Proteins Present in ≥X Males and zero females.

Table A2- 9. 92 Proteins identified in individual, either male or female.

Table A2- 10. 214 Uncharacterized proteins identified in our dataset.

Table A2- 11. Sixteen proteins related to the actin family identified in this study.

Table A2- 12. Six proteins related to tropomyosins identified in this study.

Table A2- 13. α- and β-Tubulin identified in this study.

Table A2- 14. Three proteins related to the tyrosine 3-monooxygenase/tryptophan activation protein β-polypeptide identified in this study.

Table A2- 15. Both keratin protein types identified in our data.

Table A2- 16. List of heat-shocked proteins identified in our study.

Table A2- 17. Protein-Protein Interaction- STRING network in Figure S1. The full network is available online at

(https://string-db.org/cgi/network?taskId=bybNmeXaeGFU&sessionId=boleulT8hMV6)

Table A2- 18. Top 20 in network ranked by Degree method.

Table A2- 19. String PPI network visualization of top 20 high-degree proteins in the otolith of *Gadus morhua*.

Figure A2- 1. The full Protein-Protein Interaction- STRING network.